Muller, Joanne (2006) ***Reconstructing climate change of the last 55 kyr: the Lynch's Crater peat mire record, NE-QLD, Australia.*** **PhD Thesis, James Cook University.**

Reconstructing climate change of the last 55 kyr: The Lynch’s Crater peat mire record, NE-QLD, Australia

Thesis submitted by
Joanne Muller B.Sc. (Hons)

in September 2006
for the degree of Doctor of Philosophy
in the School of Earth Sciences,
James Cook University, Queensland, Australia

ELECTRONIC COPY

I, the undersigned, the author of this work, declare that the electronic copy of this thesis provided to the James Cook University Library, is an accurate copy of the print thesis submitted, within the limits of the technology available.

Signature

Date

Statement of Access

I, the undersigned, author of this work, understand that James Cook University will make this thesis available for use within the University Library and, via the Australian Digital Theses network, for use elsewhere.

I understand that, as an unpublished work, a thesis has significant protection under Copyright Act and;

I do not wish to place any further restriction on access to this work, with the exception of the following:

All users consulting this thesis are required to sign the following statement:

"In consulting this thesis I agree not to copy or closely paraphrase it in whole or in part without the written consent of the author, and to make proper written acknowledgement for any assistance which I have obtained from it"

----------------------------------- ------------------------

Joanne Muller 2006

Statement of Sources

Declaration

I declare that this thesis is my own work and has not been submitted in any other form for another degree or diploma at any university or other institution of tertiary education. Information derived from the published or unpublished work of others has been acknowledged in the text and a list of references is given.

-----------------------------------   ------------------------

Joanne Muller   2006

Statement of Contribution by Others

This thesis has benefited greatly from the contribution of others to the formulation of ideas, the development of research approaches, and the interpretation and critical review of data. Acknowledgement of many of these contributors is made at the conclusion of relevant chapters, but is here due to several individuals.

Raphael Wüst was instrumental in providing the initial momentum to investigate geochemistry at Lynch's Crater and he secured the funding through an Australian Research Council Discovery Grant. Raphael Wüst has also contributed to acquisition and interpretation of data herein. The importance of his contribution to this research is apparent in his status as co-author to published or manuscripts submitted for publication, however, he recognises this authors role as chief investigator in these studies, and as having acquired the majority of the data, formulating the bulk of the interpretations, preparing drafts, and refining the manuscripts.

Dominik Weiss, Malin Kylander and Antonio-Martinez-Cortizas provided analytical and interpretive expertise. The contribution of these individuals is recognised by their status as co-authors on the manuscripts presented herein and all recognise this authors role as chief investigator in this particular avenue of research. This project would not have been possible without primary funding from the Australian Research Council (DP0456515) and the Australian Institute of Nuclear Sciences and Engineering (PGR8/03).

Acknowledgements

Funding for this project was provided by the Australian Research Council (DP0456515) and the Australian Institute of Nuclear Sciences and Engineering (PGR8/03). In part the field campaign was supported by the National Geographic.

This project has benefited greatly from collaboration and discussions with many people, including Robert Carter, Micheal O'Leary, Gavin Schmidt, Jerry McManus, Anthony Brocolli, Tim Jennerjahn, Hermann Behling, Peter Kershaw, Chris Turney, Susan Rule and William Anderson. Laboratory assistance from Raquel Garcia Sanchez, Barry Coles, Yi Hu, Maureen Soon and Gordon Warria and field assistance from David Holliday, Jonathan Brown, Damien Kelleher, Sarah Davies and Patrick Moss is greatly appreciated.

Special collaborations that I would like to acknowledge include, an undeniably valuable collaboration with Malin Kylander who assisted me greatly in laboratory work, paper writing and general support. Also the collaboration with Antonio Martinez Cortizas, who has taught me a great deal about organic geochemistry and peat ecology and has offered immense support and motivation in paper writing.

Special thanks go to my two supervisors, Raphael Wust, who set up a most impressive project and supported me with funds, which allowed me to travel to laboratories and conferences across the globe and to Dominik Weiss, whose never failing support and encouragement has given me great confidence as a researcher. I would like to thank them both for their support in the writing of my thesis.

Thanks to all at JCU who helped me throughout this project, especially to Mick, Loui, Bushy, Antwun and especially to Kirsten who has been a wonderful proof reader, office mate and friend over the years. Finally to my amazing family, mum, dad, Benny and Pauli – thank you.

ABSTRACT

This study provides new information on past climate conditions in equatorial regions through the application of geochemical proxies to an uncharacteristically long (55 kyr) peat record of Lynch's Crater in the Southern Hemisphere. Lynch's Crater is an extinct volcanic crater (>200 kyr) within the basaltic field of the Atherton Tablelands, NE Australia, from which a 13 m peat record was extracted. The peats consist of 1.5 m of ombrotrophic peat underlain by a minerotrophic peat. The ombrotrophic section has low ash yield (<5%) and low pH (~4-5), while the minerotrophic section has low to high ash yield (often <8%) and a more neutral pH (~7). Geochemical analyses were used to identify local, regional and global signals of environmental change over the past 55 kyr.

Principal component analyses (PCA) of trace, major and rare earth elements identified the crater wall (basaltic and schist bedrock) as the primary source of the peat's inorganic constituents. The PCA of the geochemical data are used to differentiate pathways and processes of elements that occur within the peat deposit and the information is used to interpret climate changes such as changes in precipitation, weathering and dust influx. Two distinct sources (local and long range) have contributed to the lithogenic and chalcophile elemental composition throughout the deposit. Most of the inorganic fractions have the same geochemical signatures as the rocks and sediments of the crater wall, with low As and high Al, Ti and Sc concentrations. From 55-35 kyr BP, low inorganics (<7%) and elemental concentrations coincide with rainforest vegetation in the vicinity of the crater, which reduced catchment soil erosion. The low catchment influx allows a long-range dust signature to be distinguished in this section of the deposit, as indicated

by increased As and V concentrations. Leading up to the Holocene (~35,000-10,000 kyr) the influence of dust may be still present but local sources become more dominant. During the Holocene lithogenic and chalcophile influx decreases significantly and coincides with the lowest ash values (~4%) indicating that little weathering of the catchment soils occurred during this period. This interpretation is supported by previous pollen studies that show established rainforest vegetation at this time.

Within the minerotrophic section of Lynch's Crater, several layers with abundant sponge spicules, diatom fragments and detrital quartz occur indicating high algal and protista productivity that signal high water tables and standing water. These layers are characterised by high (up to 50%) ash yield that further indicate persistent flooding of Lynch's Crater deposits and signal a change in the precipitation regime in North Queensland, Australia. High ash yield layers are synchronous with high biogenic silica, high Si/Al ratios, high Cyperaceae/Poaceae ratios, heavier $\delta^{15}N$ isotopes and low C and O concentrations. These intervals span the following periods: 34-37 kyr, 28-30 kyr, 22-25 kyr, 14.5-16 kyr, 12.5-13.5 kyr and 8.5 kyr which are contemporaneous with Heinrich events, the Younger Dryas and the 8.2 kyr event, all of which are characterised in the Northern Hemisphere as abrupt climate events. These layers also provide evidence for an extended southward migration of the Intertropical Convergence Zone (ITCZ) in the Southern Hemisphere Pacific region during major climate perturbations of the last 55 kyr. This interpretation is supported by a general circulation model (GCM), which shows a southward propagation of the ITCZ in response to a Heinrich like simulation where freshwater forcing is applied in the North Atlantic. The record provides insight into climate shifts in the Southern Hemisphere and more specifically the western Pacific Ocean during these millennial-scale climate perturbations in the low latitudes.

Post-depositional remobilisation of elements occurs within the peat deposit and provides evidence of previous environmental conditions of the peat ecosystem. Concentration profiles of Ca, Mg, Sr, Fe and S show a change between high values in the minerotrophic and low values in the ombrotrophic section of the mire, this is primarily a result of groundwater influence in the minerotrophic deposits. In addition small enrichments are associated with some of the interpreted wet events and indicate increased input of Ca, Mg, Sr, Fe and S cations from the catchment. The study also shows post-depositional diagenetic response of Mn that is regulated by Eh-pH conditions and results in increasing Mn concentrations with depth, where conditions generally become more anoxic and alkaline.

To date, research into historical distribution of halogens in peat has been limited, yet some studies have assumed Cl to be conservative in peat thereby reflecting changes in the halogen concentrations of rainwater. The present study also suggests that Cl variations in Lynch’s Crater reflect a high-resolution record of precipitation change over the past 55 kyr. At Lynch’s Crater the Cl concentration profile shows a remarkable similarity to the vegetation and precipitation phases suggested by pollen analysis from the area. Stable C isotope values show some similarity to that of the Cl record and indicate changes within the soil moisture regime. Lynch’s Crater shows similarities to other Australian paleo-precipitation records, for example increased Cl values coincide with the early Holocene and also possible periods of intense monsoon activity between 42-55 kyr. During most of the late Pleistocene (~18-30 kyr) however, low Cl concentrations indicate dry conditions across the Tablelands and possibly throughout NE Australia. It is possible that the Cl record shows increased precipitation in the tropics associated with warm periods know as Dansgaard-Oeschger cycles generally recorded in high northern latitudes. Here a detrended Cl concentration profile displays a remarkable resemblance to the oxygen isotope records from the Greenland Ice Core Project, implying the presence of a global climate signature in the Southern Hemisphere tropics.

The initial geochemistry investigation of the Lynch's Crater peat cores has uncovered important information on past climate change in the equatorial Southern Hemisphere. Future work would benefit from improved dating techniques allowing better correlation of the deposit with other paleorecords. This may provide answers to important paleoclimate questions, such as 'what is a feedback and what is a trigger of abrupt climate change?'. In addition, geochemical analysis should be undertaken on more samples to obtain higher resolution records for past climatic interpretation and more time must be spent on individual elements that are poorly understood. This is a unique opportunity to study past climate dynamics in an area of the world that is poorly constrained by paleorecords.

TABLE OF CONTENTS

CHAPTER 3..33

LIST OF FIGURES

CHAPTER 2

CHAPTER 3

CHAPTER 4

CHAPTER 5

LIST OF TABLES

CHAPTER 2

CHAPTER 3

List of Appendicies

CHAPTER 1

Introduction

View of Lynch's Crater from northeastern crater wall (July 2003)

Climate change is with us. A decade ago, it was conjecture, now it unfolds before our eyes. Canada's Inuit see receding Arctic ice and permafrost, Latin Americans and south Asians see lethal storms and floods, Europeans notice diminishing glaciers, increased forest fires and fatal heat waves. In Australia it manifests as drought, rising sea surface temperatures and ecosystem loss, including the undeniable threat to our Great Barrier Reef.

Most long, continuous records of past climate change have been sourced from ice (GRIP, GISP, EPICA) (Brook et al., 1996; Delmonte et al., 2004; Shackleton, 1987; Stuiver et al., 1997), marine e.g. (Fairbanks et al., 1980; Kennett and Venz, 1995; Tamburini et al., 2003) and terrestrial e.g. (Adegbie et al., 2003; Mora et al., 2002; Woolfenden, 2003) records. Most of these records are from mid to high latitudes and few records are from equatorial regions, and this is a major pit fall for global paleoclimate research, especially now with new work (Clement et al., 2001; Hendy and Kennett, 1999) demonstrating that the equatorial region is a “key player” in global climate dynamics.

Terrestrial paleorecords have an advantage over ocean and ice records in that they record climate change as it occurs on land, with relatively authentic timing and without the associated lags that may be experienced in ocean and ice studies. Peat is known to provide excellent terrestrial records of past climate change. As with other paleorecords the majority of peat studies to date have used high latitude records with little input from equatorial regions. Few peat studies from equatorial regions have proved their importance for interpreting past climate change, but many of these studies go back no further than the Holocene and the very late Pleistocene (~20 kyr). (Bonnefille and Chalié, 2000; Page et al., 2004; Weiss et al., 2002).

This study focuses on geochemical proxies from a peat core extracted from Lynch's Crater in the Atherton Tableland, NE Australia, to interpret past environments and climate. Lynch's Crater (17° 37′ S, 145° 70′ E) is situated at 760 m elevation on the undulating plateau of the Atherton Tableland, 30 km from the east coast of north Queensland, Australia. Lynch's Crater is a volcanic crater filled with lake and peat sediments. At present 70% of the annual rainfall in the area (2570 mm) falls during the austral summer months of November through March (www.bom.gov.au) as a result of seasonal ITCZ migration. The high rainfall allows for present day growth of luxurious and diverse rainforest vegetation and also favours peat and lake sediment accumulation in depressional settings. The deposits was first studied in the 1970's (Kershaw, 1974) and since then palynological studies from Lynch's Crater have identified major vegetation changes over the last ~200,000 years (Kershaw, 1978; Kershaw, 1986; Kershaw et al., 1993) and peat humification studies have identified climate variations at millennial and orbital time scales over the last 50 kyr (Turney et al., 2004). The upper peat deposits have also been reinvestigated, in the mid 1990's, in order to document human arrival in Australia (pollen and charcoal) (Turney et al., 2001).

The thesis consists of six chapters. Chapter 1 contains the introduction, Chapters 2-5 contain the main results of the thesis, and Chapter 6 contains the conclusions. The four central chapters (2-5) are set up as individual publications for peer-reviewed journals and the details are as follows:

1) Chapter 2: **Geochemical Evidence of Environmental Change at Lynch's Crater, Queensland, Australia** describes core LC1 from the centre of Lynch's Crater. The main focus is an introductory study to the Lynch's Crater site. In this chapter we determine the trophic status and stratigraphic nature of the peat

deposits from core LC1, which is 6.6 m (~30 kyr). Aluminiun, Ca and Mg are discussed in relation to the trophic status and stratigraphy. Some concluding remarks are made about vegetation, hydrology and atmospheric dust changes in the Lynch's Crater deposit in order to better understand past environmental changes. Co-authors on this paper are Raphael Wüst, Dominik Weiss and Yi Hu. This paper is published in 'Global and Planetary Change'.

Joanne Muller was primarily responsible for the generation of all data and it's interpretation in this chapter. Yi Hi supervised Joanne Muller in all trace and major elemental chemistry preparation and the running of these samples on ICP-OES at JCU. Analysis for radiocarbon was done by Australian Nuclear Sciences and Technology Organisation (ANSTO) staff on Tandem Accelerator as part of Joanne Muller's Australian Institute of Nuclear Sciences and Engineering Postgraduate Research Award. Joanne Muller was responsible for chemical preparation of samples at the ANSTO radiocarbon facility. Raphael A.J. Wüst and Dominik J. Weiss (PhD supervisors) assisted Joanne Muller with interpretation and corrections for this chapter.

2) Chapter 3: **Processes affecting trace and major elemental distribution in a 55 kyr peat deposit in tropical Australia: implications to paleoclimate.** This chapter presents a comprehensive evaluation and discussion of trace and major elemental geochemistry from the long peat core LC2, which constitutes 13 m. This core is the focus of Chapter 3-5 and the 13 m represent ~55,000 years of organic matter accumulation. The chapter focuses on geochemical data (specific elements such as; Sc, Al, Cu, Pb, As, V, Fe, Mg and Cl) and their suitability for paleo-environmental interpretations including weathering, atmospheric dust flux, vegetation and precipitation regimes, and trophic status. Principle component

analyses (PCA) of the geochemical data was performed to reduce the dimensionality of the data and identify the most important (i.e. defining) parts/elements whilst simultaneously filtering “noise”. The statistical analysis allows the differentiation of groups of geochemical variables with similar behaviour, thereby reducing results to sets of variables. Co-authors on this paper are Malin Kylander, Antonio Martinez-Cortizas, Raphael Wüst, Dominik Weiss, Kevin Blake, Barry Coles, and Raquel Garcia-Sanchez. This paper has been submitted to ‘Geochimica et Cosmichimica Acta’.

Analysis for radiocarbon was done by Australian Nuclear Sciences and Technology Organisation (ANSTO) staff on Tandem Accelerator as part of Joanne Muller’s Australian Institute of Nuclear Sciences and Engineering Postgraduate Research Award. Joanne Muller was responsible for chemical preparation of samples at the ANSTO radiocarbon facility. Joanne Muller and Malin Kylander prepared the samples for geochemical analysis under the supervision of Barry Coles at the Imperial College, London. Barry Coles and Raquel Garcia-Sanchez assisted in running samples on ICP-MS and OES. Lead isotopes were determined on an *Isoprobe* MC-ICP-MS by Joanne Muller and Malin Kylander under the supervision of Dominik Weiss and Barry Coles at the Natural History Museum, London. Kevin Blake assisted Joanne Muller with image collection on a JEOL 840A Electron Microprobe, which enabled high-resolution imaging and constituent determination of samples by Scanning Electron Microscopy (SEM) and Electron Probe Microanalyzer (EPMA). Raphael Wüst, Dominik Weiss (PhD supervisors) and Malin Kylander assisted Joanne Muller with interpretation and corrections for this chapter.

3) Chapter 4: **Wet phases in tropical Australia during Heinrich events detected in a terrestrial palaeorecord from Lynch's Crater.** This chapter focussed on several different proxies (ash yield, Si/Al ratios, Cyperaceae/Poaceae ratios and $\delta^{15}N$ isotopes) from LC2 linking environmental and climate changes in order to identify atmospheric and oceanic teleconnections between the North Atlantic and western Pacific Ocean. A fully coupled atmosphere/ocean climate model is included and supports this interpretation. This chapter demonstrates a direct relationship between a southern ITCZ migration over the Pacific Ocean and increased precipitation during millennial scale Heinrich events in Lynch's Crater. Few paleoclimate records of the Southern Hemisphere tropics have investigated the influence of Heinrich events on climate changes during the last glacial period. This paper has been submitted to 'Proceedings of the National Academy of Sciences'. Co-authors on this paper are Malin Kylander, Raphael Wüst, Dominik Weiss, Antonio Martinez-Cortizas, Allegra N. LeGrande, Tim Jennerjahn, Herman Behling, William Anderson and Geraldine Jacobson.

Analysis for radiocarbon was done by Australian Nuclear Sciences and Technology Organisation (ANSTO) staff on Tandem Accelerator as part of Joanne Muller's Australian Institute of Nuclear Sciences and Engineering Postgraduate Research Award. Joanne Muller was responsible for chemical preparation of samples at the ANSTO radiocarbon facility, where Geraldine Jacobson acted as ANSTO supervisor. X-ray fluorescence (XRF) analysis (Si and Al) were undertaken by Antonio Martinez-Cortizas at RIAIDT XRF facility at the University of Santiago in Spain. Nitrogen isotopes were analysed by Mark Kershaw and William Anderson at the SERC Stable Isotope Laboratory, Florida International University, Miami, USA. Biogenic silica was determined by Maureen Soon at the

University of British Columbia, Vancouver, Canada, after preparation at JCU by Joanne Muller. Allegra N. LeGrande from NASA Goddard Institute for Space Studies and Center for Climate Systems Research, Columbia University, New York City, USA, used GISS ModelE-R, to run a fully coupled atmosphere/ocean general circulation model. Hermann Behling and Tim Jennerjahn supplied Joanne Muller with radiocarbon and Fe/Ca data from previously published works. All co-authors assisted Joanne Muller in the development of ideas and corrections of this paper.

4) Chapter 5: **Factors affecting peat composition and evolution in a 55 kyr mire deposit in tropical Australia.** This chapter complements Chapter 4 by using several other geochemical elements, including tracers, majors and isotopes from core LC2 from Lynch's Crater, in order to address paleo-environmental changes related to precipitation dynamics. Principle component analysis (PCA) of the geochemical data was also used to identify trends and similarities of elements such as carbon (TC), nitrogen (TN), oxygen (TO), and sulfur (TS), along with chlorine (Cl) and potassium (K) values, and stable C and N isotopic analysis of organic matter (OM). The results from Lynch's Crater were compared to paleorecords (Atherton Tablelands and Lake Eyre) that show precipitation changes in Australia during the last 55 kyr. The statistical analysis shows ~1500 yr cyclicity that may be compared to Dansgaard-Oeschger cycles (D-O cycles) of rapid warming events (interstandials) followed by slow cooling episodes (stadials). The data strongly supports evidence of global forcing recorded in Lynch's Crater. This paper is intended for submission to 'Earth and Planetary Science Letters' and co-authors on this paper include Antonio Martinez-Cortizas, Raphael A.J. Wüst, William Anderson and Dominik Weiss.

Analysis for radiocarbon was done by Australian Nuclear Sciences and Technology Organisation (ANSTO) staff on Tandem Accelerator as part of Joanne Muller's Australian Institute of Nuclear Sciences and Engineering Postgraduate Research Award. Joanne Muller was responsible for chemical preparation of samples at the ANSTO radiocarbon facility, where Geraldine Jacobson acted as ANSTO supervisor. X-ray fluorescence (XRF) analysis (Cl and O) were undertaken by Antonio Martinez-Cortizas at RIAIDT XRF facility at the University of Santiago in Spain. Carbon 13 isotopes were analysed by Mark Kershaw and William Anderson at the SERC Stable Isotope Laboratory, Florida International University, Miami, USA. Carbon, N and S analysis were done on an Elementar Vario Max CNS Analyzer at James Cook University (Raphael Wust). Co-authors assisted Joanne Muller in the development of ideas in this paper and corrections.

During the thesis project another manuscript with focus on the rare earth elemental and Pb isotope geochemistry of Lynch's Crater was produced and published: Kylander, M.E., Muller, J., Wust, R.A.J., Gallagher, K., Garcia-Sanchez, R., Coles, B.J., and Weiss, D.J., 2007, Rare earth element and Pb isotope variations in a 52 kyr peat core from Lynch's Crater (NE Queensland, Australia): Proxy development and application to paleoclimate in the Southern Hemisphere: Geochimica et Cosmochimica Acta, v. 71, p. 942-960. The abstract of that manuscript is attached in the appendix.

REFERENCES

Adegbie, A.T., Schneider, R.R., Röhl, U. and Wefer, G., 2003. Glacial millenial-scale fluctuations in central African precipitation recorded in terrigenous sediment supply and freshwater signals offshore Cameroon. Palaeogeography, Palaeoclimatology, Palaeoecology, 197(3-4): 323-333.

Bonnefille, R. and Chalié, F., 2000. Pollen-inferred precipitation time-series from equatorial mountains, Africa, the last 40 kyr BP. Global and Planetary Change, 26(1-3): 25-50.

Brook, E.J., Sowers, T. and Orchardo, J., 1996. Rapid variations in atmospheric methane concentration during the past 110,000 years. Science, 273: 1087-1091.

Clement, A., Cane, M. and Seager, R., 2001. An orbitally driven tropical source for abrupt climate change. Journal of Climate, 14(11): 2369-2376.

Delmonte, B., Basile-Doelsch, I., Petit, J.-R., Maggi, V., Revel-Rolland, M., Michardd, A., Jagoutz, E. and Grousset, F., 2004. Comparing the EPICA and Vostok dust records during the last 220,000 years: stratigraphical correlation and provenance in glacial periods. Earth-Science Reviews, 66(1-2): 36-87.

Fairbanks, R.G., Wiebe, P.H. and Be, A.W.H., 1980. Vertical distribution and isotopic composition of living planktonic foraminifera in the western North Atlantic. Science, 207: 61-63.

Hendy, E. and Kennett, J., 1999. Latest quaternary north pacific surface-water responses imply atmosphere-driven climate instability. Geology, 27(4): 291-294.

Kennett, J.P. and Venz, K., 1995. Late Quaternary climatically related planktonic foraminiferal assemblage changes: Hole 893A, Santa Barbara Basin, California. In: J.P. Kennett, J.G. Baldauf and M. Lyle (Editors), Ocean Drilling Program, scientific results, pp. 281-293.

Kershaw, A.P., 1974. A long continuous pollen sequence from north-eastern Australia. Nature, 251: 222-223.

Kershaw, A.P., 1978. Record of last interglacial-glacial cycle from northeastern Queensland. Nature, 272: 159-161.

Kershaw, A.P., 1986. Climatic change and Aboriginal burning in north-east Australia during the last two glacial/interglacial cycles. Nature, 322: 47-49.

Kershaw, A.P., McKenzie, G.M. and McMinn, A., 1993. A Quaternary vegetation history of northeastern Queensland from pollen analysis of ODP Site 820. In: J.A. McKenzie et al. (Editors), Proceedings of the Ocean Drilling Program, scientific results, 133: 107-114. Texas A & M University, Ocean Drilling Program, College Station, TX, United States.

Mora, G., Pratt, L.M., Boom, A. and Hooghiemstra, H., 2002. Biogeochemical characteristics of lacustrine sediments reflecting a changing alpine neotropical ecosystem during the Pleistocene. Quaternary Research, 58(2): 189-196.

Page, S.E., Wüst, R.A.J., Weiss, D., Rieley, J.O., Shotyk, W. and Limin, S.H., 2004. A record of Late Pleistocene and Holocene carbon accumulation and climate change from an equatorial peat bog (Kalimantan, Indonesia): implications for past, present and future carbon dynamics. Journal of Quaternary Science, 19(7): 625-635.

Shackleton, N.J., 1987. Oxygen isotopes, ice volume and sea level. Quaternary Science Reviews, 6: 183-190.

Stuiver, M., Braziunas, T.F. and Grootes, P.M., 1997. Is there evidence for solar forcing of climate in the GISP2 oxygen isotope record? Quaternary Research, 48: 259-266.

Tamburini, F., Adatte, T., Föllmi, K.B., Bernasconi, S.M. and Steinmann, P., 2003. Investigating the history of East Asian monsoon and climate during the last glacial–interglacial period (0–140000 years): mineralogy and geochemistry of ODP Sites 1143 and 1144, South China Sea. Marine Geology, 201(1-3): 147-168.

Turney, C.S.M., Kershaw, A.P., Clemens, S.C., Branch, N., Moss, P.T. and Fifield, L.K., 2004. Millennial and orbital variations of El Niño/Southern Oscillation and high-latitude climate in the last glacial period. Nature, 428: 306-310.

Turney, C.S.M., Kershaw, A.P., Moss, P., Bird, M.I., Fifield, L.K., Cresswell, R.G., Santos, G.M., Di Tada, M.L., Hausladen, P.A. and Zhou, Y., 2001. Redating the onset of burning at Lynch's Crater (North Queensland): implications for human settlement in Australia. Journal of Quaternary Science, 16(8): 767-771.

Weiss, D., Shotyk, W., Rieley, J.O., Page, S.E., Gloor, M., Reese, S. and Cortizas-Martinez, A., 2002. The geochemistry of major and selected trace elements in a forested peat bog, Kalimantan, SE Asia, and its implications for past atmospheric dust deposition. Geochimica et Cosmochimica Acta, 66(13): 2307-2323.

Weiss, D. et al., 2002. The geochemistry of major and selected trace elements in a forested peat bog, Kalimantan, SE Asia, and its implications for past atmospheric dust deposition. Geochimica et Cosmochimica Acta, 66(13): 2307-2323.

Woolfenden, W.B., 2003. A 180,000-year pollen record from Owens Lake, CA: terrestrial vegetation change on orbital scales. Quaternary Research, 59(3): 430-444.

CHAPTER 2

Geochemical and stratigraphic evidence of environmental change at Lynch’s Crater, Queensland, Australia

Adapted from a paper published in:

Global and Planetary Change (2006), Vol 53, pp 269-277

ABSTRACT

This is one of the first applications of geochemical proxies to define changes in vegetation, hydrology and atmospheric dust influence on a peat deposit in the Southern Hemisphere. A 6.6 m deep peat record from Lynch's Crater in NE-Queensland, Australia, provides a sensitive ~5, 000 to 30,000 cal yrs BP archive of environmental change. The deposit consists of 1.5 m of ombrotrophic peat underlain by a minerotrophic peat. Within the minerotrophic section sponge spicules and diatom fragments offer evidence of prolonged flooding of the peat environment resulting in several layers containing (up to 50%) high inorganic material. The Ca and Mg data display episodes of enhanced dust influx and nutrient recycling and support previous palynological studies that show a Pleistocene to Holocene switch from sclerophyll woodlands to rainforest vegetation.

1. INTRODUCTION

Peat deposits are capable of capturing local, regional and global environmental changes (Velichko et al., 1997). Such records represent a window into how terrestrial environments have previously adapted to natural climate change and may also provide insights into anthropogenic impact on the environment.

North American and European mire ecosystems have been the focus of geochemical investigations, primarily characterising the anthropogenic impact recorded in these systems but also natural environmental changes (Dunlap et al., 1999; Klaminder et al., 2003; Martínez-Cortizas et al., 1997; Shotyk et al., 1998; Weiss et al., 1997). To date, few geochemical studies have been conducted in the Southern Hemisphere, though studies from peat bogs in Indonesia have identified interesting environmental differences and similarities between Southern and Northern hemisphere peat deposits (Page et al., 1999; Weiss et al., 2002).

Continental Australia has many different environments from arid lands to tropical rainforests. In tropical north Queensland at Lynch's Crater, a terrestrial peat record has demonstrated its potential to unveil global climate cycles as well as local and regional climate changes (Kershaw, 1986; Kershaw et al., 1993; Turney et al., 2004). These studies have focussed on climate proxies such as pollen, charcoal and peat humification. In this paper we use stratigraphic and geochemical data as further proxies. The aim of this study is to assess vegetation, hydrology and atmospheric dust changes in the Lynch's Crater deposits in order to better understand past environmental changes. To do this we will: (a) assess the stratigraphy, ash content (=combustion residue) and chronology of the core; (b) quantify the vertical distribution of Ca, Mg and Al, utilising Al as a conservative element, and (c) compare the geochemical data with past pollen records from Lynch's Crater.

2. MATERIALS AND METHODS

2.1. Site description

Lynch's Crater (17°37'S, 145°70'E; altitude 760 m) is situated on the Atherton Tablelands (Fig. 1). Prior to clearance it was surrounded by complex lowland to lower montane rainforest supported by seasonally distributed annual rainfall of about 2,600 mm (Australian Govt Bureau of Meteorology http://www.bom.gov.au).

Tertiary to Quaternary basalts (clinopyroxene, plagioclase, and olivine) dominate the northern part of the Atherton Basalt Province (Stephenson et al., 1980). These volcanic rocks erupted over a variety of basement rocks of the Devonian to Early Permian, including metamorphosed sediments and granitic rocks (Hodgkinson formation). Up to 22 possible phases of volcanism have been identified that resulted in a complex series of multi-layered basalt units, interspersed with highly weathered soil profiles (Pearce, 2002).

The crater itself was formed by an explosive local volcanic event and subsequently filled with about 65 metres of lake and peat deposits. The slope on the most exposed northern side of the crater is ~45 degrees and in other locations ranges between ~5-20 degrees. The crater is ~350 m in diameter and the 6.6 m core of this study was collected in the central part of the crater. Because of the small catchment area of about 0.6 km^2 the site may be one of the best archives for studying subtle changes in the regional environment. The water table of the peat deposit varies but sits at ~50 cm depth, however during dry months the water table can drop to ~80 cm depth and close to drainage channels the water table can exceed 100 cm depth.

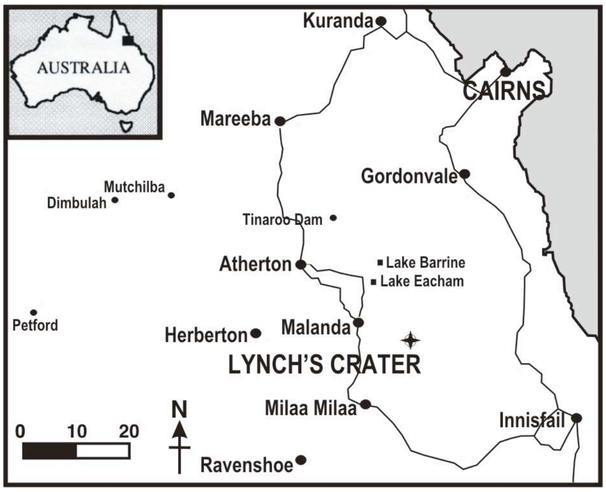

Figure 1: Location of Lynch's Crater in north Queensland, Australia.

2.2. Sample collection, preparation and ash content analysis

A 6.6 m long core (LC1) was collected using a Russian D-section corer (0.1-6.6) in July 2003. The top 10 cm were collected by cutting a monolith with a stainless steel knife and was subsequently divided into 2 cm increments and packed into plastic bags. The stratigraphy of the 50 cm core increments was described in the field, Munsell colour and pH were determined immediately and the sections were then wrapped in aluminium foil. In the laboratory the cores were split into 10 cm increments, placed in plastic bags and freeze-dried. Once dried, samples for geochemistry were cut and milled by hand using a mortar and pestel, then sieved with a 500 μm sieve, milled again and put through a 250 μm sieve, rootlets were subsequently picked under a microscope. All utensils were thoroughly cleaned with ethanol between samples. One gram of dried milled peat was placed in an oven at 550°C overnight and used to determine the ash content. In this study the ash content refers to the weight - % of the residue after combustion compared to the weight of the sample before combustion.

2.3. Radiocarbon dating

Ages were obtained by accelerated mass spectrometry at the Australian Nuclear Sciences and Technology Institute (ANSTO, Lucas Heights, Australia) (Table 1). The dried, milled samples were pre-treated with HCl-NaOH-HCl and washed with milli-Q and then freeze dried for AMS analysis, detailed analytical procedures are outlined in Fink et al. (Fink et al., 2004). The radiocarbon ages (<20,000 yrs) were calibrated using the IntCal04 (CAL 5.0.1; http://radiocarbon.pa.qub.ac.uk/calib/) and the ages >20,000 yrs BP were calibrated using Fairbanks 1204 (Fairbanks et al., 2005).

Sample ID	Lab. ID	Sample type	Depth (cm)	Radiocarbon age (14C yr BP)	Calibrated years (cal yr BP)	σ2 Error	Comments
LC1-27	OZHO71	Peat	27-28	5450	6250	73	
LC1-47	OZHO72	Peat	47-48	6440	7349	92	
LC1-67	OZHO73	Peat	67-68	7250	8071	106	
LC1-117	OZHO74	Peat	117-118	8960	10066	179	
LC1-167	OZHO75	Peat	167-168	7150	7952	107	Inversion
LC1-217	OZHO76	Peat	217-218	10390	12225	190	
LC1-267	OZHO77	Peat	267-268	14900	18215.5	362.5	
LC1-317	OZHO78	Peat	317-318	14280	17069	492	Inversion
LC1-367	OZHO79	Peat	367-368	15400	18747	137	
LC1-417	OZHO80	Peat	417-418	19090	22762	468	
LC1-467	OZHO81	Peat	467-468	21870	*26361	176	Inversion
LC1-517	OZHO82	Peat	517-518	19620	23340	499	
LC1-567	OZHO83	Peat	567-568	24000	*28574	184	
LC1-617	OZHO84	Peat	617-618	22390	*26901	165	Inversion
LC1-657	OZHO85	Peat	657-658	22040	*26537	142	Inversion

* Calibration based on Fairbanks (2005)

Table 1: Conventional radiocarbon age dates (^{14}C yr BP) and calibrated ages (cal yrs BP). CALIB 5.0.1 and Fairbanks 1204 (2005) were used to calibrate radiocarbon data.

2.4. Chemical analysis of peats

Calcium, Mg and Al were analysed by inductively coupled plasma atomic emission spectroscopy (ICP-AES). Approximately 0.15 g of sample was taken up in 2 ml HNO_3, then 0.2 ml of HF and 0.5 ml of H_2O_2 were added. This mixture was left for several hours prior to microwave-assisted digestion. Analytical precision was assessed by repeat analysis of a standard during the sample measurement and the precision was found to be within 3%. Analytical accuracy was determined using certified spruce needles (BCR 101) and certified tealeaf (GBW 07605). Measurements for Ca, Mg and Al were within 8% of the certified values.

Studies have shown that Al is effectively conserved in soil that has undergone chemical weathering (Nesbitt and Marcovics, 1997) and that Al is essentially immobile post-deposition (Norton and Kahl, 1991). As a result, studies have normalised elemental concentrations against Al in order to compensate for natural variations in the amount of dust supplied to a deposit and for bulk density differences within the profile (Shotyk et al., 2002). Here we use Al as a conservative reference element by calculating the ratios: (Ca) sample / (Al) sample and (Mg) sample / (Al) sample.

2.5. Establishing baselines for geochemical records

Geochemical records of peat deposits often use a base line to reference elemental changes and to discriminate anthropogenic impacts (Shotyk et al., 1998; Weiss et al., 2002). Determining geochemical baselines for natural climate change is not as straightforward and selecting a baseline can cause controversy amongst readers. Because Lynch's Crater has not preserved the past 5,000 years, the anthropogenic influx is not as evident as in other studies. In addition, the underlying mineral soil has not been cored, so a mineral soil background or baseline is not available. Also, a "normal" climate signature is hard to define. As a consequence, this study has selected a baseline as the average of the samples that have the lowest ash contents and the most stable accumulation rates, which is the section with a consistent geochemical composition between 0.4 – 1.5 m. The baseline has been determined from the total average of all values between these depths.

2.6. Distinguishing ombrogenic from minerotrophic peats

Ombrotrophic peats receive hydrological enrichment solely from rainwater, whereas minerotrophic peats do so from both rainwater and surface and/or groundwater. One method to determine whether an ombrotrophic zone exists within a peat deposit is to compare the Ca/Mg molar ratio of the peat with local rainwater values (Shotyk, 2002; Steinmann, 1995; Weiss et al., 1997). The notion in this approach is that peats with Ca/Mg ratios comparable to rainwater are ombrotrophic, whereas peats exceeding this value have an additional source of Ca and are therefore minerotrophic. Rainwater values from the region (Atherton and Mareeba, Fig. 1) are plotted against the Ca/Mg peat ratios (Fig. 2). There is no obvious explanation for the difference in the rainwater ratios in Atherton to those of Mareeba, however with Atherton being closer in proximity to Lynch's Crater the Atherton value is used as the primary rainwater value.

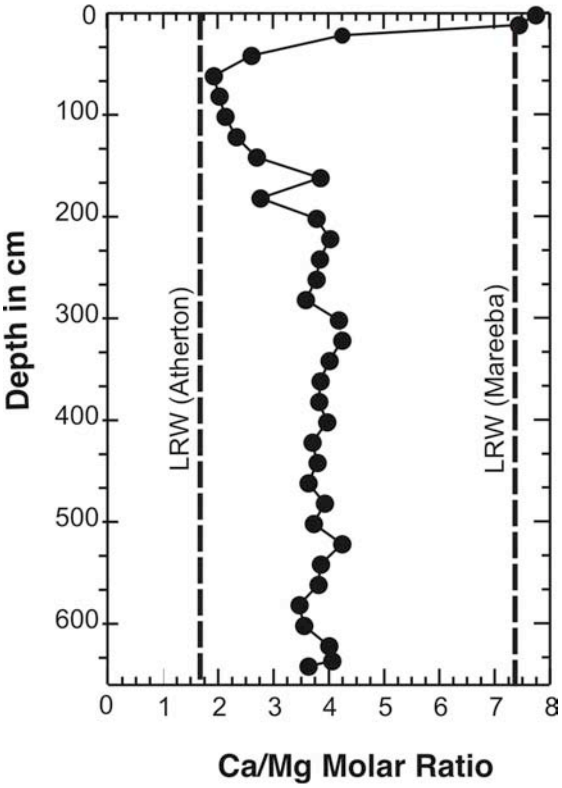

Figure 2: The Ca/Mg molar ratio in peat at Lynch's Crater. The two vertical dotted lines indicate Ca/Mg molar ratio in rainwater from Atherton and Mareeba (Douglas, 1968).

2.7. Determining constituents of high inorganic layers

Several samples had high ash values (>13%) and a polarizing microscope was used in order to identify silicon fragments and their properties. Samples of special interest were characterised using a Scanning Electron Microscope (JEOL JSM-5410LV) allowing high-resolution photography, and by Electron Microprobe (JEOL 840A) allowing qualitative elemental composition of individual constituents.

3. RESULTS

3.1. Stratigraphy and ash content

From 6.6-6.46 m a black sapric peat containing few short fibres is present underlying a dark greyish fine-grained layer (6.46-6.38 m) (A, Fig. 3). The layer contains abundant fragments of sponge spicules, diatom frustules and detrital quartz (Fig. 4). Between 2.6-6.38 m the core consists of mostly black sapric peat and little root fragments. Within this section of the core another layer with elevated ash content (13%) contains diatom and sponge fragments, it occurs between 5.38-5.16 m (C). Changes in peat colour occur between 5.2-5.1 m (brown) and between 6.42-6.1 m (banded dark brown and black) and a section of increased root material can be found between 2.92-2.82 m. Above this peat section, between 2.6-1.8 m (E) significant amounts of sponge spicules and diatoms with quartz grains can be found. A unit of brown hemic peat at 1.84-1.6 m is overlain by black sapric peat (0.16-1. m) with abundant long (up to 30 cm) root material (Fig. 3). The top 10 cm of the core is a dark brown organic-rich peat.

The most prominent difference between the sections showing lake influence (Sections A, C and E, Fig. 3) is the abundance of the sponge spicules and the abundance and properties of the quartz grains. In section C, sponge spicules and quartz grains are sparse and the quartz grains are significantly smaller than in section A. In section E sponge spicules and quartz grains are more abundant than section C but less abundant than section A. The quartz grains are smaller, perhaps indicating the activity of the catchment.

The ash content ranges between 4-11% from the base of the deposit to 2.6 m depth with the exception of elevated values at 6.46 (55%) and 5.2 (13%) m depth.

The ash content ranges between 10-33% from 2.6-1.8 m with an excursion at 1.9 m (33%). Between 1.8-0.01 m the ash content is low (2-5%) but increases in the top 10 cm of the core to ~30%.

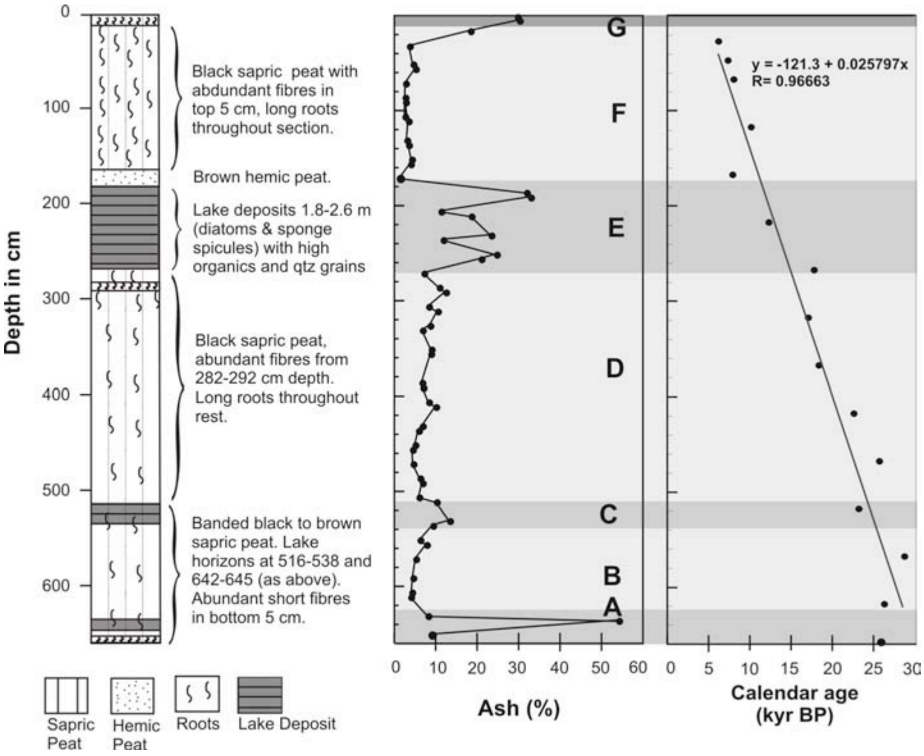

Figure 3: Stratigraphy, ash content (in wt-%), and age model of core LC1.

3.2. Radiocarbon dates

The age model of the profile is constructed from 15 calibrated AMS dates (Table 1). Within the entire profile five age dates are inverted. At present we cannot fully account for these five significantly younger ages, however two of the inversions (LC1-317 and LC1-617) have ages very close to the samples below them, suggesting that they belong to the same period. Interestingly the inversions commonly occur near boundary layers where the ash changes markedly, such as between sections G-F, E-D and C-B. The age model (Fig. 3) uses a linear regression curve for the accumulation rate even though rates of accumulation may not have been steady during the evolution of the peat deposit (see for eg. layers A, C and E, Fig. 3). It is also possible that younger root material in older layers is the cause of inversions.

Previous work (Turney et al., 2004) on an 11 m core from Lynch's Crater, taken very nearby to LC1, shows a similar age model with a linear regression. This age model yields a calendar age of ~30 kyr at 7 m, very similar to the age-depth relationship of the LC1 model.

3.3. Calcium, Mg, and Al concentrations

The Ca and Mg profiles show similar trends (Fig. 4A) from the base of the core to 2.6 m depth and more fluctuations are observed in the upper section (2.6-0 m). A steady upward decrease in Ca and Mg concentrations occurs between 2.6-1.6 m. Between 1.6-0.2 m concentrations are low (Ca = 3,000 and Mg = 2,500 ppm) with no significant enrichment or depletion in reference to the baseline. A decrease in Mg (1,500 ppm) and an increase in Ca (5,000 ppm) can be observed in the top 0.2 m, probably due to biocycling at the top of the core.

In the lower part of the core, between 6.6-2.6 m depth, Al concentration are comparable to the baseline value (2,273 ppm) with one significant enrichment at ~6.4 m (~5,250 ppm). Between 2.6-1.7 m, Al is significantly enriched (up to 5,300 ppm) in comparison to the baseline and above this section Al concentrations generally follows the same trend along the baseline as Ca and Mg do in the upper 1.7 m. It is important to note that the concentration profiles of Ca and Mg show a completely different trend to that of Al in the top 4.1 m.

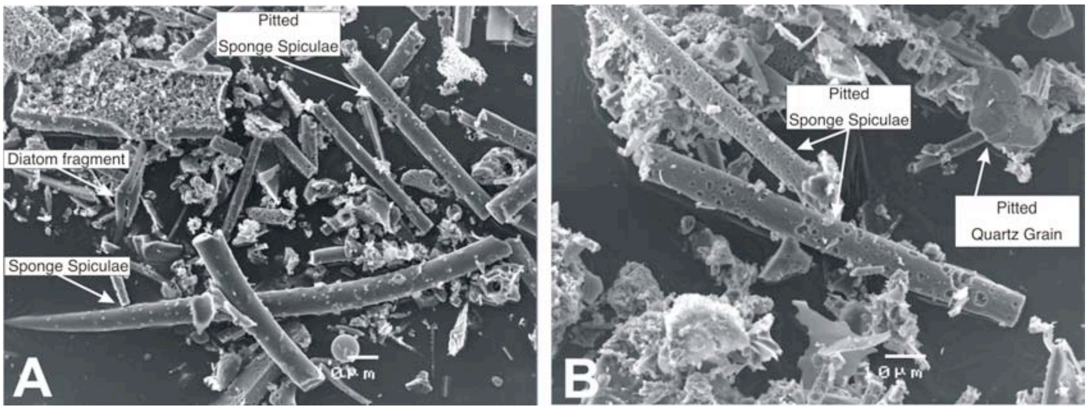

Figure 4: SEM images of layer 6.4-6.41 m showing diatom fragments, sponge spicules and quartz grains. Most constituents show strong corrosive features, probably due to an acidic environment.

3.4. Al normalised profiles

Normalisation of Ca and Mg to Al was carried out in order to compensate for the bulk density differences within the peat (Fig. 4B). The normalised profiles have similar trends to the concentration profiles. For the entire profile the ratios are higher than that of the Upper Continental Crust (UCC) where Ca/Al = 0.4 and Mg/Al = 0.2 (Wedepohl, 1995), however, from the base to 2.6 m the ratios are higher than UCC where ratios from 2.6 m to the top of the core are closer to UCC.

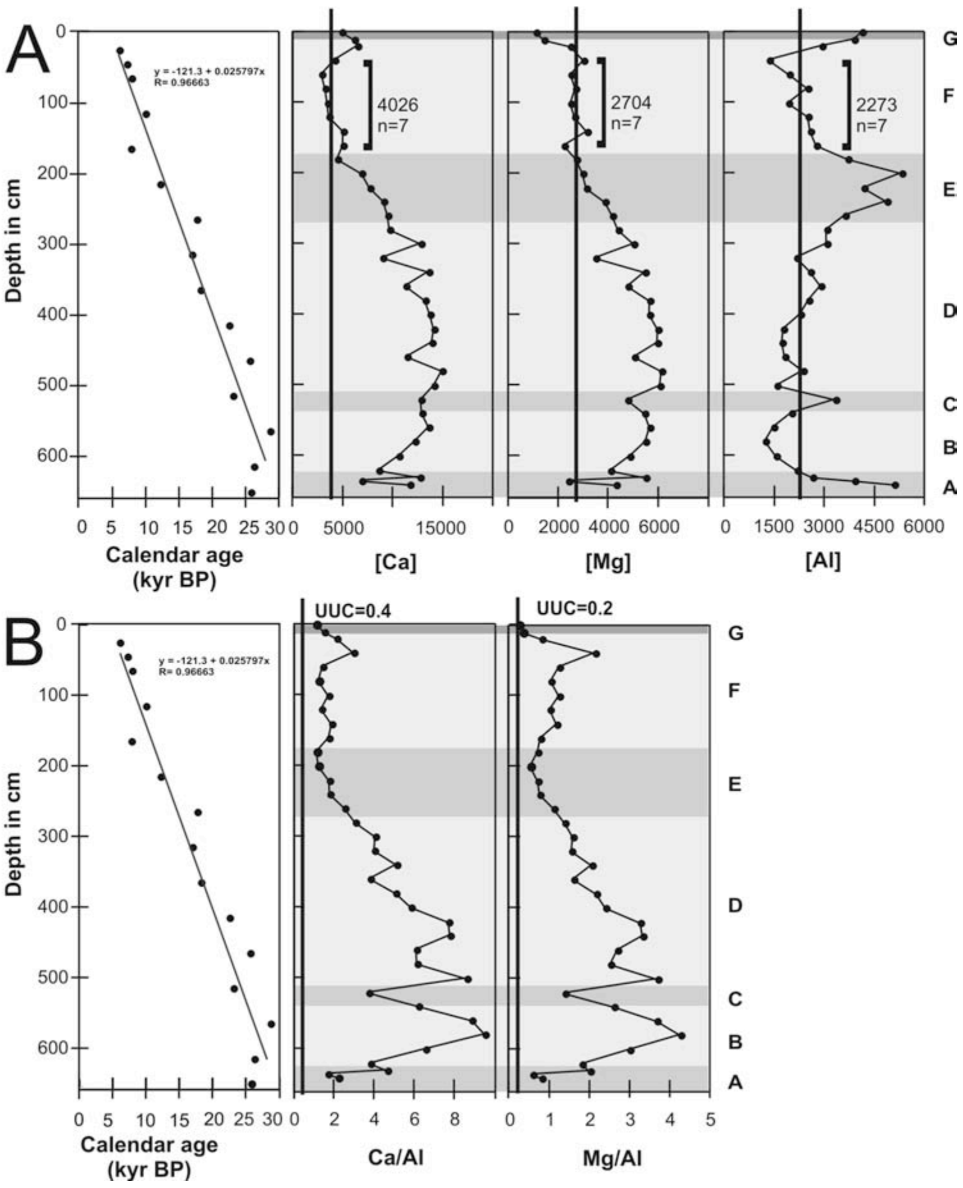

Figure 5: A) Concentration profile of Ca and Mg and Al (ppm). Baseline concentrations from between 42 and 163 cm are also given. B) Calcium and Mg normalised against Al.

4. DISCUSSION

The peat record of Lynch's Crater presents many interesting changes in stratigraphy and geochemistry. Here we use these proxies to interpret the nature of the peat deposit and its vegetation, hydrological and atmospheric dust changes.

4.1. The nature of the peat mire

The peat deposits in Lynch's Crater exhibit aspects of minerotrophic and ombrotrophic conditions, as demonstrated by comparing the Ca/Mg molar ratio of the peat with local rainwater values (Fig. 2). Another method to distinguish between an ombrotrophic and minerotrophic setting is to use the major cation Ca, because it is a limited input in ombrotrophic peats (Verhoeven, 1986). The Ca concentration of the peat in Lynch's Crater supports this differentiation. Both Ca and Mg concentrations in Lynch's Crater are higher in the lower deposits (~6.6-1.5 m) and decrease in the top 1.5 m of the deposit. The Ca/Mg with ash data (Fig. 3 and 5) suggest that prior to the early Holocene (6.6-1.5 m) peat conditions were minerotrophic, while during the early Holocene (top 1.5 m) the conditions were ombrotrophic. As a consequence, all geochemical changes in the deposit of the early Holocene reflect either changes in atmospheric dust influx or are associated with plant-induced bio-cycling of elements. On the other hand, Al shows similar concentrations within the ombrotrophic and minerotrophic sections because it is immobile after deposition and is not subject to diagenetic changes in the minerotrophic deposits. In this study the Al concentrations approach the value of the baseline after each high ash unit (indicating flooding episodes of the swamp) and therefore it is suggested that Al is essentially a safe atmospheric dust indicator within the minerotrophic and ombrotrophic peat sections of Lynch's Crater (Fig. 5).

The minerotrophic sections of the core can be divided into periods with high ash contents, when significant flooding with the possible development of shallow ponds or lake systems occurred. Flooding of the peat environment and development of high biogenic silica deposits are marked by layers with elevated "ash" contents and occur in: layer A at 6.38-6.46 m (55%), layer C at 5.16-5.38 m (13%) and layer E at 1.8-2.6 m (33%) (Fig. 3). SEM and light microscope analyses demonstrate that the inorganic fraction of these layers is composed of freshwater sponges with subordinate diatoms (Fig. 4). These layers also contain large sub-angular quartz grains (20-100 μm) that are often pitted (Fig. 4). The pitting may be the result of post-depositional corrosion within the slightly acidic peat environment as demonstrated from peat deposits of Malaysia (Wüst and Bustin, 2001).

It is possible that the top section was much thicker at some stage during the late Holocene and that changes in precipitation or hydrology at the site have resulted in a positive net oxidation of the peat. The very low accumulation rate (0.05 cm/yr) and the high ash content in the top 10 cm of the core support this theory (Fig. 3). Water drainage channels were completed at Lynch's Crater in the 1960s, and peat degradation started or increased, but it is unlikely that 170 cm of peat (assuming a constant peat accumulation rate of 0.28 mm/yr) further down the core could oxidise in such a short time. The high ash content in the topsoil is most likely due to: 1) higher influx of dust; 2) enhanced decomposition of organic matter and enrichment of inorganic material since the mid-Holocene (Fig. 3); and/or 3) a combination of 1 and 2. These changes could be the result of a climate shift.

4.2. Vegetation dynamics

The plant essential elements Ca and Mg reflect two different geochemical environments. Below 2.6 m, the Ca and Mg show a similar trend as Al, whereas above 2.6 m the signature is completely different. The effects of a change from minerotrophic to ombrotrophic conditions have been addressed above, but don't take into account the possible vegetation effects. Palynological work of (Kershaw et al., 1993) determined dominant sclerophyll taxa indicative of a woodland forest between 10,000-26,000 yrs BP followed by the introduction of rainforest cover, which emerged from retreats in response to a sharp increase in rainfall at the beginning of the Holocene ~10,000 yrs BP (Kershaw, 1978; Moss and Kershaw, 2000). An increased precipitation would imply more extensive vegetation cover that existed during the Holocene on Lynch's Crater. The peat stratigraphy also shows abundant long root fragments that penetrated the top layer during the Holocene and it is possible that the vegetation on Lynch's Crater during the Holocene has had some effect on changing the pre-Holocene Ca and Mg signature and left the peat depleted in these elements.

Studies of tropical peat deposits from Indonesia and Malaysia have shown that during the fast biomass turnover plant nutrients show high mobility within the root zone and that the plant essential elements are readily recycled in order to reduce any loss by the leaching process (Page et al., 1999; Wüst and Bustin, 2003). This process highlights the importance of identifying zones with significant recycling of plant essential elements. For accurate environmental interpretation of such sections, the geochemical focus should be on the immobile elements, such as Al.

The top soil in Lynch's Crater is depleted in Ca and Mg, unlike other tropical peat deposits where Ca and Mg are enriched in the root zone (Weiss et al., 2002; Wüst and Bustin, 2003). This may imply that the nutrient recycling processes in the peat deposits of Lynch's Crater are different to such processes in Indonesia and Malaysia, which may simply be the result of the change in vegetation, since the drainage of the site was constructed in the 1970's.

4.3. Atmospheric dust

This initial study illustrated that the post depositional affects may overprint the original signature of atmospheric dust. The ombrotrophy of the upper 1.5 m of Lynch's Crater should show the signature of dust, however little change in the lithogenic element Al can be seen in this section (Section F, Fig. 5). Within the high ash layers (Sections A, C and E, Fig. 3) it is difficult to utilise elemental data to identify atmospheric flux because a great degree of the components have been transported into the deposit via terrigenous pathways overprinting the atmospheric dust signature (Sections A, C and E, Fig. 3). In order to understand more about the atmospheric input into Lynch's Crater more lithogenic elements are needed.

5. CONCLUSIONS

This paper describes the stratigraphy, ash content, chronology and Ca, Mg and Al geochemistry of a peat core from Lynch's Crater in tropical, North Queensland, Australia and its relation to environmental changes over the past 30,000 yrs BP. The primary conclusions of this study are:

1) An increase in Ca and Mg concentration can be used to identify the boundary where a minerotrophic peat turns into an ombrotrophic peat. It shows that within the top 1.5 m of Lynch's Crater atmospheric dust is the sole source of inorganic constituents in the ombrotrophic deposits, while in the minerotrophic deposits additional sources of Ca and Mg are present.
2) In tropical peat deposits Ca and Mg can undergo remobilisation via nutrient recycling, particularly, within the root zone. Here, the

vegetation cover may have had a significant effect on this remobilisation during the Holocene.

3) The Al concentration remains consistent throughout the minerotrophic and ombrotrophic sections indicating its sole source as atmospheric and its immobility post-deposition. Aluminium can therefore be used as an indicator of atmospheric dust in the peat deposits of Lynchs Crater.
4) The ash and elemental data suggest a wetter climate during the early Holocene that in turn allowed net accumulation of peat. Some time after the mid-Holocene, climate changes influenced peat accumulation and a positive degradation of organic matter occurred.
5) Evidence of persistent flooding of the peat deposits of Lynch's Crater signals periods of change in precipitation in North Queensland. The deposits of these flood periods have significant changes in the composition of the sediments (organic material with various amounts of diatoms, sponges and quartz grains) indicating that these climatic changes differed from each other markedly.

ACKNOWLEDGMENTS

The research was supported by grants from the Australian Research Council (DP0451565) and the Australian Nuclear Sciences and Technology Organisation (AINSTU0803). We would like to acknowledge K. Blake, G. Warria and S. Ness at the Advanced Analytical Centre, James Cook University, and H. Van Der Gaast and G. Jacobson at the ANSTO for laboratory assistance and helpful discussion. J.M thanks especially D. Mather and B. Thompson at AINSE for making travel and laboratory work possible and to K. Perry for review. Special thanks go to A. Martinez-Cortizas and two anonymous reviewers for review and constructive comments.

REFERENCES

Australian Government, B.o.M., 2006. Annual rainfall for Atherton Tablelands.

Douglas, I., 1968. The effects of precipitation chemistry and catchment area lithology on the quality of river water in selected catchments in eastern australia. Earth Science Journal, 2(2): 126-144.

Dunlap, C.E., Steinnes, E. and Flegal, A.R., 1999. A synthesis of lead isotopes in two millennia of European air. Earth and Planetary Science Letters, 167: 81-88.

Fairbanks, R.G., Mortlocka, R.A., Chiua, T., Caoa, L., Kaplana, A., Guildersonc, T., Fairbankse, T., Bloomf, A., Grootesg, P. and Nadeaug, M.J., 2005. Radiocarbon calibration curve spanning 0 to 50,000 years BP based on paired 230Th/ 234U/ 238U and 14C dates on pristine corals. Quaternary Science Reviews, 24: 1781-1796.

Fink, D., Hotchkis, M., Hua, Q., Jacobsen, G., Smith, A.M., Zoppi, U., Child, D., Mifsud, C., Van der Gaast, H., Williams, A. and Williams, M.A.J., 2004. The ANTARES AMS facility at ANSTO. Nuclear instruments and methods in physics research section B: Beam interactions with materials and atoms, 223-224: 109-115.

Kershaw, A.P., 1978. Record of last interglacial-glacial cycle from northeastern Queensland. Nature, 272: 159-161.

Kershaw, A.P., 1986. Climatic change and Aboriginal burning in north-east Australia during the last two glacial/interglacial cycles. Nature, 322: 47-49.

Kershaw, A.P., McKenzie, G.M. and McMinn, A., 1993. A Quaternary vegetation history of northeastern Queensland from pollen analysis of ODP Site 820. In: J.A. McKenzie et al. (Editors), Proceedings of the Ocean Drilling Program, Scientific Results, 133: 107-114. Texas A & M University, Ocean Drilling Program, College Station, TX, United States.

Klaminder, J., Renberg, I., Bindler, R. and Emteryd, O., 2003. Isotopic trends and background fluxes of atmospheric lead in northern Europe: Analyses of three ombrotrophic bogs from south Sweden. Global Biogeochemical Cycles, 17: 1019

Martínez-Cortizas, A., Pontevedra-Pombal, X., Nóvoa-Muñoz, J.C. and García-Rodeja, E., 1997. Four thousand years of atmospheric Pb, Cd, and Zn deposition recorded by the ombrotrophic peat bog of Penido Vello (Northwestern Spain). Water, Air and Soil Pollution, 100: 387-403.

Moss, P.T. and Kershaw, A.P., 2000. The last glacial cycle from the humid tropics of northeastern Australia: comparison of a terrestrial and a marine record. Palaeogeography, Palaeoclimatology, Palaeoecology, 155: 155-176.

Nesbitt, H.W. and Marcovics, G., 1997. Weathering of granodioritic crust, long-term storage of elements in weathering profiles, and petrogenesis of siliclastic sediments. Geochimica et Cosmochimica Acta, 61(8): 1653-1670.

Norton, S.A. and Kahl, J.S., 1991. Progress in understanding the chemical stratigraphy of metals in lake sediments in relation to acidic precipitation. Hydrobiologia, 214: 77-84.

Page, S.E., Rieley, J.O., Shotyk, W. and Weiss, D., 1999. Interdependence of peat and vegetation in a tropical peat swamp forest. Phil. Trans. R. Soc. Lond. B, 354: 1885-1897.

Pearce, B., 2002. Report on compilation of a geological conceptual model for the Atherton Tableland basalts, Queensland Department of Natural Resources and Mines, Brisbane.

Shotyk, W., 2002. The chronology of anthropogenic, atmospheric Pb deposition recorded by peat cores in three minerogenic peat deposits from Switzerland. The Science of the Total Environment, 292: 19-31.

Shotyk, W., Krachler, M., Martinez-Cortizas, A., Cheburkin, A.K. and Emons, H., 2002. A peat bog record of natural, pre-anthropogenic enrichments of trace elements in atmospheric aerosols since 12 370 14C yr BP, and their variation with Holocene climate change. Earth and Planetary Science Letters, 199: 21-37.

Shotyk, W., Weiss, D., Appleby, P.G., Cheburkin, A.K., Frei, R., Gloor, M., Kramers, J.D., Reese, S. and Van Der Knaap, W.O., 1998. History of Atmospheric Lead Deposition Since 12,370 ^{14}C yr BP from a Peat Bog, Jura Mountains, Switzerland. Science, 281: 1635-1640.

Steinmann, P., 1995. Geochemistry of atmospheric inputs and pore water genesis in two contrasting Sphagnum bog preofiles, Jura Mountains, Switzerland. PhD Thesis, University of Berne, Switzerland.

Stephenson, P.J., Griffin and Sutherland, 1980. Cainozoic volcanism in north-eastern Australia. Geological Society of Australia, Brisbane, 349–374 pp.

Turney, C.S.M., Kershaw, A.P., Clemens, S.C., Branch, N., Moss, P.T. and Fifield, L.K., 2004. Millennial and orbital variations of El Niño/Southern Oscillation and high-latitude climate in the last glacial period. Nature, 428: 306-310.

Velichko, A.A., Andreev, A.A. and Klimanov, V.A., 1997. Climate and vegetation dynamics in the tundra and forest zone during the Late Glacial and Holocene. Quaternary International, 41/42: 71-96.

Verhoeven, J.T.A., 1986. Nutrient dynamics in minerotrophic peat mires. Aquatic Botany, 25: 117-137.

Wedepohl, K.H., 1995. The composition of the continental crust. Geochimica et Cosmochimica Acta, 59(7): 1217-1232.

Weiss, D., Shotyk, W., Cheburkin, A.K., Gloor, M. and Reese, S., 1997. Atmospheric lead and dust deposition from 12,400 to 2,100 yrs BP in a peat bog profile, Jura Mountains, Switzerland. Water, Air and Soil Pollution, 100: 311-324.

Weiss, D., Shotyk, W., Rieley, J.O., Page, S.E., Gloor, M., Reese, S. and Cortizas-Martinez, A., 2002. The geochemistry of major and selected trace elements in a forested peat bog, Kalimantan, SE Asia, and its implications for past atmospheric dust deposition. Geochimica et Cosmochimica Acta, 66(13): 2307-2323.

Wüst, R.A.J. and Bustin, R.M., 2001. Low ash peat deposits from a dendritic, intermontane basin in the tropics: A new model for good quality coals. International Journal of Coal Geology, 46(3-4): 179-206.

Wüst, R.A.J. and Bustin, R.M., 2003. Opaline and Al–Si phytoliths from a tropical mire system of west Malaysia: abundance, habit, elemental composition, preservation and significance. Chemical Geology, 200(3-4): 267-292.

CHAPTER 3

Processes affecting trace and major elemental distribution in a 55 kyr peat deposit in tropical Australia: implications to paleoclimate

Adapted from a paper submitted to:

Geochimica et Cosmichimica Acta (2006)

ABSTRACT

The Lynch's Crater peat deposits in NE Queensland, Australia, are a sensitive geochemical archive of past environmental change in the tropical Southern Hemisphere. The deposit reveals that ecosystem changes link directly to changes of climate over the last 55 kyr. This study investigated trace and major element geochemistry of a 13 m peat core from Lynch's Crater, where the ombrotrophic-minerotrophic boundary occurred at ~1.5 m depth. Several periods of significant influx from atmospheric and/or terrigenous run-off from the crater catchment were identified based on ash yield and trace element concentrations. Principle component analysis (PCA) was used to assess the geochemical behavior of selected major and trace elements and to identify potential synergies between elements. Elements, such as Sc, Al, Cu, and Pb were used to evaluate periods of increased soil erosion. Arsenic and V demonstrate that a long-range atmospheric dust source is present in the deeper parts of the peat deposit, where the local source rocks were found to contain very low concentrations of these elements. Chlorine was used to identify changes in precipitation, which was found to have varied significantly in the region during the last 55 kyr and is likely to be linked to monsoon activity in NE-Australia. This geochemical archive presents a unique, continuous record of environmental change in Australia and the Southern Hemisphere.

1. INTRODUCTION

Geochemical archives have long been used to successfully reconstruct climate change in the past. Through the use of geochemical tools, it has been possible to establish atmospheric dust records from ice cores (Delmonte et al., 2002) and marine cores (Hesse and McTainsh, 2003), productivity records from marine cores (Caldeira and Wickett, 2003) and ocean circulation records from marine cores (McManus et al., 2004). Peat records are another important media on which geochemistry can be used to observe previous climate change, they are widely distributed across the globe and offer a unique opportunity to study past atmospheric dust regimes (Weiss et al., 2004), precipitation changes (Page et al., 2003) and weathering dynamics (Shotyk, 1988).

Early studies show peat deposits to be repositories of a variety of major and trace elements (Mattson et al., 1944; Shotyk, 1988), in more recent years there has been considerable interest in using geochemical peat records in paleoclimate reconstruction (Gorham and Janssens, 2005; Mauquoy et al., 2002; Wüst and Bustin, 2003). Such reconstructions have concentrated on boreal and humid temperate peats (Martínez-Cortizas et al., 1999; Shotyk et al., 1990; Weiss et al., 2002), leaving the dynamics and evolution of tropical peatlands poorly understood (Anshari et al., 2001; Page et al., 1999; Wüst and Bustin, 2004). Most tropical peat mires occur under tropical rain forest and these differ markedly in composition and texture to those of humid temperate peat deposits (Wüst et al., 2003; Yonebayashi et al., 1992).

The two main types of peat deposits need to be distinguished when undertaking a geochemical reconstruction, they are rainwater-fed (ombrotrophic) deposits that receive input of inorganic material solely from the atmosphere and the mixed rainwater and groundwater-fed (minerotrophic) deposits that receive additional inorganic input via runoff or through groundwater movement. The two deposit types generally have markedly different chemical conditions, for example, ombrotrophic sites often have a pH of 3-4 where a minerotrophic peat will have a pH of 4.5-7, in addition the mobility of elements such as, Fe or Mn, can depend strongly on these chemical conditions (Weiss et al., 2002)

Lynch's Crater is a volcanic crater on the Atherton Tablelands in NE-Queensland, Australia, that contains a 65 m thick lake sediment and peat sequence. The record is ideal for addressing current debates on the extent, nature and cause of climate change in the tropical Southern Hemisphere (SH) and the role tropical regions play for global climate change (Kershaw, 1974; Turney et al., 2004). This study presents trace, major and isotope geochemistry of the top 13 m of peat material from the Lynch's Crater deposit and attempts to decipher paleo-environmental components such as, weathering, atmospheric dust, vegetation, precipitation regimes, and trophic status. This complexity of variables usually results in a wealth of data from the peat deposits and it is often problematic to disentangle the information. Hence, in this study, we also applied a principle component analysis (PCA) of the geochemical data to simplify interpretations. This application allows the differentiation of groups of geochemical variables with similar behaviour, thereby reducing results to sets of variables. Within the deposit groups of elements are described both individually and collectively and post-depositional processes are taken into account in order to assess biologic, terrigenous and atmospheric changes. The 13 m long core record represents a ~55 kyr old peat deposit. The objectives of this study are to assess: (a) the stratigraphy of the core and to characterise the type of peat deposit; (b) the major and trace elemental dynamics of the deposit; (c) possible atmospheric dust contribution; and (d) environmental changes deduced from the stratigraphic and geochemical analyses.

2. MATERIALS AND METHODS

2.1. Site Description

Lynch’s Crater (17°37’S, 145°70’E; altitude 760 m) is situated on the Atherton Tablelands in NE-Australia (Fig. 1). Prior to forest clearance in the late 19th and early 20th century it was surrounded by complex lowland to lower montane rainforest supported by seasonally distributed annual rainfall of about 4400 mm (www.bom.gov.au). The crater was formed by an explosive volcanic event ~200,000 years ago and subsequently filled with about 65 m of lake and peat deposits.

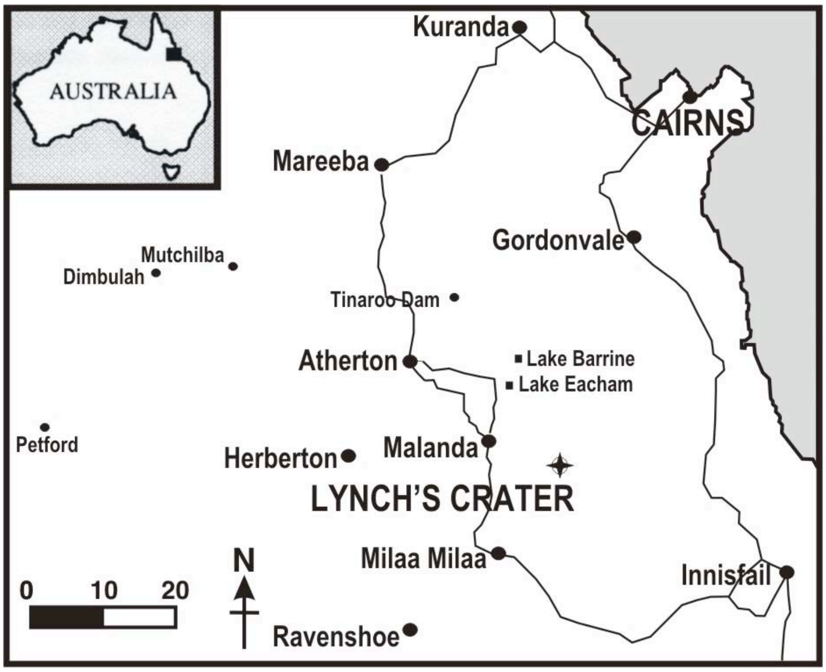

Figure 1: Location of Lynch’s Crater in NE-Australia.

Local rock consists primarily of basalts with clinopyroxene, plagioclase and olivine of the northern part of the Atherton Basalt Province (Stephenson et al., 1980), that have been active over the last 4 Ma. Several flows and eruptions penetrated the overlying Devonian to Early Permian basement deposits that include, metamorphosed sediments and the granitic rocks of the Hodgkinson Formation. Up to 22 possible phases of volcanism have been identified in this complex series of multi-layered basalt units interspersed with highly weathered soil profiles (Pearce, 2002).

2.2. Radiocarbon Dating

Radiocarbon ages were obtained from bulk peat samples by accelerated mass spectrometry (AMS) at the Australian Nuclear Sciences and Technology Organisation (ANSTO, Lucas Heights, Australia) (Table 1). Peat material was dried and sieved with a 500 and then 250 μm sieve and remaining root material was picked out under a microscope. Samples were subsequently milled with a mortar and pestle and milled samples were pre-treated with HCl-NaOH-HCl, washed with milli-Q water and then freeze dried for AMS analysis; detailed analytical procedures are outlined in Fink et al., (2004). The ^{14}C data were calibrated using both IntCal04 (http://radiocarbon.pa.qub.ac.uk/calib/) and Cariaco Basin datasets (Blockley et al., 2004). Bayesian analysis of the data defined the robust chronology.

Previous work (Turney et al., 2004) on an 1100 cm core from Lynch's Crater, taken very nearby to LC2, shows an age model that yields a calendar age of ~30 kyr at 700 cm, this age model has a very similar age-depth relationship to the LC1 model (Chapter 2). We believe that the LC2 age model is more accurate than both the Turney et al., 2004 and LC1 models. This is especially significant in the bottom layers, where the Turney et al., 2004 model is constrained by only 4 radiocarbon dates between 600-1100 cm and the LC1 model contains 2 radiocarbon dates between 550-700 cm, both of which are inverted.

Table 1: Radiocarbon ages with calibrated years (cal yrs BP). All radiocarbon ages 20,000 yrs BP or older were calibrated using the calibration of Bard et al. (1998) and ages younger than this have been calibrated using IntCal04.

Core	**Sample**	**Sample**	**Lab**	**C14**	**Cal**	**±**	**Calibration**	**Standard**
	Depth (cm)	**ID.**	**No.**	**Age**	**yrs BP**		**Method**	**Deviation**
LC2	4.5	LC2-4	OZI460	1595	1465	98	SHCal04	48.75
LC2	9.5	LC2-9	OZH600	2670	2757	34	SHCal04	17.00
LC1	27.5	LC1-27	OZH071	5450	6235	53	SHCal04	26.50
LC1	47.5	LC1-47	OZH072	6440	7345	95	SHCal04	47.25
LC1	67.5	LC1-67	OZH073	7250	8055	119	SHCal04	59.25
LC2	104.5	LC2-104	OZH601	7630	8397	52	SHCal04	25.75
LC1	117.5	LC1-117	OZH074	8960	9875	229	SHCal04	114.25
LC2	120.5	LC2-120	OZI461	9110	10005	375	SHCal04	187.50
LC2	164.5	LC2-164	OZI164	10340	12160	220	IntCal04	109.75
LC2	182.5	LC2-182	OZI463	11220	13070	88	IntCal04	44.00
LC2	248.5	LC2-248	OZI464	13180	15480	240	IntCal04	119.75
LC2	387.5	LC2-387	OZI465	20340	24225	206	IntCal04	102.75
LC2	484.5	LC2-484	OZH603	24370	29150	200	Bayesian	100.00
LC2	560.5	LC2-560	OZH604	27480	31885	330	Bayesian	165.00
LC2	720.5	LC2-720	OZI471	30740	34750	280	Bayesian	140.00
LC2	810.5	LC2-810	OZH591	32310	36450	520	Bayesian	260.00
LC2	860.5	LC2-860	OZH592	34310	39400	460	Bayesian	230.00
LC2	935.5	LC2-935	OZH593	36510	41425	700	Bayesian	350.00
LC2	987.5	LC2-987	OZH594	38320	42625	820	Bayesian	410.00
LC2	1040.5	LC2-1040	OZH596	40429	43350	930	Bayesian	465.00
LC2	1154.5	LC2-1154	OZH597	41330	43775	1100	Bayesian	550.00

2.3. Sample Collection and Preparation, pH, and Loss on Ignition Analysis

A 13 m long core (LC2) was collected using a D-section Russian corer from the centre of Lynch’s Crater in July 2003. From 0-10 cm a monolith was cut from a hummock using a stainless steel knife and divided into 2 cm increments then packed in plastic bags. The core was described in the field and the sections wrapped in aluminium foil. In the laboratory samples at 10 cm increments were placed in plastic bags and freeze-dried. Once dried, samples for geochemistry were cut and milled by hand using a mortar and pestle, then passed through a 500 μm sieve, milled again and put through a 250 μm sieve; rootlets were removed with the aid of a microscope. All utensils were thoroughly cleaned with ethanol between samples. Two soil cores from the crater wall and rocks from the crater and surrounds were collected in November 2004. A sample from the base of the sediments in the crater at a depth of 62.75 m was also analysed. After drying, both rock and soil samples were ground to < 20 μm for sample analysis.

Peat samples were placed in preheated acid-washed porcelain crucibles and re-dried at 105°C for 4 hrs to determine moisture content, after cooling in a desiccator, dry weight was determined. Loss on ignition (LOI) was established by heating sample material at 450°C overnight and cooling in a desiccator for 15 min. The weight loss was used to calculate the ash yield or inorganic content (=100% - LOI), expressed as dry weight.

2.4. Determining Constituents of High Inorganic Layers

Inorganic constituents were identified in samples with high ash yield (>13%) using a polarizing microscope. Selected samples were also characterised using a Scanning Electron Microscope (SEM) (JEOL JSM-5410LV) and an Electron Microprobe (JEOL 840A). These analyses were used to obtain qualitative elemental composition of individual constituents.

2.5. Chemical Analysis of Peats

One hundred and thirty samples were prepared for trace and major element analyses at the Imperial College, London. Digestion of the material was obtained by the following: 0.5 g of peat was placed in poly-tetra-fluoro-ethylene (PTFE) test tubes and 8 ml HNO_3 added and heated to 50°C overnight, then 5 ml HF and 1-2 ml $HClO_4$ was added and heated to 90°C for 3 hours, followed by 3 hours at 140°C and finally overnight at 170°C. Total dryness was achieved by the end of this heating program. After cooling 2 ml 5M HCl was added and samples were leached for an hour at 60°C. The material was cooled and 8 ml of H_2O was added, the solutions were mixed using a vortex mixer and decanted into new test tubes and diluted with 2% HNO_3 for analysis by inductively coupled plasma mass spectroscopy (ICP-MS).

The rock and soil samples were prepared in PTFE test tubes, to which 0.1 g material was added and digested with a sequence of 2.0 ml HNO_3, then 1.0 ml $HClO_4$ and 5.0 ml HF. Samples spent 3 hours at 90°C, 3 hours at 140°C and 10 hours at 190°C. Tubes were removed from the heating block and cooled. Then, 2.0 ml of 4M HCl was added and the tubes replaced in the heating block for an hour at 70°C. After cooling 8 ml 0.3M HCl was added. Solutions were mixed using a vortex mixer and decanted into new test tubes. Solutions were then diluted with 2% HNO_3 for analysis by ICP-MS.

Trace element concentrations (Pb and Sc) were determined using a Varian ICP-MS at the Natural History Museum, London. Detection limits were <3 ppt and blank levels for trace elements were 100 ppt or lower. Additional elements (Ti, Al, Sr, Fe, Ca, Mg, Mn, Cu, V and As) were determined using a Varian Vista Pro ICP-OES at the Imperial College London. Solutions were later diluted for ICP-MS and

ICP-OES and detection limits were <0.01 µg/g and <0.05 µg/g for trace and major elements, respectively, in solution. Blank levels were <2 µg/g for As, Cu, Ti, V; <50 µg/g for Ca and Mg, and <30 µg/g for Al, Fe and Mn. Chlorine was measured by X-ray fluorescence under vacuum and standard reference materials NIST-1515, NIST-1547 and NIST-1632 were used to calibrate the equipment and detection limit was <10 µg/g.

2.6. Baselines, Enrichment Factors

Geochemical records of peat deposits often use a baseline against which to reference elemental changes and to discriminate anthropogenic impacts (Weiss et al., 2004). This study has selected a baseline as the average of the samples that have low ash yield, stable accumulation rates and a consistent geochemical composition between 920-1300 cm depth. The baseline has been determined from the total average of all values between these depths.

Enrichment factors relative to local rock (EF_{LR}) were calculated in order to observe possible post-depositional remobilisation of elements. The enrichment factor is given as: $EF_{LR} = (X/Sc)_{sample}/(X/Sc)_{LR}$ for local rock where X represents the selected element.

2.7. Principle Component Analysis

Principle component analysis (PCA) is often used in geochemical studies of peatlands and is a useful technique for highlighting statistical associations of elements (Kalahne et al., 2000; Worralla, 2005). PCA was carried out using ash yield and the concentrations of the analysed elements as variables using the statistical package for the social sciences (SPSS). Factor analysis, which reduces the number of observed variables to fewer variables (factors), was also done in order to obtain insights into the variability among variables. The observed variables are modeled as linear combinations of the factors and this statistical approach identifies the most important (i.e. defining) parts or elements whilst simultaneously filtering “noise” within the dataset. Each element has a loading that shows the contribution of that element to a particular depth in the deposit, negative loadings reflect low contributions, while positive loadings reflect high contributions of that element.

3. RESULTS

3.1. Trophic Status: Minerotrophic vs. Ombrotrophic

Conventionally, ombrotrophic peat deposits have an inorganic content of <5% and minerotrophic deposits have an inorganic content of >5% (Tolonen, 1984), pH values in ombrotrophic peats are generally more acidic (3-4) than those of minerotrophic peats (4-7) (Fig. 2). Here we also estimate the amount of Sr deposited on the peat surface by atmospheric soil dust as: [Sr] *atmospheric* = [Sc] *sample* × (Sr/Sc) *Earth’s crust*, where Sr/Sc in the Earth’s crust is (333 mg/kg)/(16 mg/kg) (Wedepohl, 1995). Using the equation: [Sr] *diagenetic* = [Sr] *total* – [Sr] *atmospheric* we can estimate the excess diagenetic Sr representative for each sample (Fig. 2).

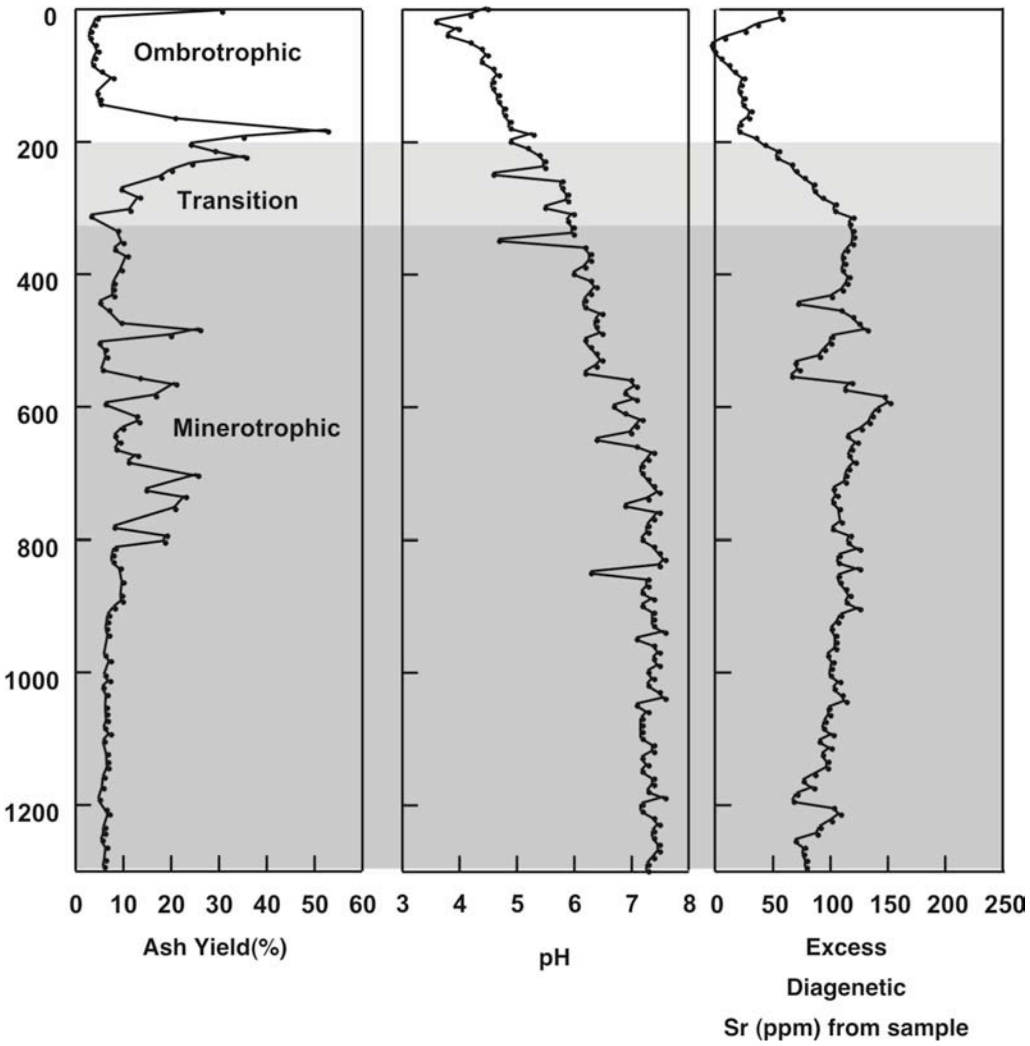

Figure 2: Ash yield, pH and excess diagenetic Sr showing ombrotrophic-minerotrophic boundary in Lynch's Crater.

3.2. Ash Yield and Biogenic Silica Layers

In the top 140 cm of the deposit, the ash yield is the lowest (2-5%) with a high value in the top 10 cm (31%). Low ash yields are also observed between 900-1300 cm (<8%) in the lowermost section of the core and between 610-690 cm (8-10%) and 370-470 cm (7-10%) (Fig. 3). Between 150-800 cm, four distinct horizons with a sharp increase in ash yield are seen at: 690-720 cm (25%), 560-610 cm (18%), 480-500 cm (25%) and 150-270 cm (53%).

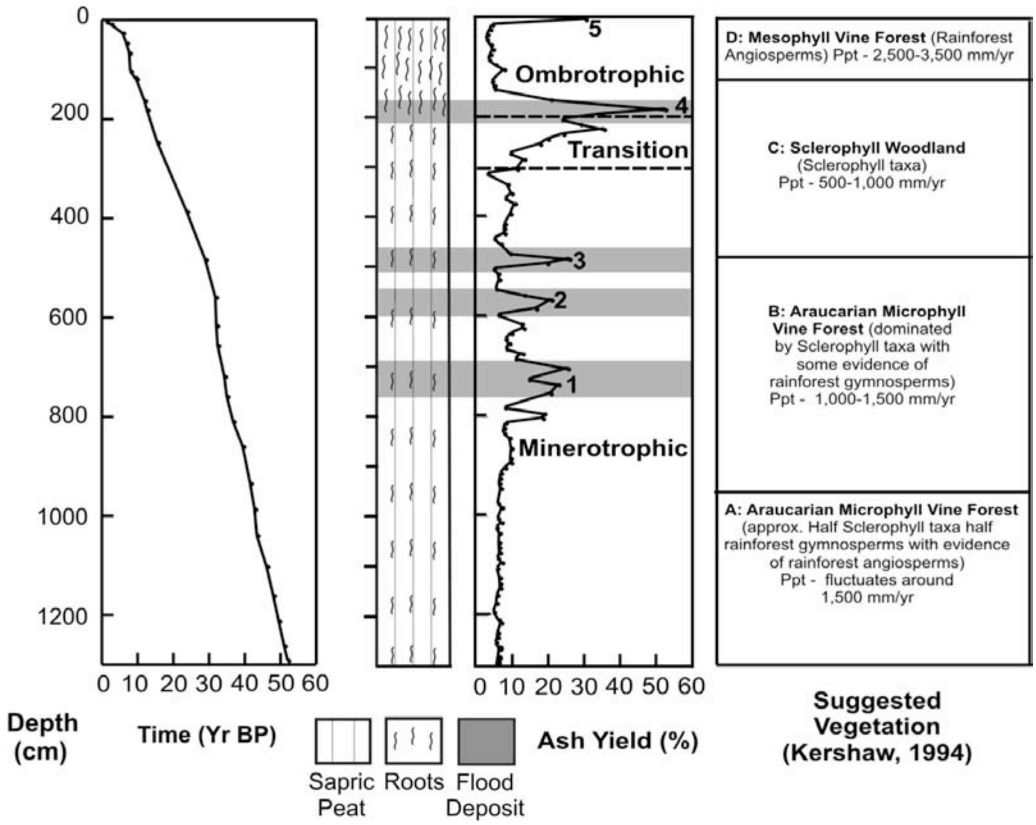

Figure 3: Age model from radiocarbon dates, peat composition, ash yield and dominant vegetation type with predicted annual rainfall (Ppt) in the vicinity of Lynch's Crater.

SEM analysis of the four layers (1-4) with high ash yield (Fig. 3) reveals that they contain abundant sponge spicules (Fig. 4) and some samples also contain diatom fragments (Fig. 4, 2B). Image analysis shows that the inorganic composition of the four layers differs from one another. Layer 1 (25% ash yield) contains abundant spicules that are both moderately and highly weathered with some very small (~10 μm) angular quartz grains and significant amounts of clay material (Fig. 4, 1A and 1B). Layer 2 (18% ash yield) has abundant sponge spicules that are less weathered than those in layer 1 (Fig. 4, 2A and 2B) and diatoms and sponge spicules are well preserved with some pitting. Some quartz grains are also present (~50 μm) these appear more rounded and show some pitting.

The preservation of the biogenic silica constituents indicates less chemical and physical weathering than in layer 1. Layer 3 (25% ash yield) contains abundant highly weathered sponge spicules with significant amounts of clay material (Fig. 4, 3A and 3B). Layer 4 (53% ash) contains abundant sponge spicules that range between well preserved and highly weathered (Fig. 4, 4A and 4B). Most sponge spicules belong to the family Spongillidae (Fig. 4, 4B) and possibly all spicules belong to the same family, which is difficult to confirm due to dissolution processes. A comparison of SEM and geochemical data shows that high concentrations of most trace and major elements coincide with all four layers with high-ash yields (Fig. 5).

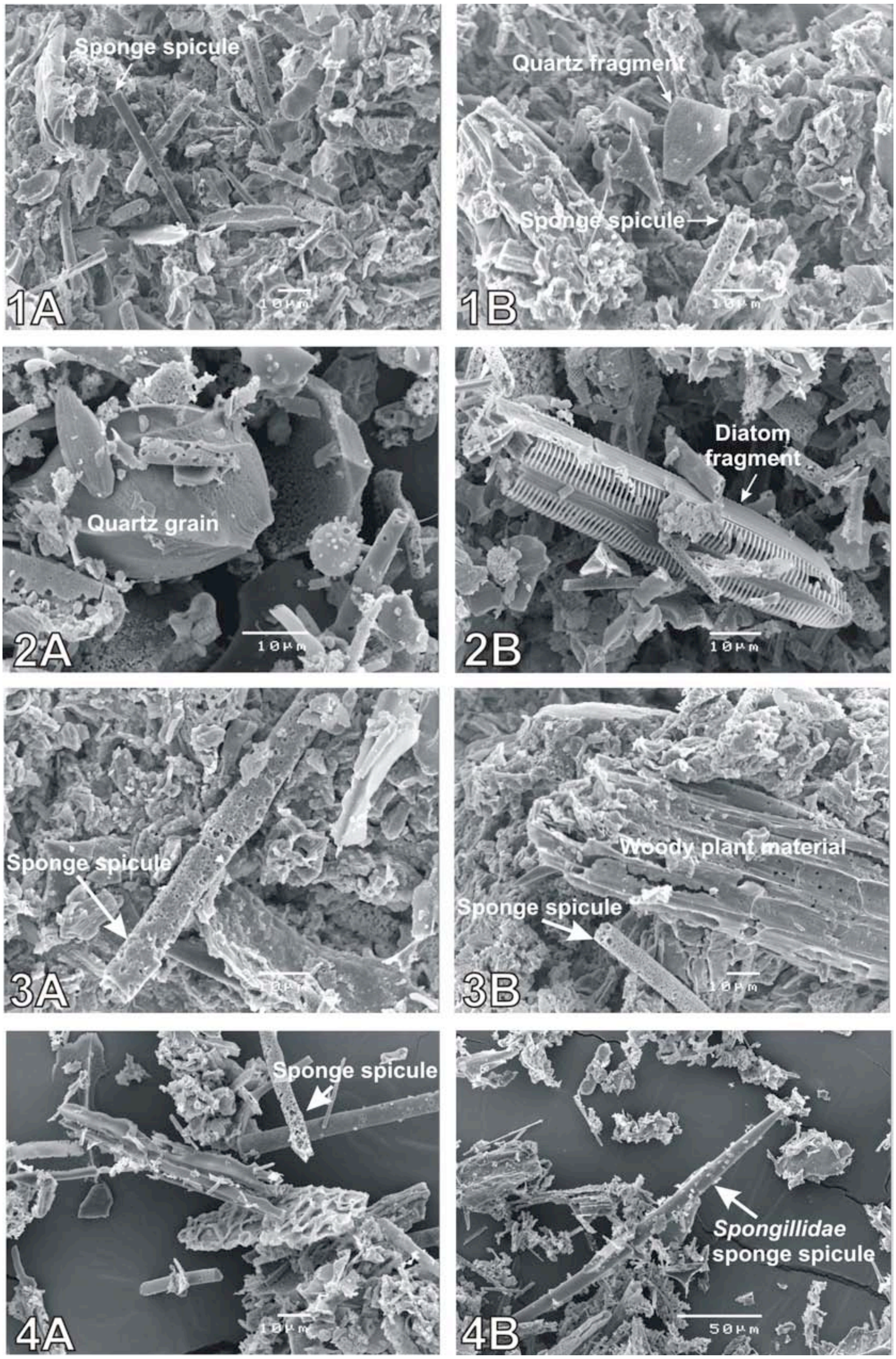

Figure 4. SEM micrographs of the four layers with high ash yield (Layer 1-4) as seen in Fig 3 &5. Note the different degrees of chemical and physical weathering of the individual constituents.

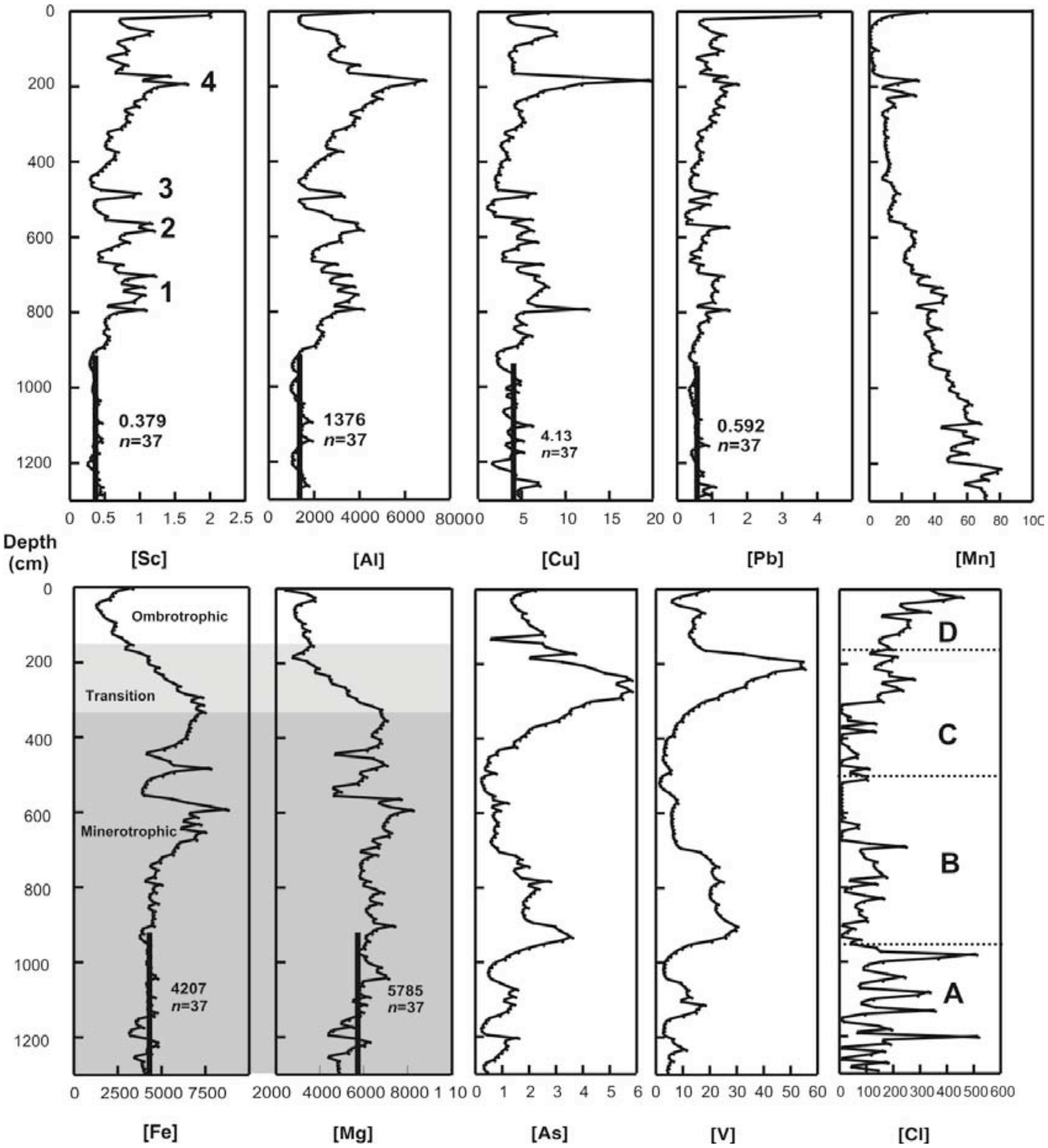

Figure 5: Elemental concentrations of the Lynch's Crater peat deposit showing selected baseline (n-37) (between 900-1300 cm). High ash yield layers are denoted 1, 2, 3 and 4. A, B, C and D represent periods with significant vegetation changes after Kershaw (1994) (description of vegetation changes can be located in Fig. 2).

3.3. Elemental Profiles

The Sc, Al, Cu and Pb concentration profiles (Fig. 5) show similar trends. Scandium concentrations follow a baseline of 0.38 μg/g (900-1300 cm) with sharp deviations in the same four distinct peat layers as discussed in ash yield (layers 1-4).

These occur at 690-800 cm (maximum of ~1 µg/g), 550-590 cm (~1.2 µg/g), 480-500 cm (1 µg/g) and 190-210 cm (~1.8 µg/g). A gradual increase from the baseline (~0.38 µg/g) to peak 4 (~1.8 µg/g) is seen between 420-180 cm. In the top 10-180 cm of the core, concentrations are ~0.7 µg/g, with a high concentration in the top 10 cm (2.1 µg/g). The Al concentration profile shows the same sharp deviations as Sc from the baseline (1376 µg/g) at 690-800 cm (maximum of ~4300 µg/g), 550-590 cm (~4400 µg/g), 480-500 cm (~3500 µg/g) and 190-210 cm (~7200 µg/g). In the uppermost section, between 10-190 cm depth, concentrations decrease to ~1600 µg/g followed by high concentrations in the top 10 cm of the core (5000 µg/g). For Cu, baseline concentrations of 4.13 µg/g occur between 900-1300 cm depth. The four layers 1-4 with high ash yield have increased concentrations of ~13 µg/g, ~7 µg/g, ~7 µg/g and ~20 µg/g, respectively. Between 10-190 cm, concentrations decrease to ~4.5 µg/g. The top 10 cm has a concentration of 8 µg/g. For Pb, baseline concentrations of 0.6 µg/g occur between 900-1300 cm depth (Fig. 5). The same four layers (layers 1-4) show increased concentrations at depths of 800 cm (~ 1.5 µg/g), 550-590 cm (~1.5 µg/g), 480-500 cm (~1.1 µg/g) and 190-210 cm (~1.8 µg/g). Above this, concentrations decrease to ~0.6 µg/g, followed by high concentrations (4 µg/g) in the top 10 cm of the core.

The Fe profile shows similar trends to that of Mg (Fig. 5). The concentrations remain constant at ~4200 µg/g between 700-1300 cm and increase towards 595 cm (7250 µg/g), two significant peaks are observed at 600 and 430 cm (~8750 and ~8100 µg/g). Iron concentration decreases to baseline levels briefly at 440 cm and then rises to ~8000 µg/g at 290 cm. Between 0-290 cm a gradual decrease in Fe concentrations to ~1600 µg/g is seen at 50 cm depth. Concentration in the surface layer is ~3300 µg/g. Magnesium concentrations are ~5800 µg/g between 700-1300 cm depth and they increase towards 600 cm (9000 µg/g). Concentrations drop back to the baseline (5785 µg/g) briefly at 550 cm and then increase once again to a peak of ~7500 µg/g at 480 cm depth. Again concentrations decrease to the baseline at 450 cm and then rise to ~7000 µg/g, where they remain between 320-400 cm. From 320 cm depth, concentrations gradually decrease to low levels of ~2000 µg/g at the surface.

The As profile shows similar trends to that of V (Fig. 5). Small deviations from the baseline (1.7 µg/g) are seen between 1000-1300 cm with concentrations ~0.6 µg/g. Between 750-1000 cm depth, two peaks occur at 940 (4.3 µg/g) and 800 cm (4.1 µg/g). Concentration decreases below the baseline between 440-740 cm and begins to increase again between 280-440 cm to a peak at 280 cm (5.3 µg/g). Between 180-280 cm concentration levels decrease to ~2.5 µg/g and at 180 cm concentration levels decrease again to approach the baseline. In general, concentrations remain stable at baseline values in the top section. The V concentration profile shows small deviations between 1000-1300 cm depth. Like As, two peaks occur at 940 cm (~30 µg/g) and 800 cm (~23 µg/g). Concentrations decrease between 400-700 cm (~15-1 µg/g) and increase between 200-400 cm to a peak (52 µg/g) at 200 cm depth. At 180 cm depth, concentrations decrease markedly (15 µg/g) and remain low and close to baseline values in the top section of the core.

The Mn concentration profile is significantly different to any of the other elements (Fig. 5). The general trend of the profile is a decrease in concentration from 70 µg/g in the bottom of the core to near zero at 40 cm. An enrichment of 50 µg/g is observed in the surface layers. Similar to Mn, the Cl concentration profile is significantly different to any of the other elements (Fig. 5), however the elemental concentrations exhibit large fluctuations in the bottom of the core between 1300-970 cm, with four peaks at depths of 1200 cm (500 μg/g), 1120 cm (375 μg/g), 1080 cm (370 μg/g) and 980 cm (500 μg/g). These peaks constitute the highest concentrations of Cl within the profile. Between 970-660 cm, Cl levels are relatively low. In the bottom of this section values are below the detection limit (10 μg/g) increasing to higher values (~200 μg/g) around 670 cm depth. Between 660-320 cm, Cl concentrations are again low (10-120 μg/g) and sometimes drop below the detection limit. Concentrations begin to rise steadily between 320 cm (150 μg/g) and the surface (450 μg/g).

3.4. Factor Analysis

Four factors have eigen-values greater than 1 and explain 88% of the total variance. Factor 1 (F1) accounts for a large proportion of the variance (45%) and is dominated by the high positive loadings (0.74-0.92) of ash yield, Al, Sc, Ti, Pb, Cu, and V and the moderate negative loadings of Mg, Ca, and Sr (-0.47 to –0.67) (Fig. 6). Variation in F2 (26% of total variance) is mainly associated with Mg, Ca, Sr, and Fe, which show factor loadings greater than 0.71 (Fig. 6). F3 (As) and F4 (Mn) account for similar amounts of the total variance (9 and 8% respectively). Almost all elements have very high communalities (>0.75, see total length of the bar in Fig. 7), i.e. their records can be explained in terms of the four main factors. Only Cl shows a low communality (0.50) suggesting that the variation in Cl concentrations is not controlled by the same processes as the majority of the other elements. With the exception of Cl, Ti, Sc and Fe, all almost exclusively associated to one factor, the other elements have a significant proportion of their total variance (sections of enrichment of As to LR may indicate an additional source of As in the Lynch's Crater deposits. In contrast, the chalcophile element Cu is depleted in relation to the LR, while the alkaline earths (Ca, Mg), particularly calcium, show enrichments in relation to LR. Both Ca and Mg are more strongly enriched in the lower part (235-1300 cm) of the deposit that correlates with increased concentrations of alkaline earth elements (Fig. 8).

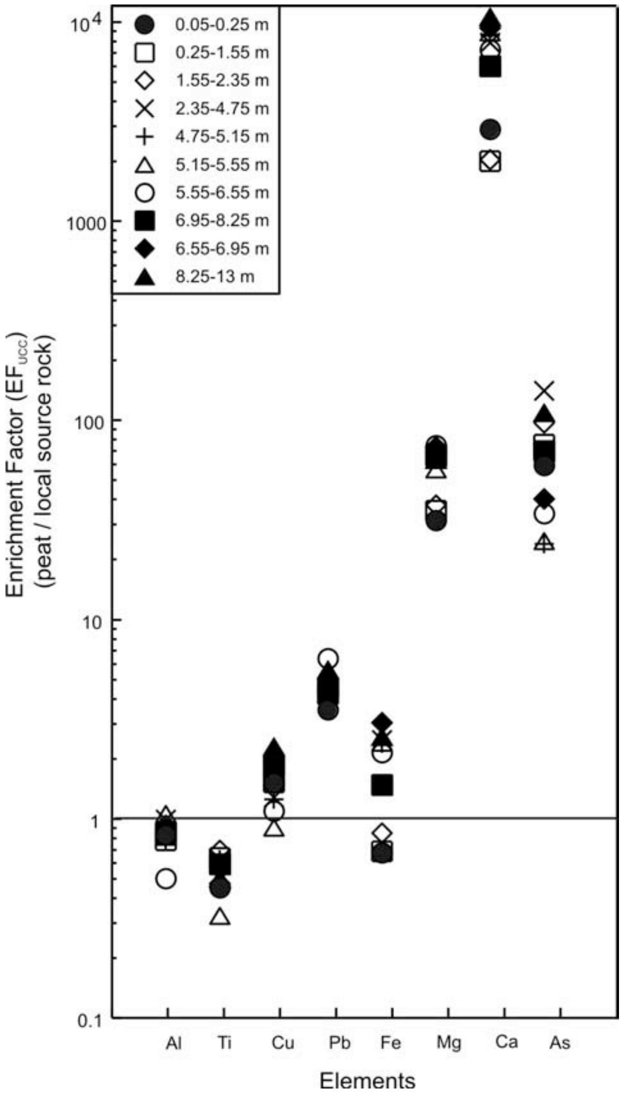

Figure 8: Enrichment factors (EF_{LR}) for major and trace elements in different sections throughout the deposit relative to local rock (LR). Notice the heavy enrichment of Mg, Ca and As compared to Local Rock.

4. DISCUSSION

4.1. Trophic Status: Minerotrophic vs. Ombrotrophic

Boundaries between minerotrophic and ombrotrophic peat units in peat deposits are determined by several, mostly chemical methods. The boundary is important for geochemical analysis because it defines the layer where groundwater can become another factor influencing geochemical compositions. In this study, ash and pH are combined with the analysis of excess diagenetic Sr that is assumed to represent minerotrophic conditions. The pH profile at Lynch's Crater shows neutral values in the lower most deposit (550-1300 cm) but becomes more acidic (3.5-6) in the top 550 cm while the ash yield is lowest (<5%) in the top 150 cm of the core. The excess diagenetic Sr is mainly confined to the lower part and changes towards the top where the ombrotrophic-minerotrophic boundary is interpreted to lie at 150 cm depth. The zone between 350-150 cm depth is regarded as transition zone (Fig. 2).

4.2. High biogenic silica layers

Several high ash yield layers occur in the peat core containing abundant biogenic silica (Fig. 4). Within six layers SEM analysis identified abundant biogenic silica components, namely freshwater sponge spicules (Family spongillidae) and some well-preserved diatom frustules, which is attributed to high bioproductivity. Microscope analysis of the deposits between the high ash yield layers shows little evidence of the presence of diatom or sponge spicules; the layers have <1.1% total opaline silica content. Coinciding with these high biogenic silica layers are enrichments in Sc, Al, Pb, Cu. Interestingly, sponge spicules and diatom frustules rarely contain Sc, Al, Pb, Cu etc., and therefore the elevated trace metal concentrations are attributed to other material, such as clay materials. The layers have been interpreted (Muller et al., 2006) as wet events where increased elemental enrichment from crater-catchment-runoff and detrital influx is evident. Environmental changes at Lynch's Crater during the formation of the high ash yield layers must have involved elevated water levels above the peat surface. Under increased wet conditions, excess runoff from the catchment may have increased nutrient levels, which fostered diatom and sponge growth leading to these high biogenic silica layers. Similarly, peat deposits with abundant biogenic silica are documented from a Malaysian mire system where water levels of >1 m above peat surface can be reached during the monsoon seasons resulting in algal blooms (Wüst and Bustin, 2003).

4.3. Factors Affecting Elemental Composition at Lynch's Crater

4.3.1. Factor 1(Al, Sc, Pb, Cu, and V) and Factor 2 (Mg, Ca, Sr, and Fe)

F1 is positively correlated to ash yield in the peat and to elements largely immobile during weathering and pedogenesis of volcanic materials (Martinez Cortizas et al., In press), while F2 is positively correlated to largely mobile and easily leached elements. Latter elements also show a negative loading in F1. Thus the results for the first two factors suggest two main mechanisms controlling the elemental composition of the peat deposits: the input of inorganic mineral matter in particulate form due to soil erosion (surface runoff and dust deposition) and the contribution of dissolved solutes (soluble Ca, Mg and Fe) leached from the catchment soils as mineral weathering progresses. The negative loading in F1 of the elements associated with F2 may be due to the fact that these are relatively diluted during periods of high mineral matter input.

In peat deposits, lithogenic elements such as Al and Sc are strongly related to mineral matter (Shotyk, 1988). Therefore elements associated with F1 were most likely deposited through sedimentation (runoff) and atmospheric dust deposition of soil material eroded within the catchment. Work on the REE and Pb isotopes in Lynch's Crater found that the primary source of elements is constrained by local sources (Group 1 and 2) with low radiogenic ^{206}Pb/^{207}Pb (Group 1 = 1.19-1.23 and Group2 = 1.24-1.29) signatures and low Eu /Eu*PAAS (Group 1 = 1.19-1.38 and Group 2 = 0.96-1.09). Eu /Eu*PAAS is the normalized Eu$_{sample}$ to Eu post-Archean Australian shale (Taylor and McLennan, 1985). Both groups are described as local sources most likely from the same rock, but where group 2 is a more weathered version of group 1. Group 1 dominates the Lynch's Crater deposit with increased contribution of group 2 between 105-895 cm. These groups have been attributed to the rock signatures of the Atherton Province (Zhang et al., 2003).

The concentration profiles of elements associated to F2 show a change between high values in the minerotrophic and low values in the ombrotrophic section of the mire (Fig. 5). Small enrichments are associated with some of the interpreted wet events (at 430 and 600 cm), and indicate increased input from the catchment.

The Fe concentration in the deposit is quite similar to those of the mobile elements (Mg, Ca and Sr). It is also noticeable that the Fe record does not show evidences of post-depositional remobilization linked to the progressive incorporation of the peats into the catotelm, where anoxic conditions prevail (Chesworth et al., 2006) as it is discussed later for Mn. One possible explanation is that most of the Fe input to the mire was as Fe-humus complexes, mainly Fe complexed to dissolved organic carbon (DOC) and thus shares properties or behaviour similar to the mobile elements. This hypothesis is consistent with the fact that most of the residual variance of Al concentrations (16%; Fig. 8) is also dominated by F2 and shows the same pattern as Mg, Ca, Sr and Fe. In andic soils, high proportions of both Al and Fe are linked to organic matter as metal-humus complexes (Shoji et al, 1993) so they can potentially be leached with DOC in the waters draining the catchment soils. In general the stability of Al-humus complexes is greater than those of Fe-humus ones (Shoji et al, 1993), this may be responsible for the relatively larger Fe concentrations. Some studies have also suggested that Fe has the potential to be affected by ombrotrophic-minerotrophic conditions, similar to Mg (Shotyk, 1988), which would explain why Fe resembles the Ca and Mg profiles in Lynch's Crater.

The interpretation of two main mechanisms for the input of particulate matter and dissolved solutes is supported by SEM analysis that showed an increase in mineral content (clay and quartz grains) in layers with high ash yield. It is also coherent with the depletion of immobile and the enrichment of mobile elements, in the peats compared to the local sources (rocks and soils of the catchment). In Figure 9 the F1/F2 projection, accounting for 71% of the variance of sample scores shows three main groups: 1) Group 1 with moderate positive loadings in F1 and negative loadings in F2, 2) Group 2 with negative loadings both in F1 and F2; and 2) Group 3 that spreads from negative to positive loadings in F1 but has positive loadings in F2. Group 1 includes samples of the upper 150 cm that are from the Holocene (<11.5 kyr); Group 2 includes the samples below 900 cm depth and two other small sections (500-550 cm and 430-450 cm). The ages of these three horizons are approximately 36-55 kyr, 22.8-24.4 kyr and 20.5-21.1 kyr respectively. Group 3 includes the remainder of the samples. Group 1 not only contains the younger samples but the samples in the ombrotrophic section of the deposit, so differences may, in part, be due to the change in the geochemical nature of the mire and the different sources of the elements deposited in the peat. Major nutrients such as Mg and Ca usually have limited input in ombrotrophic peats, as the sole supplier is atmospheric dust (Verhoeven, 1986). This distinction can be observed at Lynch's Crater where, for example, high Mg concentrations occur at greater depth and decrease in the ombrotrophic section. The pattern of Mg in the Lynch's Crater deposit demonstrates that many factors, such as trophic status of the deposit and groundwater fluctuations can significantly influence the concentrations of these elements (Fig. 5).

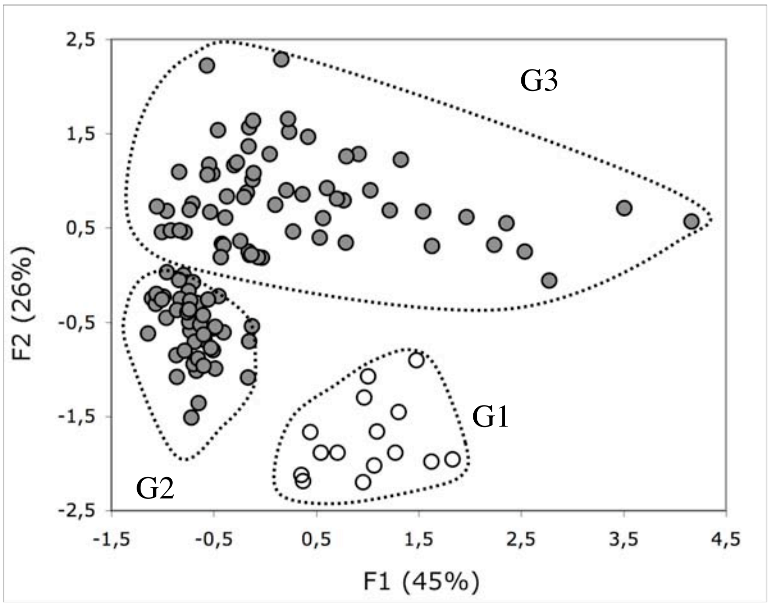

Figure 9: PCA F1/F2 projection of samples scores of the Lynch's Crater record.

The influx of mineral matter and dissolved solutes explains 71% of the variations in concentrations of all the elements and are the two main controls on elemental composition in the deposit. The influx is dependant on the geomorphological evolution including weathering and runoff rates and most of the composition depends on local rather than distant sources.

Another interesting finding is that although the ash yield has a greater proportion of its variance associated to F1 (55%), it also has a significant proportion associated to F2 (23%) (Fig. 8). This indicates that the total inorganic content of the deposit depends largely on inorganic influx and less on dissolved solutes.

4.3.2. Factor 3 (As and V) and Factor 4 (Mn)

Arsenic is dominated by F3, although a significant proportion of the variance of this element (19%) is associated with F1 (Fig. 8). The association with F1 indicates that As concentrations are in part related to the flux of inorganic material, but most of it must be related to a different control (72% of the variance). Vanadium is also associated by F3 where variations are ~30% suggesting a link between these two elements, with rather different geochemical behaviour, but similar concentration profiles (Fig, 5).

Factor 4 is almost exclusively related to one of the analysed elements. Communality analysis reveals that Mn is mainly dominated by F4 (75%) (Fig.8). The Mn record is typical of an element that undergoes post-depositional diagenetic remobilization. Due to the change in the geochemical environment as the peat deposit grows from the oxic conditions prevailing at the time of deposition at the surface of the mire to anoxic conditions characteristic of the catotelm (Chesworth et al., 2006). Manganese also shows high mobility under anoxic conditions or from very acidic to moderately alkaline environments (Brookins, 1988; Chesworth et al., 2006). Studies on ombrotrophic peat deposits show that Mn is often concentrated in the surface peat due to biological recycling (Damman, 1978; Norton, 1990). In minerotrophic settings it is common for elements such as Mn, to undergo diagenetic remobilisation regulated by the Eh-pH conditions, so Mn is lost under anaerobic conditions (Mattson and Koutler-Andersson, 1955). Previous studies on peat deposits have shown that Mn can increase with depth out of proportion with ash yield. Iron is also commonly affected by Eh-pH conditions within mire deposits, but in Lynch's Crater Fe does not follow the trend of Mn (Fig. 5). In an oxidizing, slightly acid to slightly alkaline environment the dominant Mn form is Mn^{2+} while Fe is present as a hydroxide or an oxide. Although under these conditions Mn will be mobile, Fe will not, this does not explain why the Fe record is similar to those of Mg, Ca and Sr.

Copper also has a significant component associated with F4 (14%) that represents diagenetic alteration, and the distribution of its residual variance shows a record quite similar to that of Mn (Fig. 5). This suggests that part of the Cu incorporated to the peat may have undergone diagenetic remobilization.

4.4. Chlorine

Chlorine has the lowest communality of all the analyzed elements and a significant but moderate negative loading in F2 (-0.54) (Fig. 8), suggesting that its concentration follows a pattern somewhat opposite to that of the very mobile elements and the concentration depends on processes other than those related to F1, F2, F3 and F4 (i.e. weathering of local bedrock, mobility, long-range dust or diagenetic alteration). From the elements analysed, it appears that Cl may be the only element affected purely by external sources.

Principal Cl sources are mainly chlorine bearing sedimentary rocks and seawater and influx is driven by water and hence its deposition is a strong indicator of wetness variations. Limited research has been conducted on the historical distribution of halogens in peat and some studies have assumed chlorine to be conservative in peat and thereby reflect changes in halogen concentrations in rainwater (Shotyk, 1997). Recent studies on halogen content in peat cores have demonstrated that almost all Cl present in the peat is in the form of organo-chlorinated compounds (up to 95%) (Biester et al., 2004), while studies on organic soil horizons found that the spatial distribution of organic chlorine is closely related to that of chloride, which depends on atmospheric deposition (i.e. precipitation) (Johanson et al., 2003). At Lynch's Crater the Cl concentration profile shows a remarkable similarity to the vegetation and precipitation phases suggested by Kershaw (Kershaw, 1994) from pollen analysis (Fig. 3). Phase A corresponds to a period of ~1,500 mm/yr precipitation, when the catchment was largely vegetated (mixed sclerophyll rainforest). The average Cl concentration is 168 μg/g, but large variations occur with most samples having between 45 and 250 μg/g (Fig. 5). A few samples have values below the detection limit (<10 μg/g) and four peaks with concentrations between 300 and 520 μg/g exist that possibly indicate intense variability of precipitation. Phase B has been interpreted as reduced precipitation (~1,000-1500 mm/yr) with sub-humid to humid conditions and less vegetation cover (dominated by sclerophyll taxa and some remnants of rainforest taxa). The average Cl concentration in this section is also lower than that of the previous phase (94 μg/g). Phase C has the lowest precipitation (~500-1000 mm/yr) indicating arid to semiarid conditions and the vegetation was dominated by sclerophyll taxa. In this section many samples have Cl concentrations below the detection limit and the average Cl is ~36 μg/g. Phase D contains mainly rainforest vegetation with the highest precipitation levels (~2,500-3,500 µg/g) and hyper-humid conditions. In this section of the deposit, average Cl concentrations have highest values (216 µg/g).

4.5. Chronology of Geochemical Changes and the Implications for Environmental Change

Elemental composition of the peat deposits of Lynch's Crater show that distribution is controlled by several factors. A number of other studies have demonstrated this previously (e.g. Shotyk, 1988) however the application of statistical analysis allows further differentiation of processes influencing elemental distribution. There are at least five dominant processes or factors that can be differentiated: 1) detrital influx (catchment and dust); 2) mobilization within the peat due to chemical changes (pH, eh, DOC, etc); 3) biocycling of plant essential elements within the active root layer; 4) diagenetic alteration within the profile, most likely associated with groundwater flux along with aerobic/anaerobic changes; and 5) quantity and/or composition changes of rainwater.

This section will discuss different processes throughout the deposit and changes in process intensity based on the elemental concentration profiles and PCA analysis. The time variation of sample scores for each factor (Fig. 10) is assumed to represent a measure of the intensity of each of the processes identified. The most consistent low F1 scores (i.e. low mineral matter input) occur at depths with ages between 36 and 55 kyr, and three short periods centered at 28.1 kyr, 23.7 kyr and 21.8 kyr. After 36 kyr inorganic influxes peak at 32.2-29.4 kyr, 25 kyr, 22.5 kyr, 12.2 kyr and 8.3 kyr (Fig. 10A). The largest peak corresponds to an age of 12.2 kyr but the flux started to increase around 16.5-16 kyr. The period between 36-55 kyr coincides with pollen phase A and shows extensive vegetation cover (Kershaw,

1994) implying reduced soil erosion and mineral matter transport to the mire. The onset of the arid trend at ~36 kyr on the Atherton Tablelands (Kershaw, 1994), with the subsequent changes in vegetation cover, is in agreement with the increase in inorganic mineral matter input to the mire (Fig. 5) as a possible result of less vegetation cover and increased erosion. An increase in atmospheric dust also occurs in sediment cores from the Tasman Sea (S-Australia), which indicates a widespread aridification across Australia (Calvo et al., 2004; Kawahata, 2002).

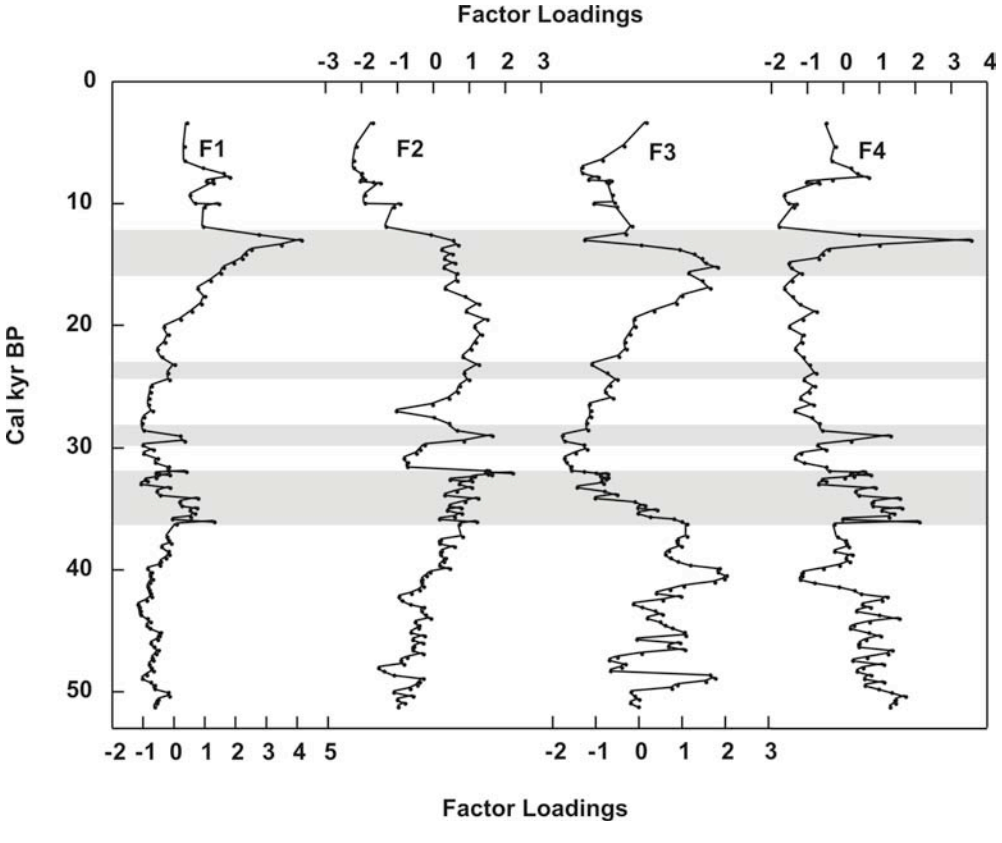

Figure 10: Variations of factor scores (F1-F4) through time of the Lynch's Crater deposit.

The flux of dissolved solutes (F2, Fig. 10) shows low values in peat sections older than 36 kyr (phase A, Fig. 3), high values from 36 kyr to 12.2 kyr (phases B and C) with two short and sharp decreases at 24.4-22.8 kyr and 21.5-20.1 kyr, and very low values for the last 11.5 kyr (phase D). This pattern seems to be related to a coupling between climate (i.e. precipitation) and vegetation type and cover. During phases of higher precipitation the greater expansion of forest vegetation may have led to a greater recycling of soil nutrients (Mg, Ca and Sr) in the catchment and a lower export to the mire. On the contrary, during sub-humid and semi-arid phases the lower cover and a change to more shrubby vegetation may have promoted more runoff. Previous studies have shown that well-established vegetation with extensive root systems may induce biocycling of nutrients and other essential elements enriching top soils in nutrients; while in areas where low recycling takes place elements may be lost (Page et al., 1999; Wüst and Bustin, 2003). This interpretation is supported by the fact that the two excursions, dated at 45.2 kyr and 38.6 kyr, occurring during phase A, also coincide with the highest Cl concentrations (i.e. high precipitation). More difficult to explain are the two excursions at the end of phase B and at the beginning of phase C, which happen after two wet events. It is possible that once the aridification conditions were established and the vegetation modified its response to short abrupt climate changes may have not been as rapid as during long wet phases.

Interpretations of long-range input to the peat deposits relies on elements either restricted or absent in the bedrocks of the catchment area. At Lynch's Crater, both As and V, associated with F3 (Fig. 10) show high concentrations in the oldest deposits (>36 kyr), and low values during the sub-humid and, particularly, the semiarid phases when vegetation cover was much lower and erosion increased. It is most likely that during periods of high runoff and local influx, the effect of long-range dust is masked. The large variability of F3 during 48-46 kyr, 37-43 kyr and 15-12 kyr may indicate that atmospheric circulation patterns and source areas changed considerably during the last 55 kyr. Rare earth elements and Pb isotope studies from the same core at Lynch's Crater (Kylander, submitted) indicate a long-range dust contribution through a change in the Eu anomaly. The Eu/Eu*PAAS show higher values in the bottom section of the core (900-1300 cm), which are not characteristic of the local source rock. The volcanic material of northern Queensland has less differentiated lavas with no plagioclase separation and therefore low Eu/Eu*PAAS. The study identifies a contribution from the volcanic rocks of central Queensland in the bottom of the core (900-1200). The large variability of the F3 records and the observation of high concentration values of F3 elements during the late Pleistocene (48-46, 37-34 and 15-12 kyr) may indicate that atmospheric circulation patterns and source areas changed considerably during the last 55 kyr.

The pattern of diagenetic remobilization (F4, Fig. 10) affects the minerotrophic section of the peat deposit, where it shows as an increase in scores values to the base. This trend is only interrupted in four sections where higher scores correspond to the same periods of elevated inorganic matter (F1, Fig. 10), this suggests an extra input over the base flux of elements associated with this factor (Mn and to a lower extent Cu).

The Cl concentration record provides more supporting evidence for its use as a proxy of precipitation variations, in particular through its strong correlation to the pollen record (Kershaw, 1994). The data show that the lowermost peat deposits (55-42 kyr Fig. 5) experienced strong fluctuations in precipitation levels that cannot be deduced from pollen studies. The Cl record shows periods B and C (42-12 kyr) to have low precipitation. A steady increase in precipitation can be deduced from the Cl record into the Holocene where changes are more consistent and the Cl reaches its maximum concentration at ~4 kyr. The negative association between Cl and the flux of dissolved solutes to the mire may be an indirect consequence of the coupling between rainfall, forest vegetation cover and nutrient recycling. Under more humid climates the greater forest cover may have induced a lower mineral matter flux to the mire. The Cl record is also in good agreement with paleoenvironmental studies that have found the Australian summer monsoon to be most effective from 65-45 kyr, least effective during 45-10 kyr, and moderately effective during the Holocene (<10 kyr) (Johnson et al., 1999).

5. CONCLUSIONS

Geochemical and statistical data analyses of peat deposits, such as Lynch's Crater, are powerful tools for interpreting past environmental conditions. At Lynch's Crater, regional climate changes influenced precipitation, vegetation cover and hence weathering, dust influx and groundwater table, which ultimately links to local pH, eH, and oxic/anoxic changes. The climate is the primary driver behind geochemical processes influencing composition and processes associated with peat deposits. Our record, that spans the past 55 kyr allows the following conclusions:

1) Studies of the Lynch's Crater peat mire emphasize the importance of determining the ombrotrophic-minerotrophic boundary. The mobility of some elements, such as Fe and Mg can be influenced by redox conditions and thus it is important to define the groundwater boundary and thus the ombrotrophic-minerotrophic boundary.
2) The results of PCA suggest that the elemental composition of Lynch's Crater peats were controlled by five main factors: 1) the input of inorganic matter from local bedrock (F1); 2) the influx of dissolved solutes (F2); 3) the

input of long-range dust (F3); 4) diagenetic processes *in-situ* (F4); and 5) variations in precipitation (Cl).

3) Marked changes in the catchment's contribution to mineral matter indicates times of abrupt precipitation changes on the peat mire at 32.2-29.4 kyr, 25 kyr, 22.5 kyr, and 12.2 kyr and. This is also supported by the abundance of sponge spicules and diatom frustules, these deposits are likely to represent evidence of global climate events such as the Younger Dryas. In turn, increases in local source rock contribution may indicate weathering of the catchment during dry periods, where catchment vegetation is reduced and the soil is more exposed.
4) At Lynch's Crater the Cl record shows marked similarities with the pollen record but at a higher resolution, this allows the definition of high-resolution changes in precipitation over the last 55 kyr.

Acknowledgements

This project was funded by the Australian Research Council (DP0456515) and the Australian Institute of Nuclear Sciences and Engineering (PGR8/03). We acknowledge helpful discussions with Robert Carter and Kirsten Perry (JCU) and laboratory assistance of Gordon Warria and David Holliday (JCU). We would like to thank Andrew Smith, Andrew Jenkinson, David Fink and Geraldine Jacobsen (ANSTO) for assistance with radiocarbon dating.

REFERENCES

Anshari, G., Kershaw, A.P. and van der Kaars, S., 2001. A Late Pleistocene and Holocene pollen and charcoal record from peat swamp forest, Lake Sentarum Wildlife Reserve, West Kalimantan, Indonesia. Palaeogeography, Palaeoclimatology, Palaeoecology, 171(3-4): 213-228.

Bard, E., Arnold, M., Hamelin, B., Tisnerat-Laborde, N. and Cabioch, G. (Editors), 1998. Radiocarbon Calibration by Means of Mass Spectrometric 230Th/234U and 14C Ages of Corals: An updated database including samples from Barbados, Mururoa, and Tahiti. Radiocarbon, 40, 1085-1092 pp.

Biester, H., Keppler, F., Putschew, A., Martinez-Cortizas, A. and Petri, M., 2004. Halogen retention, organohalogens, and the role of organic matter decomposition on halogen enrichment in two Chilean peat bogs. Environ. Sci. Technol., 38: 1984-1991.

Blockley, S.P.E., Lowe, J.J., Walker, J.C., Asioli, A., Trincardi, F., Coope, G.R., Donahue, R.E. and Pollard, A.M., 2004. Bayesian analysis of radiocarbon chronologies: examples from the European Late-glacial. Journal of Quaternary Science, 19(2): 159-175.

Brookins, D.G., 1988. Eh-pH diagrams for geochemistry. Springer-Verlag, New York, 176 pp.

Caldeira, K. and E.Wickett, M., 2003. Anthropogenic carbon and ocean pH: The coming centuries may see more ocean acidification than the past 300 million years. Nature, 425: 365.

Calvo, E., Logan, G. and De Deckker, P., 2004. Dust-induced changes in phytoplankton composition in the Tasman Sea during the last four glacial cylcles. Palaeogeography, 19: PA2020.

Chesworth, W., Martínez-Cortizas, A. and García-Rodeja, E., 2006. Peatlands, Evolution and Records of Environmental and Climate Changes. Developments in Earth Surface Processes, 9. Elsevier science, Amsterdam.

Damman, A.W.H., 1978. Distribution and movement of elements in ombrotrophic peat bogs. OIKOS, 30: 480-495.

Delmonte, B., Petit, J.-R. and Maggi, V., 2002. Glacial to Holocene implications of the new 27000-year dust record from the EPICA Dome C (East Antarctica) ice core. Climate Dynamics, 18(8): 647-660.

Fink, D., Hotchkis, M., Hua, Q., Jacobsen, G., Smith, A.M., Zoppi, U., Child, D., Mifsud, C., Van der Gaast, H., Williams, A. and Williams, M.A.J., 2004. The ANTARES AMS facility at ANSTO. Nuclear instruments and methods in physics research section B: Beam interactions with materials and atoms, 223-224: 109-115.

Gorham, E. and Janssens, J., 2005. The distribution and accumulation of chemical elements in five peat cores from the mid-continent to the eastern coast of North America. Wetlands, 25(2): 259-278.

Hesse, P.P. and McTainsh, G.H., 2003. Australian dust deposits: modern processes and the Quaternary record. Quaternary Science Reviews, 22(18-19): 2007-2035.

Johanson, E., Sanden, P. and Oberg, G., 2003. Spatial patterns of organic chlorine and chloride in Swedish forest soils. Chemosphere, 52: 391-397.

Johnson, B.J., Miller, G.H., Fogel, M.L., Magee, J.W., Gagan, M.K. and Chivas, A.R., 1999. 65,000 years of vegetation change in central Australia and the Australian summer monsoon. Science, 284: 1150-1152.

Kalahne, R., Amim, M., Sobottka, J., and Sauerbrey, R., 2000. Methods of multivariate data analysisnext term applied to the investigation of fen soils. Analytica Chimica Acta, 420: 205-216.

Kawahata, H., 2002. Shifts in oceanic and atmospheric boundaries in the Tasman Sea (Southwest Pacific) during the Late Pleistocene: evidence from organic carbon and lithogenic fluxes. Palaeogeography, Palaeoclimatology and Palaeoecology, 184(2002): 225-249.

Kershaw, A.P., 1974. A long continuous pollen sequence from north-eastern Australia. Nature, 251: 222-223.

Kershaw, A.P., 1994. Pleistocene vegetation of the humid tropics of northeastern Queensland, Australia. Palaeogeography, Palaeoclimatology, Palaeoecology, 109: 399-412.

Kylander, M.E., Muller, J., Weiss, D.J., Wust, R.A., Coles, B.J., Garcia-Sanchez, R. and Gallagher, K., Submitted. Rare Earth Element and Pb isotope variations in a 55,000 year old peat core from Lynch's Crater (NE Queensland, Australia): Proxy development and application to paleoclimate in the Southern Hemisphere. Geochemica et Cosmochimica Acta.

Martinez Cortizas, A., Nova Munoz, J.C., Pontevedra, X., Taboada, T., Garcia-Rodeja, E. and Chesworth, W., In press. Elemental composition of refernce European volcanic soils. In: O. Arnalds et al. (Editors), Soils of volcanic regions of Europe.

Martínez-Cortizas, A., Pontevedra-Pombal, X., García-Rodeja, E., Nóvoa-Muñoz, J.C. and Shotyk, W., 1999. Mercury in a Spanish peat bog: Archive of climate change and atmospheric metal deposition. Science, 284: 939-942.

Mattson, S. and Koutler-Andersson, E., 1955. Geochemistry of a raised bog. Annals of the Royal Agricultural College of Sweden, 21: 321-366.

Mattson, S., Sandberg, G. and Terning, P.-E., 1944. Electro-chemistry of soil formation, VI. Atmospheric salts in relation to soil and peat formation and plant composition. Ann. R. Agric. Coll. Sweden, 12: 101-118.

Mauquoy, D., van Geel, B., Blaauw, M. and van der Plicht, J., 2002. Evidence from northwest European bogs shows "Little Ice Age" climatic changes driven by variations in solar activity. The Holocene, 12(1): 1-6.

McManus, J.F., Francois, R., Gherardi, J., Keigwin, L.D. and Brown-Leger, S., 2004. Collapse and rapid resumption of Atlantic meridional circulation linked to deglacial climate changes. Nature, 428: 834-837.

Muller, J., Wüst, R.A.J., Weiss, D.J. and Hu, Y., 2006. Geochemical and stratigraphic evidence of environmental change at Lynch’s Crater, Queensland, Australia. Global and Planetary Change, 53: 269-277.

Norton, S.A., 1990. Geochemistry of selected Maine peat deposits, Maine Geological Survey - Department of Conservation, Maine.

Page, M.C., Dickens, G.R. and Dunbar, G.B., 2003. Tropical view of Quaternary sequence stratigraphy: Siliciclastic accumulation on slopes east of the Great Barrier Reef since the Last Glacial Maximum. Geology, 31(11): 1013-1016.

Page, S.E., Rieley, J.O., Shotyk, W. and Weiss, D., 1999. Interdependence of peat and vegetation in a tropical peat swamp forest. Phil. Trans. R. Soc. Lond. B, 354: 1885-1897.

Pearce, B., 2002. Report on compilation of a geological conceptual model for the Atherton Tableland basalts, Queensland Department of Natural Resources and Mines, Brisbane.

Shotyk, W., 1988. Review of the inorganic geochemistry of peats and peatland waters. Earth-Science Reviews, 25: 95-176.

Shotyk, W., 1997. Atmospheric deposition and geochemical mass balance of major and trace elements in two oceanic peat bog profiles, northern Scotland and the Shetland Islands. Chemical Geology, 138(1-2): 55-72.

Shotyk, W., Nesbitt, H.W. and Fyfe, W.S., 1990. The behavior of major and trace elements in complete vertical peat profiles from three Sphagnum bogs. International Journal of Coal Geology, 15: 163-190.

Stephenson, P.J., Griffin and Sutherland, 1980. Cainozoic volcanism in north-eastern Australia. Geological Society of Australia, Brisbane, 349–374 pp.

Taylor, S.R. and McLennan, S.M., 1985. The continental crust: Its composition and evolution. Blackwell, Oxford.

Tolonen, K., 1984. Interpretation of changes in the ash content of ombrotrophic peat layers. Bull. Soc. geol. Finland, 56 207–219.

Turney, C.S.M., Kershaw, A.P., Clemens, S.C., Branch, N., Moss, P.T. and Fifield, L.K., 2004. Millennial and orbital variations of El Niño/Southern Oscillation and high-latitude climate in the last glacial period. Nature, 428: 306-310.

Verhoeven, J.T.A., 1986. Nutrient dynamics in minerotrophic peat mires. Aquatic Botany, 25: 117-137.

Wedepohl, K.H., 1995. The composition of the continental crust. Geochimica et Cosmochimica Acta, 59(7): 1217-1232.

Weiss, D., Kober, B., Gallagher, K., Dogopolova, A., Mason, T.F., Coles, B.J., Kylander, M.E., LeRoux, G. and Spiro, B., 2004. Accurate and precise Pb isotope measurements in environmental samples using MC-ICP-MS. International Journal of Mass Spectrometry, 232: 205-215.

Weiss, D., Shotyk, W., Rieley, J.O., Page, S.E., Gloor, M., Reese, S. and Cortizas-Martinez, A., 2002. The geochemistry of major and selected trace elements in a forested peat bog, Kalimantan, SE Asia, and its implications for past atmospheric dust deposition. Geochimica et Cosmochimica Acta, 66(13): 2307-2323.

Worralla, F., Burtb, T., and Adamsonc, J., 2005. The rate of and controls upon DOC loss in a peat catchment. Journal of Hydrology, 321: 311-325.

Wüst, R.A.J. and Bustin, R.M., 2003. Opaline and Al–Si phytoliths from a tropical mire system of West Malaysia: abundance, habit, elemental composition, preservation and significance. Chemical Geology, 200(3-4): 267-292.

Wüst, R.A.J. and Bustin, R.M., 2004. Late Pleistocene and Holocene development of the interior peat-accumulating basin of tropical Tasek Bera, Peninsular Malaysia. Palaeogeography, Palaeoclimatology, Palaeoecology, 211(3-4): 241-270.

Wüst, R.A.J., Bustin, R.M. and Lavkulich, L.M., 2003. New classification systems for tropical organic-rich deposits based on studies of the Tasek Bera Basin, Malaysia. CATENA, 53(2): 133-163.

Yonebayashi, K., Okazaki, M. and Pechayapisit, J., 1992. Woody fragments in tropical peat soils. In: K. Kyuma, P. Vijarnsorn and A. Zakaria (Editors), Coastal lowland ecosystems in southern Thailand and Malaysia. Showado-Printing Co., Sakyoku, Kyoto, pp. 233-247.

Zhang, G., Germaine, J.T., Martin, R.T. and Whittle, A.J., 2003. A simple sample-mounting method for radndom powder X-ray diffraction. Clays and Clay Minerals, 51(2): 218-225.

CHAPTER 4

Wet phases in tropical Australia during Heinrich events detected in the terrestrial peat record of Lynch's Crater

Adapted from a paper submitted to:

Proceedings of the National Academy of Sciences

ABSTRACT

A terrestrial site in NE Australia presents new evidence of an extended southward propagation of the Intertropical Convergence Zone (ITCZ). Located in the Southern Hemisphere Pacific region the site records major climate perturbations of the last 55 kyr. Distinct climate events are identified: Increased precipitation/wetness of the region during Heinrich events (H1-4); the Younger Dryas (YD); and the 8.2 kyr abrupt event. Several proxies recorded these events from the peat deposit. These data indicate large-scale shifts of the austral summer ITCZ position that is known to control monsoonal precipitation in NE Australia. Our interpretation is well supported by a fully coupled atmosphere/ocean climate model, which simulated high freshwater influx to the North Atlantic Ocean. The model shows precipitation anomalies including a southward migration of the ITCZ and a zonal shift in mid-latitude storm tracks over the Southern Hemisphere equatorial region. To date southward ITCZ propagation has only been identified in records from the tropical Atlantic Ocean and Brazil. The Lynch's Crater record clearly demonstrates the involvement of the tropical western Pacific Ocean in ITCZ propagation during abrupt climate events that has not been shown in previous studies. Defining such past migrations will offer further insight into the importance and role of the equatorial region in global climate dynamics.

During the last glacial period the semi-periodic instability of ice sheets, known as Heinrich events (Dansgaard et al., 1993), resulted in abrupt and massive iceberg discharges to the North Atlantic, this influenced the subsequent shutdown of the ocean conveyor system and forced dramatic drops in Northern Hemisphere temperatures. Co-existing with Heinrich events are Dansgaard-Oeschger (D-O) events, these are high-frequency climate oscillations with 1000-, 1450-, and 3000-year cyclicities (Dansgaard et al., 1993). The Heinrich events and D–O cycles are arranged in "Bond Cycles" each of which consists of a major D–O interstadial (warm period) followed by a series of shorter and less intense interstadials, then by a long stadial (cold period) that is terminated by a Heinrich event (Bond et al., 1993). The above are termed "abrupt climate events", along with these Bond Cycles, other events, such as the Younger Dryas (YD) (~11 kyr) and the 8.2 kyr event are also described as abrupt. The majority of evidence for such events is from the Northern Hemisphere, usually in the form of marine sediments and ice cores (Alley et al., 2003; Broecker, 1994; Heinrich, 1988). Past studies suggest that polar regions were critical to global climate change but more recent work points to the tropics being key to forcing abrupt climate change (Hendy and Kennett, 2000).

Paleoclimate records of the last glacial from Africa and South America show elevated precipitation in association with a southward migration of the Intertropical Convergence Zone (ITCZ) (Behling et al., 2000; Gasse, 2000; Jennerjahn et al., 2004; Peck et al., 2004). The ITCZ is an equatorial region that encircles the Earth, where trade winds of the Northern and Southern Hemispheres converge (Wells, 1997). Intense humidity is responsible for almost perpetual thunderstorms within this zone and thus the ITCZ becomes the primary supplier of precipitation to equatorial regions. Changes in the ITCZ location may result in severe wet and dry periods for intertropical landmasses (Broccoli et al., 2006). For this reason, short and long-term variations in the ITCZ position are of primary importance to nearby regions where vegetation depends on the availability of water supplied by this system.

Few paleoclimatologists working on records from the Southern Hemisphere tropics have investigated the influence of Heinrich events on climate changes during the last glacial period. Most Heinrich event studies (Fig. 1) to date have focused on marine sediments from the Atlantic Ocean (Arz et al., 1998; Behling et al., 2000; Jennerjahn et al., 2004) and speleothem records from Brazil (Wang et al., 2004). Such records show a direct relationship between a southern ITCZ migration over the Atlantic Ocean and increased precipitation during millennial scale Heinrich events. This Lynch's Crater record presents new high-resolution geochemical evidence for the effects of Heinrich events and millennial-scale climate changes. The tropical NE Australian location is influenced by the western Pacific Ocean austral summer monsoon system, the ITCZ and the austral winter SE trades. This study focuses on several different proxies that link environmental and climate change in order to identify atmospheric and oceanic teleconnections between the North Atlantic and the Southern Hemisphere's Western Pacific region.

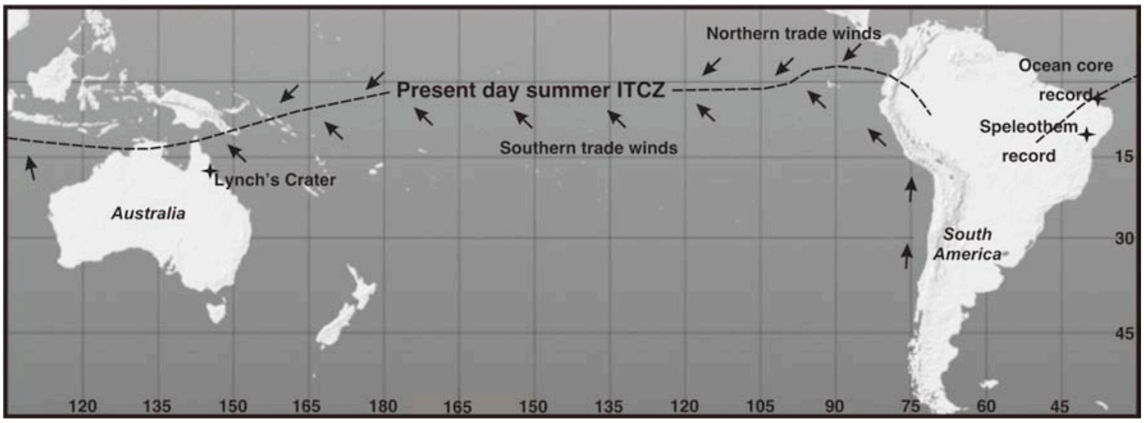

Figure 1: Locations of records from Lynch's Crater (this study), the tropical western Atlantic (Jennerjahn et al., 2004) and NE Brazilian speleothems (Wang et al., 2004). The present day summer position for the ITCZ with its associated atmospheric trade winds (dashed line).

Lynch's Crater (17° 37′ S, 145° 70′ E) is situated at 760 m elevation on the undulating plateau of the Atherton Tableland, 30 km from the east coast of north Queensland, Australia (Fig. 1). At present 70% of the annual rainfall in the area (2570 mm) falls during the austral summer months of November through March (www.bom.gov.au) as a result of seasonal ITCZ migration. The high rainfall allows for the present day growth of luxurious and diverse rainforest vegetation, it previously favoured peat and lake sediment accumulation in depressional settings. The crater itself is approximately 800 m in diameter and contains over 60 m of lake and peat sediments and was formed by an explosive volcanic event ~200,000 years ago (Kershaw, 1978). This study has focussed on the peat deposits of the top 13 m.

Lynch's Crater is a rare site in Australia in that it contains a continuous climate record ideal for high-resolution studies. Palynological work on a core (LC3) from Lynch's Crater has identified major vegetation changes in the last ~200,000 years (Kershaw, 1978; Kershaw, 1986; Kershaw et al., 1993). A peat humification study found climate variations at millennial and orbital time scales over the last 50 kyr (Turney et al., 2004) in response to variations in precipitation regimes. From ~50 kyr, the pollen record reveals a progression from rainforest to an environment dominated by sclerophyll woodland towards the end of the Pleistocene that illustrates decreasing precipitation, later, with higher precipitation a mesophyll vine forest environment dominated the Holocene (Kershaw, 1978; Kershaw, 1986; Kershaw et al., 1993). The peat humification study showed a strong correlation between a high degree of humification and millennial-scale dry periods, in turn these were associated with periods of frequent El Niño events that correlated to Dansgaard-Oeschger warm events in the North Atlantic. Humification is a measure of the decomposition of the organic matter and is influenced by microbial activity and oxidation. Generally, increased humification indicates drier conditions as decomposition increases due to lower groundwater tables, caused by either less precipitation or high peat accumulation rates. However, increased humification can also signal higher seasonal precipitation changes (Mohr et al., 1972).

In 2004 a continuous 13 m peat core (LC2) was obtained from Lynch's Crater using a D-section corer and samples were taken at 10 cm intervals. Twenty-one AMS radiocarbon dates were measured at the Australian Nuclear Sciences and Technology Organisation (ANSTO) and ^{14}C data were calibrated using both IntCal04 and Cariaco Basin datasets (Blockley et al., 2004). Bayesian analysis of the data defined the robust chronology. Peat material was analysed for loss on ignition (LOI) after samples were ignited at 450°C for 12 hrs to provide the 'ash yield' (i.e. content of the inorganic material determined as; ash yield in wt-% = 100 % - LOI). Scanning Electron Microscopy (SEM) analysis was undertaken at the Advanced Analytical Centre (JEOL JSM-5410LV) at James Cook University to assist with the identification of the inorganic fraction. X-ray Fluorescence

Spectroscopy (XRF) was undertaken at the Faculty of Biology, University of Santiago, to determined Si and Al concentrations. The Si content was normalised to Al to approximate a Si content derived from diatom and sponge debris (assuming diatoms/sponges contain no Al) versus Si from other sources (atmospheric dust or terrigenous sediments). The proxy of the Si/Al ratio is used to identify more clearly the transitions between peat sections and layers with high biogenic silica contents. Total biogenic opal content as a percentage of the ash yield was also determined (Mortlock and Froelich, 1989). As a comparison to our proxies, we used the Cyperaceae (sedge) to Poaceae (grass) ratio (Turney et al., 2004) from the LC3 core to reveal temporal change in relative abundance and/or coverage of either sedges or grasses. Higher soil moisture (precipitation) conditions favour high Cyperaceae/Poaceae ratios while lower moisture conditions have low ratios representing paleohydrological conditions. Any changes were further examined by nitrogen isotope data as another hydrological and nutrient proxy. Nitrogen isotope analyses were obtained using a standard elemental analyser isotope ratio mass spectrometer (EA-IRMS). The mass spectrometer was used to combust organic material that in turn forms N_2 and CO_2, which were measured on a Thermo Electron Delta C IRMS in a continuous flow mode at the SERC Stable Isotope Laboratory, Florida International University.

Ash yield for the majority of the peat core was <8 wt-%, with six layers >8 wt-% (Fig. 2). Age and ash yield of these six layers in ascending order from the bottom of the core are as follows: 34-37 kyr (25 wt-%), 28-30 kyr (18 wt-%), 22-25 kyr (25 wt-%), 14.5-16 kyr (36 wt-%), 12.5-13.5 kyr (53 wt-%), and 8.5 kyr (8.5 wt-%). Within these six layers SEM analysis identified abundant biogenic silica components, namely freshwater sponge spicules (Family spongillidae) and some well-preserved diatom frustules, which is attributed to high bioproductivity. A marked change of biogenic silica productivity is also evident from the Si/Al ratios, which are strongly elevated in the aforementioned layers. Low ash yield peat layers have Si/Al ratios of ~1, whereas high ash yield layers have ratios between 7 and 35. Layers 1, 2, 4, and 5 have values of ~20, while layer 3 and 6 have values of 6-7. Opaline silica measurements further confirmed the presence of biogenic silica with values for layers 1-5 of 55%, 50%, 34%, 44% and 56% respectively, for these periods (no data is available for the 8.2 kyr event). Outside these layers microscope analysis shows no evidence of diatom or sponge contributions and the average opaline silica content is <1.1%.

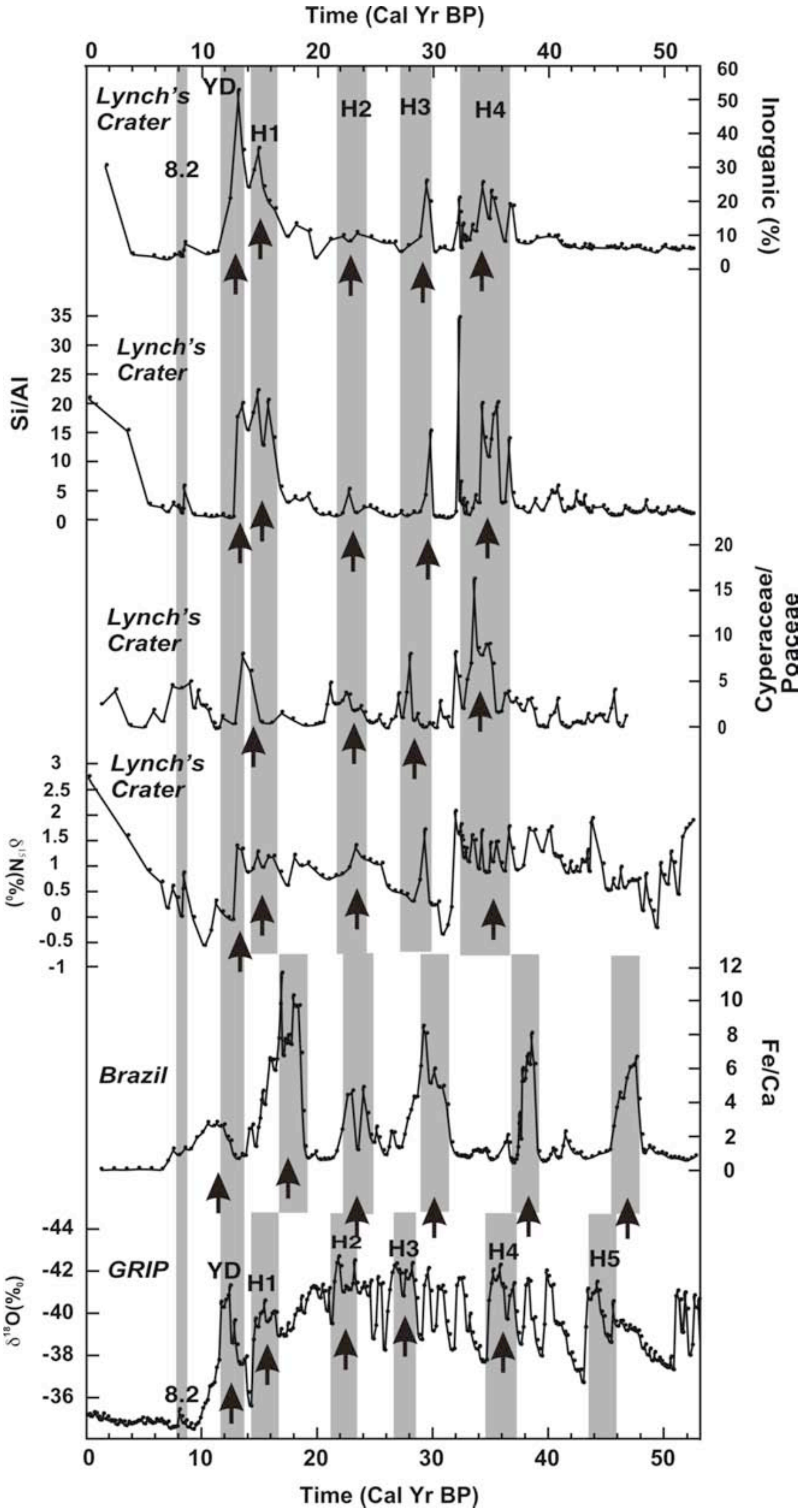

Figure 2: Ash yield (inorganics), Si/Al ratios, Cyperaceae/Poacea ratio (Turney et al., 2004) and $\delta^{15}N$ values, illustrating several wet periods in Lynch's Crater related to the 8.2 kyr event, the Younger Dryas and Heinrich events and correlated with similar precipitation events found in ocean sediments offshore NE Brazil (Jennerjahn et al., 2004) and the $\delta^{18}O$ in summit ice core (GRIP).

An alteration in the Lynch's Crater peat environment must have taken place in order to accommodate the presence of these layers of high biogenic silica within this organic rich deposit. One explanation for the sponge and diatom blooms is that periods of increased precipitation that temporarily elevated water level above the peat surface. Under increased wet conditions, runoff from the crater wall catchment is likely to have contributed superfluous nutrients to the crater floor so periods of standing water masses would have fostered diatom and sponge growth. This is documented from Malaysian peat-forming environments that have standing water for a few months of the year (Wüst and Bustin, 2003).

Other supporting data for significant precipitation changes during the last glacial stem from pollen studies (Turney et al., 2004). Layers with high ash yield coincide with high Cyperaceae/Poaceae ratios, also indicating increased soil moisture content during these periods (Fig. 2). At times the Cyperaceae/Poaceae ratios lag behind the Si/Al, which is most likely due to a slower response time of vegetation compared with that of the chemical changes within the peat deposit, such lags are also evident in other studies (Jennerjahn et al., 2004). A coupled precipitation-vegetation change as indicated by the Cyperaceae/Poaceae ratio is also expressed by the $\delta^{15}N$ data. In Lynch's Crater, heavier $\delta^{15}N$ values are associated with higher Cyperaceae/Poaceae ratios (Fig. 2). Variations are probably due to changing nitrogen sources. While fixation of atmospheric N ($\delta^{15}N = 0$ ‰) is a major N source of land plants, dissolved inorganic nitrogen (DIN, $\delta^{15}N \approx 5\text{-}10$ ‰) is the major N source for aquatic algae (e.g. (Middelburg and Nieuwenhuize, 2001; Wada and Hattori, 1990). Aquatic plants discriminate against ^{15}N during DIN uptake leading to a lower $\delta^{15}N$ than in the DIN reservoir (Talbot and Laerdal, 2000). It is conceivable that during wet periods increased nutrient input promoted primary production of predominantly siliceous algae and sponges leading to the observed higher δ^{15}N values. During dry periods aquatic primary production was less significant, any N deposited would have been primarily derived from atmospheric fixation, resulting in the observed lower δ^{15}N values.

In summary, the peat deposits of Lynch's Crater show several distinct layers (Fig. 2) with synchronous high ash yield, high Si/Al ratios, high Cyperaceae/Poaceae ratios and heavier δ^{15}N isotopes over the last 55 kyr. The layers span the following periods: 34-37 kyr, 28-30 kyr, 22-25 kyr, 14.5-16 kyr, 12.5-13.5 kyr and 8.5 kyr; they are contemporaneous with Heinrich events, the Younger Dryas and the 8.2 kyr event. These timings are all characterised in the Northern Hemisphere as abrupt climate events (Alley and Ágústsdóttir, 2005; Broecker, 1994). The proxy analyses of the peats of Lynch's Crater indicate increased precipitation during these periods. This interpretation is in line with that of other records of the low latitudes from the Atlantic region, for example in speleothem growth phases from caves in NE Brazil (Wang et al., 2004) and terrigenous discharge events identified in ocean sediments, from offshore NE Brazil (Arz et al., 1998; Behling et al., 2000; Jennerjahn et al., 2004) (Fig. 1). The increased precipitation signal corresponds to that of abrupt climate events in the high latitudes.

Our record demonstrates a probable link between the last four Heinrich events, the Younger Dryas and the 8.2 kyr event in the North Atlantic and abrupt precipitation changes at Lynch's Crater. Concomitantly, we can attempt to determine the impact of climate shifts in the Southern Hemisphere and more specifically the western Pacific Ocean during these millennial-scale climate perturbations. Our record also shows that the YD, around 12.5-13.5 kyr, was a significant climate event in tropical Australia which may have lasted for ~1 kyr. The YD event is recorded in Lynch's Crater as the period with highest ash yield (55%) we note that the Si/Al ratios and biogenic silica concentrations for this event are similar to those of the H1 event. The 8.2 kyr event in Lynch's Crater lasted about 400 years and shows lowest ash yield, Si/Al ratios, Cyperaceae/Poaceae ratios and $\delta^{15}N$ isotopes relative to the other abrupt events described above. This is consistent with paleorecords and climate simulations that describe the climate anomalies of the 8.2 kyr abrupt event as smaller, shorter-lived and less extensive than those of older origin (LeGrande et al., 2006).

Heinrich events are linked to large-scale ice discharge into the North Atlantic that disrupt the North Atlantic Thermohaline Circulation. Modeling studies consistently indicate a resulting slowdown in North Atlantic Deep Water (NADW) formation, the so-called ‘ocean conveyor' in response to this large freshwater forcing. Previous climate simulations of the 8.2 kyr event used coupled general circulation models (GCM's) and showed a slowing down of NADW formation with subsequent cooling in the Northern Hemisphere and southward shift of the ITCZ in ocean basins (LeGrande et al., 2006); this is consistent with our record that favours wet conditions at ~8.2 kyr.

In this study a Heinrich-like event was simulated by adding 1 Sv of freshwater over 100 years to the North Atlantic. The simulation resulted in global climate responses including widespread cooling in the Northern Hemisphere and alterations in precipitation patterns (Fig. 3). Specifically, precipitation anomalies include a southward migration of the ITCZ and a zonal shift in mid-latitude storm tracks. Our record of increased precipitation during Heinrich events and the Younger Dryas at Lynch's Crater (17° S) also suggests that these periods coincided ocean/atmosphere system in driving millennial-scale cycles (Clement et al., 2001). Paleorecords from the Santa Barbara Basin suggest that the tropical ocean may have played an important role in high-latitude warming during the last glacial (Hendy and Kennett, 1999). Some climate model simulations have also identified the possible trigger for abrupt events as changes in mean sea surface temperatures in the tropical Pacific caused by variations in insolation (Clement et al., 2001). This all points to abrupt climate events such as Heinrich events having been triggered by "global warming" or shifts in climate systems that originated in the low latitudes.

It is plausible that an initial warming of the equatorial latitudes increased the inter-hemispheric temperature gradient and triggered ITCZ migration before ice-rafting episodes. Interestingly, the records of ITCZ migrations in sediments from the western tropical Atlantic predate the timing of ice rafting in the northern high latitudes (Fig. 2). It is possible that the western tropical Atlantic record shows the initial warming in the Southern Hemisphere tropics. The major question here is whether this temperature gradient is initiated by a warming in the Southern Hemisphere tropics or a cooling in Northern Hemisphere high latitudes. Higher chronological resolution and a combination of different dating techniques of long paleoclimate records that show evidence of past ITCZ migrations would allow us to better address these questions. The role and migration of the ITCZ may be more important than previously thought and could play an important role in the current debate about climate change and ice sheet collapses. In this respect our study provides new evidence from a region in NE Australia/western Pacific where information on millennial-scale climate change from the late Quaternary is scarce.

ACKNOWLEDGEMENTS

This project was funded by the Australian Research Council (DP0456515) and the Australian Institute of Nuclear Sciences and Engineering (PGR8/03). Fieldwork was supported by National Geographic. Thanks to Prof. John Chappell and Damien Kelleher of the ANU, Canberra for field support. For help with isotope analysis thanks to the SERC Stable Isotope Laboratory staff, Florida International University. We acknowledge helpful discussions with Prof. Robert Carter, Kirsten Perry, Dr Jerry McManus, Dr Gavin Schmidt, Dr Pauline Treble, Dr Erica Hendy and Dr Anthony Broccoli and are grateful for the laboratory assistance of Dr Maureen Soon (UBC), Dr Mark Kershaw (FIU), Gordon Warria, Dr Kevin Blake and David Holliday (JCU).

REFERENCES

Australian Government, B.o.M., 2006. Annual rainfall for Atherton Tablelands.

Alley, R.B. and Ágústsdóttir, A.M., 2005. The 8k event: cause and consequences of a major Holocene abrupt climate change. Quaternary Science Reviews, 24(10-11): 1123-1149.

Alley, R.B., Marotzke, J., Nordhaus, W.D., Overpeck, J.T., Peteet, D.M., Jr., R.A.P., Pierrehumbert, R.T., Rhines, P.B., Stocker, T.F., Talley, L.D. and Wallace, J.M., 2003. Abrubt climate change. Science, 299(5615): 2005-2010.

Arz, H.W., Patzold, J. and Wefer, G., 1998. Correlated millenial-scale changes in surface hydrography and terrigenous sediment yield inferred from last glacial marine deposits off northeastern Brazil. Quaternary Research, 50: 157-166.

Behling, H., Arz, H.W., Patzold, J. and Wefer, G., 2000. Late Quaternary vegetational and climate dynamics in northeast Brazil, inferences from marine core GeoB 3104-1. Quaternary Science Reviews, 19: 981-994.

Blockley, S.P.E., Lowe, J.J., Walker, J.C., Asioli, A., Trincardi, F., Coope, G.R., Donahue, R.E. and Pollard, A.M., 2004. Bayesian analysis of radiocarbon chronologies: examples from the European late-glacial. Journal of Quaternary Science, 19(2): 159-175.

Bond, G., Broecker, W., Johnsen, S., McManus, J., Labeyrie, L., Jouzel, J. and Bonani, G., 1993. Correlations between climate records from North Atlantic sediments and Greenland ice. Nature, 365: 143-147.

Broccoli, A.J., Dahl, K.A. and Stouffer, R.J., 2006. Response of the ITCZ to Northern Hemisphere cooling. Geophysical Research Letters, 33(LO1702): 1-4.

Broecker, W.S., 1994. Massive iceberg discharges as triggers for global climate change. Nature, 372: 421-424.

Clement, A., Cane, M. and Seager, R., 2001. An orbitally driven tropical source for abrupt climate change. Journal of Climate, 14(11): 2369-2376.

Dansgaard, W., Johnsen, S.J., Clausen, H.B., Dahl-Jensen, D., Gundestrup, N.S., Hammer, C.U., Hvidberg, C.S., Steffensen, J.P., Sveinbjörnsdottir, A.E., Jouzel, J. and Bond, G., 1993. Evidence for general instability of past climate from a 250-kyr ice-core record. Nature, 364: 218-220.

Gasse, F., 2000. Hydrological changes in the African tropics since the Last Glacial Maximum. Quaternary Science Reviews, 19(1-5): 189-211.

Heinrich, H., 1988. Origin and consequences of cyclic ice rafting in the northeast Atlantic Ocean during the past 130,000 years. Quaternary Research, 29: 142-152.

Hendy, I.L. and Kennett, J.P., 1999. Latest Quaternary north Pacific surface-water responses imply atmosphere-driven climate instability. Geology, 27(4): 291-294.

Hendy, I.L. and Kennett, J.P., 2000. Dansgaard-Oeschger cycles and the California current system: planktonic foraminiferal response to rapid climate change in Santa Barbara Basin, Ocean Drilling Program hole 893A. Paleoceanography, 15(1): 30-42.

Jennerjahn, T., Venugopalan, I., Helge, W., Arz, H.W., Behling, H., Patzold, J. and Wefer, G., 2004. Asynchronous terrestrial and marine signals of climate change during Heinrich events. Science, 306: 2236-2239.

Kershaw, A.P., 1978. Record of last interglacial-glacial cycle from northeastern Queensland. Nature, 272: 159-161.

Kershaw, A.P., 1986. Climatic change and Aboriginal burning in north-east Australia during the last two glacial/interglacial cycles. Nature, 322: 47-49.

Kershaw, A.P., McKenzie, G.M. and McMinn, A., 1993. A Quaternary vegetation history of northeastern Queensland from pollen analysis of ODP Site 820. In: J.A. McKenzie et al. (Editors), Proceedings of the Ocean Drilling Program, Scientific Results, 133: 107-114. Texas A & M University, Ocean Drilling Program, College Station, TX, United States.

LeGrande, A.N., Schmidt, G.A., Shindell, D.T., Field, C.V., Miller, R.L., Koch, D.M., Faluvegi, G. and Hoffmann, G., 2006. Consistent simulations of multiple proxy responses to an abrupt climate change event. PNAS, 103(4): 837-842.

Middelburg, J.J. and Nieuwenhuize, J., 2001. Nitrogen isotope tracing of dissolved inorganic nitrogen in tidal estuaries. Estuarine, Coastal and Shelf Science, 53: 385-391.

Mohr, E.C.J., Van Baren, F.A. and Van Schuylenborgh, J., 1972. Factors governing the formation and decomposition of organic matter. In: E.C.J. Mohr, F.A. Van Baren and J. Van Schuylenborgh (Editors), Tropical Soils - a comprehensive study of their genesis. Mouton - Ichtiar Baru - Van Hoeve, pp. 168-187.

Mortlock, R.A. and Froelich, P.N., 1989. A simple method for the rapid determination of biogenic opal in pelagic marine sediments. Deep-Sea Research, 36(9): 1415-1426.

Peck, J.A., Green, R.R., Shanahan, T., King, J.W., Overpeck, J.T. and Scholz, C.A., 2004. A magnetic mineral record of late Quaternary tropical climate variability from Lake Bosumtwi, Ghana. Palaeogeography, Palaeoclimatology and Palaeoecology, 215: 37-57.

Schmidt, G.A., LeGrande, A.N. and Hoffman, G.L., Submitted. Water isotope expressions of intrinsic and forced variability in a coupled ocean-atmosphere model. Journal of Geophysical Research.

Talbot, M.R. and Laerdal, T., 2000. The Late Pleistocene - Holocene palaeolimnology of Lake Victoria, East Africa, based upon elemental and isotopic analyses of sedimentary organic matter. Journal of Paleolimnology, 23: 141-164.

Turney, C.S.M., Kershaw, A.P., Clemens, S.C., Branch, N., Moss, P.T. and Fifield, L.K., 2004. Millennial and orbital variations of El Niño/Southern Oscillation and high-latitude climate in the last glacial period. Nature, 428: 306-310.

Wada, E. and Hattori, A., 1990. Nitrogen in the sea: Forms, abundances, and rate processes. CRC Press, Boca Raton, 224 pp.

Wang, X., Auler, A., Edwards, L., Cheng, H., Cristall, P., Smart, P.L., Richards, D.A. and Shen, C.-C., 2004. Wet periods in northeastern Brazil over the past 210 kyr linked to distant climate anomalies. Nature, 432: 740-743.

Wells, N., 1997. The atmosphere and ocean: a physical introduction. John Wiley & Sons Ltd, West Sussex.

Wüst, R.A.J. and Bustin, R.M., 2003. Opaline and Al–Si phytoliths from a tropical mire system of west Malaysia: abundance, habit, elemental composition, preservation and significance. Chemical Geology, 200(3-4): 267-292.

CHAPTER 5

Factors affecting peat composition and evolution in a 55 kyr mire deposit in tropical Australia

Adapted from a paper intended for submission to:

Earth and Planetary Science Letters

ABSTRACT

This study endeavors to define the geochemical processes of trace and major element concentrations of Ca, Sr, Mg, Fe, Na, K, P, Si, Al, Ti, La, C, O, N, S, Se, Cl, and Mn along with stable isotopes signatures of N and C, in a tropical peat bog in eastern Australia. Previous studies have extensively researched the dynamics of some elements in peat deposits, we use these alongside elements that are poorly understood in the hope of better defining their processes and activity. A principle component analysis (PCA) is applied in order to define patterns and variability among the elements. It was found that six primary factors affected the elements used in this study: Calcium, Mg, Sr, N and S, are largely controlled by leaching processes and recycling via vegetation; Al, Ti, Si, C and O are essentially regulated by mineral fluxes and the subsequent loss of organic matter. The processes affecting K and Se in Lynch's Crater are not yet understood. Stable C and N isotopes principally reflect changes in the C fractionation, most likely linked to changes in vegetation type influenced by precipitation and humidity variance.

The study also identified Cl as being fundamentally controlled by changes in precipitation. Chlorine variations in Lynch's Crater provide a continuous, high-resolution record of regional precipitation change over the past 55 kyr. This record shows broad scale similarities to other Australian paleo-precipitation records, where increased Cl values coincide with the early Holocene and possible periods of intense monsoonal activity at about 42-55 kyr. The low Cl values coincide with the late Pleistocene (~18-30 kyr), known as a significantly dry period across Australia. A detrended Cl record indicates increased precipitation in the tropics that can be associated with warm periods in the high northern latitudes know as Dansgaard-

Oeschger cycles. Variations display a remarkable resemblance to the oxygen isotope records from the Greenland Ice Core Project (GRIP), implying a global climate signature in the Southern Hemisphere tropics.

1. INTRODUCTION

The global climate of the last 55 kyr was strongly influenced by Dansgaard-Oeschger cycles (D-O cycles) and Heinrich events detected in both GRIP and GISP ice core records (e.g. Bond, 1993). D-O cycles are climate fluctuations that represent ~1500 yr successions of rapid warming events termed interstandials, which are followed by slow cooling episodes termed stadials. These cycles have been documented in both terrestrial and marine records around the world and indicate global forcing (Leuschner and Sirocko, 2000). Heinrich events are related to D-O events in that they disrupt the climate by altering North Atlantic Thermohaline Circulation (NATC) causing cooling in the Northern Hemisphere (Broecker, 1994). Although records from New Zealand (Hellstrom et al., 1998) and South America (Jennerjahn et al., 2004) demonstrate direct links to climate shifts during these events, the implications for climate in Australia remain unclear. A few studies have documented cyclic changes (De Deckker, 2001; De Deckker et al., 1991; Skilbeck et al., 2005; Turney et al., 2004) in Australia over the last 55 kyr, of which only a pollen and peat humification record of Lynch's Crater in NE Australia illustrated possible D-O cycles and Heinrich events in Australia (Turney et al., 2004).

Paleoclimate work from Australia show marked rapid changes in precipitation during the late Pleistocene and Holocene these studies used various proxies in a range of records are used, such as pollen and peat humification of peat deposits (Bralower et al., 2002; Haberle, 2006; Turney et al., 2001), sedimentary changes in lake deposits (Bowler et al., 2001; Magee et al., 2004) and C-isotopes of emu egg shells (Johnson et al., 1999). Together these records show broad scale precipitation trends in Australia during the past 55 kyr. Interestingly, the records show that 45-55 kyr ago, it may have been wetter than it is today and all records show largely drier conditions between 35-16 kyr ago (Bralower et al., 2002; Bowler et al., 2001; Johnson et al., 1999; Magee et al., 2004).

Peat deposits are important paleoenvironmental repositories so are invaluable archives of past climate and ecology. Interest in the geochemical record preserved in peat as a means to understanding past environmental and even climate changes has increased in the past three decades (Bindler, In press). Peat deposits are similar to lake sediments where the continuous deposition of organic material allows the preservation of past geochemical signatures (Martínez-Cortizas et al., 1999; Shotyk et al., 1998; Weiss et al., 2002; Wüst and Bustin, 2003). Most records studied span only the last 10-14 kyr and only a few peat records provide information on the late Pleistocene (Anshari et al., 2001; Maloney, 1995)

This study investigated the peat deposits of Lynch's Crater because of its potential of providing a long, high-resolution record of climate change. The deposit lies on the Atherton Tablelands in NE Australia (17°37'S, 145°70'E), an area characterised by high precipitation (3500-5400 mm/yr) and rainforest vegetation (forest clearance took place during the early 20th century). Lynch's Crater is a volcanic crater filled in with lake and peat sediments, it was first studied in the 1970's (Kershaw, 1974). The uppermost 15 m (~50-60) are composed of peat and were investigated in the mid 1990's in order to document human arrival in Australia (pollen and charcoal) (Turney et al., 2001). This new study presents geochemical proxies of a 13 m (~55 kyr) peat core collected in 2003 including total; carbon (TC), nitrogen (TN), oxygen (TO), and sulfur (TS), along with chlorine (Cl) and potassium (K), and stable C and N isotopes. The objectives were to examine: (a) the elemental dynamics of the peat deposit; (b) the potential of geochemical proxies for reconstructing past precipitation; (c) the use of geochemical data for identifying climate change and climate cyclicity; and d) environmental changes recorded in Lynch's Crater in comparison with other records from Australia.

2. GEOCHEMICAL PROXIES FOR PALEOHYDROLOGY IN PEAT

2.1. Chlorine in peat

Chlorine in peat deposits is mainly sourced from Cl bearing sedimentary rocks and seawater, its influx is driven by water and hence values may indicate both source and/or wetness variations (Shotyk, 1997). The few studies that have focused on halogens in organic deposits have demonstrated conservative behaviour of Cl and shown that almost all Cl (up to 95%) occurs as organo-chlorinated compounds (Biester et al., 2004; Johanson et al., 2003). The distribution of organic Cl in the deposits is closely related to chloride that is a measure of the concentration in the atmosphere and thus Cl values in peat deposits may be entirely controlled by halogen values in rainwater.

2.2. Stable isotopes in peat deposits

Isotopic composition of peat material provide information of ecological conditions and biogeochemical processes, such as vegetation, nutrient status, and water stress (Anderson et al., 2005). Carbon isotope ratios in plants are regulated by photosynthetic fixation of CO2, which is transferred through stomatal openings or diffuses through the cellular membranes (Anderson and Fourqurean, 2003). The isotopic signature of most terrestrial plants typically falls within two groups, determined by photosynthetic pathway (C3 or C4). C3 plants have bulk δ^{13}C values of -22 to -33‰ (average -27‰), while C4 plants exhibit $\delta^{13}C$ values of -9 to -16‰ (average -13‰) (Street-Perrott et al., 1997; Deines, 1980).

The marked difference between C3 and C4 plants is that the first product of C3 plants (most trees and shrubs) during photosynthesis is a three-C acid, which makes them susceptible for physiological droughts (Street-Perrott et al., 1997). In contrast, C4 plants (e.g. most savanna grasses and sedges) possess a CO_2-concentrating mechanism that makes them more efficient than C3 plants in low moisture conditions. The $\delta^{13}C$ of C3 plants is sensitive to variations in humidity or precipitation and is mainly influenced by soil-water-content or precipitation (Francey and Farquhar, 1982; Sternberg et al., 1984; White et al., 1994) as determined in variations of $\delta^{13}C$ in tree rings (Anderson et al., 1998; Sauer and Siegenthaler, 1989; Stuiver and Braziunas, 1987).

Stable N isotopes also offer information about past ecological conditions and biogeochemical processes in peat deposits. Often variations in N isotopes are due to changing nitrogen sources. While fixation of atmospheric N ($\delta^{15}N = 0$ ‰) is a major N source of land plants, dissolved inorganic nitrogen (DIN, $\delta^{15}N \approx 5$-10 ‰) is the major N source for aquatic algae (e.g. Middelburg and Nieuwenhuize, 2001; Wada and Hattori, 1990). Algae discriminate against ^{15}N during DIN uptake leading to a lower $\delta^{15}N$ than in the DIN reservoir (Talbot and Laerdal, 2000). Therefore, during wetter conditions where primary production (algae) increases a change to heavier $\delta^{15}N$ values may be observed and vice versa for dry periods where any N deposited is predominantly derived from atmospheric fixation, resulting in lower $\delta^{15}N$ values.

3. MATERIALS AND METHODS

3.1. Site Description, Sample Collection, pH and Ash Yield Determination

Lynch's Crater (17°37'S, 145°70'E; altitude 760 m) is situated on the Atherton Tablelands in NE-Australia (Fig. 1). Prior to forest clearance in the late 19th and early 20th century it was surrounded by complex lowland to lower montane rainforest supported by seasonally distributed annual rainfall of about 2600 mm (www.bom.gov.au). The crater was formed by an explosive volcanic event ~200,000 years ago and subsequently filled with about 65 m of lake and peat deposits. A 13 m long core (LC2) was collected using a D-section Russian corer from the centre of Lynch's Crater in July 2003. From 0-10 cm a monolith was cut from a hummock using a stainless steel knife and divided into 2 cm increments then packed in plastic bags. The core was described in the field and the sections wrapped in aluminium foil.

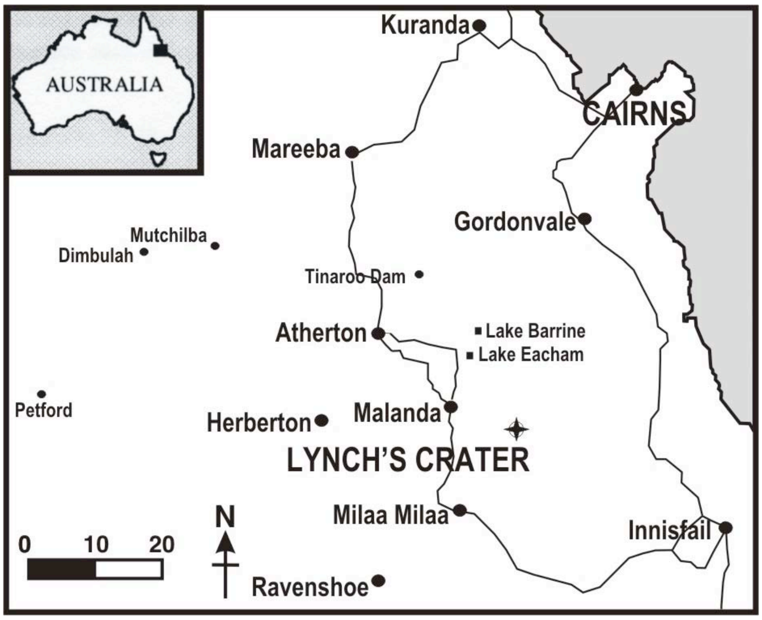

Figure 1: Location of Lynch's Crater in north Queensland, Australia.

In the laboratory samples taken at 10 cm increments were placed in plastic bags and freeze-dried. Once dried, samples for geochemistry were cut and milled by hand using a mortar and pestle, then passed through a 500 μm sieve, milled again and put through a 250 μm sieve; rootlets were removed with the aid of a microscope. All utensils were thoroughly cleaned with ethanol between samples. Loss on ignition (LOI) was determined by heating sample material at 450°C overnight and cooling in a desiccator for 15 min. The weight loss was used to calculate the ash yield or inorganic content (=100% - LOI), expressed as dry weight.

3.2. Radiocarbon Dating

Radiocarbon ages were obtained from bulk peat samples by accelerated mass spectrometry (AMS) at the Australian Nuclear Sciences and Technology Institute (ANSTO, Lucas Heights, Australia) (Table 1, Chapter 3). Peat material was dried and sieved with a 500 μm and then 250 μm sieve and remaining root material was removed under a microscope. Samples were subsequently milled with a mortar and pestle and milled samples were pre-treated with HCl-NaOH-HCl, washed with milli-Q water and then freeze dried for AMS analysis. Detailed analytical procedures are outlined in Fink et al., (2004). The radiocarbon ages were calibrated using a Bayesian calibration by means of OxCal and the IntCal04 and Cariaco Basin datasets (Blockley et al., 2004). The age models were bounded. Data points were extrapolated using a linear regression to obtain chronology for the bottom section 1040-1300 cm.

3.3. Chemical Analysis and Isotope Measurements

Peat samples were oven dried and homogenised before chemical pre-treatment. Carbon, S and N were measured by an Elementar Vario Max CNS Analyzer. The detection ranges for C, N, and S are > 0.02-200 mg, 0.02-30 mg, and 0.02-15 mg, respectively. The precision is <0.5% rel. Ground sample material was used for the analysis. Chlorine, Si and O were measured by X-ray fluorescence under vacuum and standard reference materials NIST-1515, NIST-1547 and NIST-1632 were used to calibrate the equipment, detection limits for these elements are 10 µg/g and 100 µg/g respectively. Oxygen was measured using Carlo Erba EA 1008 with a detection limit of 0.01%.

Isotopes were determined at the SERC Stable Isotope Laboratory (Florida International University, Miami) using standard elemental analyzer isotope ratio mass spectrometer (EA-IRMS) procedures. The EA is used to combust organic material forming N_2 and CO_2, which were measured on a Thermo Electron Delta C IRMS in a continuous flow mode. The samples' isotopic ratios (R, ^{13}C/^{12}C or ^{15}N/^{14}N) are reported in the standard delta notation (‰): _ (‰) = {(R_{sample}/$R_{standard}$)-1} ¥ 1000. These results are presented with respect to the international standards of atmospheric N (AIR, N_2) and Vienna Pee Dee belemnite (V-PDB) for C. Analytical reproducibility of this study based on sample replicates (n=22) is better than ± 0.23‰ for δ^{15}N and ± 0.09‰ for δ^{13}C. The δ^{13}C deviation from the δ^{13}C mean of all samples is given (Fig. 3).

3.4. Principle Component Analysis

Principle component analysis (PCA) was done using ash yield and the selected geochemical data using the statistical package for the social sciences (SPSS) to reduce the multidimensional dataset to a lower dimensional dataset. Factor analysis, which reduces the number of observed variables to fewer variables (factors), was also applied in order to obtain insights into the variability among variables. The observed variables are modeled as linear combinations of the factors, this statistical approach identifies the most important (i.e. defining) parts or elements whilst simultaneously filtering “noise” within the dataset.

4. RESULTS

4.1. Ash Yield

In the top 140 cm of the deposit, the ash yield is lowest (2-5%) with a high value in the top 10 cm (31%). Low ash yield is indicative of ombrotrophic peat and previous work has shown the ombrotrophic/minerotrophic boundary resides at 150 cm depth (Muller et al., 2006). Low ash yields are also seen in the lowermost section of the core between 900-1300 cm (<8%) cm, between 610-690 cm (8-10%) and between 370-470 cm (7-10%) (Fig. 2). Between 150 and 800 cm, there are four distinct horizons (1-4) with a sharp increase in ash yield observed at: 690-720 cm (25%), 560-610 cm (18%), 480-500 cm (25%) and 150-270 cm (53%).

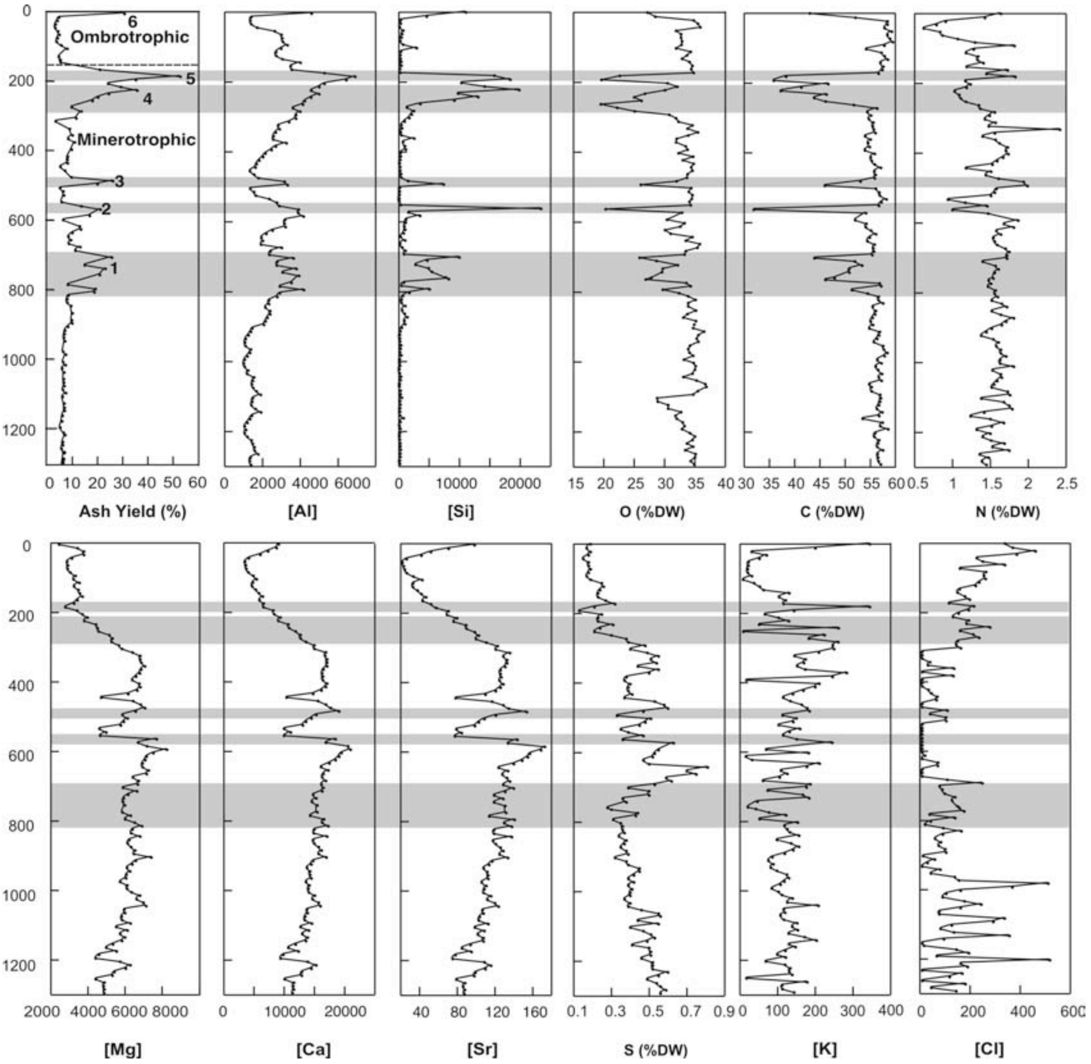

Figure 2. Ash yield and elemental concentration and content profiles of the Lynch's Crater peat deposit. Shading indicates high ash yield layers.

4.2. Elemental Profiles

Aluminium and Si concentrations show similar trends to that of the ash yield and Si concentration profiles (Fig. 2). Concentrations reveal four (1-4) units with increased values at 690-800 cm (maximum ~4300 µg/g), 550-590 cm (~4400 µg/g), 480-500 cm (~3500 µg/g) and 190-210 cm (~7200 µg/g) with an average background concentration of ~1400 µg/g. In the uppermost section, between 10-190 cm depth, concentrations decrease to ~1600 µg/g followed by high concentrations in the top 10 cm (5000 μg/g). Silica concentrations (Fig. 2) are also increased in the layers where Al concentrations are high: 690-800 cm (maximum of ~100000 μg/g), 550-590 cm (~235000 μg/g), 480-500 cm (~74000 μg/g) and 190-210 cm (~199000 μg/g) against background concentrations of ~3000 μg/g. Near the surface, concentrations increase again to 111000 μg/g.

Oxygen and C contents show similar trends (Fig. 2). Oxygen values decrease from 35% in the bottom of the profile to 28% at 1100 cm. At 1090 cm values return to 35% and remain constant at ~35% between 850-190 cm with the exception of four distinct units (1-4) that show sharp negative deviations. These occur at 690-800 cm (maximum of ~25%), 550-570 cm (~20%), 480-500 cm (26%) and 190-220 cm (~19%). In the top 10-180 cm of the core values return to ~34%, with a decrease in values in the top 10 cm to 47%. Carbon contents show similar trends to O contents. Values are constant at ~57% from 190-1300 cm (Fig. 2) with the exception of the four distinct units (1-4) at 690-800 cm (maximum C content of ~44%), 550-570 cm (~32%), 480-500 cm (45%) and 190-220 cm (~35%). In the top 10 cm the C content decreases to 43%.

Nitrogen contents range from 1.2 to 1.8% between 1000-1300 cm (Fig. 2). Between 700-1000 cm values are ~1.6% and then increase to ~1.8% between 590-700 cm. Between 560-590 cm values decrease to ~0.9% and increase again to a peak of ~1.9% at 500 cm. Between 350-500 cm ratios are ~1.6% with a sharp increase of 2.4% observed at 350 cm. Between 200-350 cm values decrease to 1.2% and then increase to ~1.7% between 80-200 cm. At 40 cm depth the lowest values of 0.7% occur and then increase again to baseline values in the surface.

The C/N ratios are ~35 between 600-1300 cm depth and increase to ~60 towards 530 cm depth before decreasing to 25 towards 490 cm depth. Ratios increase again to ~50 between 450-490 cm then decrease to ~30 at 380 cm. Ratios decrease once again at 330 cm to ~25 then increase to ~35 between 200-330 cm. Between 180-200 cm ratios decrease to ~20 and then begin to rise between 180-40 cm to the highest ratio within the record of ~95 and then decrease to ~25 between 40 cm and the surface.

Potassium concentrations (400 µg/g) decrease slightly from the base of the core to a depth of 700 cm (170 µg/g) (Fig. 2). Between 700-230 cm the values generally increase and show large variability. A sharp decrease (9 µg/g) is observed at 250 cm, with an increase to a peak (345 µg/g) at 180 cm. Concentrations steadily decrease (33 µg/g) to a depth of 20 cm after which K concentration increases sharply to 345 µg/g within the surface layer.

Magnesium concentrations show similar trends to that of the Ca and Sr (Fig. 2). Concentrations of Mg increase from ~5000-6000 µg/g between 1000-1300 cm and remain ~6400 µg/g between 700-1000 cm depth. Concentrations increase up to 8270 µg/g towards 600 cm, then decrease to ~6400 µg/g briefly at 550 cm and increase again to a peak of ~7000 µg/g at 480 cm depth. Again concentrations decrease to ~6400 µg/g at 450 cm and then rise to ~6000 µg/g at 400 cm depth where they remain up to 320 cm depth. Concentrations gradually decrease to low levels of ~2500 µg/g at the surface. Calcium concentrations increase from 12500 µg/g to ~15000 µg/g between 1000-1300 cm and remain at ~15000 µg/g between 1000-720 cm. After 720 cm depth, values increase to ~20000 µg/g at a depth of 600 cm then decrease to ~9000 µg/g between 400-550 cm with a peak of ~17500 µg/g at 480 cm depth and then rise to ~15000 µg/g, where concentrations remain between 320-400 cm. From 320 cm depth, concentrations gradually decrease to low levels of ~5000 µg/g at the surface. Strontium concentrations increase from 80-

120 μg/g between 1000-1300 cm and follow concentrations of 120 μg/g up to 650 cm depth. Concentrations increase to 170 μg/g towards 600 cm, then decrease to ~70 μg/g briefly at 550 cm and increase again to a peak of ~150 μg/g at 480 cm depth. Values decrease to ~70 μg/g at 450 cm and then rise to 120 μg/g between 320-400 cm. From 320 cm depth values gradually decrease to levels of ~20 μg/g at 40 cm and increase to 100 μg/g in the surface layers.

Sulfur shows similar trends to Ca, Mg and Sr, with some differences. Values continuously decrease with small fluctuations from ~0.5 to 0.3% between the base and 800 cm depth then increase steadily to 0.8% at 640 cm depth (Fig. 2). Values decrease to 0.5 % at 630 cm and then increase again to 0.6 % at 570 cm. Between 440-570 cm several peaks of up to ~0.7 % occur, most have a value of ~0.4%. Values of 0.4% are observed between 380-440 cm depth that slightly decrease between 380-440. Between 270-380 cm values are slightly elevated at ~0.6 % and decrease between 190-270 cm to their lowest value of ~0.1% at 190 cm. Briefly, values return to 0.38% at 170 cm and then steadily decrease to ~0.2 % towards the surface.

Significant fluctuations in Cl concentrations are seen at the base of the core between 970-1300 cm, with four peaks at depths of 1200 cm (500 μg/g), 1120 cm (375 μg/g), 1080 cm (370 μg/g) and 980 cm (500 μg/g). These peaks constitute the highest concentrations of Cl within the profile. Between 660-970 cm, Cl concentrations are low and several samples had values below the detection limit (10 μg/g). Concentrations increase to higher values (~200 μg/g) in the top of the section around 670 cm. Between 320-660 cm Cl concentrations are again low (10-120 μg/g) and sometimes drop below the detection limit. Concentrations begin to increase steadily between 320 cm (150 μg/g) and the surface (450 μg/g).

4.3. Carbon and Nitrogen Isotopes

The heaviest C isotope values (– 22‰) occur between 1200-1300 cm depth (Fig. 3). Between 1000-1200 cm deviations from values of -27‰ to -28‰ occurs with one significant deviation of –25‰ at 1180 cm. The uppermost 1000 cm of the deposit shows values of –27‰, with one excursion between 530-550 cm of –28.5‰ and heavier isotopic composition in the surface layer of –25‰.

The N isotope analysis shows that the basal 20 cm has heavy N isotope values (~2‰) followed by fluctuations (–0.8‰ and 1.6‰) between 1150-1280 cm depth. Between 1050-1150 cm values are steady at ~0.7‰ but become heavy at 1030 cm (2‰). Between 600-1030 cm isotopic compositions are ~1.2‰ and become heavy (2‰) again at 550 cm. A significant drop to negative isotopic values (-0.3‰) is observed between 520-540 cm, which increase quickly to a peak of 1.8‰ at 480 cm. Another quick drop in values to 0.3‰ is observed at 450 cm and then values begin to increase steadily again to 1.7‰ between 270 -450 cm. Between 190-270 cm depth, isotopic values are ~1.2‰ but become rapidly lighter (0‰) at 180 cm. From 180 cm to the surface isotopic values increase steadily to 2.8‰ with a two small peaks at 100 cm (0.8‰) and 140 cm (0.3‰).

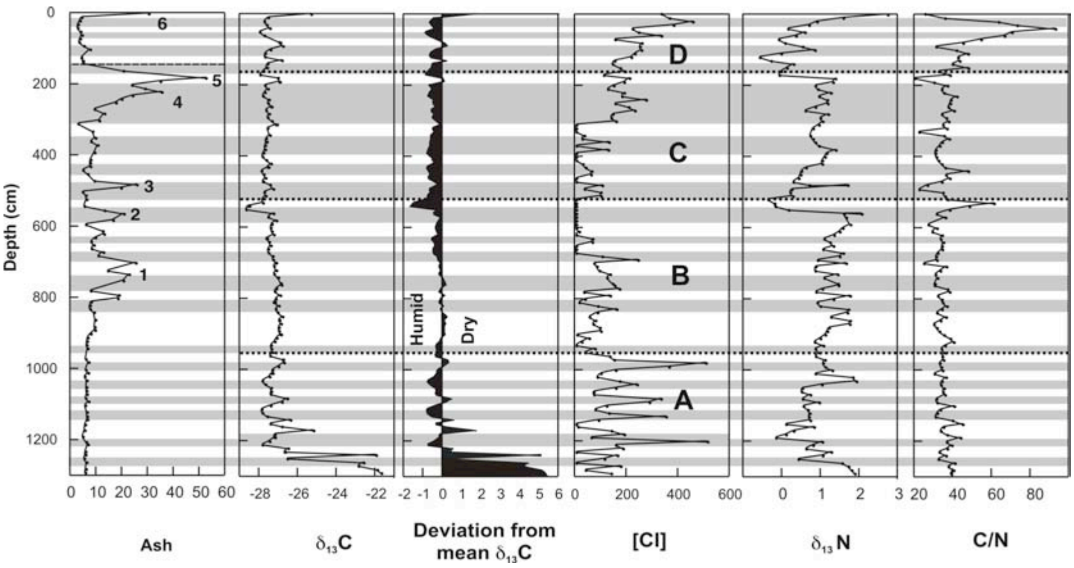

Figure 3: Carbon and nitrogen isotope profiles, with ratio profiles of the Lynch's Crater peat deposit. Shading indicates higher moisture conditions.

4.4. Principle Component Analysis

Factor analysis of the geochemical data of Lynch's Crater shows that six factors explain 85% of the total variance (Fig. 4). Factor 1 (F1) explains 28.7% of the variance and the higher factor loadings of this group includes Ca, Sr, Mg and Na (>0.8). Moderate loadings include N, δ^{15}N and S (0.67-0.58) and lower negative loadings are shown by Cl and Se (-0.40 and –0.34) (Fig. 4). Factor 2 (F2) explains 24.1% of the total variance, where elements Si, P, Al and La have high positive loadings (>0.7). Moderate positive loadings are shown with La and Ti (0.67 and 0.6) and high negative loadings are shown by C and O (-0.93 and -0.80). Factor 3 (F3) explains a 12.3% of the total variance showing positive loadings for Se (0.79), Ti (0.69) and La (0.54), while Mn has a negative loading (-0.72). Factor 4 (F4) explains 7.9% of the variance and is dominated by the δ^{13}C record (0.93), but it is also partly associated with Mn (0.5) and δ^{15}N (0.46). Factor 5 (F5) explains 6.6% of the variance and is dominated by Cl (0.79) and has low negative loadings for S,

5. DISCUSSION

5.1. Elemental Dynamics in the Lynch's Crater Peat Deposits

The composition and elemental dynamics of peat deposits can vary significantly from site to site. Many peat deposits from N-Europe and N-America, have been geochemically characterized and are thus well understood, however little information is know on the geochemical characteristics of tropical peats (Gorham and Janssens, 2005; Martínez-Cortizas et al., 1997; Norton, 1990; Shotyk et al., 1990). It is critical to understand the topographic setting and hydrology including trophic status, of these deposit prior to geochemical studies. Several factors influence the geochemical composition and elemental concentrations, some of these are: influx rate, organic matter accumulation rate, vegetational composition, rate of leaching, pH and precipitation changes. Such factors may change over evolution of the peat deposit. The following section discusses these factors and their importance throughout the Lynch's Crater peat.

5.1.1. Factor 1 (Ca, Mg, Sr, N, S and δ^{15}N)

Factor 1 (F1) includes elements that are highly mobile in peat deposits (Ca, Mg, Sr) it also shows some association with N and S and part of the variance of the δ^{15}N record (Fig. 4). In general, positive scores of F1 (~1) occur in the minerotrophic section; slightly negative scores are observed in the lowermost deposits (1040-1300 cm) and at two periods, centered at 520 and 440 cm depth, relatively positive values were recorded (1-2.8) between 560-700 cm. Mobility of elements in peat deposits is controlled by factors including the trophic status, biocycling, bioavailability, nutrient requirements of living plants and precipitation and the groundwater flow.

The characteristic patterns of elements associated with F1 (Fig. 5) are high values in the deeper, minerotrophic peat and low values in the uppermost ombrotrophic section (Fig. 2). Previous studies have shown that ground water is a major control on elements such as Ca, Mg and Sr with up to 200 fold increases in elemental concentrations within minerotrophic settings (Wüst and Bustin, 2003). Ions can enter the peat column as dissolved species via diffusion and subsequent transport in groundwater they will eventually fix to ions surrounding peat layers, this ‘binding’ of ions is the likely explanation for the enrichment of Ca, Mg and Sr (Steinmann and Shotyk, 1997). Previous work has shown the influence of vegetation on post-depositional remobilisation of elements such as Ca, Mg and Sr, these are known to be the plant essential elements (PEE). There is often significant enrichment of PPE in the surface layers due to the biocycling of PEE within the root zone (Weiss et al., 2002; Wüst and Bustin, 2003), this is seen at Lynch’s Crater, where the surface layer has higher PEE concentrations than the subsurface. This is common for an ombrotrophic peat deposit that receives limited nutrient input where the plants rely more on biocycling of PEEs because free elements are generally less abundant. This is also evident from the low F1 scores that most likely represent lower nutrients availability/input. In the minerotrophic setting (150-1300 cm) PEE are abundant, this may indicate that less biocycling has occurred in the lower deposits of Lynch’s Crater.

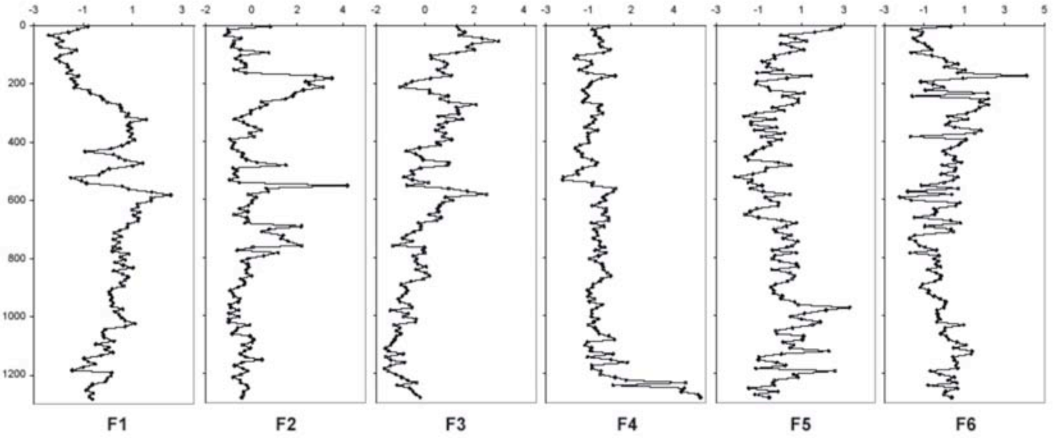

Figure 5: Variations of factor scores (F1-F6) against depth of the Lynch's Crater deposit.

The S content has a similar trend to the bio-essential elements discussed above and is strongly associated with F1 (Fig. 2). However, S is not solely confined to F1, in fact, 23% of its variance is unexplained by the 5 primary factors. The S in this deposit shows subtle differences in its concentration profile compared to that of the bio-essential elements. In other freshwater peat deposits almost all S occurs in a reduced form and ~75% to 85% of the total S is organically bound, the remaining portion is inorganic S, generally in the form of iron sulfides (Mandernack et al., 2000). At Lynch's Crater it is possible that part of the S has undergone geochemical change in the more anoxic part of the catotelm, resulting in the formation of inorganic sulfides. A study from freshwater peats in Malaysia has shown abundant inorganic S (framboidal pyrite) deposited within plants cells as a result of microbial activity and chemical changes probably associated with burial and hence oxidation of the organic matter (Wüst et al., 2002). In Malaysia water table fluctuations are common throughout the year as precipitation depends on monsoonal activity, such water table changes are critical for oxidation processes in peatlands and are known to increase organic sulfate oxidation in peat deposits from Europe (Steinmann, 1997). Groundwater fluctuations also have significant implications for the distribution of Ca, Mg and Sr, however, some other controlling factors are responsible for the S concentration profile, possibly due to oxidation processes that increase the organic sulfate oxidation in Lynch’s Crater.

Nitrogen and N isotopes are also associated to F1 (Fig. 4). Nitrogen concentrations are moderately associated to F1, they show a definite affinity to post-depositional remobilisation. In the minerotrophic section the N content is relatively high, this may be due to the availability of N in groundwater. Where there is limited groundwater in the ombrotrophic section the N content is low, however, due to its low availability, this element will be precious to living organisms such as plants, actynomycetes, and other microbes, their use of N will further lowering it’s concentration. Nitrogen is not solely confined to F1, half of its variance is unexplained by the 6 primary factors and this variation is difficult to understand. There are many other processes that may explain N variability, for example, mineralization, erosion, denitrification, grazing, and burning. It is unlikely that mineralization or erosion substantially contributes to N variation in Lynch’s Crater because the N profile shows little resemblance to F2, this is addressed in the following section. Studies have shown that (Lucas, 1982) that those peat deposits composed of reeds, sedges and trees are generally two to four times higher in nitrogen than those formed of *Sphagnum* mosses, which can contain less than 1 percent N even though the original plant materials contain 1-5 percent. It is possible that vegetation type had a strong influence on the distribution of this element, but further exploration would require a high-resolution pollen record. In order to better understand the dynamics of N in Lynch's Crater further work will be needed.

The heavier N isotopes dominate layers with higher inorganic material (Layer 1-5, Fig. 3) where sponge and diatom fragments occur and nutrient concentrations increased (Muller et al., submitted). These changes of the isotopic values may be the result of different fractionation processes associated with the vegetation at the time of deposition. Isotopic fractionation of aquatic plants may result in heavier isotopic values as terrestrial material is depleted in ^{15}N relative to aquatic plants by at least 4‰ (Letolle, 1980). High nutrient concentration has been associated with high N isotope fractionation when there is a low rate of nutrient utilization (Montoya, 1994). It is likely that during periods of increased precipitation at Lynch's Crater nutrient input also increased, fostering primary productivity and organic matter enriched in δ^{15}N.

5.1.2. Factor 2 (Al, Ti, Si, C and O)

Factor 2 (F2) is strongly associated with Al, Ti, Si, C and O (Fig. 4) and shows very similar trends. The lithophile elements Al, Ti and Si show remarkably similar trends to each other. These elements are typically derived from weathering of the Earth's crust and consequently have a continental origin (Berner and Berner, 1997; Rahn, 1999). Previous studies from Lynch's Crater define the crater wall as the primary source of lithophile elements (Muller et al., Submitted), therefore F2 scores identify periods of increased and decreased weathering of the crater catchment. The F2 scores (Fig. 5) are characterized by a relatively constant low background with high values at 780, 760-790, 550, 480, 250-170 and 90 cm, that also coincide with high ash yield. Previous work identified biogenic silica in the form of diatoms and sponge spicules in the above layers and concluded that their deposition most likely took place during wet events (layers 1-6), where standing water and run off from the catchment fostered their growth (Muller et al., Submitted). These events would also contain Si that is transported to the deposit in clays. In this case significant increases in Si values identify episodes of prolonged standing water on the mire and Si along with other lithogenic elements (Al and Ti) may signify sedimentation/runoff and atmospheric dust deposition of soil eroded within the catchment.

Carbon and O contents exhibit almost opposite trends to Al, Ti, and Si and their association to F2 is due to this mirrored trend. These elements are most abundant in the organic matter and thus respond to the relative proportions of organic material from various sources. Therefore C and O are often controlled by environmental conditions e.g. wetter conditions may result in increased primary productivity, surface run-off, and most likely a high input of terrigenous material and nutrients to the peat deposit, where dry conditions may reduce land productivity and the input of material to peat environments (Gorham and Janssens, 2005). Highly decomposed peats have higher C values than those of lesser decomposed, however the difference is never more than 10 percent (Ekono, 1981) therefore, it is unlikely that the significant changes in C content in Lynch's Crater are associated with the decomposition of peat. Significant decreases in O and C values (45-32%) correspond to the high inorganic layers discussed above (1-5, Fig. 3), therefore it is more likely that the abrupt halt in peat production, as a result of this environmental change, is the primary reason for decreases in C and O values and the association of C and O to F2.

5.1.3. Factor 3 (Se, Ti, La and Al)

Factor 3 (F3) is strongly associated to Se, but also has positive contributions from Ti, La, and Al, and negative contributions from Mn. As discussed above Ti and Al are also strongly associated to F2 whose likely source is from weathering of the crater wall. The Se record displays no obvious trends, our understanding of this element at Lynch's Crater is limited. However, researchers have found correlations between carbon content and Se (Tamari, 1978) and in a previous investigation of Lynch's Crater we hypothesized that part of the Al may have been transported to the peat deposit as organo-Al compounds (Muller et al., Submitted). Predominantly, weathering of the crater wall produces andic soils in which contain abundant organo-Al compounds (Martinez Cortizas et al., In press). There are increases in F3 coinciding with increases in F2 due to increased weathering from the catchment at approximate depths of 780, 760-790, 550, 480, 250-170 and 90 cm. In this case it is possible that F3 may reflect the contribution of Se, Al, Ti and La to the peat mire in clays and subsequent fixation onto organic matter within the peat deposit. At this stage the above interpretation is speculative and more work is need on this topic in order to test this interpretation.

5.1.4. Factor 4 ($\delta^{13}C$ and $\delta^{15}N$)

Factor 4 is dominated by the isotopes C and to a lesser extent (0.46% of the variance) N. Previous work has shown that isotopic fractionation processes are largely dependent on plant type (C3 vs C4) and therefore $\delta^{13}C$ values often reflect vegetation type (Street-Perrott et al., 1997; Deines, 1980). However, in some deposits $\delta^{13}C$ is confined to a C3 signature and as a result differentiation between vegetation type is not viable. Studies have shown that deposits consisting of dominant C3 signatures may be used to illustrate past soil water content or precipitation, due to the sensitivity of C3 plants to moisture (Francey and Farquhar, 1982; Sternberg et al., 1984; White et al., 1994). A study from China demonstrated that high $\delta^{13}C$ values of peat cellulose represented lower soil moisture or precipitation and *vice versa* (Hong et al., 2001).

The above interpretation was also applied to Lynch's Crater where $\delta^{13}C$ values show a dominant C3 plant signature and C isotope data are plotted against the mean to assess past soil moisture changes. Positive deviations denote lower than average soil moisture or precipitation and negative shifts higher soil moisture or precipitation (Fig. 3). At Lynch's Crater, the deviations are modest, except for in the basal 300 cm. Between 1000-1300 cm conditions vary between relatively humid and dry environments, with the driest conditions recorded by the $\delta^{13}C$ proxy between 1250-1300 cm. Between 700-1000 cm conditions are largely dry and between 580-700 cm the $\delta^{13}C$ values indicate humid conditions, however the $\delta^{13}C$ values between 580-1000 remain close to the mean value, indicating that environmental changes may not have been significant during these periods. Between 580-550 conditions on the mire became more humid with the largest negative deviation from the mean at 540 cm and after this conditions remain humid to the top of the core.

As discussed in Chapter 4 $\delta^{15}N$ values are mainly associated to changing nitrogen sources. Here, fixation of atmospheric N ($\delta^{15}N = 0$ ‰) is a major N source of land plants, dissolved inorganic nitrogen (DIN, $\delta^{15}N \approx 5\text{-}10$ ‰) is the major N source for aquatic algae. However, aquatic plants discriminate against ^{15}N during DIN uptake leading to a lower $\delta^{15}N$ than in the DIN reservoir. It is conceivable that during wet periods increased nutrient input promoted primary production of predominantly siliceous algae and sponges leading to the observed higher $\delta^{15}N$ values. During dry periods aquatic primary production was less significant, any N deposited would have been primarily derived from atmospheric fixation, resulting in the observed lower $\delta^{15}N$ values. Therefore, it is likely that the role of $\delta^{15}N$ values in Factor 4 is most likely related to the changing moisture conditions at Lynch's Crater.

5.1.5. Factor 5

Factor 5 (F5) is dominated by Cl, with S and Na has a small contribution, but all loadings are negative. Interestingly the F5 profile shows marked similarities to the precipitation reconstruction inferred from pollen analysis in Lynch's Crater (Kershaw, 1994). From the base to the top, the four main sections of the F5 record correspond to the environments suggested by the pollen: humid (below 950 cm), sub-humid between (670 and 950 cm), semi-arid (320 and 670 cm), and the return to humid climatic conditions (from 320 cm to the top). This implies that F5 may be primarily affected by past precipitation changes (Fig. 3), this is supported by other peat studies that show the strong association between precipitation and Cl (Biester et al., 2004; Hong et al., 2001; Shotyk, 1997).

Chlorine and C isotopes behave differently to one another in peat, where Cl is not associated to plant material and C isotopes are. However this work shows that both proxies may be primarily controlled by precipitation and/or humidity so a correlation between them may be feasible. Most interesting is the variation in C isotopes and the Cl concentrations between 900-1300 cm (grey bars in Fig. 3). The lowermost peat deposition occurred between 42-53 kyr ago when ENSO was active and influenced the climate in Australia (Johnsen et al., 1993) explaining these large shifts between humid and dry conditions. Relatively low Cl values between 700-900 cm correspond the $\delta^{13}C$ deviations that are mostly higher than the overall mean values of the peat. This period was less humid according to the pollen analysis (Kershaw, 1976) that described this time as a transition between a rainforest and a sclerophyll environment. Between 600-700 cm Cl values are relatively high, this is also a time when the $\delta^{13}C$ deviations begin to increase into values higher than the mean, an indicator of relatively humid conditions. Between 520-600 cm Cl values are under the detection limit, this indicates dry conditions concurrently the $\delta^{13}C$ deviates slightly under the mean $\delta^{13}C$ values, but not significantly (-0.5%). This period also resides in the transition between rainforest and sclerophyll environment (Kershaw, 1976), which would explain the low Cl values and $\delta^{13}C$ mean. Between 520 cm and the top of the core, Cl values increase steadily and $\delta^{13}C$ values also move into lower than mean deviations representing humid conditions, however these deviations remain at similar values (~ -1) and do not show the same trend of increasing humidity to the top of the core. This period coincides with the transition of sclerophyll into rainforest (Kershaw, 1976). The Cl record shows marked similarities with the precipitation changes based on Kershaw’s pollen record (Kershaw1994). Similar findings are reported from other organic soils in Sweden where the spatial distribution of Cl is closely related to that of chloride. Here a strong correlation between Cl concentration and Cl (atmospheric deposition) from precipitation was inferred (Johanson et al., 2003).

5.1.6. *Factor 6*

Factor 6 (F6) exclusively contains K implying a different pathway and behaviour than other mobile cations in the Lynch's Crater mire. The factor score variations (Fig. 5) show also the same trend as the K concentration record (Fig. 2). There has been little work done on K, however studies have shown that K resides in the mineral fraction (K-feldspars) of peat (Steinmann and Shotyk, 1997). We do not see this association in Lynch's Crater, as the F6 trend is dissimilar to F2. As with Se, we do not fully understand the dynamics of K and further work is needed in order to use this element as a paleoclimate proxy.

5.2. Precipitation changes in tropical NE Australia

The value of the Cl concentration record as a proxy for past humidity changes was tested by its detrended record, this was compared to other Australian paleorecords (Fig. 6). The basal deposits (~43-52 kyr) with highly variable Cl values correspond to the Araucarian microphyll vine forest of the region, where rainforest gymnosperms and angiosperms and sclerophyll taxa dominated (Kershaw, 1994). As suggested by Johnson (1999) this period was influenced by a highly affective monsoon, which would explain the high Cl values in Lynch's Crater during this time. The Cl profile shows lower and less erratic changes between ~30-42 kyr in Lynch's Crater (Fig. 6), where Kershaw's pollen study (Bralower et al.) identified a transition between an Araucarian microphyll vine forest and sclerophyll forest and Magee (2004) noted low-level lake conditions in the Lake Eyre basin (Magee et al., 2004). It is likely that this period corresponds to an overall reduced precipitation. The detrended Cl record shows the lowest and least variable pattern in precipitation between ~18-30 kyr, which is in agreement with the other Australian records (Fig. 6) of this relatively dry period in Australia. Between ~18 kyr to present the Cl record infers precipitation changes most closely described by a pollen record from Lake Euramoo close to Lynch's Crater on the Tablelands (Haberle, 2006), there, precipitation increased after 16 kyr into the Holocene, showing highest values in the early Holocene. After 4 kyr insufficient Cl data makes precipitation interpretations difficult

Comparisons of the detrended Cl record of Lynch's Crater with the Greenland (GISP) $\delta^{18}O$ record (Fig. 6) shows an in-phase relationship of the paleohumidity levels at Lynch's Crater with the D-O cycles. Over this trend a higher frequency pattern is superimposed, suggesting a cyclic component. Below 670 cm the cyclicity is more regular, showing a peak every ~40 cm, which, considering the peat accumulation rates in this section, may correspond to a 1500-1600 yr cycle (Fig. 7). D-O cycles are climate fluctuations that represent ~1500 yr successions of rapid (decades) warming events (interstandials) followed by slow cooling episodes (stadials) (Leuschner and Sirocko, 2000). Similar warm cycles have been observed in equatorial and sub-equatorial deposits, such as stalagmites from Socotra Island in the Indian Ocean (Burns et al., 2003), marine sediments from the Arabian Sea (Leuschner and Sirocko, 2000) and marine sediments from offshore Brazil in the Atlantic (Arz et al., 1998). Due to the relatively low resolution of the Cl record and current dating methods we cannot be certain of the cyclicity in Lynch's Crater furthermore, possible phase differences between Lynch's Crater and the above records are hard to deduce. This limits possible conclusions on the forcing mechanisms, but the evidence from the tropics and subtropics has implications for the discussion of climate variations on D-O time scales. It is apparent that these cycles are not unique to the Northern Hemisphere or the high latitudes. The important question to address is whether all D-O records respond to the same forcing and if they do, which physical mechanism controls the phase relations between low and high latitudes?

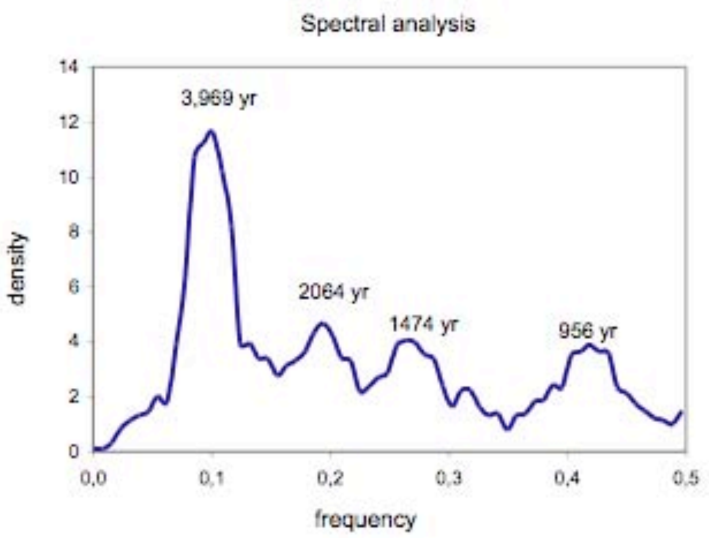

Figure 7: Spectral Analysis to the depth/time series of the detrended Cl profile.

6. CONCLUSIONS

1) The principle component analyses show that six primary factors affect the elements used in this study. F1 is associated to mobile elements (Ca, Mg, Sr, N and S) and is largely controlled by leaching processes and recycling by vegetation. F2 is associated to immobile elements (Al, Ti, and Si, C and O) and is mainly controlled by terrigenous and atmospheric dust influx. F4 is associated to $\delta^{13}C$ and $\delta^{15}N$ and is essentially controlled by changes in the C fractionation possibly linked to changes in vegetation type and/or humidity changes. F5 is dominated by Cl and is fundamentally controlled by precipitation changes. The processes involved in F3 and F6 are undefined.
2) The broad scale precipitation changes recorded in this study show similar dynamics to other Australian paleorecords. Between 42-53 kyr high, but variable precipitation may reflect strong monsoonal patterns in

Australia. Reduced and less variable precipitation is recorded between 30-42 kyr and the lowest precipitation is between 18-30 kyr. A steady increase in precipitation is noted from 18-8 kyr with the high precipitation at 8 kyr, comparable to that of 42-53 kyr. Precipitation appears to decrease between 8-4 kyr and after that (4 kyr – present) there is insufficient data to interpret.

3) A detrended Cl concentration record of the peat deposit of Lynch's Crater demonstrates cyclicities of precipitation change over the last 53 kyr. These span ~1500 yr and coincide with D-O oscillations cycles reported in the GRIP and GISP ice cores.

ACKNOWLEDGEMENTS

This project was funded by the Australian Research Council (DP0456515) and the Australian Institute of Nuclear Sciences and Engineering (PGR8/03). We acknowledge laboratory assistance from Southeast Environmental Research Centre (SERC), Florida International University and the helpful field assistance of David Holliday, James Cook University (JCU). We would like to thank Andrew Smith, Andrew Jenkinson, David Fink and Geraldine Jacobsen Australian Nuclear Sciences and Technology Organisation (ANSTO) for assistance with radiocarbon dating.

REFERENCES

Anderson, W.T., Bernasconi, S.M. and McKenzie, J.A., 1998. Oxygen and carbon isotopic record of climatic variability in tree ring cellulose (*Picea abies*): An example from central Switzerland (1913-1995). Journal of Geophysical Research, 103(D24): 31,625-31,636.

Anderson, W.T. and Fourqurean, J.W., 2003. Intra- and interannual variability in seagrass carbon and nitrogen stable isotopes from south Florida, a preliminary study. Organic Geochemistry, 34(2): 185-194.

Anderson, W.T., Sternberg, L., Pinzon, M.C., Gann-Troxler, T., Childers, D.L. and Duever, M., 2005. Carbon isotopic composition of cypress trees from South Florida and changing hydrologic conditions. Dendrochronologia, 23: 1-10.

Anshari, G., Kershaw, A.P. and van der Kaars, S., 2001. A late Pleistocene and Holocene pollen and charcoal record from peat swamp forest, Lake Sentarum Wildlife Reserve, West Kalimantan, Indonesia. Palaeogeography, Palaeoclimatology, Palaeoecology, 171(3-4): 213-228.

Arz, H.W., Patzold, J. and Wefer, G., 1998. Correlated millenial-scale changes in surface hydrography and terrigenous sediment yield inferred from last glacial marine deposits off Northeastern Brazil. Quaternary Research, 50: 157-166.

Berner, E.K. and Berner, R.A., 1997. Global Environment: Water, Air, and Geochemical Cycles. Prentice Hall, Englewood Cliffs: NJ.

Biester, H., Keppler, F., Putschew, A., Martinez-Cortizas, A. and Petri, M., 2004. Halogen retention, organohalogens, and the role of organic matter decomposition on halogen enrichment in two Chilean peat bogs. Environ. Sci. Technol., 38: 1984-1991.

Bindler, R., In press. Mired in the past - looking to the future: Geochemistry of peat and the analysis of past environmental changes. Global and Planetary Change.

Blockley, S.P.E., Lowe, J.J., Walker, J.C., Asioli, A., Trincardi, F., Coope, G.R., Donahue, R.E. and Pollard, A.M., 2004. Bayesian analysis of radiocarbon chronologies: examples from the European Late-glacial. Journal of Quaternary Science, 19(2): 159-175.

Bond, G., Broecker, W., Johnsen, S., McManus, J., Labeyrie, L., Jouzel, J. and Bonani, G., 1993. Correlations between climate records from North Atlantic sediments and Greenland ice. Nature, 365: 143-147.

Bowler, J.M., Wyrwoll, K.-H. and Lu, Y., 2001. Variations of the northwest Australian summer monsoon over the last 300,000 years: the paleohydrological record of the Gregory (Mulan) Lakes System. Quaternary International, 83-85: 63-80.

Bralower, T.J., Silva, I.P., Malone, M.J., 2002. New evidence for abrupt climate change in the Cretaceous and Paleogene: An Ocean Drilling Program expedition to Shatsky Rise, northwest Pacific. GSA Today, 12(11): 4-10.

Broecker, W.S., 1994. Massive iceberg discharges as triggers for global climate change. Nature, 372: 421-424.

Burns, S.J., Fleitmann, D., Matter, A., Kramers, J. and Al-Subbary, A.A., 2003. Indian Ocean climate and an absolute chronology over Dansgaard/Oeschger Events 9 to 13. Science, 301(1365-1367).

De Deckker, P., 2001. Late Quaternary cyclic aridity in tropical Australia. Palaeogeography, Palaeoclimatology, Palaeoecology, 170: 1-9.

De Deckker, P., Corrège, T. and Head, J., 1991. Late Pleistocene record of cyclic eolian activity from tropical Australia suggesting the Younger Dryas is not an unusual climatic event. Geology, 19: 602-605.

Deines, P., 1980. Handbook of environmental isotope geochemistry, 1. Elsevier, Amsterdam, 329-406 pp.

Ekono, 1981. Report on energy use of peat, Nairobi.

Fink, D., Hotchkis, M., Hua, Q., Jacobsen, G., Smith, A.M., Zoppi, U., Child, D., Mifsud, C., Van der Gaast, H., Williams, A. and Williams, M.A.J., 2004. The ANTARES AMS facility at ANSTO. Nuclear Instruments and Methods in Physics Research Section B: Beam Interactions with Materials and Atoms, 223-224: 109-115.

Francey, R.J. and Farquhar, G.D., 1982. An explanation of 13C/12C variations in tree rings. Nature, 297: 28-31.

Gorham, E. and Janssens, J., 2005. The distribution and accumulation of chemical elements in five peat cores from the mid-continent to the eastern coast of North America. Wetlands, 25(2): 259-278.

Haberle, S.G., 2006. A 23,000-yr pollen record from Lake Euramoo, wet tropics of NE Queensland, Australia. Quaternary Research, 64: 343-356.

Hammond, R.F., 1971. Survey of peat deposits on Makandudu, Milandu and Forkaidu Islands in Miladummandulu, North Atoll, Maldives

Hellstrom, J., McCulloch, M. and Stone, J., 1998. A detailed 31,000-year record of climate and vegetation change, from the isotope geochemistry of two New Zealand Speleothems. Quaternary Research, 50: 167-17.

Hong, Y.T., Wang, Z.G., Jiang, H.B., Lin, Q.H., Hong, B., Zhu, Y.X., Wang, Y., Xu, L.S., Leng, X.T. and Li, H.D., 2001. A 6000-year record of changes in drought and precipitation in northeastern China based on a $d^{13}C$ time series from peat cellulose. Earth and Planetary Science Letters, 185: 111-119.

Jennerjahn, T., Venugopalan, I., Helge, W., Arz, H.W., Behling, H., Patzold, J. and Wefer, G., 2004. Asynchronous terrestrial and marine signals of climate change during Heinrich events. Science, 306: 2236-2239.

Johanson, E., Sanden, P. and Oberg, G., 2003. Spatial patterns of organic chlorine and chloride in Swedish forest soils. Chemoshere, 52: 391-397.

Johnsen, R.I., Grahl-Nielsen, O. and Leunestad, B.T., 1993. Environmental distribution of organic waste from a marine fish farm. Aquaculture, 118: 229-244.

Johnson, B.J., Miller, G.H., Fogel, M.L., Magee, J.W., Gagan, M.K. and Chivas, A.R., 1999. 65,000 years of vegetation change in central Australia and the Australian summer monsoon. Science, 284: 1150-1152.

Kershaw, A.P., 1974. A long continuous pollen sequence from north-eastern Australia. Nature, 251: 222-223.

Kershaw, A.P., 1976. A Late Pleistocene and Holocene pollen diagram from Lynch's Crater, Northeastern Queensland, Australia. New Phytologist, 77: 469-498.

Kershaw, A.P., 1994. Pleistocene vegetation of the humid tropics of northeastern Queensland, Australia. Palaeogeography, Palaeoclimatology, Palaeoecology, 109: 399-412.

Letolle, R., 1980. Nitrogen-15 in natural environment. In: P. Fritz and J.-C. Fontes (Editors), Handbook of environmental geochemistry. Elsevier Science Publications, New York.

Leuschner, D.C. and Sirocko, F., 2000. The low-latitude monsoon climate during Dansgaard-Oeschger cycles and Heinrich Events. Quaternary Science Reviews, 19: 243-254.

Lucas, R.E., 1982. Organic Soils (Histosols). Formation, distribution, physical and chemical properties and management for crop production, Michigan State University.

Magee, J.W., Miller, G.H., Spooner, N.A. and Questiaux, D.G., 2004. Continuous 150 k.y. monsoon record from Lake Eyre, Australia: Insolation-forcing implications and unexpected Holocence failure. Geology, 32(10): 885-888.

Maloney, B.K., 1995. Evidence for the Younger Dryas climatic event in Southeast Asia. Quaternary Science Reviews, 14: 949-958.

Mandernack, K.W., Lynch, L., Krouse, H.R. and Morgan, M.D., 2000. Sulfur cycling in wetland peat of the New Jersey pinelands and its effect on stream water chemistry. Geochimica et Cosmochimica Acta, 64(23): 3949-3964.

Martinez Cortizas, A., Nova Munoz, J.C., Pontevedra, X., Taboada, T., Garcia-Rodeja, E. and Chesworth, W., In press. Elemental composition of refernce European volcanic soils. In: O. Arnalds et al. (Editors), Soils of volcanic regions of Europe.

Martínez-Cortizas, A., Pontevedra-Pombal, X., García-Rodeja, E., Nóvoa-Muñoz, J.C. and Shotyk, W., 1999. Mercury in a Spanish peat bog: Archive of climate change and atmospheric metal deposition. Science, 284: 939-942.

Martínez-Cortizas, A., Pontevedra-Pombal, X., Nóvoa-Muñoz, J.C. and García-Rodeja, E., 1997. Four thousand years of atmospheric Pb, Cd, and Zn deposition recorded by the ombrotrophic peat bog of Penido Vello (Northwestern Spain). Water, Air and Soil Pollution, 100: 387-403.

Middelburg, J.J. and Nieuwenhuize, J., 2001. Nitrogen isotope tracing of dissolved inorganic nitrogen in tidal estuaries. Estuarine, Coastal and Shelf Science, 53: 385-391.

Montoya, J.P., 1994. Nitrogen isotope fractionation in the modern ocean. Implications for the sedimentary record. In: R. Zahn, M. Kaminski, L.D. Labeyrie and T. Pedersen (Editors), Carbon cycling in the glacial ocean: constraints on the oceans role in global change. Springer, Heidelberg, pp. 259-279.

Muller, J., Kylander, M.E., Martinez Cortizas, A., Wust, R.A., Weiss, D.J., Blake, K., Coles, B.J. and Garcia-Sanchez, R., Submitted. Processes affecting trace and major elemental distribution in a 55 kyr peat deposit in tropical Australia: implications to paleoclimate Geochemica et Cosmochimica Acta.

Muller, J., Wüst, R.A.J., Weiss, D.J. and Hu, Y., 2006. Geochemical and stratigraphic evidence of environmental change at Lynch's Crater, Queensland, Australia. Global and Planetary Change, 53: 269-277.

Norton, S.A., 1990. Geochemistry of selected Maine peat deposits, Maine Geological Survey - Department of Conservation, Maine.

Rahn, K.A., 1999. A graphical technique for determining major components in a mixed aerosol. I. Descriptive aspects. Atmospheric Environment, 33, 9: 1441-1455.

Sauer, M. and Siegenthaler, U., 1989. 13C/12C isotope ratios in tree are sensitive to relative humidity. Dendrochronologia, 7: 9-13.

Shotyk, W., 1997. Atmospheric deposition and geochemical mass balance of major and trace elements in two oceanic peat bog profiles, northern Scotland and the Shetland Islands. Chemical Geology, 138(1-2): 55-72.

Shotyk, W., Nesbitt, H.W. and Fyfe, W.S., 1990. The behavior of major and trace elements in complete vertical peat profiles from three sphagnum bogs. International Journal of Coal Geology, 15: 163-190.

Shotyk, W., Weiss, D., Appleby, P.G., Cheburkin, A.K., Frei, R., Gloor, M., Kramers, J.D., Reese, S. and Van Der Knaap, W.O., 1998. History of atmospheric lead deposition since 12,370 ^{14}C yr BP from a peat bog, Jura Mountains, Switzerland. Science, 281: 1635-1640.

Skilbeck, C.G., Rolph, T.C., Hill, N.G., Woods, J. and Wilkens, R.H., 2005. Holocene millennial/centennial-scale multiproxy cyclicity in temperate eastern Australian estuary sediments. Journal of Quaternary Science, 20: 327-347.

Steinmann, P. and Shotyk, W., 1997. Geochemistry, mineralogy, and geochemical mass balance on major elements in two peat bog profiles (Jura Mountains, Switzerland). Chemical Geology, 138: 25-53.

Sternberg, L., DeNiro, M.J. and Johnson, H.B., 1984. Isotope ratios of cellulose from plants having different photosynthetic pathways. Plant Physiology, 74: 557-561.

Street-Perrott, F.A., Huang, Y., Perrott, R.A., Eglinton, G., Barker, P., Ben Khelifa, L., Harkness, D.D. and Olago, D.O., 1997. Impact of lower atmospheric carbon dioxide on tropical mountain ecosystems. Science, 278(5342): 1422-1426.

Stuiver, T.F. and Braziunas, T.F., 1987. Tree cellulose 13C/12C isotope ratios and climate change. Nature, 328: 58-60.

Talbot, M.R. and Laerdal, T., 2000. The Late Pleistocene - Holocene palaeolimnology of Lake Victoria, East

Africa, based upon elemental and isotopic analyses of sedimentary organic matter. Journal of Paleolimnology, 23: 141-164.

Tamari, Y., 1978. Studies on the state analysis of selenium in sediments Kinki University Higashi-Osaka City.

Turney, C.S.M., Kershaw, A.P., Clemens, S.C., Branch, N., Moss, P.T. and Fifield, L.K., 2004. Millennial and orbital variations of El Niño/Southern Oscillation and high-latitude climate in the last glacial period. Nature, 428: 306-310.

Turney, C.S.M., Kershaw, A.P., Moss, P., Bird, M.I., Fifield, L.K., Cresswell, R.G., Santos, G.M., Di Tada, M.L., Hausladen, P.A. and Zhou, Y., 2001. Redating the onset of burning at Lynch's Crater (North Queensland): implications for human settlement in Australia. Journal of Quaternary Science, 16(8): 767-771.

Wada, E. and Hattori, A., 1990. Nitrogen in the sea: Forms, abundances, and rate processes. CRC Press, Boca Raton, 224 pp.

Weiss, D., Shotyk, W., Rieley, J.O., Page, S.E., Gloor, M., Reese, S. and Cortizas-Martinez, A., 2002. The geochemistry of major and selected trace elements in a forested peat bog, Kalimantan, SE Asia, and its implications for past atmospheric dust deposition. Geochimica et Cosmochimica Acta, 66(13): 2307-2323.

White, J.W.C., Cials, P., Figgo, R.A., Kenny, R. and Markgraf, V., 1994. A high-resolution record of atmospheric CO_2 content from carbon isotopes in peat. Nature, 365: 153-156.

Wüst, R.A.J. and Bustin, R.M., 2003. Opaline and Al–Si phytoliths from a tropical mire system of West Malaysia: abundance, habit, elemental composition, preservation and significance. Chemical Geology, 200(3-4): 267-292.

Wüst, R.A.J., Ward, C.R., Bustin, R.M. and Hawke, M.I., 2002. Characterization and quantification of inorganic constituents of tropical peats and organic-rich deposits from Tasek Bera (Peninsular Malaysia): Implications for coals. International Journal of Coal Geology, 49(4): 215-249.

CHAPTER 6

Conclusions

1) Important tools for paleoclimate reconstructions of peat deposits: Geochemical analysis and statistics

This thesis presents new evidence for the importance of statistical data analysis for reconstructing our past climate. Peat deposits have been utilised for decades as "archives" of past environmental conditions and many geochemical investigations have been done. This thesis has not only applied geochemical analysis to possibly the longest peat record of the southern hemisphere, but demonstrates that applying statistical analysis to the geochemical data may provide new means to solve data interpretations. Hence, principle component analysis applied in this work is a novel approach in defining processes affecting elements within peat deposits. This is particularly important since peat deposits are very complex sedimentary systems and several factors and processes contribute to their composition, such as runoff, atmospheric dust, intensity of catchment weathering, vegetation dynamics, hydrology, precipitation regimes, etc. This thesis shows that elements can be clearly differentiated from each other, and controlling factors/processes may be determined through the statistical analysis. The study reveals, however, that several elements (e.g. As, N, Se, K) that were thought to be clearly defined in terms of their controlling factors/processes show a more complex pattern and require further investigations in future research projects. Future projects should focus on: 1) elemental distributions in plants and plant material associated with peat forming environments; 2) the role of organic compounds and acids for elemental mobilisation in peat forming environments; and 3) role of mobilisation/immobilisation of fluctuating groundwater levels in peat forming environments.

2) Climate change recorded in Lynch's Crater: Sensitivity for past climate change and evidence of global connectivity

Investigations of Lynch's Crater started in the 70's by Kershaw, and numerous other studies followed (Kershaw and co-workers), mainly focusing on pollen and charcoal analysis. All studies demonstrated that Lynch's Crater is an amazingly long, almost continuous and hence rare record of Australia's climate that extends back to over 200,000 years. This thesis has focus on the top 13 m peat deposits, which span the last 55,000 years and used geochemistry as another proxy for paleoclimate reconstructions. The thesis has produced some significant new findings including evidence that climate changed throughout the past 55,000 years and the environment had to adapt to erratic changes. In particularly well recorded are the Heinrich events (H1-4), the Younger Dryas (YD), and the 8.2 kyr event, during which more precipitation was received in this part of the world, interpreted as southward migration of the Intertropical Convergence Zone (ITCZ). The shifts in ITCZ position have also been shown in paleoclimate records from Brazil and Africa, however, this is the first time they have been positively identified in Australia. This may provide new evidence on the importance and role of the Pacific Ocean and the equatorial region in abrupt climate change. The study also recognises Cl variations as a high-resolution precipitation proxy and shows good agreement with pollen records from the area. In addition, Cl displays a remarkable resemblance to the O-isotope records and their Dansgaard-Oeschger cycles from the Greenland Ice Core Project illustrating Lynch's Crater as a sensitive global climate archive. The study suggests that future investigations at even higher resolution may indeed provide some compelling new evidence for climate change and the significance of the tropics for global climate.

Appendix 1

LC1 - Ash Yield Results

Ash Yield LC1					
Depth (cm)	**Ash Content (%)**	**Depth (cm)**	**Ash Content (%)**	**Depth (cm)**	**Ash Content (%)**
2	29.99	232	23.61	457	4.69
6	30.42	237	12.06	472	4.81
17	18.61	252	24.90	487	6.46
33	3.90	257	21.22	492	7.01
52	4.78	272	7.39	507	6.22
57	5.38	287	11.13	512	10.43
72	2.96	292	12.68	532	13.63
107	2.82	307	8.57	537	9.54
87	2.91	312	10.69	552	6.45
92	3.03	327	8.87	557	8.06
112	3.65	332	7.04	572	5.44
132	3.26	352	9.17	592	4.74
137	3.74	357	9.07	607	4.49
152	4.45	387	6.94	612	4.21
157	4.19	392	7.22	632	8.40
172	1.60	407	8.54	637	54.39
187	32.16	412	10.27	652	9.31
192	33.11	432	7.01		
207	11.55	437	6.12		
212	18.83	452	5.30		

Appendix 1: Ash Yield LC1

Appendix 2

LC1 - Moisture Content Results

Moisture							
Content LC1							
Depth (cm)	**Wet (g)**	**Dry (g)**	**% Moisture**	**Depth (cm)**	**Wet (g)**	**Dry (g)**	**% Moisture**
10-20	73.59	39.11	53.15	180-190	86.98	20.31	23.36
20-30	75.01	25.99	34.64	190-200	88.24	28.53	32.33
30-40	101.68	29.50	29.01	200-210	75.41	20.44	27.11
40-50	100.90	31.84	31.56	210-220	86.06	25.46	29.58
50-60	85.70	28.66	33.44	220-230	84.44	21.16	25.06
60-70	79.50	24.29	30.55	230-240	79.53	17.67	22.22
70-80	91.60	24.51	26.76	240-250	80.27	20.07	25.00
80-90	98.66	24.83	25.17	250-260	72.12	21.84	30.29
90-100	100.65	25.07	24.91	260-270	75.29	17.34	23.03
100-110	85.53	19.40	22.68	270-280	88.55	18.47	20.86
110-120	74.87	17.79	23.76	280-290	90.61	18.04	19.91
120-130	68.21	12.77	18.72	290-300	93.68	20.91	22.33
130-140	68.33	12.01	17.58	300-310	80.51	17.83	22.14
140-150	66.80	11.74	17.58	310-320	88.77	23.67	26.67
150-160	57.70	10.60	18.37	320-330	90.28	18.86	20.89
160-170	86.75	24.41	28.14	330-340	91.01	17.31	19.02
170-180	86.00	18.89	21.96	340-350	87.28	17.21	19.72

Appendix 2: Moisture Content LC1

Moisture Content LC1							
Depth (cm)	**Wet (g)**	**Dry (g)**	**% Moisture**	**Depth (cm)**	**Wet (g)**	**Dry (g)**	**% Moisture**
350-360	89.07	17.57	19.73	510-520	79.29	15.11	19.06
360-370	77.09	15.31	19.87	520-530	85.37	23.40	27.41
370-380	87.17	15.71	18.03	530-540	82.35	19.29	23.42
380-390	82.43	14.59	17.69	540-550	68.31	13.81	20.22
390-400	85.06	16.54	19.45	550-560	77.71	13.86	17.83
400-410	90.93	16.71	18.38	560-570	63.71	11.71	18.39
410-420	75.46	19.59	25.96	570-580	74.80	12.37	16.54
420-430	88.09	15.53	17.63	580-590	80.36	13.87	17.26
430-440	84.65	15.56	18.38	590-600	83.30	14.64	17.58
440-450	83.00	14.30	17.23	600-610	77.41	13.04	16.85
450-460	75.44	12.94	17.16	610-620	77.33	13.70	17.72
460-470	72.82	13.23	18.17	620-630	90.85	16.04	17.66
470-480	76.03	15.01	19.75	630-640	77.26	17.53	22.69
480-490	78.67	15.86	20.16	640-650	75.51	21.20	28.08
490-500	70.97	14.29	20.13	650-660	68.71	14.47	21.06
500-510	64.50	12.97	20.11				

Appendix 2: Moisture Content LC1

Appendix 3

LC1 - Radiocarbon Results

Radiocarbon						
LC1						
		Sample		**Radiocarbon age**		
Sample ID	**Lab. ID**	**type**	**Depth (cm)**	**(14C yr BP)**	**Calibrated years (cal yr BP)**	**Comments**
LC1-27	OZHO71	Peat	27-28	5450	6280, 6217, 6212	
LC1-47	OZHO72	Peat	47-48	6440	7415, 7393, 7369, 7350, 7331	
LC1-67	OZHO73	Peat	67-68	7250	8106, 8093, 8028	
LC1-117	OZHO74	Peat	117-118	8960	10176	
LC1-167	OZHO75	Peat	167-168	7150	7960	Age Inversion
LC1-217	OZHO76	Peat	217-218	10390	12332	
LC1-267	OZHO77	Peat	267-268	14900	17825	
LC1-317	OZHO78	Peat	317-318	14280	17112	Age Inversion
LC1-367	OZHO79	Peat	367-368	15400	18400	
LC1-417	OZHO80	Peat	417-418	19090	22647	
LC1-467	OZHO81	Peat	467-468	21870		Age Inversion
LC1-517	OZHO82	Peat	517-518	19620	23257	
LC1-567	OZHO83	Peat	567-568	24000		
LC1-617	OZHO84	Peat	617-618	22390		Age Inversion
LC1-657	OZHO85	Peat	657-658	22040		Age Inversion

Appendix 3: Radiocarbon Dates LC1

Appendix 4

LC1 - Peat Geochemistry ICP-AES

ICP-AES							
LC1							
Depth (cm)	**Al**	**As**	**Ca**	**Cu**	**Fe**	**Hg**	**K**
2	4060.00	0.00	5310.00	6.33	2550.00	0.04	0.50
12	4110.00	0.18	6680.00	8.55	3410.00	0.01	173.00
22	3140.00	0.00	7280.00	5.67	2710.00	0.02	0.50
42	1540.00	0.00	5780.00	6.55	2430.00	0.02	262.00
62	1890.00	0.00	2980.00	7.36	1070.00	0.02	0.50
82	2710.00	0.04	3700.00	4.48	1690.00	0.02	0.50
102	2460.00	0.19	3890.00	2.76	1820.00	0.02	0.50
122	2280.00	0.02	3980.00	2.08	1770.00	0.00	0.50
142	2640.00	0.29	5840.00	3.59	1970.00	0.02	0.50
162	3100.00	0.06	5420.00	15.40	2790.00	0.02	0.50
182	3560.00	1.70	5320.00	5.05	2780.00	0.00	0.50
202	4820.00	0.85	7260.00	9.02	3640.00	0.02	0.50
222	3960.00	2.20	8060.00	5.63	4050.00	0.01	0.50
242	4700.00	3.04	10400.00	5.62	5110.00	0.00	0.50
262	3380.00	3.03	10300.00	4.02	5030.00	0.01	0.50
282	3070.00	4.62	10600.00	3.64	4870.00	0.02	168.00
302	2800.00	3.29	13900.00	2.98	6450.00	0.00	0.50
322	2590.00	1.76	12500.00	3.52	5600.00	0.00	0.50

Appendix 4: ICP-MS LC1

ICP-AES							
LC1							
Depth (cm)	**Al**	**As**	**Ca**	**Cu**	**Fe**	**Hg**	**K**
342	2400.00	1.82	14100.00	2.61	6150.00	0.00	0.50
362	2630.00	1.56	12000.00	3.97	5320.00	0.05	0.50
382	2250.00	0.85	14200.00	2.57	5700.00	0.00	378.00
402	1820.00	0.61	14000.00	2.61	5460.00	0.01	0.50
422	1560.00	0.40	12500.00	3.07	4660.00	0.08	0.50
442	1600.00	0.48	15500.00	1.83	5410.00	0.02	56.60
462	1830.00	0.55	13000.00	1.85	5000.00	0.01	179.00
482	2040.00	0.27	16500.00	3.42	6160.00	0.00	0.50
502	1540.00	0.11	16000.00	2.23	5360.00	0.00	0.50
522	2780.00	1.01	13600.00	5.10	5330.00	0.00	0.50
542	1750.00	0.00	13300.00	2.92	4910.00	0.00	110.00
562	1250.00	0.00	14000.00	1.79	4560.00	0.00	0.50
582	1190.00	0.00	13100.00	1.13	4160.00	0.01	0.50
602	1340.00	0.00	11200.00	0.90	3720.00	0.01	143.00
622	2930.00	0.41	5400.00	19.90	2890.00	0.00	0.50
637	7120.00	4.47	13900.00	28.70	7740.00	0.00	0.50
642	2270.00	1.08	9950.00	3.07	4120.00	0.00	92.00

ICP-AES							
LC1							
Depth (cm)	**Mg**	**Na**	**Pb**	**Ti**	**Zn**	**Sc**	**Sr**
2	1130.00	215.00	4.32	109.00	13.90	0.14	16.90
12	1480.00	76.40	3.50	105.00	2.89	1.42	42.90
22	2830.00	145.00	3.25	95.80	6.57	1.62	56.00
42	3660.00	99.10	0.80	102.00	0.01	4.71	181.00
62	2560.00	121.00	0.93	106.00	0.01	0.80	16.70
82	3010.00	146.00	1.23	69.30	0.01	1.00	17.20
102	3010.00	186.00	0.66	62.20	0.01	1.20	26.70
122	2820.00	221.00	0.53	48.70	0.01	0.81	27.60
142	3570.00	173.00	0.95	50.00	1.90	0.71	26.80
162	2320.00	113.00	2.38	77.50	6.88	0.96	48.70
182	3170.00	190.00	0.85	117.00	15.70	1.88	56.10
202	3170.00	139.00	1.97	129.00	0.01	1.22	39.70
222	3300.00	112.00	1.45	91.10	0.69	1.60	54.80
242	4470.00	172.00	1.39	112.00	0.01	1.62	75.70
262	4500.00	207.00	1.21	97.30	10.10	1.60	87.70
282	4870.00	239.00	0.57	88.70	0.01	1.35	82.20
302	5480.00	235.00	0.84	70.10	0.01	1.21	88.90
322	4860.00	143.00	0.95	67.10	8.64	1.35	114.00

Appendix 4: ICP-MS LC1

ICP-AES							
LC1							
Depth (cm)	**Mg**	**Na**	**Pb**	**Ti**	**Zn**	**Sc**	**Sr**
342	5790.00	194.00	0.61	56.40	0.01	1.51	103.00
362	5140.00	306.00	1.08	67.00	0.28	1.33	116.00
382	6120.00	159.00	1.12	56.60	0.01	1.34	90.30
402	5810.00	276.00	0.63	43.90	0.01	1.14	107.00
422	5560.00	223.00	0.54	36.00	1.70	1.24	102.00
442	6740.00	345.00	0.54	29.50	0.01	1.41	109.00
462	5900.00	344.00	0.53	31.70	0.01	1.39	125.00
482	6920.00	265.00	0.89	64.40	0.51	1.20	96.80
502	7070.00	312.00	0.53	33.60	0.72	0.21	136.00
522	5280.00	222.00	1.27	76.40	3.38	<= 0.0001	126.00
542	5690.00	237.00	1.13	44.70	10.20	0.13	114.00
562	6050.00	273.00	0.84	26.90	0.55	<= 0.0001	107.00
582	6220.00	255.00	0.41	19.80	0.01	<= 0.0001	115.00
602	5190.00	242.00	0.22	17.30	0.01	<= 0.0001	104.00
622	2220.00	95.20	3.90	153.00	0.01	0.26	88.30
637	5640.00	242.00	8.00	245.00	6.11	0.37	47.80
642	4520.00	228.00	0.54	44.80	2.69	<= 0.0001	83.20

Appendix 5

LC2 - Ash Yield Results

Ash Yield LC1					
Depth (cm)	**Ash Content (%)**	**Depth (cm)**	**Ash Content (%)**	**Depth (cm)**	**Ash Content (%)**
5	30.78	235	24.57	505	5.16
15	4.71	245	20.27	515	6.50
25	4.20	255	18.04	526	6.79
35	3.47	273	9.79	545	5.89
45	3.27	285	13.60	557	13.66
55	4.41	305	11.60	567	21.25
65	4.96	314	3.41	585	16.94
75	4.26	335	9.05	597	6.37
85	3.81	354	10.17	615	13.03
95	5.65	364	8.39	624	13.49
105	8.13	374	11.05	634	10.15
128	4.72	395	9.84	645	8.51
137	5.38	415	8.26	655	9.56
144	5.45	424	8.17	665	8.72
165	20.97	434	8.23	675	13.22
185	52.95	444	5.26	685	11.31
195	35.29	455	7.19	705	25.76
205	24.27	474	9.74	727	14.93
215	29.33	485	26.22	737	23.21
225	35.81	494	20.10	755	20.98

Appendix 5: Ash Yield LC2

Ash Yield LC1					
Depth (cm)	**Ash Content (%)**	**Depth (cm)**	**Ash Content (%)**	**Depth (cm)**	**Ash Content (%)**
783	8.24	945	7.13	1136	6.99
795	19.26	975	6.40	1145	7.06
805	18.86	984	7.56	1159	6.21
814	8.49	1005	6.38	1175	5.99
824	8.12	1014	7.39	1193	5.22
834	8.08	1024	5.96	1208	6.61
844	9.64	1035	6.85	1215	7.27
865	10.18	1054	6.67	1235	6.36
885	9.85	1064	6.80	1244	6.33
894	10.03	1074	6.87	1254	5.78
904	8.38	1085	6.34	1265	6.72
915	7.21	1094	7.48	1284	6.48
925	6.99	1105	6.18	1294	6.19
935	6.75	1124	6.91		

Appendix 5: Ash Yield LC2

Appendix 6

LC2 - pH Results

pH LC2													
Depth (cm)	**pH**	**Depth (cm)**	**pH**	**Depth (cm)**	**pH**	**Depth (cm)**	**pH**	**Depth (cm)**	**pH**	**Depth (cm)**	**pH**	**Depth (cm)**	**pH**
0	4.5	200	4.9	400	6	600	6.7	800	7.2	1000	7.3	1200	7.2
10	4.2	210	5.2	410	6.3	610	6.9	810	7.4	1010	7.4	1210	7.2
20	3.6	220	5.4	420	6.4	620	7.2	820	7.5	1020	7.3	1220	7.4
30	4	230	5.5	430	6.3	630	7.1	830	7.6	1030	7.5	1230	7.5
40	3.8	240	5.5	440	6.2	640	7	840	7.5	1040	7.6	1240	7.4
50	4.2	250	4.6	450	6.2	650	6.4	850	6.3	1050	7.1	1250	7.4
60	4.4	260	5.8	460	6.5	660	7.1	860	7.3	1060	7.3	1260	7.5
70	4.5	270	5.8	470	6.4	670	7.4	870	7.3	1070	7.2	1270	7.5
80	4.4	280	5.9	480	6.4	680	7.3	880	7.2	1080	7.2	1280	7.4
90	4.6	290	5.9	490	6.5	690	7.2	890	7.4	1090	7.2	1290	7.3
100	4.7	300	5.5	500	6.2	700	7.2	900	7.2	1100	7.2	1300	7.3
110	4.6	310	6	510	6.3	710	7.3	910	7.4	1110	7.4		
120	4.6	320	5.9	520	6.4	720	7.4	920	7.4	1120	7.4		
130	4.7	330	6	530	6.5	730	7.5	930	7.4	1130	7.2		
140	4.7	340	6	540	6.4	740	7.3	940	7.6	1140	7.3		
150	4.8	350	4.7	550	6.2	750	6.9	950	7.1	1150	7.2		
160	4.8	360	6.2	560	7	760	7.5	960	7.4	1160	7.4		
170	4.9	370	6.3	570	7.1	770	7.4	970	7.5	1170	7.4		
180	4.9	380	6.3	580	6.9	780	7.3	980	7.4	1180	7.3		
190	5.3	390	6.2	590	7.1	790	7.3	990	7.5	1190	7.6		

Appendix 6: pH LC2

Appendix 7

LC2 - Radiocarbon results

Radiocarbon LC1 & LC2

Core	Sample Depth (cm)	Sample ID.	Lab No.	C14 Age	Cal yrs BP	±	Calibration Method	Standard Deviation
LC2	4.5	LC2-4	OZI460	1595	1465	98	SHCal04	48.75
LC2	9.5	LC2-9	OZH600	2670	2757	34	SHCal04	17.00
LC1	27.5	LC1-27	OZH071	5450	6235	53	SHCal04	26.50
LC1	47.5	LC1-47	OZH072	6440	7345	95	SHCal04	47.25
LC1	67.5	LC1-67	OZH073	7250	8055	119	SHCal04	59.25
LC2	104.5	LC2-104	OZH601	7630	8397	52	SHCal04	25.75
LC1	117.5	LC1-117	OZH074	8960	9875	229	SHCal04	114.25
LC2	120.5	LC2-120	OZI461	9110	10005	375	SHCal04	187.50
LC2	164.5	LC2-164	OZI164	10340	12160	220	IntCal04	109.75
LC2	182.5	LC2-182	OZI463	11220	13070	88	IntCal04	44.00
LC2	248.5	LC2-248	OZI464	13180	15480	240	IntCal04	119.75

Appendix 7: Radiocarbon dates LC1 &LC2

Radiocarbon LC1 & LC2								
Core	**Sample**	**Sample**	**Lab**	**C14**	**Cal**	**±**	**Calibration**	**Standard**
	Depth (cm)	**ID.**	**No.**	**Age**	**yrs BP**		**Method**	**Deviation**
LC2	387.5	LC2-387	OZI465	20340	24225	206	IntCal04	102.75
LC2	484.5	LC2-484	OZH603	24370	29150	200	Bayesian	100.00
LC2	560.5	LC2-560	OZH604	27480	31885	330	Bayesian	165.00
LC2	720.5	LC2-720	OZI471	30740	34750	280	Bayesian	140.00
LC2	810.5	LC2-810	OZH591	32310	36450	520	Bayesian	260.00
LC2	860.5	LC2-860	OZH592	34310	39400	460	Bayesian	230.00
LC2	935.5	LC2-935	OZH593	36510	41425	700	Bayesian	350.00
LC2	987.5	LC2-987	OZH594	38320	42625	820	Bayesian	410.00
LC2	1040.5	LC2-1040	OZH596	40429	43350	930	Bayesian	465.00
LC2	1154.5	LC2-1154	OZH597	41330	43775	1100	Bayesian	550.00

Appendix 7: Radiocarbon dates LC1 &LC2

Appendix 8

LC2 - Peat Geochemistry ICP-AES and ICP-MS

AES LC2												
Depth (cm)	**Al**	**As**	**Ba**	**Be**	**Ca**	**Co**	**Cr**	**Cu**	**Fe**	**K**	**La**	**Li**
Error	47	0.5	0.93	0.00	92	0.06	0.20	0.64	121	3.83	0.04	0.05
5	4603	2.9	35.08	0.655	9110	4.96	18.70	8.02	3370	345	8.23	0.63
15	1403	2.4	7.08	0.127	8750	3.69	4.51	3.52	2390	200	1.65	0.30
25	1373	1.9	4.68	0.112	7340	3.45	4.06	3.65	2250	31	1.545	0.25
35	1413	1.7	2.88	0.077	6080	2.87	4.53	4.42	2080	71.5	1.295	0.18
45	1723	1.8	1.43	0.07	4150	2.66	8.55	7.98	1430	52	1.48	0.08
55	2653	2.0	1.53	0.093	3530	2.73	10.20	8.95	1330	23	2.05	0.07
65	3013	2.1	1.93	0.128	3660	2.75	12.20	9	1570	23	2.42	0.09
75	3053	2.0	1.83	0.128	3730	2.53	13.80	6.85	1690	21	2.205	0.08
85	3083	2.5	1.83	0.132	4050	3.08	14.80	6.19	1910	21	1.85	0.09
95	3333	2.4	2.83	0.2	4900	2.78	26.10	4.24	2410	32	2.365	0.15
105	2993	2.4	7.58	0.198	5470	3.18	26.40	4.41	2400	8.5	2.55	0.20
115	2733	2.3	2.68	0.085	4810	3.07	34.80	3.62	2300	37.5	1.02	0.12
125	2733	2.7	3.73	0.075	4700	3.17	26.10	3.91	2230	53	1.175	0.16
135	3063	2.4	3.98	0.087	5310	3.34	21.90	4.21	2730	63	1.21	0.19
145	4023	2.8	5.88	0.103	5820	3.36	23.10	4.07	3020	131	2.145	0.30
155	3503	2.9	5.83	0.106	6440	3.15	14.90	4.12	3380	104	1.71	0.31
165	3553	3.3	5.83	0.067	5910	3.28	15.80	4.1	2950	122	1.29	0.29

AES LC2												
Depth (cm)	**Mg**	**Mn**	**Mo**	**Na**	**Ni**	**P**	**Pb**	**S**	**Sr**	**Ti**	**V**	**Zn**
Error	80	0.5	0.02	14.14	0.10	2.64	0.05	84	1.10	2.31	0.15	1.76
5	2450	35.3	0.45	288	10.45	607	4.00	1390	98.40	507.54	19.50	8.12
15	3450	14.1	0.15	193	6.27	165	0.80	1230	71.00	207.54	15.20	1.38
25	3790	7.3	0.15	205	5.85	112	0.80	1180	52.10	209.54	8.96	0.90
35	3790	4.4	0.10	203	4.89	81.6	0.60	1170	42.10	191.54	5.98	0.57
45	3140	1.8	0.15	198	4.79	70	0.80	1290	26.40	306.54	8.94	1.86
55	2880	1.1	0.15	220	4.25	75.2	0.80	1370	22.00	369.54	15.30	2.29
65	2930	1.0	0.20	239	4.97	71.6	1.20	1510	23.50	345.54	18.20	0.23
75	2910	1.1	0.15	249	5.83	72.6	1.00	1410	24.50	244.54	16.30	0.27
85	3050	1.1	0.20	270	6.39	82.6	0.80	1390	26.50	188.54	13.90	0.24
95	3340	1.5	0.20	289	7.45	87.6	0.80	1370	33.50	236.54	14.50	6.47
105	3230	5.8	0.30	324	6.79	157	1.20	1590	43.00	258.54	14.50	2.23
115	3550	1.4	0.35	399	6.47	83.6	0.60	2160	33.20	130.54	13.50	1.22
125	3250	2.1	0.35	371	6.33	91	0.60	1880	33.00	241.54	12.50	0.48
135	3500	2.2	0.30	395	8.43	87.6	0.60	1940	38.00	171.54	14.10	0.67
145	3570	3.4	0.25	387	7.53	100	0.80	1700	42.00	512.54	14.50	2.07
155	3720	2.9	0.25	404	9.73	84.8	1.00	1650	47.20	219.54	16.20	8.70
165	3440	3.0	0.25	400	7.21	92.2	0.60	1830	43.40	207.54	18.50	2.25

AES LC2												
Depth (cm)	**Al**	**As**	**Ba**	**Be**	**Ca**	**Co**	**Cr**	**Cu**	**Fe**	**K**	**La**	**Li**
175	5283	3.9	11.18	0.129	6590	3.36	26.10	12	3740	116	2.635	0.53
185	6913	1.7	18.68	0.153	6580	2.77	28.90	19.8	4290	345	3.53	0.75
195	6443	2.9	15.58	0.181	8190	2.27	27.10	11.9	4310	144	3.3	0.82
205	5273	4.0	13.28	0.141	8340	2.40	25.90	9.83	4310	66	2.52	0.75
215	5013	4.0	16.08	0.134	9370	2.38	27.60	7.44	4860	103	2.6	0.71
225	4573	4.6	16.08	0.098	9030	2.41	27.30	6.82	4650	130	2.345	0.67
235	5003	5.3	16.88	0.103	10700	2.51	30.50	5.6	5110	51	2.135	0.83
245	4573	5.4	15.28	0.106	10800	2.86	31.40	4.43	5250	262	1.905	0.86
255	4243	4.7	18.48	0.131	11900	2.71	31.00	4.28	5660	9	2.35	0.86
265	4143	4.9	16.08	0.098	12700	2.95	31.50	5.05	6090	225	1.81	0.97
275	3613	5.2	13.98	0.075	12700	2.89	31.40	4.79	5910	183	1.38	0.88
285	4003	4.9	17.88	0.095	13600	2.74	33.40	5.2	6380	261	1.89	1.17
295	3783	4.7	19.58	0.102	15000	2.52	34.60	5.38	7360	247	1.865	1.26
305	3773	3.8	19.08	0.111	15000	2.58	28.90	4.97	6730	250	1.93	1.32
315	3413	3.4	20.88	0.084	16900	2.45	29.40	4.36	7410	210	1.695	1.48
325	2833	3.1	16.78	0.05	16800	2.30	27.80	3.13	7000	145	1.08	1.32
335	2913	3.1	18.38	0.054	17100	2.78	42.50	4.02	7500	175	1.29	1.34

AES LC2												
Depth (cm)	**Mg**	**Mn**	**Mo**	**Na**	**Ni**	**P**	**Pb**	**S**	**Sr**	**Ti**	**V**	**Zn**
175	3260	8.4	0.20	407	12.25	103	1.40	1970	52.20	530.54	32.50	1.14
185	2780	30.1	0.15	466	18.15	79.6	2.00	958	57.60	788.54	41.80	1.61
195	3420	17.6	<0.1	425	9.43	94.4	1.80	1060	70.80	607.54	54.70	3.31
205	3710	8.4	0.15	434	8.71	101	1.20	1620	69.40	430.54	54.00	2.86
215	3980	20.0	0.20	480	8.65	88.8	1.40	1690	79.90	418.54	55.50	2.44
225	3810	28.5	0.15	519	9.05	75.8	1.40	1630	76.40	411.54	44.30	2.54
235	4450	10.9	0.15	523	7.71	81.6	1.20	1930	89.50	362.54	41.70	2.04
245	4530	15.3	0.15	480	7.37	85.6	1.20	1980	90.00	352.54	36.20	2.56
255	4590	16.0	0.10	471	7.29	78	1.40	1810	98.70	364.54	33.70	5.37
265	5160	11.3	0.15	504	7.71	80	1.20	2350	103.00	290.54	33.60	4.24
275	5340	8.3	0.20	509	7.95	84.4	1.00	3240	100.00	239.54	28.80	1.00
285	5290	11.2	0.15	518	7.93	82	1.00	3090	111.00	317.54	24.60	3.08
295	5680	10.3	0.15	518	9.95	76.8	1.20	3270	123.00	269.54	23.30	1.73
305	5850	10.1	0.20	524	7.81	87.2	1.20	3430	121.00	310.54	18.10	4.57
315	6410	10.7	0.20	541	8.17	79.8	1.20	3900	136.00	257.54	16.00	2.48
325	6840	9.4	0.25	563	6.53	85.2	1.00	5230	129.00	157.54	13.80	1.94
335	6840	11.6	1.30	553	33.25	87.4	1.00	4950	133.00	212.54	12.10	1.50

AES LC2												
Depth (cm)	**Al**	**As**	**Ba**	**Be**	**Ca**	**Co**	**Cr**	**Cu**	**Fe**	**K**	**La**	**Li**
345	2713	2.8	17.88	0.052	17100	2.24	21.40	3.55	7040	170	1.195	1.37
355	2593	2.7	16.18	0.038	17100	2.09	19.60	2.7	6940	152	0.99	1.31
365	2573	2.3	16.08	0.039	16500	2.12	15.60	2.86	6650	174	1.055	1.33
375	3283	2.1	18.38	0.048	16300	2.41	13.90	3.34	6690	284	1.535	1.42
385	2713	2.1	18.18	0.05	16400	2.06	12.20	3.41	6600	246	1.33	1.39
395	2483	3.0	18.88	0.054	16400	1.99	11.70	3.63	6490	17.5	1.325	1.28
405	2163	2.3	18.58	0.044	17100	1.83	9.33	2.66	6470	211	1.12	1.28
415	2043	2.1	17.58	0.035	16900	1.88	8.94	2.81	6140	200	1	1.20
425	1833	2.3	16.18	0.03	16200	1.99	8.41	2.48	5800	169	0.83	1.07
435	1701	1.2	14.17	0.023	14800	2.15	7.64	2.56	5170	141	0.635	0.94
445	1641	1.4	9.97	0.013	10400	3.42	7.27	2.01	4170	115	0.42	0.55
455	1341	1.0	16.47	0.032	15600	1.64	9.64	2.35	4870	134	0.705	1.02
465	1561	0.9	20.07	0.041	16900	1.36	11.15	2.2	5490	164	0.94	1.16
475	1801	0.9	20.57	0.043	17700	1.47	12.75	2.32	5720	179	0.955	1.23
485	3171	0.6	33.57	0.087	19100	1.51	16.65	6.6	7820	185	2.385	1.79
495	3341	1.2	23.27	0.074	15300	2.49	16.45	5.64	5720	113	1.96	1.42
505	1351	0.6	17.37	0.039	14500	1.68	7.49	1.79	5080	150	0.815	0.89

AES LC2												
Depth (cm)	**Mg**	**Mn**	**Mo**	**Na**	**Ni**	**P**	**Pb**	**S**	**Sr**	**Ti**	**V**	**Zn**
345	6890	10.2	0.25	565	6.01	91.8	1.00	5020	133.00	180.54	10.30	2.37
355	7090	10.5	0.25	582	5.55	80.6	1.00	5030	131.00	147.54	10.10	0.75
365	6880	10.5	0.20	599	5.01	87.2	0.80	4130	126.00	166.54	7.82	4.64
375	6810	11.7	0.20	611	4.97	82	1.00	3660	126.00	308.54	7.64	2.71
385	6610	11.3	0.20	580	4.99	88.2	1.00	3340	127.00	232.54	6.88	14.40
395	6400	12.1	0.25	518	4.97	80.4	1.00	2810	125.00	245.54	7.02	9.38
405	6780	12.8	0.20	548	3.99	83.6	1.00	2870	129.00	179.54	4.16	11.20
415	6840	12.5	0.20	557	3.75	80.8	0.80	2930	126.00	155.54	3.94	1.07
425	6670	12.1	0.20	550	3.67	82.6	0.80	2920	121.00	119.54	3.74	1.76
435	6180	10.8	0.25	533	3.23	83	1.00	2920	110.00	74.77	3.32	2.02
445	4720	8.3	0.30	498	2.39	85.8	0.60	2590	78.40	61.57	3.96	4.46
455	6450	13.6	0.25	593	3.25	86.8	0.60	3960	117.00	84.07	2.78	1.12
465	6860	15.1	0.30	620	3.35	76.4	0.80	5100	129.00	112.07	3.68	0.53
475	7090	15.6	0.30	593	3.61	84	0.80	4040	135.00	133.07	4.62	1.18
485	6590	18.8	0.10	606	5.61	61.4	1.40	2580	154.00	387.07	5.76	1.36
495	5860	14.8	0.40	572	5.45	111	1.20	3260	121.00	344.07	5.60	4.77
505	6150	16.0	0.15	510	3.67	77.8	0.80	3270	109.00	86.67	2.28	6.99

AES LC2												
Depth (cm)	**Al**	**As**	**Ba**	**Be**	**Ca**	**Co**	**Cr**	**Cu**	**Fe**	**K**	**La**	**Li**
515	1561	0.8	15.87	0.031	13600	1.77	7.36	1.79	4390	142	0.67	0.75
525	1651	0.7	14.77	0.026	13100	1.67	7.26	1.12	4190	103	0.57	0.73
535	2371	0.8	13.27	0.026	10000	2.66	8.09	1.97	4100	160	0.65	0.57
545	2771	0.6	13.87	0.031	11100	1.91	10.65	1.98	3950	132	0.765	0.61
555	2891	1.0	12.77	0.027	9980	2.16	11.95	6.25	4010	115	0.64	0.55
565	3921	1.0	26.47	0.058	18500	1.77	18.55	3.92	5630	151	1.855	1.35
575	3901	1.5	29.37	0.103	16900	6.10	21.05	5.57	6520	245	2.05	1.33
585	4181	0.9	44.77	0.158	20600	2.39	21.85	6.38	7780	69.5	3.1	1.96
595	3191	1.3	36.27	0.081	21000	4.49	21.05	4.94	8810	183	1.715	1.77
605	3171	1.8	36.37	0.075	19500	1.80	21.35	4.53	6620	16	1.515	1.70
615	3221	1.8	38.87	0.075	19100	2.03	22.45	6.86	7100	32.5	1.575	1.74
625	2541	1.4	36.17	0.07	18500	2.22	19.15	4.6	6290	212	1.27	1.46
635	2211	1.6	32.17	0.055	17500	3.46	17.15	4.64	7270	178	1.06	1.32
645	1951	1.2	23.87	0.034	16100	2.82	16.75	2.9	6140	109	0.58	1.09
655	2031	1.3	27.47	0.042	17300	3.75	17.75	3.2	7540	126	0.71	1.24
665	1931	1.3	25.17	0.032	16500	3.53	16.65	2.88	6960	106	0.57	1.15
675	3031	0.9	35.67	0.077	16300	2.59	15.75	7.44	7020	61.5	1.515	1.45

AES LC2												
Depth (cm)	**Mg**	**Mn**	**Mo**	**Na**	**Ni**	**P**	**Pb**	**S**	**Sr**	**Ti**	**V**	**Zn**
515	5940	14.4	0.20	519	2.93	87	0.60	3270	103.00	76.67	1.96	1.11
525	5780	13.5	0.20	501	3.03	81.8	0.40	3120	98.80	44.47	1.72	0.66
535	4620	11.9	0.30	475	3.19	109	0.40	2860	79.10	88.17	2.82	1.46
545	4990	13.7	0.45	448	3.55	105	0.40	3200	84.90	72.47	5.06	1.21
555	4660	12.7	0.55	456	3.81	117	0.60	3380	77.70	79.67	6.78	1.52
565	7730	22.2	0.55	589	5.19	135	0.60	5510	144.00	192.07	8.02	0.70
575	6720	22.1	0.60	539	7.93	110	1.60	4280	134.00	213.07	8.28	1.02
585	7200	28.6	0.20	586	9.81	90.8	1.20	3320	173.00	300.07	6.88	1.39
595	8270	25.9	0.30	593	6.35	91.8	1.20	5990	169.00	147.07	6.44	7.64
605	7540	28.0	0.30	605	5.85	90.8	1.00	3710	157.00	217.07	6.02	1.66
615	7170	28.1	0.20	588	7.09	88	1.00	3600	155.00	271.07	6.44	1.13
625	7100	27.5	0.15	567	5.77	83	0.80	3600	149.00	201.07	6.20	0.79
635	6950	24.6	0.20	568	6.29	87.4	1.00	5610	140.00	157.07	6.34	2.83
645	6960	22.3	0.25	546	5.23	94	0.60	5560	124.00	78.87	6.74	6.81
655	7290	22.7	0.25	571	5.75	96.2	1.00	6390	134.00	96.07	6.98	0.74
665	7180	21.7	0.20	562	5.63	92.8	0.60	6050	128.00	68.27	6.78	0.69
675	6430	26.4	0.15	555	8.89	88.4	1.00	3480	133.00	267.07	7.60	0.96

AES LC2												
Depth (cm)	**Al**	**As**	**Ba**	**Be**	**Ca**	**Co**	**Cr**	**Cu**	**Fe**	**K**	**La**	**Li**
685	2431	1.1	33.77	0.076	16900	2.31	17.85	4.53	6010	187	1.175	1.36
695	2371	1.1	30.97	0.078	16200	2.70	18.95	4.85	5950	177	1.105	1.27
705	3661	1.1	44.97	0.151	16500	2.01	29.75	7	5760	73.5	2.165	1.58
715	2791	2.0	34.97	0.102	16300	3.20	25.35	6.53	5690	167	1.245	1.29
725	2761	2.3	32.17	0.093	14800	3.57	19.75	7.49	5000	184	1.145	1.13
735	3811	2.0	41.37	0.126	15300	2.78	19.65	8.11	4960	46.5	1.76	1.69
745	3061	2.4	36.77	0.101	14600	2.66	19.35	7.24	4390	21	1.39	1.24
755	3941	1.9	42.77	0.129	15500	2.42	19.55	6.76	4840	42.5	1.81	1.72
775	3541	2.1	44.07	0.126	15500	2.53	20.65	5.72	4660	77.5	1.98	1.49
785	2921	3.1	30.07	0.062	14300	3.03	17.45	6.84	4100	123	0.8	1.15
795	4201	4.1	49.27	0.128	16600	2.27	16.35	12.7	5040	52	2.025	1.93
805	2921	3.9	37.37	0.082	16300	2.52	18.45	5.16	4560	154	1.205	1.31
815	2791	3.5	36.47	0.063	17300	2.68	17.45	4.43	4720	118	0.97	1.40
825	2351	3.0	34.87	0.061	15000	2.76	15.85	4.74	4350	126	0.92	1.02
835	2351	2.8	36.47	0.065	14900	2.66	15.15	5.53	4450	133	0.83	1.10
845	2161	2.6	44.77	0.078	17100	2.14	13.85	4.19	4840	157	1.115	1.22
855	2411	2.7	34.57	0.06	14800	2.78	17.35	4.82	4290	98.5	0.72	0.98

AES LC2												
Depth (cm)	**Mg**	**Mn**	**Mo**	**Na**	**Ni**	**P**	**Pb**	**S**	**Sr**	**Ti**	**V**	**Zn**
685	6760	26.9	0.15	553	6.49	93.8	0.80	3830	136.00	168.07	7.90	0.84
695	6700	26.1	0.20	548	6.61	107	0.80	4080	129.00	148.07	9.44	1.59
705	5890	36.8	0.15	547	8.15	91.4	1.00	2510	140.00	355.07	16.70	2.38
715	6660	30.2	0.20	544	6.33	97.4	1.20	3970	131.00	211.07	18.60	1.16
725	6180	30.8	0.25	543	6.17	112	1.00	3490	119.00	221.07	20.40	3.55
735	5940	45.0	0.20	556	7.29	106	0.80	2560	129.00	362.07	21.20	3.06
745	5900	38.0	0.25	564	6.11	109	1.20	2610	119.00	284.07	23.50	1.87
755	6000	47.2	0.20	524	7.13	102	1.00	2290	131.00	369.07	21.00	3.99
775	5870	45.2	0.20	541	6.05	97.6	1.00	2260	132.00	365.07	22.20	4.45
785	6320	29.2	0.30	506	5.89	109	0.60	2970	114.00	168.07	25.20	4.63
795	6010	40.9	0.25	533	8.39	107	1.20	2060	141.00	366.07	22.20	3.76
805	6530	36.1	0.15	542	5.85	114	0.80	2680	130.00	208.07	20.60	6.74
815	6930	36.9	0.20	583	5.73	109	1.00	2740	138.00	130.07	20.70	14.30
825	6410	36.0	0.20	537	5.67	108	1.00	2680	119.00	163.07	20.30	6.30
835	6330	37.6	0.20	512	6.21	106	0.60	2650	119.00	184.07	21.50	2.70
845	6830	44.2	0.20	515	5.69	106	0.80	2510	138.00	166.07	23.30	0.58
855	6240	34.2	0.25	474	5.43	94	0.80	2790	118.00	132.07	22.50	0.55

AES LC2												
Depth (cm)	**Al**	**As**	**Ba**	**Be**	**Ca**	**Co**	**Cr**	**Cu**	**Fe**	**K**	**La**	**Li**
865	2411	2.5	38.47	0.079	15000	2.40	16.45	6.2	4650	136	0.97	1.09
875	2271	2.5	39.97	0.075	15700	2.21	16.65	5.13	4570	157	1.07	1.14
885	2171	2.4	39.97	0.075	16200	2.09	17.45	5.08	4620	142	1.015	1.14
895	2081	2.7	39.37	0.065	15700	2.19	18.75	4.54	4520	119	0.91	1.03
905	1471	3.4	40.87	0.04	17000	2.33	12.85	2.92	4590	86.5	0.585	1.12
915	1401	3.6	34.97	0.036	14800	2.82	12.55	2.19	3930	75.5	0.52	0.85
925	1271	4.2	35.97	0.04	14500	2.93	12.85	2.43	4000	89	0.505	0.85
935	1121	4.3	34.17	0.033	13800	2.89	13.15	2.33	3800	82	0.46	0.75
945	1081	3.9	36.87	0.039	14300	2.58	11.85	2.59	4050	98.5	0.51	0.82
955	1110	3.1	40.65	0.046	14300	1.97	11.21	3.26	4390	125	0.655	0.89
965	1400	2.5	39.35	0.039	14500	2.14	9.91	4.08	4310	130	0.705	1.03
975	1350	2.1	38.75	0.042	13600	2.42	8.59	4.25	4210	118	0.67	0.92
985	1210	1.9	40.25	0.038	14200	2.58	9.22	4.87	4380	108	0.665	0.95
995	1070	1.6	39.95	0.033	14000	2.40	6.00	4.83	4330	85	0.525	0.84
1005	1020	1.1	38.95	0.029	14100	3.52	4.22	3.27	4190	103	0.55	0.87
1015	1070	1.5	41.65	0.027	15100	3.53	4.32	4.64	4400	112	0.58	0.94
1025	1250	2.2	41.15	0.031	14700	3.52	3.60	3.34	4340	140	0.715	0.86

AES LC2												
Depth (cm)	**Mg**	**Mn**	**Mo**	**Na**	**Ni**	**P**	**Pb**	**S**	**Sr**	**Ti**	**V**	**Zn**
865	6150	36.8	0.25	475	6.27	94	0.80	2670	121.00	161.07	22.70	0.66
875	6340	38.2	0.25	481	5.55	101	0.80	2690	126.00	160.07	24.10	1.68
885	6560	39.4	0.25	485	5.79	94.8	0.60	2800	129.00	140.07	25.40	1.11
895	6480	38.9	0.25	483	5.77	93.8	0.60	2940	125.00	125.07	27.90	0.65
905	7430	43.8	0.10	550	4.77	83.8	0.60	2740	134.00	66.57	30.60	0.86
915	6590	37.4	0.15	518	4.35	83.4	0.60	2760	117.00	58.97	29.80	2.06
925	6400	38.3	0.20	521	4.61	93	0.60	2820	114.00	64.87	27.10	0.87
935	6110	37.4	0.30	507	4.67	98.4	0.60	3090	108.00	57.07	26.10	1.59
945	6280	40.3	0.30	514	5.13	104	0.60	3000	112.00	71.17	20.90	0.73
955	6090	49.1	0.30	492	4.94	105	0.60	2910	113.00	97.83	13.10	0.84
965	6070	48.5	0.30	522	5.20	108	0.60	3030	113.00	93.13	9.88	2.02
975	5740	47.5	0.25	492	5.32	103	0.80	2920	106.00	97.53	7.56	1.48
985	6130	51.3	0.30	497	5.46	98.8	0.60	2980	111.00	95.83	5.56	0.83
995	6110	51.9	0.25	486	4.62	93.4	0.60	2860	109.00	58.03	4.48	8.45
1005	6370	49.2	0.20	539	4.52	89.8	0.60	2860	108.00	58.73	3.54	1.12
1015	6820	54.5	0.30	569	4.62	97.8	0.60	3090	116.00	63.33	3.36	0.77
1025	6630	54.7	0.30	556	4.46	108	0.60	3090	112.00	90.33	3.34	0.57

AES LC2												
Depth (cm)	**Al**	**As**	**Ba**	**Be**	**Ca**	**Co**	**Cr**	**Cu**	**Fe**	**K**	**La**	**Li**
1035	1190	2.0	45.55	0.034	15700	3.63	3.52	4.23	4650	126	0.725	1.00
1045	1560	1.1	48.45	0.04	16000	3.17	3.90	4.42	4790	209	1.015	1.08
1055	1500	1.8	43.95	0.04	13800	2.33	7.11	4.38	4210	117	0.71	0.80
1065	1450	2.1	45.75	0.043	13900	2.12	6.99	3	4230	120	0.77	0.83
1075	1510	2.4	44.15	0.038	13500	1.60	7.69	3.32	4380	108	0.745	0.78
1085	1690	2.2	45.35	0.069	13400	1.91	8.27	3.94	4230	117	0.82	0.80
1095	1910	2.1	50.35	0.066	14600	2.10	15.11	4.39	4660	152	1.025	1.01
1105	1490	1.6	35.55	0.032	12700	1.73	5.91	6.29	4210	139	0.72	0.73
1115	1470	2.2	44.35	0.041	14100	1.53	6.52	3.66	4450	154	0.905	0.89
1125	1420	1.9	40.85	0.046	13000	1.52	5.41	3.55	4230	129	0.875	0.79
1135	1640	1.7	47.55	0.058	13900	1.68	9.26	4.08	4770	172	1.17	0.95
1145	1930	1.3	46.65	0.067	13600	1.94	7.82	5.23	4590	204	1.215	0.92
1155	1440	1.0	40.75	0.038	11900	2.19	9.91	3.22	3650	130	0.825	0.64
1165	1350	1.1	37.75	0.035	10700	2.01	5.64	3.86	3590	148	0.86	0.56
1175	1210	0.9	40.95	0.052	12400	1.98	5.55	5.24	4000	121	1.065	0.68
1185	1070	0.9	35.65	0.034	9860	1.71	5.11	3.82	3260	99	0.78	0.48
1195	1130	1.0	34.55	0.031	9420	1.52	5.90	4.06	3230	122	0.835	0.43

AES LC2												
Depth (cm)	**Mg**	**Mn**	**Mo**	**Na**	**Ni**	**P**	**Pb**	**S**	**Sr**	**Ti**	**V**	**Zn**
1035	7000	60.2	0.30	552	4.52	88	0.60	3040	120.00	88.83	3.50	1.01
1045	7150	62.9	0.25	600	4.06	88.8	0.80	3070	124.00	162.43	4.58	0.80
1055	5970	58.2	0.40	422	4.64	98.6	0.60	3330	107.00	87.53	9.36	4.73
1065	6010	60.0	0.40	433	4.32	90.2	0.60	3530	108.00	83.73	10.80	4.33
1075	5830	59.1	0.45	431	4.68	89	0.80	3730	104.00	80.93	12.40	83.10
1085	5850	61.0	0.30	416	4.52	89.6	0.80	3570	103.00	89.83	11.70	2.05
1095	6310	68.5	0.30	433	5.44	85.4	0.80	4150	113.00	133.43	13.40	1.63
1105	5530	44.5	0.40	474	18.02	101	0.60	3310	98.70	104.43	9.46	3.32
1115	6140	59.3	0.55	497	4.62	115	0.80	3750	109.00	103.43	18.40	0.90
1125	5740	57.9	0.45	479	4.44	100	0.60	3480	102.00	107.43	16.00	1.33
1135	6020	66.6	0.35	489	5.32	109	0.80	3880	108.00	142.43	15.10	9.43
1145	5840	63.5	0.30	488	4.02	82.4	0.80	3490	108.00	163.43	10.40	4.41
1155	5360	52.9	0.20	492	4.44	88.4	1.00	3670	94.20	100.43	5.06	2.85
1165	4990	50.4	0.20	494	4.48	102	0.60	3340	85.00	100.43	3.66	6.34
1175	5560	61.0	0.25	487	6.12	87.4	0.60	3720	95.20	91.43	3.46	1.94
1185	4600	49.0	0.20	470	5.24	95	0.60	3430	78.20	68.33	3.32	2.31
1195	4420	48.5	0.30	487	4.38	109	0.60	3740	75.30	84.53	3.30	2.06

AES LC2												
Depth (cm)	**Al**	**As**	**Ba**	**Be**	**Ca**	**Co**	**Cr**	**Cu**	**Fe**	**K**	**La**	**Li**
1205	1060	2.3	44.45	0.029	13900	1.31	4.40	1.69	4330	69	0.76	0.81
1215	1210	3.4	38.55	0.047	15300	1.70	4.37	2.37	4810	120	1.025	0.94
1225	1430	3.0	44.95	0.057	14500	1.85	7.78	3.83	4810	134	1.06	0.92
1235	1490	2.7	42.65	0.045	12900	2.16	9.01	4.36	4190	131	0.86	0.73
1245	1590	2.3	39.45	0.074	12900	2.21	9.71	4.29	4450	139	1.095	0.78
1255	1600	1.6	40.45	0.044	10100	1.58	4.32	6.88	3480	17.5	1.08	0.56
1265	1780	1.7	21.65	0.07	11600	1.80	4.25	7.11	4000	179	1.26	0.69
1275	1370	1.1	37.75	0.083	11500	2.30	4.24	4.82	3930	112	1.19	0.59
1285	1340	1.1	43.45	0.091	11600	2.28	5.01	4.67	4060	113	1.24	0.60
1295	1400	1.2	42.45	0.099	11400	2.30	6.35	4.89	4070	144	1.24	0.60

AES LC2												
Depth (cm)	**Mg**	**Mn**	**Mo**	**Na**	**Ni**	**P**	**Pb**	**S**	**Sr**	**Ti**	**V**	**Zn**
1205	5740	68.1	0.30	399	3.48	63	0.80	3990	109.00	32.23	6.70	1.78
1215	6300	80.7	0.30	422	4.32	68.4	0.80	3850	116.00	70.53	6.68	4.28
1225	6050	78.7	0.30	426	4.98	78.8	0.80	3860	110.00	100.43	9.08	3.29
1235	5430	68.6	0.40	415	4.66	79.8	0.80	4140	99.40	90.83	11.50	1.44
1245	5320	73.2	0.30	402	5.72	90	0.60	3680	98.20	138.43	6.64	2.39
1255	4420	58.7	0.65	467	4.98	121	0.80	3630	79.20	157.43	4.96	8.43
1265	4900	68.7	0.40	455	4.30	93.4	1.00	4200	88.30	180.43	6.58	1.81
1275	4850	70.7	0.20	425	4.00	82.8	0.80	3920	86.60	120.43	5.20	2.21
1285	4900	71.8	0.15	423	4.26	83.8	1.00	4200	88.20	132.43	4.92	2.33
1295	4880	71.3	0.20	441	5.10	90.8	0.60	4360	87.40	132.43	4.54	2.03

ICP-MS Trace											
LC2											
Depth (cm)	**Sc45 mg/L**	**Ti47 mg/L**	**Cr52 mg/L**	**Co59 mg/L**	**Cu65 mg/L**	**Ga69 mg/L**	**As75 mg/L**	**Rb85 mg/L**	**Sr88 mg/L**	**Cd111 mg/L**	**Ba137 mg/L**
5	2.01	475.3507	20.3877	4.0524	7.9457	2.3844	2.2399	1.6268	100.0546	0.0613	33.5142
15	0.5946	178.4723	5.59855	3.1763	3.60905	0.7166	1.67865	0.97645	74.1101	0.02235	7.1562
25	0.7145	182.4257	5.1558	2.973	3.6706	0.4927	1.4144	0.3464	51.4086	0.0195	4.8431
35	0.752	164.8291	5.3581	2.3835	4.293	0.4824	1.3733	0.1282	39.6674	0.0152	3.0217
45	0.8579	267.7253	9.2107	1.9974	7.4721	0.6434	1.4909	0.1258	24.4305	0.0177	1.6714
55	1.1853	318.6025	10.7432	1.9268	8.2802	0.9405	1.6067	0.0796	20.8153	0.0283	1.7379
65	1.1418	298.8803	12.4542	1.9849	8.2761	1.1058	1.8968	0.0834	22.0824	0.0253	2.138
75	0.9127	209.6995	14.1425	1.9836	6.3467	1.0557	1.7514	0.067	22.8916	0.0219	2.0986
85	0.6877	155.0773	14.6206	2.5589	5.7811	1.0075	1.9775	0.0539	24.7447	0.0203	2.0005
95	0.7802	200.6469	25.7677	2.2475	4.1074	0.886	2.0245	0.0898	31.7515	0.0391	2.9034
105	0.8418	234.9554	27.4662	2.7057	4.5459	1.1149	2.2815	0.316	42.1057	0.0266	7.3501
115	0.49425	107.5798	34.09525	2.6704	4.368	0.8843	2.501	0.10205	31.8726	0.02365	2.7779
125	0.5426	211.905	26.9926	2.6852	3.9533	0.957	2.5923	0.1913	31.5528	0.1063	3.8031
135	0.5946	0.5946	0.5946	0.5946	0.5946	0.5946	0.5946	0.5946	0.5946	0.5946	0.5946
145	0.8304	484.4664	24.3212	2.4935	4.3444	1.2359	2.5169	0.6042	41.5672	0.0303	5.8182
155	0.7469	200.6244	16.4504	2.8189	4.2421	1.052	2.6336	0.3565	46.7881	0.0552	5.8224
165	0.6628	193.4173	17.4345	2.9581	4.2219	1.2438	3.1864	0.4972	42.7554	0.0484	5.7958
175	1.4392	526.7059	28.8983	2.5987	12.1479	2.4428	3.7451	1.4308	53.7334	0.0567	10.9804

Appendix 8B: ICP-MS Trace LC2

ICP-MS Trace											
LC2											
Depth (cm)	**Sc45 mg/L**	**Ti47 mg/L**	**Cr52 mg/L**	**Co59 mg/L**	**Cu65 mg/L**	**Ga69 mg/L**	**As75 mg/L**	**Rb85 mg/L**	**Sr88 mg/L**	**Cd111 mg/L**	**Ba137 mg/L**
185	1.7522	722.8255	29.3816	1.41795	18.30665	3.1665	2.0542	2.46865	55.8071	0.0541	17.05875
195	1.6832	575.3391	28.8702	1.307	11.7041	2.6412	3.2513	1.344	75.5722	0.0423	15.8133
205	1.2379	398.5786	27.6609	1.7136	9.5389	2.1176	4.0709	1.0144	74.5385	0.0448	13.8144
215	1.1596	378.9007	28.7845	1.7366	7.2943	1.9876	4.4803	1.1529	84.2173	0.0404	16.0634
225	1.0628	368.2827	27.9612	1.7296	6.6061	1.9915	4.8295	1.2909	78.7905	0.0364	15.6228
235	1.0838	323.0728	31.3234	1.9274	5.4859	2.2427	5.6207	0.9723	92.8303	0.0339	16.772
245	0.9221	318.1001	32.0805	2.2712	4.4795	1.958	5.8408	0.829	93.5797	0.0302	15.2662
255	0.9953	333.7494	32.2124	2.1072	4.3555	1.8401	5.2653	0.8069	103.8423	0.0662	18.6494
265	0.7918	265.653	33.1347	2.4857	5.1618	1.8239	5.6445	0.7249	109.1208	0.0357	16.096
275	0.6337	215.7251	33.2266	2.5745	4.85455	1.66605	5.853	0.60685	108.33285	0.0702	14.11275
285	0.8101	292.7338	35.2332	2.2207	5.2654	1.7705	5.4382	0.9265	119.2053	0.0281	18.423
295	0.8525	247.3975	36.6833	2.1006	5.4249	1.7233	5.4856	0.7926	132.8239	0.0348	20.4578
305	0.791	289.2897	30.9045	2.1006	5.0439	1.6845	4.2545	0.8457	130.7847	0.0299	19.6126
315	0.7446	237.6533	31.7408	2.0816	4.5111	1.602	4.0398	0.6903	148.4657	0.0339	21.2436
325	0.547	140.2854	29.8683	2.0984	3.2815	1.3512	3.568	0.3997	139.6636	0.0274	16.7886
335	0.6015	194.1701	46.2612	2.5805	4.3485	1.4402	3.5459	0.5558	145.7315	0.0311	19.0454
345	0.5642	162.1236	23.4484	2.0063	3.6996	1.3655	3.3096	0.5009	145.7883	0.0338	18.5826
355	0.5204	133.3593	21.6241	1.9147	2.834	1.2712	3.1231	0.4133	143.6824	0.0232	16.5157

Appendix 8B: ICP-MS Trace LC2

ICP-MS Trace											
LC2											
Depth (cm)	**Sc45 mg/L**	**Ti47 mg/L**	**Cr52 mg/L**	**Co59 mg/L**	**Cu65 mg/L**	**Ga69 mg/L**	**As75 mg/L**	**Rb85 mg/L**	**Sr88 mg/L**	**Cd111 mg/L**	**Ba137 mg/L**
365	0.5272	149.2019	17.1699	1.9112	3.0126	1.2547	2.6248	0.5235	137.464	0.0251	16.4948
375	0.6949	300.1833	15.3148	1.9754	3.6065	1.6773	2.1091	1.0326	140.6195	0.0244	18.6351
385	0.6487	208.0819	13.2553	1.7098	3.5399	1.4067	2.0001	0.7822	137.7354	0.0214	18.2072
395	0.6554	227.5946	12.9916	1.6487	3.8773	1.4294	1.8869	1.0291	141.9227	0.0224	19.236
405	0.5648	170.6888	10.6865	1.6164	2.8712	1.3143	1.6702	0.7017	148.5989	0.0186	19.4683
415	0.517	146.4965	10.2361	1.6865	2.9783	1.2208	1.4492	0.6938	143.6835	0.0208	18.1217
425	0.4678	111.684	9.7448	1.8436	2.6891	1.1093	1.5571	0.5505	137.8107	0.0231	16.8078
435	0.4017	67.6309	10.1015	2.0852	2.8043	0.9224	0.8531	0.4496	126.0853	0.0244	14.8383
445	0.2989	53.3746	8.4249	3.2581	2.1566	0.7548	0.8285	0.3536	85.9736	0.026	9.9478
455	0.3376	74.634	11.5433	1.507	2.9049	0.9183	0.4988	0.3674	131.4378	0.019	16.7884
465	0.41815	102.1187	13.00455	1.20005	2.63945	1.14895	0.55285	0.49115	147.24205	0.02015	20.8295
475	0.4473	122.1266	14.7389	1.3072	2.5142	1.3219	0.4675	0.5452	152.8327	0.027	21.3504
485	1.0116	384.6849	18.8848	0.9802	6.8722	2.364	0.3899	3.4066	181.6762	0.0333	36.1869
495	0.9074	331.6208	17.9469	2.0231	5.8569	2.1444	0.7849	2.8386	138.3963	0.0283	24.4968
505	0.3735	74.9756	8.4085	1.5232	1.9543	0.9332	0.3306	0.4703	121.4956	0.0169	17.6343
515	0.3606	67.3837	8.1998	1.6474	15.6669	0.9225	0.2562	0.4735	114.8336	0.0233	15.8
525	0.3583	39.5822	7.91595	1.57875	1.8333	0.7706	0.3211	0.32965	110.19635	0.021	15.0235
535	0.4308	74.7513	8.4997	2.4332	1.9875	0.8422	0.3568	0.625	85.7191	0.0188	13.0547

Appendix 8B: ICP-MS Trace LC2

ICP-MS Trace											
LC2											
Depth (cm)	**Sc45 mg/L**	**Ti47 mg/L**	**Cr52 mg/L**	**Co59 mg/L**	**Cu65 mg/L**	**Ga69 mg/L**	**As75 mg/L**	**Rb85 mg/L**	**Sr88 mg/L**	**Cd111 mg/L**	**Ba137 mg/L**
545	0.5403	61.6818	11.3354	1.7114	3.4364	1.2082	0.4586	0.5803	92.4033	0.023	13.7202
555	0.515	68.7821	12.4319	1.9684	6.1194	1.5573	0.742	0.435	85.1856	0.0179	12.7755
565	1.1725	185.2182	20.6987	1.5959	4.0731	2.8146	0.6813	0.5195	162.6866	0.0256	27.7878
575	0.9969	204.9118	23.549	6.2166	5.6861	2.6783	1.2467	1.076	155.7426	0.0471	31.3425
585	1.2121	309.4877	25.4587	2.1732	6.6918	2.7863	0.6361	1.4028	205.0186	0.0327	49.3244
595	0.7774	141.6741	23.89455	4.6748	4.6988	2.1825	0.94795	0.6026	197.39265	0.03575	38.46305
605	0.7178	208.2647	23.8139	1.6201	4.7771	2.0814	0.6911	1.1309	179.9429	0.03	38.2522
615	0.8502	266.3987	25.481	1.7408	7.0326	2.2693	0.7129	1.328	179.326	0.0226	40.6371
625	0.6932	193.4527	21.7967	2.0778	4.8304	1.98	0.8599	0.7022	170.5513	0.1294	37.609
635	0.5911	151.5558	19.331	3.4447	4.9051	1.7583	0.8646	0.5627	161.0305	0.0327	33.3966
645	0.4111	70.6186	18.0456	2.7894	3.1265	1.374	0.717	0.299	139.3658	0.0265	24.1137
655	0.4631	87.4235	19.696	3.7673	3.4721	1.547	0.8192	0.3522	153.299	0.0292	28.0769
665	0.4228	62.6669	18.4599	3.5975	3.2176	1.4437	0.7452	0.282	146.3048	0.0299	25.5233
675	0.7623	258.4387	17.7595	2.3246	7.4938	2.1667	0.6198	1.3339	153.547	0.0288	37.3884
685	0.6423	158.7104	19.7803	2.1668	4.8513	1.8632	0.6436	0.6175	157.4148	0.0284	35.224
695	0.5923	139.9273	21.1729	2.6853	5.3661	1.7443	0.83565	0.6051	148.6901	0.0331	31.88275
705	1.2287	338.5809	31.437	1.5022	7.3674	2.6984	0.9046	1.2401	156.1676	0.0424	46.8347
715	0.8252	196.0047	27.4491	2.9946	6.5328	2.0747	1.5087	0.5362	148.8591	0.0488	36.0764

Appendix 8B: ICP-MS Trace LC2

ICP-MS Trace											
LC2											
Depth (cm)	**Sc45 mg/L**	**Ti47 mg/L**	**Cr52 mg/L**	**Co59 mg/L**	**Cu65 mg/L**	**Ga69 mg/L**	**As75 mg/L**	**Rb85 mg/L**	**Sr88 mg/L**	**Cd111 mg/L**	**Ba137 mg/L**
725	0.7474	207.4192	21.4964	3.3613	7.5055	2.1118	1.7585	0.6214	135.0635	0.0593	33.1482
735	1.075	355.2762	21.8755	2.335	8.2911	2.8205	1.5782	1.1649	148.4515	0.0317	44.0699
745	0.7728	270.3429	20.8857	2.2853	7.1041	2.2604	2.0127	0.8692	133.4509	0.0421	37.2475
755	1.0748	364.563	22.1171	1.9707	7.0228	2.925	1.4546	1.1632	150.0287	0.0338	45.6667
775	1.0342	368.3103	23.08815	2.0766	6.0948	2.73885	1.74555	1.2534	153.36775	0.03545	47.01905
785	0.551	156.7246	19.2065	2.8765	6.9718	2.1327	2.816	0.3974	128.1332	0.0321	30.7866
795	1.0935	368.535	18.65	1.8331	13.0026	3.1638	1.9999	1.2277	165.2621	0.0512	52.8771
805	0.6664	200.3609	20.4655	2.3459	5.516	2.264	2.3831	0.4694	150.2475	0.0353	38.5141
815	0.5576	123.9724	19.1472	2.6272	4.6681	2.1465	2.1968	0.3107	156.7753	0.0411	37.3916
825	0.5114	154.5098	17.6467	2.6266	4.9935	1.9839	2.0495	0.371	135.2039	0.0339	35.273
835	0.5273	178.0702	17.1527	2.5085	6.0422	2.0358	1.9062	0.4372	136.524	0.0367	37.7992
845	0.5557	161.356	15.8569	2.012	4.6006	2.262	1.7984	0.5004	159.411	0.0372	47.7072
855	0.4901	123.8471	18.8485	2.685	5.1802	2.0471	1.9829	0.3015	134.6941	0.0424	35.1501
865	0.5656	153.4563	18.2984	2.2692	6.6226	2.1088	1.7729	0.4374	138.9706	0.0361	39.7008
875	0.5645	155.8057	18.6646	2.0875	5.3825	2.1517	1.8433	0.5003	144.2065	0.039	41.8583
885	0.5318	134.4877	19.4038	2.0039	5.3651	2.0905	1.87	0.4195	148.8026	0.0341	42.3733
895	0.496	118.494	20.9078	2.1065	4.8308	2.0697	2.1532	0.345	144.1269	0.0432	41.2302
905	0.3745	62.0348	14.8737	2.3788	3.2802	1.9136	2.9709	0.2134	154.1108	0.0294	42.9712

Appendix 8B: ICP-MS Trace LC2

ICP-MS Trace											
LC2											
Depth (cm)	**Sc45 mg/L**	**Ti47 mg/L**	**Cr52 mg/L**	**Co59 mg/L**	**Cu65 mg/L**	**Ga69 mg/L**	**As75 mg/L**	**Rb85 mg/L**	**Sr88 mg/L**	**Cd111 mg/L**	**Ba137 mg/L**
915	0.3405	54.1355	14.2132	2.8434	2.5162	1.6299	3.15	0.1709	131.7733	0.0322	35.6624
925	0.3211	59.2879	14.6074	2.9176	2.6603	1.5709	3.423	0.2321	128.7232	0.031	36.8447
935	0.3024	51.9457	14.5138	2.8862	2.6265	1.4746	3.6297	0.2111	123.0436	0.0345	34.2611
945	0.3071	63.0575	12.9901	2.464	2.7529	1.5166	3.2517	0.266	123.0767	0.0325	36.4736
955	0.3425	89.0669	12.553	1.8789	3.4691	1.7762	2.5538	0.3694	127.1113	0.0328	43.4883
965	0.3631	85.7803	11.4992	2.0578	4.3539	1.7509	2.013	0.3724	126.6408	0.039	40.1904
975	0.3637	88.2956	10.3299	2.3339	4.5733	1.7297	1.616	0.3432	117.6845	0.0335	39.88
985	0.368	86.3573	11.058	2.4989	5.0025	1.7459	1.2704	0.3046	122.4201	0.0376	41.3993
995	0.3511	53.9413	7.6738	2.3853	5.0201	1.7099	1.1224	0.2271	121.8841	0.0335	41.5203
1005	0.342	55.2358	5.9304	3.5683	3.5484	1.624	0.7461	0.2677	121.7144	0.0335	41.0031
1015	0.33545	59.77435	5.70165	3.53495	4.8319	1.7788	0.6184	0.30535	128.9455	0.0316	44.14815
1025	0.3859	81.4731	4.9712	3.4068	3.5106	1.8291	0.5301	0.4	123.3485	0.0295	43.1867
1035	0.4353	82.7938	4.9784	3.6116	4.4854	2.032	0.5204	0.3742	135.8507	0.0485	49.1382
1045	0.4551	153.6776	4.848	2.9067	4.4501	2.2074	0.59875	0.6352	135.65555	0.03165	52.3562
1055	0.3587	74.66	7.6245	2.0758	4.2576	1.845	0.9129	0.3531	111.3955	0.0378	43.8723
1065	0.3684	75.9032	7.988	1.9994	3.2009	1.9773	1.2243	0.3728	119.4225	0.0394	48.468
1075	0.3634	73.1055	8.568	1.4743	3.4687	1.9251	1.5849	0.327	114.0106	0.0496	45.7532
1085	0.3926	78.1914	9.1132	1.7289	3.9469	1.9245	1.2627	0.3563	109.7196	0.044	45.4911

ICP-MS Trace											
LC2											
Depth (cm)	**Sc45 mg/L**	**Ti47 mg/L**	**Cr52 mg/L**	**Co59 mg/L**	**Cu65 mg/L**	**Ga69 mg/L**	**As75 mg/L**	**Rb85 mg/L**	**Sr88 mg/L**	**Cd111 mg/L**	**Ba137 mg/L**
1095	0.4646	124.3726	16.1591	1.87	4.4479	2.303	1.5068	0.5021	124.1669	0.0521	56.1992
1105	0.3621	93.5388	6.721	1.5782	6.2734	1.6577	1.0798	0.4572	108.0052	0.0359	37.0763
1115	0.3655	91.4401	7.2116	1.3313	3.7204	1.959	1.4773	0.4731	118.2249	0.048	46.5875
1125	0.3961	95.7913	6.2093	1.3522	3.6284	1.9536	1.3123	0.3975	111.5478	0.0429	46.0541
1135	0.4615	133.0381	10.3267	1.46	4.1379	2.1801	1.229	0.5897	118.3502	0.061	51.5414
1145	0.4648	154.3104	8.9876	1.7266	5.3162	2.3083	0.9278	0.6904	120.8118	0.0482	53.1841
1155	0.3349	88.6175	10.7978	1.993	3.3486	1.9051	0.4915	0.4162	102.4154	0.0449	41.8651
1165	0.385	89.5221	6.4627	1.8375	3.9602	1.6872	0.4182	0.5166	93.1411	0.0409	38.6917
1175	0.4246	80.7631	6.4132	1.8236	5.2928	1.8472	0.3101	0.3898	104.3945	0.0475	44.4127
1185	0.3156	59.7218	5.7861	1.5573	3.8723	1.5222	0.2567	0.3339	84.0043	0.037	35.5439
1195	0.3239	73.3174	6.5017	1.3469	4.0889	1.5439	0.4578	0.433	80.9119	0.0423	34.2304
1205	0.2618	28.567	5.1231	1.1991	1.7911	1.9157	1.6263	0.1874	115.1912	0.0396	50.6995
1215	0.3169	61.514	5.3807	1.6282	2.4573	2.2066	1.1186	0.3119	131.6155	0.0429	58.7469
1225	0.4036	90.2931	9.0662	1.7193	4.0404	2.2415	1.22	0.4227	123.5237	0.0516	56.096
1235	0.3583	76.4171	9.6562	1.9743	4.2894	2.1214	1.1737	0.4155	107.1661	0.0444	50.2019
1245	0.4207	127.9759	10.9959	2.0301	4.4627	2.2334	1.0038	0.4994	110.0763	0.0451	53.175
1255	0.43855	147.3287	5.1321	1.33745	7.04565	2.02655	0.86565	0.8151	89.38865	0.04925	44.5223
1265	0.4797	166.3021	5.0769	1.522	7.2292	2.3086	0.7333	0.7505	99.6503	0.0552	50.9421

ICP-MS Trace											
LC2											
Depth (cm)	**Sc45 mg/L**	**Ti47 mg/L**	**Cr52 mg/L**	**Co59 mg/L**	**Cu65 mg/L**	**Ga69 mg/L**	**As75 mg/L**	**Rb85 mg/L**	**Sr88 mg/L**	**Cd111 mg/L**	**Ba137 mg/L**
1275	0.4433	109.3268	5.019	2.0939	4.9618	2.0838	0.3908	0.3808	96.0651	0.0465	49.2207
1285	0.4004	117.5299	5.66965	2.03795	4.7571	2.11125	0.34725	0.36235	96.8593	0.0419	49.887
1295	0.3723	118.7954	7.1055	2.0916	5.0476	2.1633	0.4561	0.5328	96.7236	0.0446	50.0181

ICP-MS Trace - Blanks											
LC2											
Type	**Sc45 mg/L**	**Ti47 mg/L**	**Cr52 mg/L**	**Co59 mg/L**	**Cu65 mg/L**	**Ga69 mg/L**	**As75 mg/L**	**Rb85 mg/L**	**Sr88 mg/L**	**Cd111 mg/L**	**Ba137 mg/L**
BLANK	0.0977	0.4425	0.7813	0.0083	0.2255	0.0184	nd	nd	0.3082	0.0079	0.3336
BLANK	0.1159	0.7331	0.4861	0.0082	0.242	0.0127	nd	0.0029	0.2205	0.0106	0.1108
BLANK	0.103	0.3214	1.0176	0.0072	0.314	0.0099	nd	0.0026	0.2909	0.0126	0.0679
BLANK	0.1276	1.2226	0.443	0.0075	0.2758	0.0225	nd	0.0203	0.3329	0.0117	0.2541
BLANK	0.1259	0.2993	0.397	0.0047	0.1911	0.0086	nd	0.0035	0.3472	0.0075	0.0784
BLANK	0.1082	0.2634	0.6048	0.006	0.1766	0.0085	nd	0.0027	0.2677	0.0077	0.0829

ICP-MS Trace - Reference Material											
LC2											
Chinese Peach Leaves (CPL) and in House Reference Materials (HRM)											
Type	**Sc45 mg/L**	**Ti47 mg/L**	**Cr52 mg/L**	**Co59 mg/L**	**Cu65 mg/L**	**Ga69 mg/L**	**As75 mg/L**	**Rb85 mg/L**	**Sr88 mg/L**	**Cd111 mg/L**	**Ba137 mg/L**
CPL	0.2841	43.4454	1.7873	0.2267	9.0345	0.7549	0.4258	8.9302	61.4163	0.024	17.2228
CPL	0.2803	42.8677	3.185	0.2607	8.8248	0.8265	0.5085	8.9999	62.1937	0.0255	17.7937
CPL	0.2738	44.7013	1.2906	0.2195	8.8054	0.8855	0.2097	11.708	64.521	0.0287	17.0878
CPL	0.2787	46.9972	1.3135	0.2339	9.1119	0.8322	0.1426	9.2167	64.9265	0.0233	15.9279
Mean	**0.279**	**44.503**	**1.894**	**0.235**	**8.944**	**0.825**	**0.322**	**9.714**	**63.264**	**0.025**	**17.008**
StDev	0.0085	3.6612	1.7811	0.0360	0.3051	0.1073	0.3471	2.6702	3.4455	0.0048	1.5648
HRM 12	0.1825	14.2733	1.0535	0.1033	9.8705	1.112	0.3773	33.8995	7.9236	0.3708	28.1289
HRM 12	0.1824	13.9436	0.9922	0.0925	10.0846	1.1039	0.3425	31.1876	6.5333	0.3759	29.0658
Mean	**0.182**	**14.108**	**1.023**	**0.098**	**9.978**	**1.108**	**0.360**	**32.544**	**7.228**	**0.373**	**28.597**
StDev	0.0001	0.4663	0.0867	0.0153	0.3028	0.0115	0.0492	3.8352	1.9662	0.0072	1.3250
HRM 14	0.6849	113.7021	44.7316	2.9186	8.485	0.7972	0.9816	3.365	59.2155	0.1364	9.1308
HRM 14	0.6806	146.555	45.9486	2.7034	7.3032	0.7772	0.6727	3.3069	59.6873	0.1288	8.6253
HRM 14	0.57	84.0219	36.5064	2.3302	7.3056	0.6684	0.3735	3.1414	54.893	0.1146	7.8661
Mean	**0.645**	**114.760**	**42.396**	**2.651**	**7.698**	**0.748**	**0.676**	**3.271**	**57.932**	**0.127**	**8.541**
StDev	0.1303	62.5599	10.2726	0.5954	1.3632	0.1386	0.6081	0.2320	5.2847	0.0221	1.2732

ICP-MS Trace - Repeats											
LC2											
Depth (cm)	**Sc45 mg/L**	**Ti47 mg/L**	**Cr52 mg/L**	**Co59 mg/L**	**Cu65 mg/L**	**Ga69 mg/L**	**As75 mg/L**	**Rb85 mg/L**	**Sr88 mg/L**	**Cd111 mg/L**	**Ba137 mg/L**
15	0.5992	178.4715	5.9434	3.1877	3.5688	0.6856	1.8866	0.9537	72.2972	0.0238	7.2388
15	0.59	178.4731	5.2537	3.1649	3.6493	0.7476	1.4707	0.9992	75.923	0.0209	7.0736
	0.595	178.472	5.599	3.176	3.609	0.717	1.679	0.976	74.110	0.022	7.156
	0.007	0.001	0.488	0.016	0.057	0.044	0.294	0.032	2.564	0.002	0.117
	1.094	0.001	8.711	0.508	1.577	6.118	17.519	3.295	3.459	9.175	1.632
115	0.4997	111.8122	34.9951	2.7251	5.2112	0.8775	2.4221	0.1016	31.482	0.0246	2.7414
115	0.4888	103.3474	33.1954	2.6157	3.5248	0.8911	2.5799	0.1025	32.2632	0.0227	2.8144
	0.494	107.580	34.095	2.670	4.368	0.884	2.501	0.102	31.873	0.024	2.778
	0.008	5.986	1.273	0.077	1.192	0.010	0.112	0.001	0.552	0.001	0.052
	1.559	5.564	3.732	2.897	27.300	1.087	4.461	0.624	1.733	5.681	1.858
135	0.6086	152.309	22.6751	2.9244	4.0795	0.9582	2.6677	0.2196	36.2237	0.0281	3.9463
135	0.5737	141.3505	21.2133	2.7902	4.0391	0.965	2.6709	0.2086	36.8095	0.0287	4.1006
	0.591	146.830	21.944	2.857	4.059	0.962	2.669	0.214	36.517	0.028	4.023
	0.025	7.749	1.034	0.095	0.029	0.005	0.002	0.008	0.414	0.000	0.109
	4.175	5.277	4.710	3.321	0.704	0.500	0.085	3.633	1.134	1.494	2.712

ICP-MS Trace - Repeats											
LC2											
Depth (cm)	**Sc45 mg/L**	**Ti47 mg/L**	**Cr52 mg/L**	**Co59 mg/L**	**Cu65 mg/L**	**Ga69 mg/L**	**As75 mg/L**	**Rb85 mg/L**	**Sr88 mg/L**	**Cd111 mg/L**	**Ba137 mg/L**
185	1.7634	730.4501x	29.4923	1.4195	18.2625	3.0534	1.9234	2.4095	53.1963	0.0578	16.6002
185	1.741	715.2009x	29.2709	1.4164	18.3508	3.2796	2.185	2.5278	58.4179	0.0504	17.5173
	1.752		29.382	1.418	18.307	3.167	2.054	2.469	55.807	0.054	17.059
	0.016		0.157	0.002	0.062	0.160	0.185	0.084	3.692	0.005	0.648
	0.904		0.533	0.155	0.341	5.051	9.005	3.389	6.616	9.672	3.801
275	0.6432	216.8488	33.162	2.5743	4.9407	1.6652	5.8457	0.6054	108.2017	0.0407	14.3762
275	0.6242	214.6014	33.2912	2.5747	4.7684	1.6669	5.8603	0.6083	108.464	0.0997	13.8493
	0.634	215.725	33.227	2.575	4.855	1.666	5.853	0.607	108.333	0.070	14.113
	0.013	1.589	0.091	0.000	0.122	0.001	0.010	0.002	0.185	0.042	0.373
	2.120	0.737	0.275	0.011	2.510	0.072	0.176	0.338	0.171	59.429	2.640
465	0.4038	101.9829	13.2597	1.1632	2.832	1.1486	0.5168	0.4887	146.3779	0.0219	20.6452
465	0.4325	102.2545	12.7494	1.2369	2.4469	1.1493	0.5889	0.4936	148.1062	0.0184	21.0138
	0.418	102.119	13.005	1.200	2.639	1.149	0.553	0.491	147.242	0.020	20.830
	0.020	0.192	0.361	0.052	0.272	0.000	0.051	0.003	1.222	0.002	0.261
	4.853	0.188	2.775	4.343	10.317	0.043	9.222	0.705	0.830	12.282	1.251

ICP-MS Trace - Repeats											
LC2											
Depth (cm)	**Sc45 mg/L**	**Ti47 mg/L**	**Cr52 mg/L**	**Co59 mg/L**	**Cu65 mg/L**	**Ga69 mg/L**	**As75 mg/L**	**Rb85 mg/L**	**Sr88 mg/L**	**Cd111 mg/L**	**Ba137 mg/L**
525	0.3555	39.4293	7.81	1.5753	2.3473	0.7726	0.3216	0.3315	110.4695	0.0202	15.1196
525	0.3611	39.7351	8.0219	1.5822	1.3193	0.7686	0.3206	0.3278	109.9232	0.0218	14.9274
	0.358	39.582	7.916	1.579	1.833	0.771	0.321	0.330	110.196	0.021	15.024
	0.004	0.216	0.150	0.005	0.727	0.003	0.001	0.003	0.386	0.001	0.136
	1.105	0.546	1.893	0.309	39.650	0.367	0.220	0.794	0.351	5.387	0.905
695	0.592	140.2613	21.2578	2.7525	5.666	1.7396	0.8814	0.6161	148.3561	0.0331	31.7898
695	0.5926	139.5933	21.088	2.6181	5.0662	1.749	0.7899	0.5941	149.0241	0.0331	31.9757
	0.592	139.927	21.173	2.685	5.366	1.744	0.836	0.605	148.690	0.033	31.883
	0.000	0.472	0.120	0.095	0.424	0.007	0.065	0.016	0.472	0.000	0.131
	0.072	0.338	0.567	3.539	7.904	0.381	7.743	2.571	0.318	0.000	0.412
775	1.0094	363.981	22.6474	2.0634	5.9935	2.7164	1.6923	1.2696	152.2529	0.0347	47.0599
775	1.059	372.6396	23.5289	2.0898	6.1961	2.7613	1.7988	1.2372	154.4826	0.0362	46.9782
	1.034	368.310	23.088	2.077	6.095	2.739	1.746	1.253	153.368	0.035	47.019
	0.035	6.123	0.623	0.019	0.143	0.032	0.075	0.023	1.577	0.001	0.058
	3.391	1.662	2.700	0.899	2.351	1.159	4.314	1.828	1.028	2.992	0.123

ICP-MS Trace - Repeats											
LC2											
Depth (cm)	**Sc45 mg/L**	**Ti47 mg/L**	**Cr52 mg/L**	**Co59 mg/L**	**Cu65 mg/L**	**Ga69 mg/L**	**As75 mg/L**	**Rb85 mg/L**	**Sr88 mg/L**	**Cd111 mg/L**	**Ba137 mg/L**
1015	0.3408	61.8593	6.0556	3.5724	4.9356	1.7977	0.6122	0.3128	130.203	0.0325	44.5486
1015	0.3301	57.6894	5.3477	3.4975	4.7282	1.7599	0.6246	0.2979	127.688	0.0307	43.7477
	0.335	59.774	5.702	3.535	4.832	1.779	0.618	0.305	128.946	0.032	44.148
	0.008	2.949	0.501	0.053	0.147	0.027	0.009	0.011	1.778	0.001	0.566
	2.255	4.933	8.779	1.498	3.035	1.503	1.418	3.450	1.379	4.028	1.283
1045	0.4651	156.5748	5.0099	2.9611	4.5284	2.2594	0.659	0.646	137.8325	0.0332	53.2674
1045	0.4451	150.7804	4.6861	2.8523	4.3718	2.1554	0.5385	0.6244	133.4786	0.0301	51.445
	0.455	153.678	4.848	2.907	4.450	2.207	0.599	0.635	135.656	0.032	52.356
	0.014	4.097	0.229	0.077	0.111	0.074	0.085	0.015	3.079	0.002	1.289
	3.107	2.666	4.723	2.647	2.488	3.331	14.231	2.405	2.269	6.926	2.461
1255	0.4384	146.4416	5.0631	1.3397	7.0593	2.0243	0.7921	0.8925	89.3302	0.0492	45.0436
1255	0.4387	148.2157	5.2011	1.3352	7.032	2.0288	0.9392	0.7377	89.4471	0.0493	44.001
	0.439	147.329	5.132	1.337	7.046	2.027	0.866	0.815	89.389	0.049	44.522
	0.000	1.254	0.098	0.003	0.019	0.003	0.104	0.109	0.083	0.000	0.737
	0.048	0.851	1.901	0.238	0.274	0.157	12.016	13.429	0.092	0.144	1.656

ICP-MS Trace - Repeats											
LC2											
Depth (cm)	**Sc45 mg/L**	**Ti47 mg/L**	**Cr52 mg/L**	**Co59 mg/L**	**Cu65 mg/L**	**Ga69 mg/L**	**As75 mg/L**	**Rb85 mg/L**	**Sr88 mg/L**	**Cd111 mg/L**	**Ba137 mg/L**
1285	0.4037	117.8247	5.7371	2.0833	4.8355	2.1523	0.2774	0.3643	98.2658	0.0427	50.2758
1285	0.3971	117.2351	5.6022	1.9926	4.6787	2.0702	0.4171	0.3604	95.4528	0.0411	49.4982
	0.400	117.530	5.670	2.038	4.757	2.111	0.347	0.362	96.859	0.042	49.887
	0.005	0.417	0.095	0.064	0.111	0.058	0.099	0.003	1.989	0.001	0.550
	1.166	0.355	1.682	3.147	2.331	2.750	28.447	0.761	2.054	2.700	1.102

ICP-MS REE								
LC2								
Depth (cm)	**Y89 mg/L**	**Zr90 mg/L**	**Nb93 mg/L**	**La139 mg/L**	**Ce140 mg/L**	**Pr141 mg/L**	**Nd143 mg/L**	**Sm147 mg/L**
5	5.2250	8.2275	1.2436	7.1613	11.9397	1.6950	6.9106	1.4269
15	0.9344	3.6105	0.5057	1.4031	2.2996	0.3028	1.2148	0.2444
25	0.8291	3.8584	0.4983	1.3231	2.2465	0.2854	1.1268	0.2276
35	0.7042	3.5266	0.4524	1.1245	1.9832	0.2429	0.9528	0.1969
45	0.7984	5.5821	0.7485	1.2864	2.3029	0.2827	1.0981	0.2237
55	1.1491	6.6854	0.8772	1.7642	3.1305	0.3920	1.5399	0.3184
65	1.4239	6.5489	0.7626	2.0678	3.9003	0.4823	1.9085	0.3994
75	1.4334	5.0813	0.5233	1.8849	3.6867	0.4579	1.8687	0.3942
85	1.4068	4.2653	0.4195	1.5947	3.2152	0.4220	1.7599	0.3746
95	1.9324	4.7443	0.5139	2.0170	4.1406	0.5230	2.1721	0.4577
105	1.7345	4.9501	0.5620	2.1409	3.8379	0.5415	2.2229	0.4619
115	0.8855	3.3889	0.3071	0.8739	1.7685	0.2374	1.0175	0.2153
125	0.8732	4.8074	0.5263	1.0316	1.9792	0.2598	1.0654	0.2191
135	1.0053	4.2773	0.3902	1.0239	2.0514	0.2689	1.1151	0.2333
145	1.2990	8.6231	1.4182	1.9119	3.4877	0.4581	1.7987	0.3519
155	1.2382	5.1131	0.4783	1.4820	2.9155	0.3719	1.5049	0.3027
165	0.9288	5.1630	0.4981	1.1453	2.3292	0.2905	1.1914	0.2422
175	1.7438	9.9667	1.2367	2.2796	4.7252	0.5655	2.2186	0.4504
185	2.2633	12.9866	1.9383	2.9745	6.2331	0.7208	2.8138	0.5640

Appendix 8C: ICP-MS REE LC2

ICP-MS REE								
LC2								
Depth (cm)	**Eu151 mg/L**	**Gd157 mg/L**	**Tb159 mg/L**	**Dy163 mg/L**	**Ho165 mg/L**	**Er166 mg/L**	**Tm169 mg/L**	**Yb174 mg/L**
5	0.4369	1.4235	0.1981	1.0174	0.1834	0.4569	0.0573	0.3368
15	0.0718	0.2464	0.0327	0.1744	0.0319	0.0820	0.0111	0.0699
25	0.0658	0.2248	0.0308	0.1596	0.0289	0.0764	0.0098	0.0628
35	0.0568	0.1887	0.0259	0.1369	0.0247	0.0645	0.0082	0.0517
45	0.0637	0.2179	0.0303	0.1593	0.0292	0.0785	0.0104	0.0653
55	0.0943	0.3194	0.0455	0.2395	0.0431	0.1135	0.0149	0.0931
65	0.1144	0.3966	0.0560	0.3079	0.0554	0.1469	0.0197	0.1202
75	0.1142	0.3946	0.0564	0.2992	0.0556	0.1459	0.0196	0.1227
85	0.1081	0.3728	0.0518	0.2756	0.0527	0.1432	0.0193	0.1212
95	0.1310	0.4661	0.0643	0.3411	0.0651	0.1763	0.0237	0.1503
105	0.1326	0.4584	0.0638	0.3276	0.0621	0.1649	0.0216	0.1351
115	0.0579	0.2095	0.0277	0.1477	0.0290	0.0808	0.0109	0.0710
125	0.0558	0.2074	0.0268	0.1457	0.0286	0.0796	0.0113	0.0747
135	0.0595	0.2245	0.0306	0.1659	0.0326	0.0908	0.0129	0.0835
145	0.0836	0.3304	0.0430	0.2270	0.0418	0.1211	0.0171	0.1122
155	0.0776	0.2972	0.0402	0.2163	0.0419	0.1188	0.0168	0.1074
165	0.0616	0.2336	0.0313	0.1649	0.0320	0.0889	0.0124	0.0832
175	0.1115	0.4220	0.0581	0.3228	0.0619	0.1712	0.0233	0.1581
185	0.1345	0.5258	0.0741	0.4022	0.0771	0.2176	0.0296	0.2015

Appendix 8C: ICP-MS REE LC2

ICP-MS REE						
LC2						
Depth (cm)	**Lu175 mg/L**	**Hf178 mg/L**	**Ta181 mg/L**	**Pb208 mg/L**	**Th232 ppm**	**U238 ppm**
5	0.0462	0.1802	0.0969	4.0977	1.5656	0.3413
15	0.0100	0.0752	0.0369	0.8472	0.4810	0.0988
25	0.0086	0.0840	0.0384	0.7378	0.4926	0.0970
35	0.0074	0.0764	0.0345	0.6562	0.4526	0.0948
45	0.0093	0.1300	0.0558	0.8607	0.8116	0.1578
55	0.0127	0.1554	0.0657	1.0124	1.1812	0.2480
65	0.0169	0.1561	0.0591	1.3973	1.4580	0.2466
75	0.0174	0.1263	0.0417	1.1063	1.0293	0.1361
85	0.0176	0.1083	0.0331	0.9747	0.7782	0.1007
95	0.0214	0.1183	0.0419	0.9772	1.1378	0.1377
105	0.0196	0.1161	0.0441	1.3148	1.0683	0.1705
115	0.0109	0.0799	0.0214	0.5779	0.5501	0.0690
125	0.0116	0.1071	0.0379	0.5749	0.7925	0.0878
135	0.0126	0.0984	0.0266	0.6825	0.8602	0.0889
145	0.0171	0.1866	0.0972	0.8436	1.6647	0.1493
155	0.0161	0.1158	0.0353	0.9562	1.0079	0.1137
165	0.0125	0.1231	0.0358	0.6660	0.6894	0.0819
175	0.0230	0.2280	0.0942	1.4307	1.9742	0.2170
185	0.0288	0.2718	0.1355	2.0130	2.5774	0.2582

ICP-MS REE								
LC2								
Depth (cm)	**Y89 mg/L**	**Zr90 mg/L**	**Nb93 mg/L**	**La139 mg/L**	**Ce140 mg/L**	**Pr141 mg/L**	**Nd143 mg/L**	**Sm147 mg/L**
195	2.2070	11.3500	1.5283	2.6689	5.6393	0.6564	2.6163	0.5322
205	1.7273	8.3681	0.9956	2.0321	4.3540	0.5174	2.0878	0.4251
215	1.7677	7.4365	0.9694	2.0667	4.3989	0.5295	2.1246	0.4319
225	1.5494	7.2446	0.9964	1.8632	3.8652	0.4787	1.8932	0.3859
235	1.4162	6.8355	0.8708	1.6583	3.4262	0.4319	1.7516	0.3476
245	1.3310	6.4178	0.7811	1.4662	3.0168	0.3827	1.5417	0.3223
255	1.6404	6.5492	0.8555	1.8676	3.8557	0.4706	1.8731	0.3840
265	1.3552	5.9356	0.7074	1.4712	3.0655	0.3858	1.5289	0.3161
275	1.0725	5.1776	0.5951	1.1558	2.3679	0.2973	1.2137	0.2530
285	1.3718	6.4501	0.8078	1.5440	3.0966	0.3875	1.5339	0.3137
295	1.4843	5.9916	0.7137	1.5377	3.1142	0.3902	1.5556	0.3168
305	1.3640	6.6922	0.7798	1.5655	3.0454	0.3890	1.5343	0.3149
315	1.3368	4.9585	0.6847	1.4152	2.8270	0.3569	1.4192	0.2906
325	0.8866	3.7424	0.4349	0.8977	1.8179	0.2306	0.9495	0.1936
335	1.0172	4.3259	0.5565	1.0959	2.1872	0.2754	1.1025	0.2274
345	0.9102	3.7299	0.4782	1.0005	1.9886	0.2510	1.0050	0.2059
355	0.8013	3.4468	0.4048	0.8512	1.7101	0.2131	0.8616	0.1830

ICP-MS REE								
LC2								
Depth (cm)	**Eu151 mg/L**	**Gd157 mg/L**	**Tb159 mg/L**	**Dy163 mg/L**	**Ho165 mg/L**	**Er166 mg/L**	**Tm169 mg/L**	**Yb174 mg/L**
195	0.1325	0.5158	0.0704	0.3901	0.0727	0.2008	0.0271	0.1740
205	0.1070	0.4116	0.0555	0.3032	0.0580	0.1595	0.0214	0.1392
215	0.1082	0.4203	0.0576	0.3149	0.0594	0.1667	0.0229	0.1455
225	0.0908	0.3727	0.0516	0.2806	0.0532	0.1495	0.0202	0.1321
235	0.0881	0.3468	0.0481	0.2640	0.0494	0.1405	0.0187	0.1226
245	0.0822	0.3217	0.0444	0.2487	0.0481	0.1333	0.0179	0.1171
255	0.0958	0.3777	0.0525	0.2889	0.0553	0.1534	0.0213	0.1324
265	0.0766	0.3071	0.0430	0.2345	0.0446	0.1257	0.0166	0.1079
275	0.0613	0.2475	0.0330	0.1838	0.0350	0.0974	0.0135	0.0869
285	0.0743	0.3039	0.0414	0.2334	0.0449	0.1281	0.0177	0.1154
295	0.0797	0.3178	0.0432	0.2465	0.0469	0.1338	0.0185	0.1187
305	0.0767	0.3023	0.0422	0.2345	0.0447	0.1256	0.0175	0.1140
315	0.0712	0.2878	0.0399	0.2211	0.0433	0.1195	0.0168	0.1080
325	0.0487	0.1932	0.0261	0.1484	0.0283	0.0806	0.0108	0.0712
335	0.0547	0.2169	0.0299	0.1663	0.0322	0.0900	0.0121	0.0791
345	0.0500	0.1999	0.0277	0.1522	0.0297	0.0816	0.0112	0.0728
355	0.0445	0.1724	0.0247	0.1344	0.0257	0.0717	0.0099	0.0648

Appendix 8C: ICP-MS REE LC2

ICP-MS REE						
LC2						
Depth (cm)	**Lu175 mg/L**	**Hf178 mg/L**	**Ta181 mg/L**	**Pb208 mg/L**	**Th232 ppm**	**U238 ppm**
195	0.0252	0.2541	0.1196	1.7564	2.1287	0.2411
205	0.0202	0.1857	0.0740	1.2417	1.6963	0.1861
215	0.0212	0.1674	0.0708	1.4099	1.8964	0.2180
225	0.0199	0.1596	0.0750	1.3760	1.7073	0.1504
235	0.0175	0.1591	0.0693	1.1914	1.6149	0.1631
245	0.0170	0.1561	0.0601	1.1315	1.4806	0.1785
255	0.0196	0.1469	0.0633	1.3389	1.7807	0.1802
265	0.0159	0.1338	0.0480	1.0478	1.3868	0.1340
275	0.0130	0.1152	0.0389	0.8183	1.0662	0.1017
285	0.0164	0.1432	0.0562	0.9362	1.6993	0.1520
295	0.0176	0.1319	0.0492	1.1016	1.6020	0.1490
305	0.0168	0.1482	0.0556	0.9682	1.4816	0.1392
315	0.0157	0.1129	0.0470	0.8442	0.9508	0.0632
325	0.0106	0.0874	0.0276	0.6144	0.6058	0.0479
335	0.0117	0.0964	0.0358	0.7318	0.9360	0.0809
345	0.0112	0.0855	0.0328	0.7051	0.8845	0.0833
355	0.0095	0.0803	0.0262	0.5691	0.6756	0.0495

ICP-MS REE								
LC2								
Depth (cm)	**Y89 mg/L**	**Zr90 mg/L**	**Nb93 mg/L**	**La139 mg/L**	**Ce140 mg/L**	**Pr141 mg/L**	**Nd143 mg/L**	**Sm147 mg/L**
365	0.7807	3.7169	0.4425	0.8839	1.7579	0.2197	0.8735	0.1798
375	1.0483	6.1550	0.7082	1.2993	2.4698	0.3093	1.2068	0.2356
385	0.9741	4.5874	0.5690	1.1076	2.1826	0.2701	1.0775	0.2236
395	1.0187	4.6127	0.6328	1.1689	2.3274	0.2865	1.1309	0.2299
405	0.8393	3.6914	0.4707	0.9704	1.9098	0.2372	0.9359	0.1895
415	0.7561	3.5282	0.4216	0.8878	1.7446	0.2174	0.8584	0.1751
425	0.6244	2.7294	0.3260	0.7077	1.4152	0.1776	0.7142	0.1436
435	0.4742	1.8857	0.2056	0.5225	1.0678	0.1326	0.5314	0.1100
445	0.2811	1.5884	0.1644	0.3266	0.6619	0.0881	0.3591	0.0728
455	0.5230	1.6907	0.2003	0.5188	1.0351	0.1387	0.5724	0.1207
465	0.6899	2.3683	0.2862	0.7752	1.5348	0.1977	0.8004	0.1623
475	0.6874	2.6078	0.3017	0.6969	1.4024	0.1891	0.7688	0.1663
485	1.5893	6.7758	0.8562	1.7886	3.6372	0.4820	1.9193	0.4009
495	1.1807	5.9261	0.7378	1.4363	2.8208	0.3867	1.5185	0.3136
505	0.6340	1.7544	0.2087	0.5997	1.2305	0.1675	0.6812	0.1446
515	0.5149	1.6895	0.1841	0.4803	0.9840	0.1343	0.5553	0.1165
525	0.4516	1.4173	0.1274	0.4385	0.9140	0.1259	0.5157	0.1115

ICP-MS REE								
LC2								
Depth (cm)	**Eu151 mg/L**	**Gd157 mg/L**	**Tb159 mg/L**	**Dy163 mg/L**	**Ho165 mg/L**	**Er166 mg/L**	**Tm169 mg/L**	**Yb174 mg/L**
365	0.0441	0.1715	0.0238	0.1303	0.0256	0.0720	0.0098	0.0656
375	0.0576	0.2282	0.0320	0.1782	0.0356	0.0957	0.0138	0.0968
385	0.0531	0.2110	0.0296	0.1678	0.0327	0.0878	0.0122	0.0846
395	0.0577	0.2235	0.0316	0.1772	0.0346	0.0913	0.0129	0.0885
405	0.0455	0.1854	0.0258	0.1467	0.0276	0.0741	0.0106	0.0724
415	0.0432	0.1699	0.0230	0.1339	0.0255	0.0690	0.0098	0.0651
425	0.0363	0.1424	0.0199	0.1104	0.0212	0.0552	0.0077	0.0522
435	0.0274	0.1081	0.0147	0.0815	0.0154	0.0407	0.0056	0.0389
445	0.0194	0.0767	0.0107	0.0569	0.0112	0.0298	0.0042	0.0291
455	0.0308	0.1268	0.0172	0.0961	0.0190	0.0508	0.0074	0.0491
465	0.0406	0.1666	0.0231	0.1268	0.0252	0.0674	0.0092	0.0618
475	0.0420	0.1691	0.0228	0.1300	0.0252	0.0667	0.0092	0.0651
485	0.0949	0.4182	0.0560	0.3199	0.0620	0.1635	0.0237	0.1677
495	0.0763	0.3256	0.0440	0.2439	0.0462	0.1258	0.0175	0.1216
505	0.0365	0.1522	0.0210	0.1187	0.0235	0.0635	0.0092	0.0648
515	0.0301	0.1243	0.0169	0.0991	0.0194	0.0508	0.0074	0.0508
525	0.0287	0.1155	0.0162	0.0899	0.0175	0.0458	0.0064	0.0449

ICP-MS REE						
LC2						
Depth (cm)	**Lu175 mg/L**	**Hf178 mg/L**	**Ta181 mg/L**	**Pb208 mg/L**	**Th232 ppm**	**U238 ppm**
365	0.0094	0.0829	0.0283	0.5916	0.8004	0.0666
375	0.0143	0.1294	0.0458	0.7512	1.1922	0.1161
385	0.0125	0.1016	0.0382	0.6633	0.8443	0.0712
395	0.0131	0.0983	0.0424	0.7101	1.0152	0.0970
405	0.0108	0.0790	0.0305	0.6038	0.8356	0.0845
415	0.0096	0.0775	0.0283	0.5023	0.6879	0.0661
425	0.0081	0.0591	0.0214	0.4279	0.5214	0.0464
435	0.0057	0.0402	0.0126	0.5932	0.3425	0.0314
445	0.0044	0.0410	0.0118	0.4077	0.2437	0.0282
455	0.0074	0.0426	0.0158	0.4025	0.3445	0.0384
465	0.0089	0.0603	0.0226	0.4849	0.4908	0.0458
475	0.0095	0.0677	0.0261	0.5112	0.5306	0.0679
485	0.0250	0.1689	0.0694	1.1369	1.7837	0.1917
495	0.0178	0.1498	0.0609	0.9084	1.5376	0.1745
505	0.0093	0.0450	0.0163	0.3692	0.3346	0.0302
515	0.0074	0.0437	0.0142	0.9474	0.3564	0.0422
525	0.0064	0.0376	0.0095	0.3779	0.3297	0.0344

ICP-MS REE								
LC2								
Depth (cm)	**Y89 mg/L**	**Zr90 mg/L**	**Nb93 mg/L**	**La139 mg/L**	**Ce140 mg/L**	**Pr141 mg/L**	**Nd143 mg/L**	**Sm147 mg/L**
535	0.4360	1.9153	0.2191	0.4775	0.9870	0.1345	0.5389	0.1146
545	0.5073	2.2521	0.2576	0.5523	1.1756	0.1608	0.6686	0.1450
555	0.4311	2.5304	0.3117	0.4733	1.0208	0.1405	0.5707	0.1267
565	1.1910	5.0605	0.4099	1.3737	2.9025	0.3883	1.5852	0.3485
575	1.3413	4.9052	0.4951	1.5283	3.1468	0.4173	1.6773	0.3617
585	2.0868	6.0956	0.6578	2.4183	4.9213	0.6166	2.4940	0.5225
525	1.3334	3.9398	0.3590	1.4549	2.9362	0.3897	1.5923	0.3318
605	1.2030	4.4804	0.4309	1.1530	2.2719	0.3079	1.2583	0.2625
615	1.2349	5.1121	0.5599	1.2061	2.4212	0.3284	1.3378	0.2828
625	1.0254	3.9238	0.4107	0.9771	1.9659	0.2723	1.1137	0.2378
635	0.8860	3.3440	0.3226	0.8183	1.6902	0.2312	0.9408	0.2045
645	0.5666	2.7186	0.2547	0.5690	1.1785	0.1610	0.6654	0.1438
655	0.6917	3.0698	0.2942	0.7071	1.4398	0.1952	0.7999	0.1698
665	0.5739	2.7266	0.2537	0.5683	1.1940	0.1602	0.6597	0.1436
675	1.2575	5.7340	0.7054	1.4673	2.8991	0.3819	1.5029	0.3126
685	1.0496	3.9731	0.4416	1.1491	2.3282	0.3058	1.2213	0.2573
695	0.9701	3.7943	0.4068	1.0547	2.1708	0.2844	1.1460	0.2393

ICP-MS REE

LC2

Depth (cm)	Eu151 mg/L	Gd157 mg/L	Tb159 mg/L	Dy163 mg/L	Ho165 mg/L	Er166 mg/L	Tm169 mg/L	Yb174 mg/L
535	0.0298	0.1182	0.0168	0.0908	0.0171	0.0459	0.0064	0.0467
545	0.0366	0.1484	0.0200	0.1085	0.0206	0.0540	0.0073	0.0491
555	0.0322	0.1286	0.0177	0.0938	0.0182	0.0441	0.0061	0.0421
565	0.0897	0.3524	0.0485	0.2598	0.0487	0.1235	0.0159	0.1113
575	0.0922	0.3804	0.0515	0.2841	0.0540	0.1368	0.0189	0.1303
585	0.1328	0.5492	0.0733	0.4098	0.0784	0.2086	0.0282	0.1973
525	0.0873	0.3328	0.0469	0.2570	0.0499	0.1345	0.0182	0.1156
605	0.0688	0.2829	0.0384	0.2209	0.0437	0.1185	0.0165	0.1180
615	0.0730	0.2981	0.0413	0.2361	0.0456	0.1234	0.0171	0.1228
625	0.0626	0.2521	0.0340	0.1893	0.0377	0.1020	0.0139	0.0989
635	0.0531	0.2138	0.0290	0.1617	0.0319	0.0867	0.0118	0.0845
645	0.0383	0.1333	0.0196	0.1063	0.0214	0.0594	0.0079	0.0506
655	0.0456	0.1633	0.0242	0.1314	0.0258	0.0715	0.0098	0.0617
665	0.0392	0.1352	0.0200	0.1066	0.0214	0.0579	0.0081	0.0509
675	0.0785	0.2840	0.0433	0.2425	0.0488	0.1349	0.0190	0.1246
685	0.0670	0.2445	0.0356	0.1959	0.0388	0.1073	0.0144	0.0918
695	0.0635	0.2263	0.0331	0.1811	0.0360	0.0981	0.0135	0.0852

ICP-MS REE						
LC2						
Depth (cm)	**Lu175 mg/L**	**Hf178 mg/L**	**Ta181 mg/L**	**Pb208 mg/L**	**Th232 ppm**	**U238 ppm**
535	0.0069	0.0512	0.0160	0.3285	0.3417	0.0309
545	0.0073	0.0639	0.0148	0.2577	0.6572	0.0564
555	0.0061	0.0707	0.0184	0.4239	0.5377	0.0541
565	0.0157	0.1396	0.0361	0.2812	1.5011	0.1838
575	0.0189	0.1312	0.0395	1.4780	1.1622	0.1463
585	0.0279	0.1518	0.0562	0.9106	1.5957	0.1957
525	0.0174	0.1047	0.0271	0.9081	0.7514	0.0645
605	0.0175	0.1116	0.0362	0.7195	0.9727	0.1104
615	0.0191	0.1282	0.0474	0.8293	1.2397	0.1520
625	0.0146	0.1016	0.0356	0.6824	0.9519	0.1115
635	0.0130	0.0838	0.0267	0.6927	0.6668	0.0722
645	0.0077	0.0745	0.0177	0.4040	0.5501	0.0572
655	0.0094	0.0800	0.0208	0.6505	0.6782	0.0689
665	0.0082	0.0740	0.0163	0.3715	0.5382	0.0532
675	0.0186	0.1410	0.0532	0.7481	1.3724	0.1113
685	0.0136	0.0994	0.0331	0.6151	0.9841	0.0869
695	0.0129	0.0975	0.0293	0.6265	0.7407	0.0563

ICP-MS REE								
LC2								
Depth (cm)	**Y89 mg/L**	**Zr90 mg/L**	**Nb93 mg/L**	**La139 mg/L**	**Ce140 mg/L**	**Pr141 mg/L**	**Nd143 mg/L**	**Sm147 mg/L**
705	1.9872	8.3450	1.1214	2.4232	5.0343	0.6281	2.4440	0.5060
715	1.1132	4.6286	0.5500	1.1984	2.5800	0.3312	1.3211	0.2789
725	0.9790	4.5771	0.5965	1.0959	2.3266	0.2982	1.2134	0.2485
735	1.4028	7.2846	1.0197	1.6873	3.5360	0.4382	1.7098	0.3527
745	1.2185	5.7146	0.7845	1.4264	3.0023	0.3787	1.5052	0.3087
755	1.4158	7.0771	0.9912	1.6382	3.4815	0.4365	1.7285	0.3496
695	1.5866	7.4193	0.9813	1.8178	3.9186	0.4852	1.9043	0.3819
785	0.6977	3.9372	0.4996	0.7242	1.6202	0.2129	0.8765	0.1829
795	1.6117	7.5884	1.0024	1.8612	4.0705	0.5097	2.0087	0.4095
805	1.0091	4.4597	0.5736	1.0959	2.3532	0.3123	1.2599	0.2588
815	0.8278	3.2945	0.3741	0.8608	1.9325	0.2546	1.0522	0.2172
825	0.7653	3.5335	0.4382	0.8349	1.7953	0.2369	0.9674	0.2007
835	0.7696	3.8209	0.4948	0.7533	1.6033	0.2170	0.8868	0.1819
845	1.0144	3.6176	0.4559	1.0126	2.1320	0.2893	1.1658	0.2364
855	0.7374	3.3252	0.4074	0.6553	1.4853	0.1977	0.8290	0.1752
865	0.9434	3.7384	0.4695	0.9015	1.9763	0.2633	1.0789	0.2208
875	0.9891	3.7596	0.4579	0.9702	2.1283	0.2827	1.1419	0.2358

ICP-MS REE								
LC2								
Depth (cm)	**Eu151 mg/L**	**Gd157 mg/L**	**Tb159 mg/L**	**Dy163 mg/L**	**Ho165 mg/L**	**Er166 mg/L**	**Tm169 mg/L**	**Yb174 mg/L**
705	0.1341	0.4744	0.0709	0.3779	0.0728	0.1960	0.0267	0.1657
715	0.0762	0.2665	0.0395	0.2112	0.0408	0.1082	0.0144	0.0929
725	0.0689	0.2391	0.0351	0.1860	0.0362	0.0995	0.0127	0.0807
735	0.0931	0.3309	0.0495	0.2661	0.0505	0.1355	0.0180	0.1139
745	0.0824	0.2917	0.0422	0.2285	0.0447	0.1189	0.0159	0.1013
755	0.0959	0.3395	0.0501	0.2701	0.0511	0.1394	0.0182	0.1159
695	0.1049	0.3682	0.0544	0.2966	0.0576	0.1581	0.0218	0.1376
785	0.0519	0.1788	0.0250	0.1341	0.0260	0.0699	0.0092	0.0578
795	0.1106	0.3894	0.0571	0.3111	0.0608	0.1624	0.0219	0.1379
805	0.0724	0.2530	0.0355	0.1906	0.0368	0.0994	0.0130	0.0823
815	0.0606	0.2089	0.0299	0.1572	0.0304	0.0815	0.0110	0.0668
825	0.0527	0.1906	0.0270	0.1435	0.0279	0.0746	0.0102	0.0623
835	0.0526	0.1776	0.0254	0.1401	0.0275	0.0746	0.0103	0.0649
845	0.0672	0.2330	0.0332	0.1789	0.0352	0.0963	0.0131	0.0800
855	0.0517	0.1699	0.0249	0.1328	0.0265	0.0702	0.0094	0.0585
865	0.0636	0.2216	0.0317	0.1709	0.0334	0.0913	0.0125	0.0769
875	0.0656	0.2301	0.0335	0.1781	0.0352	0.0976	0.0132	0.0823

ICP-MS REE						
LC2						
Depth (cm)	**Lu175 mg/L**	**Hf178 mg/L**	**Ta181 mg/L**	**Pb208 mg/L**	**Th232 ppm**	**U238 ppm**
705	0.0242	0.1986	0.0856	1.3351	2.2315	0.2271
715	0.0134	0.1142	0.0400	1.1683	0.8880	0.0845
725	0.0116	0.1161	0.0432	1.0253	0.7984	0.0822
735	0.0169	0.1697	0.0765	1.0630	1.1755	0.0951
745	0.0151	0.1354	0.0585	1.1679	0.5439	0.0172
755	0.0174	0.1638	0.0729	1.0021	0.7519	0.0411
695	0.0203	0.1734	0.0713	1.0107	0.9859	0.0677
785	0.0088	0.0978	0.0314	0.5994	0.3179	0.0185
795	0.0209	0.1771	0.0734	1.4893	1.7373	0.1649
805	0.0123	0.1042	0.0376	0.8318	0.8706	0.0916
815	0.0103	0.0785	0.0213	0.9524	0.5623	0.0581
825	0.0099	0.0824	0.0278	0.8980	0.6963	0.0636
835	0.0099	0.0880	0.0315	0.6395	0.6030	0.0643
845	0.0121	0.0856	0.0309	0.6484	0.7906	0.0853
855	0.0090	0.0794	0.0222	0.7284	0.5412	0.0575
865	0.0114	0.0875	0.0283	0.6383	0.7062	0.0687
875	0.0126	0.0932	0.0307	0.6034	0.6160	0.0443

ICP-MS REE								
LC2								
Depth (cm)	**Y89 mg/L**	**Zr90 mg/L**	**Nb93 mg/L**	**La139 mg/L**	**Ce140 mg/L**	**Pr141 mg/L**	**Nd143 mg/L**	**Sm147 mg/L**
885	0.9635	3.3413	0.3971	0.9301	2.0398	0.2683	1.1067	0.2302
895	0.8685	3.0890	0.3542	0.8304	1.8356	0.2443	1.0101	0.2079
905	0.5844	2.0116	0.2237	0.5425	1.1788	0.1630	0.6765	0.1387
915	0.4897	1.7719	0.2203	0.4827	1.0109	0.1427	0.5953	0.1192
925	0.4743	1.7801	0.2092	0.4624	0.9758	0.1343	0.5571	0.1154
935	0.4210	1.6099	0.1854	0.4235	0.9026	0.1232	0.5022	0.1018
945	0.5469	2.0840	0.2357	0.5386	1.1514	0.1571	0.6398	0.1262
955	0.6987	2.4259	0.2815	0.7269	1.5052	0.2071	0.8271	0.1671
965	0.5772	2.0712	0.2400	0.6691	1.3615	0.1857	0.7297	0.1514
975	0.5498	2.0854	0.2422	0.6265	1.2938	0.1739	0.6895	0.1419
985	0.5875	2.2036	0.2529	0.6757	1.3966	0.1910	0.7600	0.1533
995	0.4845	1.5465	0.1613	0.4988	1.0732	0.1478	0.5996	0.1272
1005	0.4613	1.5340	0.1584	0.5178	1.0865	0.1508	0.5917	0.1218
1015	0.4999	1.6626	0.1806	0.5592	1.1791	0.1612	0.6456	0.1344
1025	0.5323	2.0392	0.2134	0.6528	1.3180	0.1767	0.7039	0.1426
1035	0.5912	2.0722	0.2214	0.6839	1.4178	0.1894	0.7648	0.1558
1045	0.8361	3.6726	0.4188	1.0436	2.0729	0.2773	1.0871	0.2198

ICP-MS REE								
LC2								
Depth (cm)	**Eu151 mg/L**	**Gd157 mg/L**	**Tb159 mg/L**	**Dy163 mg/L**	**Ho165 mg/L**	**Er166 mg/L**	**Tm169 mg/L**	**Yb174 mg/L**
885	0.0659	0.2228	0.0322	0.1720	0.0342	0.0919	0.0124	0.0753
895	0.0592	0.2074	0.0290	0.1543	0.0303	0.0816	0.0107	0.0671
905	0.0414	0.1361	0.0193	0.1025	0.0199	0.0564	0.0073	0.0462
915	0.0372	0.1177	0.0171	0.0882	0.0174	0.0471	0.0062	0.0376
925	0.0344	0.1111	0.0160	0.0870	0.0169	0.0463	0.0061	0.0389
935	0.0304	0.1009	0.0138	0.0757	0.0146	0.0405	0.0056	0.0342
945	0.0373	0.1273	0.0176	0.0980	0.0190	0.0515	0.0072	0.0450
955	0.0491	0.1601	0.0230	0.1257	0.0248	0.0697	0.0093	0.0589
965	0.0406	0.1411	0.0203	0.1069	0.0211	0.0574	0.0076	0.0500
975	0.0395	0.1354	0.0191	0.1039	0.0201	0.0554	0.0075	0.0484
985	0.0445	0.1454	0.0207	0.1091	0.0212	0.0584	0.0078	0.0496
995	0.0350	0.1161	0.0172	0.0903	0.0173	0.0488	0.0064	0.0403
1005	0.0351	0.1138	0.0165	0.0894	0.0172	0.0490	0.0066	0.0421
1015	0.0387	0.1278	0.0182	0.0958	0.0186	0.0515	0.0071	0.0436
1025	0.0410	0.1358	0.0198	0.1065	0.0209	0.0565	0.0078	0.0477
1035	0.0460	0.1521	0.0220	0.1157	0.0221	0.0622	0.0080	0.0514
1045	0.0603	0.2129	0.0302	0.1660	0.0318	0.0883	0.0121	0.0758

ICP-MS REE						
LC2						
Depth (cm)	**Lu175 mg/L**	**Hf178 mg/L**	**Ta181 mg/L**	**Pb208 mg/L**	**Th232 ppm**	**U238 ppm**
885	0.0114	0.0781	0.0241	0.5208	0.6287	0.0598
895	0.0102	0.0750	0.0213	0.4698	0.5843	0.0549
905	0.0072	0.0497	0.0128	0.4989	0.2841	0.0291
915	0.0056	0.0451	0.0121	0.3730	0.2749	0.0355
925	0.0060	0.0431	0.0128	0.3989	0.2018	0.0216
935	0.0052	0.0395	0.0109	0.5479	0.2432	0.0295
945	0.0069	0.0495	0.0158	0.5073	0.3849	0.0444
955	0.0089	0.0575	0.0206	0.5623	0.3480	0.0312
965	0.0075	0.0509	0.0175	0.5531	0.3715	0.0319
975	0.0074	0.0504	0.0172	0.6021	0.3406	0.0256
985	0.0074	0.0522	0.0182	0.5041	0.3374	0.0230
995	0.0062	0.0383	0.0102	0.4807	0.2140	0.0125
1005	0.0065	0.0394	0.0115	0.3626	0.2679	0.0161
1015	0.0066	0.0413	0.0127	0.4305	0.3486	0.0249
1025	0.0072	0.0515	0.0160	0.4112	0.4156	0.0353
1035	0.0076	0.0527	0.0171	0.4814	0.3715	0.0305
1045	0.0114	0.0870	0.0323	0.6499	1.4732	0.0518

ICP-MS REE

LC2

Depth (cm)	Y89 mg/L	Zr90 mg/L	Nb93 mg/L	La139 mg/L	Ce140 mg/L	Pr141 mg/L	Nd143 mg/L	Sm147 mg/L
1055	0.7005	2.3742	0.2754	0.7311	1.5275	0.2040	0.8439	0.1770
1065	0.6481	2.0859	0.2253	0.6942	1.4383	0.1917	0.7786	0.1604
1075	0.6650	2.0617	0.2397	0.7130	1.4605	0.1953	0.7996	0.1691
1085	0.8123	2.4255	0.2774	0.8615	1.7678	0.2344	0.9474	0.1987
1095	0.9082	3.1502	0.3641	0.9988	1.9881	0.2702	1.0744	0.2252
1105	0.5669	2.3283	0.2856	0.6513	1.3237	0.1755	0.7086	0.1449
1115	0.7574	2.4466	0.2964	0.8764	1.8268	0.2416	0.9752	0.2059
1125	0.7220	2.2637	0.3017	0.8297	1.7117	0.2235	0.9127	0.1873
1135	0.9309	2.9862	0.3498	1.1324	2.2664	0.2946	1.1797	0.2465
1145	0.9147	3.2406	0.3694	1.1000	2.1859	0.2868	1.1332	0.2367
1155	0.6730	2.2809	0.2791	0.7480	1.5045	0.1958	0.7901	0.1666
1165	0.6693	2.0285	0.2393	0.7718	1.5470	0.1998	0.8296	0.1685
1175	0.8725	1.8540	0.2125	0.9617	1.9632	0.2541	1.0661	0.2263
1185	0.6240	1.4624	0.1776	0.6946	1.3751	0.1807	0.7512	0.1578
1195	0.6878	1.7077	0.2068	0.7392	1.4424	0.1936	0.8106	0.1705
1205	0.8395	1.0899	0.1266	0.8385	1.7887	0.2346	1.0069	0.2044
1215	1.0101	1.5912	0.1851	1.0400	2.1961	0.2887	1.1914	0.2528

ICP-MS REE								
LC2								
Depth (cm)	**Eu151 mg/L**	**Gd157 mg/L**	**Tb159 mg/L**	**Dy163 mg/L**	**Ho165 mg/L**	**Er166 mg/L**	**Tm169 mg/L**	**Yb174 mg/L**
1055	0.0521	0.1720	0.0246	0.1331	0.0260	0.0717	0.0097	0.0594
1065	0.0496	0.1566	0.0227	0.1211	0.0241	0.0648	0.0088	0.0563
1075	0.0501	0.1636	0.0233	0.1264	0.0244	0.0656	0.0091	0.0540
1085	0.0601	0.2003	0.0286	0.1565	0.0300	0.0818	0.0111	0.0681
1095	0.0668	0.2210	0.0321	0.1690	0.0335	0.0902	0.0118	0.0743
1105	0.0413	0.1387	0.0204	0.1093	0.0217	0.0581	0.0080	0.0511
1115	0.0575	0.1948	0.0279	0.1472	0.0287	0.0769	0.0103	0.0646
1125	0.0544	0.1822	0.0263	0.1397	0.0273	0.0738	0.0096	0.0596
1135	0.0714	0.2378	0.0341	0.1863	0.0353	0.0947	0.0127	0.0783
1145	0.0656	0.2245	0.0326	0.1769	0.0350	0.0930	0.0130	0.0806
1155	0.0490	0.1621	0.0242	0.1312	0.0260	0.0696	0.0094	0.0571
1165	0.0503	0.1674	0.0243	0.1295	0.0250	0.0691	0.0094	0.0550
1175	0.0660	0.2164	0.0317	0.1666	0.0324	0.0859	0.0114	0.0670
1185	0.0477	0.1529	0.0222	0.1205	0.0229	0.0632	0.0080	0.0497
1195	0.0506	0.1662	0.0239	0.1271	0.0248	0.0690	0.0089	0.0559
1205	0.0645	0.2040	0.0292	0.1525	0.0297	0.0797	0.0103	0.0621
1215	0.0754	0.2426	0.0347	0.1831	0.0360	0.0953	0.0124	0.0766

ICP-MS REE						
LC2						
Depth (cm)	**Lu175 mg/L**	**Hf178 mg/L**	**Ta181 mg/L**	**Pb208 mg/L**	**Th232 ppm**	**U238 ppm**
1055	0.0092	0.0577	0.0185	0.5495	0.4513	0.0386
1065	0.0083	0.0512	0.0158	0.5027	0.4598	0.0501
1075	0.0083	0.0513	0.0166	0.5258	0.4186	0.0437
1085	0.0103	0.0599	0.0190	0.6889	0.3938	0.0294
1095	0.0113	0.0738	0.0259	0.6149	0.6722	0.0852
1105	0.0076	0.0561	0.0209	0.5398	0.3995	0.0358
1115	0.0094	0.0580	0.0206	0.5775	0.4119	0.0444
1125	0.0091	0.0557	0.0219	0.5461	0.4857	0.0520
1135	0.0115	0.0712	0.0274	0.7092	0.7125	0.0704
1145	0.0121	0.0781	0.0297	0.6330	0.8567	0.0758
1155	0.0087	0.0556	0.0186	0.9080	0.4677	0.0389
1165	0.0084	0.0488	0.0171	0.5182	0.4726	0.0374
1175	0.0101	0.0465	0.0151	0.4259	0.6368	0.0454
1185	0.0078	0.0378	0.0122	0.4803	0.4602	0.0361
1195	0.0087	0.0434	0.0147	0.5379	0.4095	0.0366
1205	0.0094	0.0290	0.0077	0.5907	0.3195	0.0284
1215	0.0112	0.0409	0.0132	0.5946	0.5097	0.0529

ICP-MS REE								
LC2								
Depth (cm)	**Y89 mg/L**	**Zr90 mg/L**	**Nb93 mg/L**	**La139 mg/L**	**Ce140 mg/L**	**Pr141 mg/L**	**Nd143 mg/L**	**Sm147 mg/L**
1225	1.0257	2.1854	0.2709	1.0997	2.2187	0.2908	1.2236	0.2475
1235	0.9353	2.5614	0.3140	0.9375	1.9622	0.2551	1.0753	0.2227
1245	0.9716	2.7252	0.3567	1.0559	2.1567	0.2804	1.1750	0.2421
1255	0.8524	2.7604	0.3897	1.0370	1.9105	0.2669	1.1006	0.2224
1265	1.0249	3.2072	0.3943	1.1675	2.1720	0.3027	1.2620	0.2577
1275	1.0155	2.5529	0.2968	1.0884	2.0756	0.2906	1.2199	0.2492
1285	1.2092	2.7267	0.3390	1.1912	2.2908	0.3234	1.3575	0.2844
1295	1.1656	2.3753	0.3444	1.1232	2.1652	0.3077	1.2763	0.2731

ICP-MS REE								
LC2								
Depth (cm)	**Eu151 mg/L**	**Gd157 mg/L**	**Tb159 mg/L**	**Dy163 mg/L**	**Ho165 mg/L**	**Er166 mg/L**	**Tm169 mg/L**	**Yb174 mg/L**
1225	0.0757	0.2488	0.0354	0.1872	0.0363	0.0977	0.0128	0.0774
1235	0.0670	0.2174	0.0323	0.1707	0.0339	0.0897	0.0120	0.0751
1245	0.0714	0.2362	0.0335	0.1801	0.0352	0.0945	0.0123	0.0757
1255	0.0659	0.2188	0.0312	0.1644	0.0321	0.0859	0.0115	0.0720
1265	0.0770	0.2552	0.0364	0.1909	0.0368	0.0995	0.0132	0.0789
1275	0.0770	0.2506	0.0357	0.1879	0.0366	0.0953	0.0125	0.0737
1285	0.0869	0.2896	0.0408	0.2191	0.0420	0.1127	0.0146	0.0893
1295	0.0825	0.2740	0.0395	0.2116	0.0416	0.1089	0.0143	0.0874

ICP-MS REE						
LC2						
Depth (cm)	**Lu175 mg/L**	**Hf178 mg/L**	**Ta181 mg/L**	**Pb208 mg/L**	**Th232 ppm**	**U238 ppm**
1225	0.0117	0.0537	0.0193	0.7539	0.6274	0.0683
1235	0.0112	0.0643	0.0205	0.7456	0.6089	0.0756
1245	0.0113	0.0660	0.0260	0.5560	0.6742	0.0585
1255	0.0108	0.0667	0.0281	0.8344	0.7166	0.0643
1265	0.0121	0.0762	0.0284	1.1049	0.7745	0.0669
1275	0.0110	0.0646	0.0193	0.7502	0.6346	0.0453
1285	0.0131	0.0694	0.0214	0.9458	0.6508	0.0473
1295	0.0127	0.0554	0.0225	0.6002	0.5596	0.0466

ICP-MS REE - Blanks								
LC2								
Type	**Y89 mg/L**	**Zr90 mg/L**	**Nb93 mg/L**	**La139 mg/L**	**Ce140 mg/L**	**Pr141 mg/L**	**Nd143 mg/L**	**Sm147 mg/L**
BLANK	0.0046	0.7128	0.0031	0.0060	0.0114	0.0013	0.0042	0.0007
BLANK	0.0025	0.1395	0.0010	0.0041	0.0086	0.0009	0.0034	0.0007
BLANK	0.0050	0.1409	0.0004	0.0056	0.0086	0.0010	0.0046	0.0007
BLANK	0.0161	0.1790	0.0193	0.0155	0.0294	0.0037	0.0156	0.0033
BLANK	0.0031	0.0779	0.0017	0.0060	0.0113	0.0014	0.0051	0.0010
BLANK	0.0037	0.0776	nd	0.0050	0.0093	0.0010	0.0036	0.0010

ICP-MS REE - Blanks								
LC2								
Type	**Eu151 mg/L**	**Gd157 mg/L**	**Tb159 mg/L**	**Dy163 mg/L**	**Ho165 mg/L**	**Er166 mg/L**	**Tm169 mg/L**	**Yb174 mg/L**
BLANK	0.0002	0.0009	0.0001	0.0007	0.0002	0.0006	0.0001	0.0007
BLANK	0.0001	0.0005	0.0001	0.0005	0.0001	0.0002	0.0000	0.0003
BLANK	0.0002	0.0009	0.0001	0.0009	0.0002	0.0004	0.0000	0.0005
BLANK	0.0007	0.0039	0.0005	0.0030	0.0007	0.0016	0.0003	0.0016
BLANK	0.0002	0.0010	0.0001	0.0007	0.0001	0.0004	0.0001	0.0004
BLANK	0.0002	0.0006	0.0001	0.0005	0.0001	0.0003	nd	0.0003

ICP-MS REE - Blanks						
LC2						
Type	**Lu175 mg/L**	**Hf178 mg/L**	**Ta181 mg/L**	**Pb208 mg/L**	**Th232 ppm**	**U238 ppm**
BLANK	0.0002	0.0140	0.0028	0.1754	0.0037	0.0013
BLANK	0.0000	0.0027	0.0016	0.1567	0.0019	0.0003
BLANK	0.0000	0.0025	0.0017	0.1090	0.0014	0.0004
BLANK	0.0003	0.0075	0.0034	0.1297	0.0149	0.0012
BLANK	nd	0.0019	0.0002	0.0956	nd	0.0001
BLANK	nd	0.0018	0.0006	0.0935	0.0012	0.0004

ICP-MS REE - Precision								
LC2								
Type	**Y89 mg/L**	**Zr90 mg/L**	**Nb93 mg/L**	**La139 mg/L**	**Ce140 mg/L**	**Pr141 mg/L**	**Nd143 mg/L**	**Sm147 mg/L**
Chinese Peach Leaves (CPL) and in House Reference Materials (HRM)								
CPL	0.2640	1.7112	0.1427	0.4299	0.8312	0.1029	0.3746	0.0703
CPL	0.2697	1.7847	0.1414	0.5005	0.9358	0.1110	0.4111	0.0755
CPL	0.2468	1.0916	0.1270	0.3497	0.6907	0.0894	0.3402	0.0692
CPL	0.2777	1.2006	0.1530	0.4676	0.8942	0.1106	0.4211	0.0832
Mean	**0.2646**	**1.4470**	**0.1410**	**0.4369**	**0.8380**	**0.1035**	**0.3868**	**0.0746**
StDev	0.0262	0.7032	0.0214	0.1298	0.2144	0.0202	0.0738	0.0128
Precision %	9.9034	48.5961	15.1653	29.7126	25.5823	19.5152	19.0880	17.1368
HRM 12	0.0874	0.4600	0.0386	0.1320	0.2303	0.0296	0.1101	0.0219
HRM 12	0.0801	0.3724	0.0343	0.1101	0.1933	0.0250	0.0931	0.0186
Mean	**0.0838**	**0.4162**	**0.0365**	**0.1211**	**0.2118**	**0.0273**	**0.1016**	**0.0203**
HRM 14	0.7213	3.7844	0.3935	0.6802	1.4411	0.1715	0.6629	0.1409
HRM 14	0.7534	3.7846	0.3568	0.8189	1.6905	0.2031	0.7838	0.1635
HRM 14	0.4931	2.2896	0.1842	0.4718	1.0424	0.1257	0.5034	0.1036
HRM 14	0.4797	2.3864	0.2247	0.4933	1.1185	0.1296	0.4949	0.1025
HRM 14	0.4181	1.8293	0.1920	0.4525	0.9373	0.1161	0.4606	0.0961
Mean	**0.5731**	**2.8149**	**0.2702**	**0.5833**	**1.2460**	**0.1492**	**0.5811**	**0.1213**

Appendix 8C: ICP-MS REE LC2

ICP-MS REE - Precision								
LC2								
Type	**Eu151 mg/L**	**Gd157 mg/L**	**Tb159 mg/L**	**Dy163 mg/L**	**Ho165 mg/L**	**Er166 mg/L**	**Tm169 mg/L**	**Yb174 mg/L**
Chinese Peach Leaves (CPL) and in House Reference Materials (HRM)								
CPL	0.0155	0.0666	0.0093	0.0502	0.0095	0.0285	0.0040	0.0269
CPL	0.0150	0.0682	0.0090	0.0486	0.0105	0.0260	0.0036	0.0250
CPL	0.0149	0.0665	0.0089	0.0498	0.0095	0.0265	0.0039	0.0271
CPL	0.0176	0.0750	0.0104	0.0578	0.0110	0.0311	0.0043	0.0285
Mean	**0.0158**	**0.0691**	**0.0094**	**0.0516**	**0.0101**	**0.0280**	**0.0040**	**0.0269**
StDev	0.0025	0.0081	0.0014	0.0084	0.0015	0.0046	0.0006	0.0029
Precision %	16.0121	11.6571	14.6381	16.2359	14.8148	16.5363	14.6165	10.7048
HRM 12	0.0078	0.0206	0.0031	0.0163	0.0033	0.0095	0.0013	0.0083
HRM 12	0.0073	0.0185	0.0025	0.0147	0.0028	0.0076	0.0011	0.0074
Mean	**0.0076**	**0.0196**	**0.0028**	**0.0155**	**0.0031**	**0.0086**	**0.0012**	**0.0079**
HRM 14	0.0332	0.1423	0.0214	0.1268	0.0258	0.0765	0.0110	0.0751
HRM 14	0.0366	0.1526	0.0217	0.1242	0.0245	0.0708	0.0103	0.0712
HRM 14	0.0249	0.1114	0.0158	0.0913	0.0187	0.0508	0.0073	0.0553
HRM 14	0.0248	0.0985	0.0152	0.0906	0.0186	0.0523	0.0078	0.0502
HRM 14	0.0226	0.0916	0.0136	0.0783	0.0157	0.0463	0.0065	0.0441
Mean	**0.0284**	**0.1193**	**0.0175**	**0.1022**	**0.0207**	**0.0593**	**0.0086**	**0.0592**

ICP-MS REE - Precision						
LC2						
Type	**Lu175 mg/L**	**Hf178 mg/L**	**Ta181 mg/L**	**Pb208 mg/L**	**Th232 ppm**	**U238 ppm**
Chinese Peach Leaves (CPL) and in House Reference Materials (HRM)						
CPL	0.0040	0.0377	0.0143	1.3292	0.2990	0.0252
CPL	0.0037	0.0366	0.0114	1.2370	0.7691	0.0492
CPL	0.0041	0.0297	0.0134	1.0652	0.3196	0.0369
CPL	0.0042	0.0298	0.0111	1.2335	0.5322	0.0485
Mean	**0.0040**	**0.0335**	**0.0126**	**1.2162**	**0.4800**	**0.0400**
StDev	0.0004	0.0086	0.0031	0.2200	0.4394	0.0227
Precision %	10.8012	25.6868	24.7055	18.0892	91.5428	56.7521
HRM 12	0.0014	0.0108	0.0034	5.9333	0.0503	0.0080
HRM 12	0.0012	0.0084	0.0037	5.6872	0.0537	0.0145
Mean	**0.0013**	**0.0096**	**0.0036**	**5.8103**	**0.0520**	**0.0113**
HRM 14	0.0116	0.0882	0.0306	9.4386	0.7881	0.2021
HRM 14	0.0107	0.0824	0.0285	10.1810	0.6120	0.1202
HRM 14	0.0079	0.0581	0.0185	8.1400	0.2657	0.0630
HRM 14	0.0079	0.0584	0.0179	9.7272	0.4569	0.1458
HRM 14	0.0065	0.0487	0.0149	9.1425	0.4635	0.1255
Mean	**0.0089**	**0.0672**	**0.0221**	**9.3259**	**0.5172**	**0.1313**

ICP-MS REE - Repeats								
LC2								
Depth (cm)	**Y89 mg/L**	**Zr90 mg/L**	**Nb93 mg/L**	**La139 mg/L**	**Ce140 mg/L**	**Pr141 mg/L**	**Nd143 mg/L**	**Sm147 mg/L**
15	0.9114	3.8140	0.4982	1.4302	2.3602	0.3117	1.2445	0.2501
15	0.9574	3.4070	0.5131	1.3759	2.2389	0.2939	1.1850	0.2386
Average	0.9344	3.6105	0.5057	1.4031	2.2996	0.3028	1.2148	0.2444
Stdev-2sig	0.0651	0.5756	0.0211	0.0768	0.1715	0.0252	0.0841	0.0163
% Precision	6.9621	15.9420	4.1673	5.4732	7.4599	8.3134	6.9270	6.6558
115	0.8788	3.2990	0.3039	0.9050	1.8452	0.2507	1.0771	0.2277
115	0.8921	3.4788	0.3103	0.8427	1.6918	0.2241	0.9579	0.2029
Average	0.8855	3.3889	0.3071	0.8739	1.7685	0.2374	1.0175	0.2153
Stdev-2sig	0.0188	0.2543	0.0091	0.0881	0.2169	0.0376	0.1686	0.0351
% Precision	2.1242	7.5032	2.9472	10.0825	12.2669	15.8459	16.5675	16.2901
135	0.9926	4.2732	0.3873	1.0466	2.1072	0.2745	1.1327	0.2335
135	1.0179	4.2814	0.3930	1.0012	1.9956	0.2633	1.0974	0.2331
Average	1.0053	4.2773	0.3902	1.0239	2.0514	0.2689	1.1151	0.2333
Stdev-2sig	0.0358	0.0116	0.0081	0.0642	0.1578	0.0158	0.0499	0.0006
% Precision	3.5593	0.2711	2.0661	6.2707	7.6936	5.8904	4.4771	0.2425

ICP-MS REE - Repeats								
LC2								
Depth (cm)	**Eu151 mg/L**	**Gd157 mg/L**	**Tb159 mg/L**	**Dy163 mg/L**	**Ho165 mg/L**	**Er166 mg/L**	**Tm169 mg/L**	**Yb174 mg/L**
15	0.0724	0.2508	0.0332	0.1772	0.0321	0.0847	0.0114	0.0702
15	0.0712	0.2419	0.0322	0.1715	0.0316	0.0793	0.0108	0.0696
Average	0.0718	0.2464	0.0327	0.1744	0.0319	0.0820	0.0111	0.0699
Stdev-2sig	0.0017	0.0126	0.0014	0.0081	0.0007	0.0076	0.0008	0.0008
% Precision	2.3636	5.1092	4.3248	4.6235	2.2201	9.3131	7.6444	1.2139
115	0.0610	0.2197	0.0292	0.1551	0.0304	0.0861	0.0112	0.0737
115	0.0548	0.1993	0.0262	0.1403	0.0275	0.0754	0.0105	0.0683
Average	0.0579	0.2095	0.0277	0.1477	0.0290	0.0808	0.0109	0.0710
Stdev-2sig	0.0088	0.0288	0.0042	0.0209	0.0041	0.0151	0.0010	0.0076
% Precision	15.1436	13.7709	15.3164	14.1709	14.1666	18.7394	9.1240	10.7560
135	0.0607	0.2256	0.0312	0.1679	0.0331	0.0908	0.0131	0.0871
135	0.0583	0.2233	0.0300	0.1639	0.0320	0.0907	0.0126	0.0799
Average	0.0595	0.2245	0.0306	0.1659	0.0326	0.0908	0.0129	0.0835
Stdev-2sig	0.0034	0.0033	0.0017	0.0057	0.0016	0.0001	0.0007	0.0102
% Precision	5.7044	1.4492	5.5459	3.4098	4.7792	0.1558	5.5028	12.1944

ICP-MS REE - Repeats						
LC2						
Depth (cm)	**Lu175 mg/L**	**Hf178 mg/L**	**Ta181 mg/L**	**Pb208 mg/L**	**Th232 ppm**	**U238 ppm**
15	0.0103	0.0830	0.0388	0.8839	0.5618	0.1232
15	0.0097	0.0674	0.0349	0.8104	0.4001	0.0744
Average	0.0100	0.0752	0.0369	0.8472	0.4810	0.0988
Stdev-2sig	0.0008	0.0221	0.0055	0.1039	0.2287	0.0690
% Precision	8.4853	29.3374	14.9673	12.2699	47.5472	69.8518
115	0.0115	0.0822	0.0231	0.6418	0.6138	0.0837
115	0.0102	0.0775	0.0197	0.5139	0.4864	0.0542
Average	0.0109	0.0799	0.0214	0.5779	0.5501	0.0690
Stdev-2sig	0.0018	0.0066	0.0048	0.1809	0.1802	0.0417
% Precision	16.9445	8.3241	22.4688	31.3019	32.7524	60.5066
135	0.0131	0.1003	0.0273	0.6864	0.8592	0.0911
135	0.0121	0.0964	0.0258	0.6785	0.8611	0.0867
Average	0.0126	0.0984	0.0266	0.6825	0.8602	0.0889
Stdev-2sig	0.0014	0.0055	0.0021	0.0112	0.0027	0.0062
% Precision	11.2239	5.6080	7.9899	1.6371	0.3124	6.9995

ICP-MS REE - Repeats								
LC2								
Depth (cm)	**Y89 mg/L**	**Zr90 mg/L**	**Nb93 mg/L**	**La139 mg/L**	**Ce140 mg/L**	**Pr141 mg/L**	**Nd143 mg/L**	**Sm147 mg/L**
185	2.1333	12.4068	1.8125	2.9340	6.1954	0.7155	2.7961	0.5592
185	2.3932	13.5663	2.0640	3.0150	6.2708	0.7261	2.8314	0.5688
Average	2.2633	12.9866	1.9383	2.9745	6.2331	0.7208	2.8138	0.5640
Stdev-2sig	0.3676	1.6398	0.3557	0.1146	0.1066	0.0150	0.0499	0.0136
% Precision	16.2401	12.6268	18.3503	3.8511	1.7107	2.0797	1.7742	2.4072
275	1.0459	5.5043	0.5766	1.1394	2.3451	0.2951	1.2036	0.2516
275	1.0991	4.8508	0.6135	1.1721	2.3907	0.2995	1.2237	0.2543
Average	1.0725	5.1776	0.5951	1.1558	2.3679	0.2973	1.2137	0.2530
Stdev-2sig	0.0752	0.9242	0.0522	0.0462	0.0645	0.0062	0.0284	0.0038
% Precision	7.0150	17.8499	8.7698	4.0013	2.7234	2.0930	2.3422	1.5095
465	0.6641	2.2245	0.2609	0.6589	1.3276	0.1762	0.7354	0.1478
465	0.7157	2.5121	0.3115	0.8914	1.7420	0.2192	0.8654	0.1768
Average	0.6899	2.3683	0.2862	0.7752	1.5348	0.1977	0.8004	0.1623
Stdev-2sig	0.0730	0.4067	0.0716	0.3288	0.5861	0.0608	0.1838	0.0410
% Precision	10.5774	17.1738	25.0032	42.4182	38.1841	30.7593	22.9695	25.2694

ICP-MS REE - Repeats								
LC2								
Depth (cm)	**Eu151 mg/L**	**Gd157 mg/L**	**Tb159 mg/L**	**Dy163 mg/L**	**Ho165 mg/L**	**Er166 mg/L**	**Tm169 mg/L**	**Yb174 mg/L**
185	0.1342	0.5190	0.0728	0.3911	0.0753	0.2115	0.0289	0.2022
185	0.1348	0.5325	0.0753	0.4132	0.0788	0.2236	0.0303	0.2007
Average	0.1345	0.5258	0.0741	0.4022	0.0771	0.2176	0.0296	0.2015
Stdev-2sig	0.0008	0.0191	0.0035	0.0313	0.0049	0.0171	0.0020	0.0021
% Precision	0.6309	3.6314	4.7745	7.7718	6.4241	7.8658	6.6888	1.0530
275	0.0591	0.2442	0.0324	0.1825	0.0347	0.0963	0.0132	0.0856
275	0.0635	0.2508	0.0335	0.1851	0.0352	0.0985	0.0137	0.0881
Average	0.0613	0.2475	0.0330	0.1838	0.0350	0.0974	0.0135	0.0869
Stdev-2sig	0.0062	0.0093	0.0016	0.0037	0.0007	0.0031	0.0007	0.0035
% Precision	10.1510	3.7712	4.7212	2.0005	2.0232	3.1943	5.2573	4.0709
465	0.0382	0.1615	0.0215	0.1193	0.0238	0.0642	0.0087	0.0617
465	0.0429	0.1716	0.0246	0.1343	0.0265	0.0705	0.0097	0.0619
Average	0.0406	0.1666	0.0231	0.1268	0.0252	0.0674	0.0092	0.0618
Stdev-2sig	0.0066	0.0143	0.0044	0.0212	0.0038	0.0089	0.0014	0.0003
% Precision	16.3916	8.5761	19.0198	16.7297	15.1824	13.2287	15.3719	0.4577

ICP-MS REE - Repeats						
LC2						
Depth (cm)	**Lu175 mg/L**	**Hf178 mg/L**	**Ta181 mg/L**	**Pb208 mg/L**	**Th232 ppm**	**U238 ppm**
185	0.0285	0.2707	0.1319	1.9465	2.4874	0.2779
185	0.0291	0.2729	0.1391	2.0795	2.6673	0.2384
Average	0.0288	0.2718	0.1355	2.0130	2.5774	0.2582
Stdev-2sig	0.0008	0.0031	0.0102	0.1881	0.2544	0.0559
% Precision	2.9463	1.1447	7.5146	9.3438	9.8713	21.6391
275	0.0128	0.1214	0.0391	0.8705	1.1103	0.1089
275	0.0131	0.1089	0.0386	0.7661	1.0220	0.0944
Average	0.0130	0.1152	0.0389	0.8183	1.0662	0.1017
Stdev-2sig	0.0004	0.0177	0.0007	0.1476	0.1249	0.0205
% Precision	3.2762	15.3519	1.8201	18.0428	11.7127	20.1732
465	0.0088	0.0573	0.0215	0.4983	0.4529	0.0498
465	0.0090	0.0633	0.0237	0.4715	0.5286	0.0418
Average	0.0089	0.0603	0.0226	0.4849	0.4908	0.0458
Stdev-2sig	0.0003	0.0085	0.0031	0.0379	0.1071	0.0113
% Precision	3.1780	14.0718	13.7667	7.8162	21.8148	24.7024

ICP-MS REE - Repeats								
LC2								
Depth (cm)	**Y89 mg/L**	**Zr90 mg/L**	**Nb93 mg/L**	**La139 mg/L**	**Ce140 mg/L**	**Pr141 mg/L**	**Nd143 mg/L**	**Sm147 mg/L**
525	0.4608	1.2884	0.1242	0.4634	0.9616	0.1309	0.5393	0.1149
525	0.4424	1.5462	0.1306	0.4135	0.8663	0.1209	0.4921	0.1080
Average	0.4516	1.4173	0.1274	0.4385	0.9140	0.1259	0.5157	0.1115
Stdev-2sig	0.0260	0.3646	0.0091	0.0706	0.1348	0.0141	0.0668	0.0098
% Precision	5.7621	25.7239	7.1044	16.0952	14.7464	11.2328	12.9437	8.7556
595	1.2846	3.5695	0.3107	1.3015	2.6022	0.3538	1.4650	0.3061
595	1.3821	4.3101	0.4072	1.6083	3.2702	0.4256	1.7195	0.3574
Average	1.3334	3.9398	0.3590	1.4549	2.9362	0.3897	1.5923	0.3318
Stdev-2sig	0.1379	1.0474	0.1365	0.4339	0.9447	0.1015	0.3599	0.0725
% Precision	10.3413	26.5843	38.0197	29.8220	32.1741	26.0561	22.6043	21.8686
695	0.9748	3.8723	0.4130	1.0364	2.1479	0.2797	1.1288	0.2354
695	0.9654	3.7163	0.4006	1.0730	2.1936	0.2890	1.1631	0.2432
Average	0.9701	3.7943	0.4068	1.0547	2.1708	0.2844	1.1460	0.2393
Stdev-2sig	0.0133	0.2206	0.0175	0.0518	0.0646	0.0132	0.0485	0.0110
% Precision	1.3703	5.8144	4.3108	4.9076	2.9773	4.6254	4.2330	4.6096

ICP-MS REE - Repeats

LC2

Depth (cm)	Eu151 mg/L	Gd157 mg/L	Tb159 mg/L	Dy163 mg/L	Ho165 mg/L	Er166 mg/L	Tm169 mg/L	Yb174 mg/L
525	0.0293	0.1191	0.0164	0.0921	0.0179	0.0459	0.0063	0.0450
525	0.0281	0.1119	0.0160	0.0877	0.0171	0.0457	0.0064	0.0448
Average	0.0287	0.1155	0.0162	0.0899	0.0175	0.0458	0.0064	0.0449
Stdev-2sig	0.0017	0.0102	0.0006	0.0062	0.0011	0.0003	0.0001	0.0003
% Precision	5.9131	8.8159	3.4919	6.9216	6.4650	0.6176	2.2271	0.6299
595	0.0801	0.3270	0.0434	0.2414	0.0464	0.1248	0.0170	0.1144
595	0.0945	0.3385	0.0503	0.2726	0.0533	0.1441	0.0194	0.1168
Average	0.0873	0.3328	0.0469	0.2570	0.0499	0.1345	0.0182	0.1156
Stdev-2sig	0.0204	0.0163	0.0098	0.0441	0.0098	0.0273	0.0034	0.0034
% Precision	23.3272	4.8876	20.8283	17.1687	19.5749	20.3007	18.6490	2.9361
695	0.0635	0.2247	0.0330	0.1801	0.0360	0.0997	0.0138	0.0868
695	0.0635	0.2278	0.0332	0.1821	0.0359	0.0965	0.0132	0.0835
Average	0.0635	0.2263	0.0331	0.1811	0.0360	0.0981	0.0135	0.0852
Stdev-2sig	0.0000	0.0044	0.0003	0.0028	0.0001	0.0045	0.0008	0.0047
% Precision	0.0000	1.9377	0.8545	1.5618	0.3934	4.6131	6.2854	5.4808

ICP-MS REE - Repeats						
LC2						
Depth (cm)	**Lu175 mg/L**	**Hf178 mg/L**	**Ta181 mg/L**	**Pb208 mg/L**	**Th232 ppm**	**U238 ppm**
525	0.0065	0.0353	0.0093	0.4575	0.3753	0.0390
525	0.0063	0.0399	0.0096	0.2983	0.2841	0.0298
Average	0.0064	0.0376	0.0095	0.3779	0.3297	0.0344
Stdev-2sig	0.0003	0.0065	0.0004	0.2251	0.1290	0.0130
% Precision	4.4194	17.3015	4.4896	59.5773	39.1193	37.8220
595	0.0166	0.0948	0.0260	0.8393	0.8409	0.0929
595	0.0181	0.1145	0.0281	0.9769	0.6619	0.0361
Average	0.0174	0.1047	0.0271	0.9081	0.7514	0.0645
Stdev-2sig	0.0021	0.0279	0.0030	0.1946	0.2531	0.0803
% Precision	12.2266	26.6221	10.9791	21.4289	33.6897	124.5385
695	0.0130	0.1003	0.0302	0.6599	0.7953	0.0668
695	0.0127	0.0947	0.0283	0.5930	0.6860	0.0457
Average	0.0129	0.0975	0.0293	0.6265	0.7407	0.0563
Stdev-2sig	0.0004	0.0079	0.0027	0.0946	0.1546	0.0298
% Precision	3.3017	8.1227	9.1863	15.1027	20.8700	53.0487

ICP-MS REE - Repeats								
LC2								
Depth (cm)	**Y89 mg/L**	**Zr90 mg/L**	**Nb93 mg/L**	**La139 mg/L**	**Ce140 mg/L**	**Pr141 mg/L**	**Nd143 mg/L**	**Sm147 mg/L**
775	1.5683	7.3355	0.9733	1.8107	3.9098	0.4823	1.8957	0.3821
775	1.6049	7.5031	0.9892	1.8248	3.9273	0.4881	1.9129	0.3817
Average	1.5866	7.4193	0.9813	1.8178	3.9186	0.4852	1.9043	0.3819
Stdev-2sig	0.0518	0.2370	0.0225	0.0199	0.0247	0.0082	0.0243	0.0006
% Precision	3.2623	3.1947	2.2916	1.0970	0.6316	1.6905	1.2773	0.1481
1015	0.4924	1.6456	0.1821	0.5555	1.1700	0.1591	0.6352	0.1327
1015	0.5073	1.6795	0.1790	0.5629	1.1881	0.1632	0.6559	0.1361
Average	0.4999	1.6626	0.1806	0.5592	1.1791	0.1612	0.6456	0.1344
Stdev-2sig	0.0211	0.0479	0.0044	0.0105	0.0256	0.0058	0.0293	0.0048
% Precision	4.2156	2.8836	2.4282	1.8715	2.1710	3.5981	4.5348	3.5776
1045	0.7294	3.3479	0.3719	0.9491	1.8731	0.2527	0.9876	0.1970
1045	0.9428	3.9972	0.4656	1.1381	2.2726	0.3018	1.1866	0.2425
Average	0.8361	3.6726	0.4188	1.0436	2.0729	0.2773	1.0871	0.2198
Stdev-2sig	0.3018	0.9182	0.1325	0.2673	0.5650	0.0694	0.2814	0.0643
% Precision	36.0953	25.0030	31.6446	25.6120	27.2561	25.0452	25.8880	29.2818

ICP-MS REE - Repeats								
LC2								
Depth (cm)	**Eu151 mg/L**	**Gd157 mg/L**	**Tb159 mg/L**	**Dy163 mg/L**	**Ho165 mg/L**	**Er166 mg/L**	**Tm169 mg/L**	**Yb174 mg/L**
775	0.1038	0.3621	0.0539	0.2974	0.0571	0.1587	0.0217	0.1368
775	0.1060	0.3743	0.0549	0.2958	0.0580	0.1575	0.0219	0.1384
Average	0.1049	0.3682	0.0544	0.2966	0.0576	0.1581	0.0218	0.1376
Stdev-2sig	0.0031	0.0173	0.0014	0.0023	0.0013	0.0017	0.0003	0.0023
% Precision	2.9659	4.6859	2.5997	0.7629	2.2116	1.0734	1.2974	1.6444
1015	0.0385	0.1249	0.0180	0.0955	0.0185	0.0516	0.0071	0.0436
1015	0.0388	0.1306	0.0183	0.0960	0.0187	0.0513	0.0070	0.0435
Average	0.0387	0.1278	0.0182	0.0958	0.0186	0.0515	0.0071	0.0436
Stdev-2sig	0.0004	0.0081	0.0004	0.0007	0.0003	0.0004	0.0001	0.0001
% Precision	1.0977	6.3100	2.3375	0.7385	1.5207	0.8246	2.0060	0.3247
1045	0.0542	0.1932	0.0269	0.1465	0.0282	0.0778	0.0106	0.0677
1045	0.0663	0.2326	0.0334	0.1855	0.0353	0.0987	0.0136	0.0839
Average	0.0603	0.2129	0.0302	0.1660	0.0318	0.0883	0.0121	0.0758
Stdev-2sig	0.0171	0.0557	0.0092	0.0552	0.0100	0.0296	0.0042	0.0229
% Precision	28.4016	26.1719	30.4888	33.2255	31.6249	33.4924	35.0631	30.2246

ICP-MS REE - Repeats						
LC2						
Depth (cm)	**Lu175 mg/L**	**Hf178 mg/L**	**Ta181 mg/L**	**Pb208 mg/L**	**Th232 ppm**	**U238 ppm**
775	0.0202	0.1719	0.0707	1.0233	1.1232	0.0855
775	0.0203	0.1749	0.0719	0.9981	0.8485	0.0498
Average	0.0203	0.1734	0.0713	1.0107	0.9859	0.0677
Stdev-2sig	0.0001	0.0042	0.0017	0.0356	0.3885	0.0505
% Precision	0.6984	2.4467	2.3802	3.5261	39.4060	74.6303
1015	0.0066	0.0400	0.0131	0.4276	0.3602	0.0233
1015	0.0066	0.0425	0.0123	0.4333	0.3369	0.0265
Average	0.0066	0.0413	0.0127	0.4305	0.3486	0.0249
Stdev-2sig	0.0000	0.0035	0.0011	0.0081	0.0330	0.0045
% Precision	0.0000	8.5710	8.9084	1.8727	9.4538	18.1746
1045	0.0100	0.0818	0.0293	0.5715	0.5019	0.0315
1045	0.0128	0.0921	0.0353	0.7283	2.4444	0.0720
Average	0.0114	0.0870	0.0323	0.6499	1.4732	0.0518
Stdev-2sig	0.0040	0.0146	0.0085	0.2217	2.7471	0.0573
% Precision	34.7351	16.7526	26.2702	34.1204	186.4786	110.6776

ICP-MS REE - Repeats								
LC2								
Depth (cm)	**Y89 mg/L**	**Zr90 mg/L**	**Nb93 mg/L**	**La139 mg/L**	**Ce140 mg/L**	**Pr141 mg/L**	**Nd143 mg/L**	**Sm147 mg/L**
1255	0.8565	2.7513	0.3902	1.0762	1.9829	0.2756	1.1274	0.2247
1255	0.8483	2.7695	0.3892	0.9977	1.8381	0.2581	1.0737	0.2200
Average	0.8524	2.7604	0.3897	1.0370	1.9105	0.2669	1.1006	0.2224
Stdev-2sig	0.0116	0.0257	0.0014	0.1110	0.2048	0.0247	0.0759	0.0066
% Precision	1.3605	0.9324	0.3629	10.7060	10.7186	9.2744	6.9005	2.9893
1285	1.1095	2.4691	0.3078	1.0967	2.1143	0.2956	1.2449	0.2635
1285	1.3089	2.9843	0.3701	1.2857	2.4672	0.3512	1.4701	0.3052
Average	1.2092	2.7267	0.3390	1.1912	2.2908	0.3234	1.3575	0.2844
Stdev-2sig	0.2820	0.7286	0.0881	0.2673	0.4991	0.0786	0.3185	0.0590
% Precision	23.3207	26.7210	25.9937	22.4384	21.7866	24.3136	23.4608	20.7395

ICP-MS REE - Repeats								
LC2								
Depth (cm)	**Eu151 mg/L**	**Gd157 mg/L**	**Tb159 mg/L**	**Dy163 mg/L**	**Ho165 mg/L**	**Er166 mg/L**	**Tm169 mg/L**	**Yb174 mg/L**
1255	0.0669	0.2235	0.0314	0.1663	0.0324	0.0857	0.0115	0.0721
1255	0.0648	0.2140	0.0310	0.1625	0.0317	0.0861	0.0114	0.0719
Average	0.0659	0.2188	0.0312	0.1644	0.0321	0.0859	0.0115	0.0720
Stdev-2sig	0.0030	0.0134	0.0006	0.0054	0.0010	0.0006	0.0001	0.0003
% Precision	4.5100	6.1417	1.8131	3.2689	3.0888	0.6585	1.2351	0.3928
1285	0.0801	0.2675	0.0376	0.2030	0.0391	0.1043	0.0136	0.0819
1285	0.0937	0.3116	0.0440	0.2351	0.0449	0.1211	0.0155	0.0966
Average	0.0869	0.2896	0.0408	0.2191	0.0420	0.1127	0.0146	0.0893
Stdev-2sig	0.0192	0.0624	0.0091	0.0454	0.0082	0.0238	0.0027	0.0208
% Precision	22.1327	21.5392	22.1837	20.7242	19.5296	21.0814	18.4674	23.2929

ICP-MS REE - Repeats						
LC2						
Depth (cm)	**Lu175 mg/L**	**Hf178 mg/L**	**Ta181 mg/L**	**Pb208 mg/L**	**Th232 ppm**	**U238 ppm**
1255	0.0108	0.0668	0.0275	0.8613	0.7043	0.0615
1255	0.0107	0.0665	0.0286	0.8074	0.7289	0.0671
Average	0.0108	0.0667	0.0281	0.8344	0.7166	0.0643
Stdev-2sig	0.0001	0.0004	0.0016	0.0762	0.0348	0.0079
% Precision	1.3155	0.6366	5.5459	9.1360	4.8548	12.3166
1285	0.0122	0.0648	0.0196	0.8920	0.5733	0.0440
1285	0.0139	0.0740	0.0231	0.9996	0.7283	0.0505
Average	0.0131	0.0694	0.0214	0.9458	0.6508	0.0473
Stdev-2sig	0.0024	0.0130	0.0049	0.1522	0.2192	0.0092
% Precision	18.4227	18.7475	23.1838	16.0890	33.6821	19.4548

Appendix 9

LC2 - Source Rock Geochemistry

ICP-AES

Source Rocks											
AES LC2											
Sample Label	**Al**	**As**	**Ba**	**Be**	**Ca**	**Cu**	**Fe**	**K**	**La**	**Li**	**Mg**
1- Rock 1	65900	14	387	1.89	703	17.85	32700	15960	56	45.2	8920
2- CW 180	130700	16	423.2	1.535	105	71.4	60800	9580	38.33	23.23	1846
4- CW 385	129500	9.5	362.2	1.665	635	82.8	43530	7390	40.68	30.1	3125
5- Rock 2	106300	11.5	691	2.94	155	34.6	45110	28800	83.2	53.7	10750
7- Rock 1	64900	14.5	372.5	1.835	620	17.05	32280	15480	57.4	45	8770
8- Rock 3	77200	< 1.	396	1.645	41630	46.75	68900	15300	34.25	8.85	37280
9- CW 280	149800	11	45	0.645	60	75.9	159500	650	22.33	15.87	782
10- Rock 4	60300	11	507	2.19	222.5	13.5	23070	18510	48.78	25.45	5910
12- Basal Clay	150100	5	342	1.32	3755	91.9	128400	1990	54.1	61.3	2032
13- ash outcrop	124800	7	105.5	1.16	172.5	108.7	144500	117.5	36.35	6.05	11340
14- CW 385	122300	7.5	340	1.56	608	78.9	44420	6640	38.02	28.73	2945
15- ash rock	139100	< 1.	155	1.175	100	135.9	126700	115	25.6	5.25	2831
RBLK	59	1.5	1.5	< .01	75	0.6	40	< 5.	< .05	< .05	3.5
RBLK	135	1	0.75	< .01	97.5	0.95	45	7.5	< .05	< .05	6

Appendix 9: Source Rocks AES LC2

Source Rocks											
AES LC2											
Sample Label	**Mn**	**Mo**	**Na**	**Ni**	**P**	**Pb**	**S**	**Sr**	**Ti**	**V**	**Zn**
1- Rock 1	169.5	0.75	9640	17.2	566	8	28.5	63	4217	49.9	47.85
2- CW 180	91.5	1.75	553	213.7	827	8	428.5	44.25	12840	141.5	64.7
4- CW 385	343	1.5	1088	214.5	1018	15	784	64.2	16500	237.7	157.4
5- Rock 2	180.5	< .5	1468	34.5	337	15	46	42.5	4652	81	67.2
7- Rock 1	164.5	< .5	9640	15	532	8	28.5	61.2	4132	49.2	45.15
8- Rock 3	731	1.25	30620	130	2230	3	14	624	10130	104.5	92.6
9- CW 280	214	3.25	220	168.1	2432	6	700	47	18940	300.6	87.5
10- Rock 4	63.5	0.75	7900	8.6	303	13	38	44.5	3323	34.6	34.95
12- Basal Clay	2939	0.75	730	204	1428	5	423.5	112.2	17950	162.2	138.8
13- ash outcrop	854	1.5	200	420.7	2991	6	252	60.7	13660	235.1	129.4
14- CW 385	385	1.5	1090	203.4	971	14	750	60.5	15510	223.5	135.1
15- ash rock	1844	1.25	197.5	639	2325	2	319	56	15600	220.1	111.4
RBLK	< 1.	< .5	< 5.	0.8	< 2.	< 2.	2.5	0.5	27.2	< .2	1.55
RBLK	2.5	< .5	< 5.	0.5	3	< 2.	8.5	0.5	25.65	< .2	3.65

Appendix 9: Source Rocks AES LC2

Source Rocks Reference Materials (Accuracy)

AES LC2

Sample Label	**Al**	**As**	**Ba**	**Be**	**Ca**	**Cu**	**Fe**	**K**	**La**	**Li**	**Mg**
GBW07406	111000	247.5	112	3.97	1340	428	58600	11100	30.48	35.08	1767
GBW07406	112900	248	113.2	3.61	1573	419.3	60900	12260	29.98	34.37	1863
Average	111950	247.75	112.6	3.79	1456.5	423.65	59750	11680	30.23	34.725	1815
RSD	1.20	0.14	0.75	6.72	11.31	1.45	2.72	7.02	1.17	1.45	3.74
Accepted	112400	220	118	4.4	1572	390	56600	14110	30	36	2050
%Bias	-0.40	12.61	-4.58	-13.86	-7.35	8.63	5.57	-17.22	0.77	-3.54	-11.46
HRM1	13810	9.5	262.7	0.345	888	4.25	8500	8280	9.75	7.2	486
HRM1	13570	10	249.7	0.34	870	4.8	8530	8140	9.05	6.9	455.5
Average	13690	9.75	256.2	0.3425	879	4.525	8515	8210	9.4	7.05	470.75
RSD	1.24	3.63	3.59	1.03	1.45	8.59	0.25	1.21	5.27	3.01	4.58
Accepted	#######	4.5	250	0.45	750	4.4	9100	9800	9	9	490
%Bias	-2.21	116.67	2.48	-23.89	17.20	2.84	-6.43	-16.22	4.44	-21.67	-3.93
HRM2	53600	177.5	691	4.17	9110	662	58100	13560	26.87	203.2	20760
HRM2	53400	164	700	4.51	8990	646	56900	13410	25.53	200	20500
Average	53500	170.75	695.5	4.34	9050	654	57500	13485	26.2	201.6	20630
RSD	0.26	5.59	0.92	5.54	0.94	1.73	1.48	0.79	3.62	1.12	0.89
Accepted	50500	180	690	4.3	9500	600	54000	16300	27	180	21200
%Bias	5.94	-5.14	0.80	0.93	-4.74	9.00	6.48	-17.27	-2.96	12.00	-2.69

Source Rocks Reference Materials (Accuracy)											
AES LC2											
Sample Label	**Mn**	**Mo**	**Na**	**Ni**	**P**	**Pb**	**S**	**Sr**	**Ti**	**V**	**Zn**
GBW07406	1295	18.25	1080	52.9	265	288	250.5	48.5	4549	94.2	93.4
GBW07406	1395	18.75	1120	54.1	282	295	250	49.25	4768	93.5	100.2
Average	1345	18.5	1100	53.5	273.5	291.5	250.25	48.875	4658.5	93.85	96.8
RSD	5.26	1.91	2.57	1.59	4.40	1.70	0.14	1.09	3.32	0.53	4.97
Accepted	1450	18	1410	53	303	314	260	39	4390	130	96.6
%Bias	-7.24	2.78	-21.99	0.94	-9.74	-7.17	-3.75	25.32	6.12	-27.81	0.21
HRM1	125	< .5	1448	5.9	413	17	162.5	44.25	1036	11.7	23.65
HRM1	120.5	< .5	1430	5.8	411	17	155	42	1040	11.4	24.5
Average	122.75		1439	5.85	412	17	158.75	43.125	1038	11.55	24.075
RSD	2.59		0.88	1.21	0.34	0.00	3.34	3.69	0.27	1.84	2.50
Accepted	140		1750	5	480	24	180	39	910	17	22
%Bias	-12.32		-17.77	17.00	-14.17	-29.17	-11.81	10.58	14.07	-32.06	9.43
HRM2	1418	3	5560	293.8	756	524	1857	1396	3579	62.7	396.4
HRM2	1404	2.25	5500	283.4	737	500	1857	1463	3470	60.7	379.4
Average	1411	2.625	5530	288.6	746.5	512	1857	1429.5	3524.5	61.7	387.9
RSD	0.70	20.20	0.77	2.55	1.80	3.31	0.00	3.31	2.19	2.29	3.10
Accepted	1600	2	5600	290	760	570	2000	1300	3200	83	430
%Bias	-11.81	31.25	-1.25	-0.48	-1.78	-10.18	-7.15	9.96	10.14	-25.66	-9.79

Appendix 9: Source Rocks AES LC2

Source Rocks Reference Materials (Precision)											
AES LC2											
Sample Label	**Al**	**As**	**Ba**	**Be**	**Ca**	**Cu**	**Fe**	**K**	**La**	**Li**	**Mg**
1- Rock 1	65900	14	387	1.89	703	17.85	32700	15960	56	45.2	8920
7- Rock 1	64900	14.5	372.5	1.835	620	17.05	32280	15480	57.4	45	8770
Average	65400	14.25	379.75	1.8625	661.5	17.45	32490	15720	56.7	45.1	8845
% Diff	1.5	3.5	3.8	3.0	12.5	4.6	1.3	3.1	2.5	0.4	1.7
4- CW 385	129500	9.5	362.2	1.665	635	82.8	43530	7390	40.68	30.1	3125
14- CW 385	122300	7.5	340	1.56	608	78.9	44420	6640	38.02	28.73	2945
Average	125900	8.5	351.1	1.6125	621.5	80.85	43975	7015	39.35	29.415	3035
% Diff	5.7	23.5	6.3	6.5	4.3	4.8	2.0	10.7	6.8	4.7	5.9

Source Rocks Reference Materials (Precision)											
AES LC2											
Sample Label	**Mn**	**Mo**	**Na**	**Ni**	**P**	**Pb**	**S**	**Sr**	**Ti**	**V**	**Zn**
1- Rock 1	169.5	0.75	9640	17.2	566	8	28.5	63	4217	49.9	47.85
7- Rock 1	164.5	< .5	9640	15	532	8	28.5	61.2	4132	49.2	45.15
Average	167	0.75	9640	16.1	549	8	28.5	62.1	4174.5	49.55	46.5
% Diff	3.0		0.0	13.7	6.2	0.0	0.0	2.9	2.0	1.4	5.8
4- CW 385	343	1.5	1088	214.5	1018	15	784	64.2	16500	237.7	157.4
14- CW 385	385	1.5	1090	203.4	971	14	750	60.5	15510	223.5	135.1
Average	364	1.5	1089	208.95	994.5	14.5	767	62.35	16005	230.6	146.25
% Diff	11.5	0.0	0.2	5.3	4.7	6.9	4.4	5.9	6.2	6.2	15.2

Appendix 10

LC2 – Source Rock Geochemistry

ICP-MS

Source Rocks										
Quadrapole										
LC2										
Sample Label	**Li7**	**Be**	**Sc45**	**V51**	**Ni60**	**Cu65**	**Rb85**	**Sr88**	**Mo98**	**Ba137**
1- Rock 1	50.4067	2.1957	10.854	70.7773	17.4458	18.6476	126.487	67.7844	0.7237	367.8550x
10- Rock 4	30.7782	2.5629	10.1412	52.3905	9.7007	16.718	166.7249	54.2803	1.1115	524.8041x
12- Basal Clay	64.3105	1.9262	32.6963	364.9184	271.0439	103.913	20.6296	129.6401	1.5788	378.6641x
13- ash outcrop	7.8682	1.5615	34.5903	652.7330x	555.1421x	162.661	0.8026	51.3569	3.4218	120.1322x
14- CW 385	29.5608	1.934	29.2851	489.6752	243.9572	83.719	97.2973	69.2528	2.4677	363.4981x
15- ash rock	6.5893	1.57	30.0353	520.0098	781.3365x	148.568	0.3687	44.8671	2.5008	172.2024x
2- CW 180	25.3673	1.9546	25.1563	245.3309	226.9461	66.3521	92.3877	34.5061	2.5938	373.7108x
4- CW 385	31.9119	2.055	28.6808	474.2279	228.017	78.2567	87.5306	59.8172	2.3948	323.8402x
5- Rock 2	58.2496	3.4503	19.9504	117.7698	37.3032	34.793	271.6225	45.3343	0.7227	665.0918x
7- Rock 1	54.0005	2.2736	11.3012	74.7153	16.4623	19.1394	131.9657	68.9342	0.4318	356.6776x
8- Rock 3	11.585	2.3755	15.23	189.8371	169.7147	51.905	35.5956	904.3892x	2.1549	441.1960x
9- CW 280	16.1358	0.9368	39.2419	617.0461x	198.9449	79.7182	4.9347	15.7306	5.064	43.1383
RBLK	0.1977	nd	0.0271	0.4805	0.7773	0.578	0.0303	0.1521	0.7577	1.0143
RBLK	0.3755	0.0047	0.0387	0.2953	0.5826	1.02	0.0717	0.2694	0.5938	0.2147

Appendix 10: Source Rocks Quad LC2

Source Rocks										
Quadrapole										
LC2										
Sample Label	**Y89 mg/L**	**Zr90 mg/L**	**Nb93 mg/L**	**La139 mg/L**	**Ce140 mg/L**	**Pr141 mg/L**	**Nd143 mg/L**	**Sm147 mg/L**	**Eu151 mg/L**	**Gd157 mg/L**
1- Rock 1	17.0321	180.7311	17.2966	52.4283	81.1242	12.0098	43.146	8.1188	1.6083	6.9767
10- Rock 4	20.1813	157.8465	19.1083	49.9738	91.8004	12.02	42.1653	7.837	1.5348	6.7653
12- Basal Clay	24.8201	453.3633	97.3421	58.2439	123.0704	12.7929	47.851	9.7594	3.1295	8.2635
13- ash outcrop	17.9158	481.285	134.1057	44.3979	100.1011	9.6722	35.6809	7.0821	2.4462	7.3967
14- CW 385	23.2271	324.8955	67.8953	41.8335	119.0643	10.2974	39.375	8.1868	2.2243	7.5936
15- ash rock	20.5192	377.7	98.1203	28.9064	91.0983	8.3418	39.391	7.9572	2.7125	8.0792
2- CW 180	11.0027	222.9954	44.0749	35.1097	63.0513	7.8614	28.0641	5.1353	1.1858	4.4274
4- CW 385	20.3233	295.0225	62.2327	35.9758	104.1548	8.8442	34.0361	7.0591	1.9368	6.6593
5- Rock 2	28.4248	161.2048	23.4561	81.8779	120.9359	18.2697	62.5114	10.7952	2.3108	9.0951
7- Rock 1	17.9774	191.194	17.3487	56.0512	86.5236	13.0656	46.4586	8.6004	1.667	7.3672
8- Rock 3	19.1816	270.506	45.567	36.8659	69.1612	8.752	34.1427	6.5364	2.2402	6.2733
9- CW 280	5.8491	359.4487	66.4278	21.0512	32.6583	3.5906	11.2293	1.9987	0.5452	1.8337
RBLK	0.0129	0.37	0.0844	0.0154	0.0241	0.0032	0.0097	0.0022	0.0008	0.0021
RBLK	0.0268	0.6301	0.0855	0.0192	0.0355	0.0039	0.0138	0.0026	0.0007	0.0038

Appendix 10: Source Rocks Quad LC2

Source Rocks										
Quadrapole										
LC2										
Sample Label	**Tb159 mg/L**	**Dy163 mg/L**	**Ho165 mg/L**	**Er166 mg/L**	**Tm169 mg/L**	**Yb174 mg/L**	**Lu175 mg/L**	**Hf178 mg/L**	**Ta181 mg/L**	**Pb208 mg/L**
1- Rock 1	0.8457	3.8666	0.6507	2.1432	0.2772	1.9539	0.3144	4.5454	1.5609	14.1334
10- Rock 4	0.8414	3.9557	0.7365	2.1701	0.3299	2.1789	0.3489	3.9686	1.9717	21.6118
12- Basal Clay	1.1066	5.5818	0.9706	2.691	0.3772	2.2452	0.3156	8.5542	5.5913	14.073
13- ash outcrop	1.0329	5.3354	0.8912	2.4089	0.3262	2.1048	0.2859	9.7589	7.5477	10.0292
14- CW 385	1.0324	5.2404	0.9233	2.535	0.3355	2.1421	0.3166	6.7263	4.3249	30.7226
15- ash rock	1.0371	5.0137	0.8361	2.1422	0.2606	1.6349	0.2347	7.4163	5.7395	8.1407
2- CW 180	0.5394	2.4994	0.4278	1.2313	0.1628	1.0989	0.1707	4.9414	2.9934	17.6873
4- CW 385	0.911	4.4975	0.7825	2.1672	0.2894	1.8298	0.2671	5.8817	3.8162	26.4949
5- Rock 2	1.1684	5.7559	1.0978	3.0703	0.4469	2.5478	0.4187	3.8552	2.0837	25.2045
7- Rock 1	0.9582	4.0889	0.7258	2.0756	0.2906	2.1654	0.3342	4.5377	1.4943	13.6691
8- Rock 3	0.8108	3.9507	0.6837	1.8265	0.218	1.2946	0.192	5.3594	2.7036	7.408
9- CW 280	0.2524	1.3231	0.2357	0.7009	0.0993	0.6697	0.098	6.8297	3.7079	11.6399
RBLK	0.0004	0.0008	0.0003	0.0007	0.0003	0.001	0.0001	0.0114	0.0022	0.5622
RBLK	0.0008	0.0039	0.001	0.003	0.0004	0.0035	0.0005	0.0202	0.0021	0.4859

Appendix 10: Source Rocks Quad LC2

Source Rocks Reference Materials (Accuracy)										
Quadrapole	**LC2**									
Sample Label	**Li7**	**Be**	**Sc45**	**V51**	**Ni60**	**Cu65**	**Rb85**	**Sr88**	**Mo98**	**Ba137**
GBW07406	33.6331	4.2109	15.5103	131.1591	57.5167	432.621	294.2674	53.78	24.7728	62.7848
GBW07406	36.523	4.031	16.3631	137.7393	59.6216	442.464	291.229	53.1445	24.1752	61.4776
Average	35.07805	4.12095	15.9367	134.4492	58.56915	437.5425	292.7482	53.46225	24.474	62.1312
RSD	5.83	3.09	3.78	3.46	2.54	1.59	0.73	0.84	1.73	1.49
Accepted	36	4.4		130	53	390		39	18	
%Bias	-2.56	-6.34		3.42	10.51	12.19		37.08	35.97	
HRM1	11.4889	0.4015	1.6032	15.9934	6.4115	5.039	45.449	50.775	0.6996	251.8794
HRM1	9.6513	0.3987	1.3944	15.3523	6.3247	5.571	48.2629	53.8843	0.7121	269.4207
Average	10.5701	0.4001	1.4988	15.67285	6.3681	5.305	46.85595	52.32965	0.70585	
RSD	12.29	0.49	9.85	2.89	0.96	7.09	4.25	4.20	1.25	
Accepted	9	0.45		17	5	4.4		39		
%Bias	17.45	-11.09		-7.81	27.36	20.57		34.18		
HRM2	210.8062	5.0789	12.4832	401.0505	338.9171	672.8619	234.3153	1840.671	4.5173	351.8815
HRM2	171.8377	4.6194	11.3215	377.5855	313.3203	623.8639	229.0237	1923.926	3.7774	378.4870
Average	191.32195	4.84915	11.90235	389.318	326.1187		231.6695		4.14735	
RSD	14.40	6.70	6.90	4.26	5.55		1.62		12.62	
Accepted	180	4.3		83	290	600		1300	2	
%Bias	6.29	12.77		369.06	12.45				107.37	

Appendix 10: Source Rocks Quad LC2

Source Rocks Reference Materials (Accuracy)										
Quadrapole	**LC2**									
Sample Label	**Y89 mg/L**	**Zr90 mg/L**	**Nb93 mg/L**	**La139 mg/L**	**Ce140 mg/L**	**Pr141 mg/L**	**Nd143 mg/L**	**Sm147 mg/L**	**Eu151 mg/L**	**Gd157 mg/L**
GBW07406	20.8551	139.149	32.5439	17.6833	41.0556	3.6068	12.3583	2.3255	0.4182	2.1952
GBW07406	21.3764	146.9797	33.2219	17.1988	40.1536	3.4514	11.9779	2.233	0.4169	2.0974
Average	21.11575	143.06435	32.8829	17.44105	40.6046	3.5291	12.1681	2.27925	0.41755	2.1463
RSD	1.75	3.87	1.46	1.96	1.57	3.11	2.21	2.87	0.22	3.22
Accepted				30						
%Bias				-41.86						
HRM1	5.3136	54.7379	3.1591	9.4847	18.7994	2.2103	8.1168	1.466	0.3302	1.3914
HRM1	5.1045	48.6731	3.328	10.1318	20.1931	2.3494	8.5583	1.4982	0.3684	1.3891
Average	5.20905	51.7055	3.24355	9.80825	19.49625	2.27985	8.33755	1.4821	0.3493	1.39025
RSD	2.84	8.29	3.68	4.67	5.05	4.31	3.74	1.54	7.73	0.12
Accepted				9						
%Bias				8.98						
HRM2	21.2561	183.9253	17.1841	13.6577	29.1276	3.6096	13.4305	2.6778	0.4773	2.4476
HRM2	19.8171	193.9074	15.8465	13.7051	29.1647	3.5831	13.5285	2.7088	0.5049	2.4106
Average	20.5366	188.91635	16.5153	13.6814	29.14615	3.59635	13.4795	2.6933	0.4911	2.4291
RSD	4.95	3.74	5.73	0.24	0.09	0.52	0.51	0.81	3.97	1.08
Accepted				27						
%Bias				-49.33						

Source Rocks Reference Materials (Accuracy)										
Quadrapole	**LC2**									
Sample Label	**Tb159 mg/L**	**Dy163 mg/L**	**Ho165 mg/L**	**Er166 mg/L**	**Tm169 mg/L**	**Yb174 mg/L**	**Lu175 mg/L**	**Hf178 mg/L**	**Ta181 mg/L**	**Pb208 mg/L**
GBW07406	0.3254	1.9119	0.3965	1.2892	0.2068	1.4633	0.2366	2.2356	3.5379	226.6705
GBW07406	0.3133	1.8349	0.3806	1.2518	0.2032	1.4323	0.2275	2.2712	3.3819	217.0802
Average	0.31935	1.8734	0.38855	1.2705	0.205	1.4478	0.23205	2.2534	3.4599	221.87535
RSD	2.68	2.91	2.89	2.08	1.24	1.51	2.77	1.12	3.19	3.06
Accepted										314
%Bias										-29.34
HRM1	0.1888	1.0308	0.1976	0.5934	0.086	0.5692	0.0897	1.2993	0.2049	22.0476
HRM1	0.1889	1.0012	0.1932	0.5919	0.085	0.5774	0.0869	1.1987	0.2532	25.084
Average	0.18885	1.016	0.1954	0.59265	0.0855	0.5733	0.0883	1.249	0.22905	23.5658
RSD	0.04	2.06	1.59	0.18	0.83	1.01	2.24	5.70	14.91	9.11
Accepted										24
%Bias										-1.81
HRM2	0.3448	1.8518	0.3643	1.1287	0.1711	1.1549	0.1814	2.2733	1.3943	354.9542
HRM2	0.3425	1.8417	0.3649	1.1384	0.1744	1.1999	0.1938	2.5744	1.3628	364.7634
Average	0.34365	1.84675	0.3646	1.13355	0.17275	1.1774	0.1876	2.42385	1.37855	359.8588
RSD	0.47	0.39	0.12	0.61	1.35	2.70	4.67	8.78	1.62	1.93
Accepted										570
%Bias										-36.87

Source Rocks Reference Materials (Precision)										
Quadrapole										
LC2										
Sample Label	**Li7**	**Be**	**Sc45**	**V51**	**Ni60**	**Cu65**	**Rb85**	**Sr88**	**Mo98**	**Ba137**
1- Rock 1	50.4067	2.1957	10.854	70.7773	17.4458	18.6476	126.487	67.7844	0.7237	367.8550
7- Rock 1	54.0005	2.2736	11.3012	74.7153	16.4623	19.1394	131.9657	68.9342	0.4318	356.6776
Average	52.2036	2.23465	11.0776	72.7463	16.95405	18.8935	129.22635	68.3593	0.57775	
% Diff	6.9	3.5	4.0	5.4	5.8	2.6	4.2	1.7	50.5	
14- CW 385	29.5608	1.934	29.2851	489.6752	243.9572	83.719	97.2973	69.2528	2.4677	363.4981
4- CW 385	31.9119	2.055	28.6808	474.2279	228.017	78.2567	87.5306	59.8172	2.3948	323.8402
Average	30.73635	1.9945	28.98295	481.95155	235.9871	80.98785	92.41395	64.535	2.43125	
% Diff	7.6	6.1	2.1	3.2	6.8	6.7	10.6	14.6	3.0	

Appendix 10: Source Rocks Quad LC2

Source Rocks Reference Materials (Precision)										
Quadrapole										
LC2										
Sample Label	**Y89 mg/L**	**Zr90 mg/L**	**Nb93 mg/L**	**La139 mg/L**	**Ce140 mg/L**	**Pr141 mg/L**	**Nd143 mg/L**	**Sm147 mg/L**	**Eu151 mg/L**	**Gd157 mg/L**
1- Rock 1	17.0321	180.7311	17.2966	52.4283	81.1242	12.0098	43.146	8.1188	1.6083	6.9767
7- Rock 1	17.9774	191.194	17.3487	56.0512	86.5236	13.0656	46.4586	8.6004	1.667	7.3672
Average	17.50475	185.96255	17.32265	54.23975	83.8239	12.5377	44.8023	8.3596	1.63765	7.17195
% Diff	5.4	5.6		6.7	6.4	8.4	7.4	5.8	3.6	5.4
14- CW 385	23.2271	324.8955	67.8953	41.8335	119.0643	10.2974	39.375	8.1868	2.2243	7.5936
4- CW 385	20.3233	295.0225	62.2327	35.9758	104.1548	8.8442	34.0361	7.0591	1.9368	6.6593
Average	21.7752	309.959	65.064	38.90465	111.60955	9.5708	36.70555	7.62295	2.08055	7.12645
% Diff	13.3	9.6		15.1	13.4	15.2	14.5	14.8	13.8	13.1

Appendix 10: Source Rocks Quad LC2

Source Rocks Reference Materials (Precision)										
Quadrapole										
LC2										
Sample Label	**Tb159 mg/L**	**Dy163 mg/L**	**Ho165 mg/L**	**Er166 mg/L**	**Tm169 mg/L**	**Yb174 mg/L**	**Lu175 mg/L**	**Hf178 mg/L**	**Ta181 mg/L**	**Pb208 mg/L**
1- Rock 1	0.8457	3.8666	0.6507	2.1432	0.2772	1.9539	0.3144	4.5454	1.5609	14.1334
7- Rock 1	0.9582	4.0889	0.7258	2.0756	0.2906	2.1654	0.3342	4.5377	1.4943	13.6691
Average	0.90195	3.97775								
% Diff	12.5	5.6								
14- CW 385	1.0324	5.2404	0.9233	2.535	0.3355	2.1421	0.3166	6.7263	4.3249	30.7226
4- CW 385	0.911	4.4975	0.7825	2.1672	0.2894	1.8298	0.2671	5.8817	3.8162	26.4949
Average	0.9717	4.86895								
% Diff	12.5	15.3								

Appendix 11

LC2 - XRF Results

XRF LC2											
Depth (cm)	**O**	**Cl**	**Al**	**Si**	**P**	**Depth (cm)**	**O**	**Cl**	**Al**	**Si**	**P**
1	27.20	340	5269	110634	832	193	19.60	195	9152	183716	409
13	28.50	371	2984	45972	510	203	30.50	155	6701	103298	657
23	34.80	462	1141	3100	112	213	32.10	132	7698	141445	481
33	35.50	387	1422	3294	140	223	30.10	195	8916	198531	449
43	35.90	227	1205	1616	66	233	26.80	187	7639	97479	476
53	31.90	252	2538	7411	224	243	25.00	281	6349	130801	249
63	32.70	340	2346	5626	168	253	26.20	161	6492	91529	348
73	32.70	160	2278	4241	69	263	19.50	213	6229	35549	326
83	32.90	264	2671	2940	164	273	22.20	237	4496	13276	223
93	32.80	257	3777	7014	217	283	25.10	151	6217	24882	346
103	31.90	263	5042	29556	397	293	30.80	145	6340	21508	312
113	34.30	237	3971	3766	163	303	31.90	164	3925	17565	217
123	33.70	223	3369	2931	127	313	32.30	10	5402	9802	263
133	32.90	159	5094	3032	183	323	34.60	10	4499	4336	234
142	34.10	150	5774	4126	149	333	33.80	10	4489	5264	220
153	34.60	180	4587	4452	244	343	35.50	41	4711	3215	367
163	34.40	199	4876	2311	73	352	33.90	33	3966	4363	298
173	34.80	116	5997	2839	147	362	32.00	137	4846	25628	302
182	22.60	216	8939	157486	331	372	31.90	10	5917	7070	407

Appendix 11: XRF LC2

XRF LC2											
Depth (cm)	**O**	**Cl**	**Al**	**Si**	**P**	**Depth (cm)**	**O**	**Cl**	**Al**	**Si**	**P**
383	33.50	134	4698	10254	249	573	32.90	10	4969	15790	490
393	33.80	10	4820	11768	289	593	30.40	10	4035	11943	221
403	32.30	10	1578	3059	91	603	33.30	10	3571	11147	402
413	34.70	10	2714	3355	110	613	32.60	21	3674	9338	341
423	33.00	35	2933	2370	94	623	30.10	10	3001	10727	253
433	34.80	46	2424	1639	114	633	31.00	73	3436	8197	287
443	34.40	70	1595	2351	166	643	34.60	72	3129	3101	349
453	34.60	67	3416	2378	313	653	33.50	10	3650	10478	357
463	33.80	10	2731	3814	243	663	35.80	10	2478	1985	313
473	33.70	10	2946	4054	387	673	35.40	10	2833	5480	390
482	32.00	111	3667	15532	338	683	33.50	110	2612	10955	374
494	26.10	41	4856	74145	371	693	33.30	249	3074	8812	228
503	34.40	105	2507	1572	204	702	25.90	79	4999	100111	508
513	34.00	106	2705	1626	232	711	28.70	90	3338	47069	367
522	34.60	10	2577	1396	200	723	32.20	99	2551	27561	386
533	34.50	10	3039	1003	204	733	29.70	141	3591	49437	461
542	34.10	10	1954	922	57	743	29.60	129	3021	54556	472
552	34.30	10	2443	3399	304	759	27.80	150	3997	77246	396
563	20.30	10	6746	234541	902	764	26.90	158	4089	82543	532

Appendix 11: XRF LC2

XRF LC2											
Depth (cm)	**O**	**Cl**	**Al**	**Si**	**P**	**Depth (cm)**	**O**	**Cl**	**Al**	**Si**	**P**
774	33.60	177	2875	8334	320	963	33.90	139	1024	3048	185
782	34.30	39	1496	4544	201	973	34.10	157	764	1963	99
793	29.70	141	3629	50878	422	982	34.70	513	974	4051	145
803	32.40	43	3776	17331	389	993	33.20	369	885	1725	195
812	33.90	21	2941	6669	270	1003	34.80	163	825	1554	61
822	35.10	93	2249	4753	197	1012	35.10	105	1461	2006	273
831	33.90	166	3586	4574	319	1022	35.00	91	797	1003	50
841	33.90	92	3071	10854	223	1033	34.60	178	664	1495	57
853	35.20	61	3490	5516	266	1043	33.10	245	1610	3958	314
863	33.80	84	2659	9481	247	1053	35.30	163	1731	2972	191
873	33.10	75	2883	14380	317	1063	36.70	77	1630	1632	152
883	35.20	102	2036	9301	181	1071	36.90	78	1692	1398	109
893	34.90	105	1833	10720	200	1083	35.50	338	3557	3099	420
903	34.70	13	1456	5105	186	1093	34.70	293	3304	2953	530
913	36.50	60	2007	2810	222	1103	28.80	127	2180	5010	229
923	35.60	31	841	1768	71	1113	28.90	83	1187	2306	95
933	35.30	10	979	1889	105	1123	30.60	136	1886	2686	323
942	35.60	82	964	2166	138	1133	30.60	358	1541	1935	194
953	34.20	44	822	3990	195	1143	32.70	96	1510	2032	147

Appendix 11: XRF LC2

XRF LC2											
Depth (cm)	**O**	**Cl**	**Al**	**Si**	**P**	**Depth (cm)**	**O**	**Cl**	**Al**	**Si**	**P**
1154	31.80	10	1258	2201	179	1232	33.70	10	1592	2401	230
1162	32.00	17	2370	7913	361	1242	34.70	170	1721	2780	251
1173	33.00	146	1752	2580	254	1252	33.40	119	1582	3315	307
1183	33.30	196	980	1413	89	1263	35.10	10	1669	2884	307
1192	32.90	68	1313	2618	206	1273	35.00	182	1826	2633	240
1203	34.20	519	2036	2167	388	1283	34.30	45	1378	1729	250
1213	35.00	163	1450	1554	249	1293	34.90	145	1608	1739	280
1223	34.60	191	785	1703	108						

Appendix 12

LC2 - Carbon, Sulfur and Nitrogen Results

Carbon											
Analyser LC2											
Depth (cm)	**N**	**C**	**S**	**Depth (cm)**	**N**	**C**	**S**	**Depth (cm)**	**N**	**C**	**S**
1	1.64	43.02	0.19	182	1.83	38.30	0.21	362	1.57	55.04	0.55
13	1.43	52.06	0.17	193	1.17	35.89	0.13	372	1.62	54.56	0.50
23	0.91	58.41	0.19	203	1.24	46.69	0.25	383	1.73	54.87	0.38
33	0.79	58.41	0.18	213	1.19	41.32	0.23	393	1.71	53.96	0.37
43	0.62	57.82	0.15	223	1.03	37.26	0.23	403	1.74	55.89	0.40
53	0.84	59.25	0.18	233	1.09	46.33	0.31	413	1.67	55.10	0.39
63	0.87	58.37	0.18	243	1.11	43.84	0.24	423	1.59	55.30	0.39
73	1.07	58.89	0.19	253	1.18	46.17	0.21	433	1.53	55.85	0.41
83	1.30	59.45	0.18	263	1.35	51.75	0.30	443	1.18	57.11	0.37
93	1.82	57.80	0.17	273	1.37	56.34	0.38	453	1.51	55.79	0.53
103	1.28	54.18	0.19	283	1.56	54.38	0.39	463	1.44	56.06	0.58
113	1.18	57.18	0.25	293	1.49	55.16	0.48	473	1.61	55.86	0.60
123	1.34	57.83	0.26	303	1.43	54.71	0.40	482	1.94	53.01	0.47
133	1.33	58.46	0.24	313	1.57	55.60	0.49	494	1.99	45.97	0.33
142	1.41	56.98	0.23	323	1.48	55.49	0.55	503	1.58	56.08	0.51
153	1.19	57.59	0.23	333	2.42	55.73	0.51	513	1.56	56.78	0.48
163	1.73	57.41	0.27	343	1.56	56.02	0.54	522	1.51	56.88	0.45
173	1.45	56.65	0.32	352	1.40	53.98	0.44	533	0.94	58.20	0.35

Carbon Analyser LC2											
Depth (cm)	**N**	**C**	**S**	**Depth (cm)**	**N**	**C**	**S**	**Depth (cm)**	**N**	**C**	**S**
542	1.17	57.18	0.39	733	1.61	50.83	0.36	913	1.45	56.87	0.38
552	1.46	56.74	0.47	743	1.56	50.85	0.38	923	1.38	56.75	0.39
563	1.00	31.94	0.36	759	1.54	47.94	0.28	933	1.54	56.36	0.45
573	1.47	54.16	0.63	764	1.48	46.11	0.30	942	1.61	55.71	0.45
593	1.87	52.01	0.55	774	1.51	56.85	0.44	953	1.58	57.56	0.42
603	1.68	54.20	0.53	782	1.47	57.15	0.43	963	1.64	57.70	0.39
613	1.81	54.10	0.52	793	1.57	51.33	0.31	973	1.64	58.40	0.42
623	1.58	55.16	0.47	803	1.56	54.48	0.35	982	1.71	57.82	0.39
633	1.64	56.13	0.50	812	1.60	56.63	0.36	993	1.63	56.35	0.41
643	1.54	54.85	0.81	822	1.52	56.66	0.36	1003	1.63	57.20	0.40
653	1.56	54.43	0.70	831	1.65	57.55	0.37	1012	1.81	56.06	0.40
663	1.59	55.85	0.75	841	1.72	55.47	0.34	1022	1.53	56.55	0.37
673	1.70	55.61	0.59	853	1.52	56.11	0.38	1033	1.64	57.31	0.40
683	1.75	55.74	0.62	863	1.64	55.94	0.37	1043	1.65	56.67	0.39
693	1.72	55.38	0.53	873	1.81	55.47	0.35	1053	1.59	57.23	0.46
702	1.72	43.93	0.39	883	1.71	55.10	0.38	1063	1.55	54.82	0.55
711	1.40	51.90	0.50	893	1.65	55.54	0.39	1071	1.52	55.23	0.56
723	1.57	53.38	0.50	903	1.52	54.81	0.32	1083	1.73	55.24	0.44

Carbon Analyser LC2

Depth (cm)	N	C	S	Depth (cm)	N	C	S	Depth (cm)	N	C	S
1093	1.76	56.95	0.55	1162	1.50	53.50	0.50	1232	1.69	56.56	0.60
1103	1.38	57.11	0.40	1173	1.68	57.44	0.51	1242	1.53	56.37	0.55
1113	1.68	56.92	0.47	1183	1.52	56.97	0.51	1252	1.75	57.50	0.49
1123	1.75	56.72	0.51	1192	1.32	58.54	0.46	1263	1.36	56.43	0.54
1133	1.79	56.30	0.53	1203	1.50	55.95	0.52	1273	1.48	56.53	0.56
1143	1.42	57.38	0.49	1213	1.40	55.77	0.52	1283	1.39	56.65	0.59
1154	1.24	56.75	0.41	1223	1.51	56.75	0.52	1293	1.45	57.09	0.56

Appendix 13

LC2 - Carbon and Nitrogen Isotope Results

Carbon and Nitrogen Isotopes

LC2

Depth (cm)	**δ^{15}N**	**δ^{13}C**	**Depth (cm)**	**δ^{15}N**	**δ^{13}C**	**Depth (cm)**	**δ^{15}N**	**δ^{13}C**	**Depth (cm)**	**δ^{15}N**	**δ^{13}C**
1	2.76	-25.26	182	1.41	-26.97	362	0.98	-27.62	542	0.20	-28.61
13	1.61	-27.48	193	1.35	-26.89	372	1.42	-27.62	552	2.09	-27.20
23	0.93	-27.67	203	0.89	-27.64	383	1.18	-27.72	563	1.63	-27.48
33	0.70	-27.55	213	0.96	-27.49	393	1.14	-27.78	573	1.69	-27.05
43	0.18	-27.39	223	1.29	-27.64	403	1.07	-27.57	593	1.83	-27.29
53	0.62	-27.91	233	0.98	-27.75	413	1.07	-27.33	603	1.60	-27.34
63	0.39	-27.68	243	1.20	-27.43	423	0.62	-27.48	613	1.52	-27.28
73			253	1.21	-27.49	433	0.53	-27.82	623	1.38	-27.18
83	0.02	-26.87	263	0.90	-27.31	443	0.51	-27.70	633	1.17	-27.56
93	0.56	-26.71	273	0.63	-27.59	453	0.46	-27.61	643	1.27	-27.42
103	0.88	-27.36	283	1.23	-27.42	463	0.32	-27.74	653	1.36	-27.34
113	0.01	-27.63	293	1.02	-27.50	473	0.74	-27.38	663	1.09	-27.47
123	-0.55	-27.64	303	1.08	-27.28	482	1.73	-27.21	673	1.61	-27.46
133	-0.25	-26.76	313	0.96	-27.06	494	0.28	-27.67	683	1.52	-27.24
142	0.33	-27.51	323	0.83	-27.51	503	0.24	-27.60	693	0.95	-27.22
153	0.12	-27.55	333	0.76	-27.39	513	0.31	-27.77	702	1.71	-27.07
163	0.01	-27.72	343	0.83	-27.58	522	-0.33	-27.75	711	0.90	-27.17
173	-0.04	-27.89	352	0.86	-27.57	533	-0.15	-28.48	723	0.89	-27.05

Carbon and Nitrogen Isotopes											
LC2											
Depth (cm)	**δ^{15}N**	**δ ^{13}C**	**Depth (cm)**	**δ^{15}N**	**δ ^{13}C**	**Depth (cm)**	**δ^{15}N**	**δ ^{13}C**	**Depth (cm)**	**δ^{15}N**	**δ ^{13}C**
733	1.47	-27.17	883	1.24	-26.92	1033	1.95	-27.77	1183	0.13	-27.13
743	1.09	-26.97	893	1.20	-26.91	1043	1.06	-27.63	1192	-0.20	-27.13
759	1.48	-26.82	903	1.20	-26.83	1053	0.55	-27.32	1203	1.07	-27.41
764	1.49	-26.79	913	1.02	-27.04	1063	0.54	-27.31	1213	0.83	-27.78
774	1.07	-27.05	923	0.87	-27.13	1071	0.76	-27.35	1223	0.65	-26.44
782	0.91	-27.14	933	1.10	-27.33	1083	0.57	-26.50	1232	1.29	-26.61
793	1.79	-26.85	942	0.89	-27.30	1093	0.99	-26.77	1242	1.08	-21.89
803	1.36	-27.08	953	0.99	-27.26	1103	0.58	-27.35	1252	0.45	-26.49
812	0.93	-27.16	963	0.90	-27.38	1113	0.70	-27.81	1263	1.58	-22.54
822	1.02	-26.92	973	1.13	-26.71	1123	0.75	-27.77	1273	1.75	-22.81
831	1.75	-27.08	982	1.09	-26.65	1133	0.73	-27.52	1283	1.83	-21.84
841	1.72	-26.98	993	1.15	-26.94	1143	0.76	-26.32	1293	1.91	-21.63
853	1.29	-26.74	1003	1.33	-27.26	1154	0.13	-27.37			
863	1.70	-26.90	1012	0.90	-27.27	1162	0.86	-26.76			
873	1.78	-26.81	1022	1.86	-27.40	1173	0.33	-25.13			

Appendix 14

LC2 - Pb Isotope Results

Pb Isotopes LC2													
Depth (cm)	**206/204**	**207/204**	**208/204**	**207/206**	**208/206**	**206/207**	**Depth (cm)**	**206/204**	**207/204**	**208/204**	**207/206**	**208/206**	**206/207**
5	17.862	15.568	37.663	0.87156	2.10848	1.14736	225	18.871	15.663	38.959	0.83000	2.06453	1.20481
15	18.808	15.676	38.792	0.83349	2.06254	1.19978	235	18.931	15.685	38.965	0.82855	2.05823	1.20692
25	18.909	15.688	38.897	0.82964	2.05706	1.20534	245	18.961	15.692	39.075	0.82762	2.06086	1.20829
35	18.951	15.693	38.953	0.82808	2.05545	1.20762	255	18.969	15.678	39.044	0.82654	2.05835	1.20986
45	18.924	15.683	38.912	0.82874	2.05627	1.20666	272.5	18.964	15.684	39.095	0.82704	2.06152	1.20914
55	19.076	15.688	39.052	0.82235	2.04715	1.21602	285	18.819	15.653	38.922	0.83175	2.06822	1.20228
65	19.104	15.690	39.076	0.82128	2.04543	1.21761	305	18.887	15.682	39.024	0.83031	2.06620	1.20437
75	19.058	15.670	39.029	0.82223	2.04789	1.21620	313.5	18.922	15.677	39.074	0.82855	2.06508	1.20693
85	18.922	15.666	38.952	0.82790	2.05852	1.20788	335	18.914	15.675	39.023	0.82872	2.06311	1.20668
95	18.963	15.670	39.010	0.82638	2.05722	1.21009	353.5	18.946	15.673	39.028	0.82725	2.05999	1.20883
105	18.257	15.607	38.192	0.85489	2.09196	1.16974	363.5	18.909	15.670	39.016	0.82873	2.06339	1.20667
127	18.901	15.657	38.955	0.82835	2.06098	1.20722	373.5	18.939	15.672	39.058	0.82752	2.06235	1.20843
136	18.934	15.665	39.026	0.82732	2.06114	1.20872	395	18.946	15.678	39.012	0.82749	2.05910	1.20848
143.5	18.816	15.667	38.887	0.83262	2.06666	1.20103	415	18.777	15.652	38.808	0.83358	2.06675	1.19964
165	18.992	15.675	39.088	0.82537	2.05816	1.21158	423.5	18.866	15.669	38.989	0.83054	2.06662	1.20404
185	19.058	15.678	39.084	0.82262	2.05073	1.21563	433.5	18.820	15.667	38.911	0.83245	2.06746	1.20127
195	19.050	15.679	39.095	0.82306	2.05224	1.21498	443	18.518	15.644	38.582	0.84477	2.08346	1.18375
205	18.912	15.670	38.962	0.82855	2.06015	1.20692	455	18.803	15.640	38.832	0.83177	2.06515	1.20225
215	18.870	15.665	38.912	0.83017	2.06213	1.20457	473.5	18.737	15.677	38.912	0.83672	2.07678	1.19514

Pb Isotopes LC2													
Depth (cm)	**206/204**	**207/204**	**208/204**	**207/206**	**208/206**	**206/207**	**Depth (cm)**	**206/204**	**207/204**	**208/204**	**207/206**	**208/206**	**206/207**
485	19.008	15.657	39.068	0.82367	2.05527	1.21408	726	18.829	15.669	38.884	0.83214	2.06506	1.20171
493.5	18.976	15.680	39.119	0.82630	2.06143	1.21021	736	18.954	15.678	39.026	0.82718	2.05897	1.20893
505	18.845	15.666	38.923	0.83128	2.06540	1.20296	755	19.008	15.686	39.083	0.82522	2.05615	1.21179
515	18.898	15.677	39.098	0.82956	2.06886	1.20545	782.5	18.406	15.635	38.415	0.84948	2.08716	1.17719
525.5	18.836	15.673	38.894	0.83206	2.06481	1.20183	795	19.058	15.686	39.136	0.82309	2.05358	1.21493
545	18.744	15.637	38.759	0.83424	2.06786	1.19869	805	18.950	15.664	39.088	0.82660	2.06266	1.20978
556	18.939	15.679	39.056	0.82789	2.06220	1.20790	813.5	18.385	15.633	38.334	0.85027	2.08504	1.17609
566	18.928	15.666	39.028	0.82770	2.06195	1.20817	833.5	18.645	15.652	38.697	0.83951	2.07551	1.19118
585	18.960	15.682	39.107	0.82709	2.06255	1.20905	843.5	18.905	15.668	38.946	0.82873	2.06002	1.20666
596	18.747	15.670	38.854	0.83587	2.07256	1.19636	865	18.603	15.646	38.678	0.84105	2.07910	1.18899
615	18.922	15.667	39.015	0.82799	2.06194	1.20775	885	18.925	15.675	38.997	0.82824	2.06058	1.20738
623.5	18.976	15.676	38.987	0.82611	2.05455	1.21049	893.5	18.889	15.678	38.974	0.83001	2.06331	1.20480
633.5	18.926	15.680	39.096	0.82851	2.06577	1.20699	903.5	18.447	15.646	38.494	0.84814	2.08675	1.17905
645	18.862	15.681	38.977	0.83134	2.06640	1.20288	915	18.925	15.673	38.972	0.82812	2.05927	1.20755
655	18.959	15.694	39.066	0.82780	2.06058	1.20803	935	18.509	15.653	38.601	0.84572	2.08557	1.18243
665	18.832	15.664	38.844	0.83180	2.06267	1.20221	944.5	18.710	15.660	38.801	0.83700	2.07383	1.19474
675	18.950	15.664	39.106	0.82658	2.06364	1.20980	975	18.518	15.630	38.517	0.84406	2.07997	1.18475
685	18.859	15.649	38.847	0.82982	2.05989	1.20509	983.5	18.533	15.637	38.553	0.84372	2.08020	1.18523
705	19.017	15.679	39.003	0.82448	2.05098	1.21288	1005	18.697	15.653	38.753	0.83715	2.07268	1.19452

Pb Isotopes LC2													
Depth (cm)	**206/204**	**207/204**	**208/204**	**207/206**	**208/206**	**206/207**	**Depth (cm)**	**206/204**	**207/204**	**208/204**	**207/206**	**208/206**	**206/207**
1013.5	18.825	15.669	38.925	0.83232	2.06772	1.20146	1158	18.920	15.682	38.992	0.82883	2.06088	1.20651
1023.5	18.612	15.660	38.674	0.84142	2.07790	1.18847	1175	18.959	15.690	39.018	0.82758	2.05796	1.20835
1035	18.947	15.687	39.009	0.82795	2.05883	1.20781	1192.5	18.615	15.665	38.656	0.84153	2.07662	1.18832
1053.5	18.763	15.645	38.760	0.83379	2.06574	1.19934	1207.5	18.679	15.652	38.695	0.83795	2.07153	1.19339
1063.5	18.740	15.665	38.818	0.83591	2.07139	1.19630	1215	18.791	15.666	38.864	0.83370	2.06818	1.19947
1073.5	18.607	15.661	38.644	0.84168	2.07686	1.18809	1235	18.929	15.677	38.958	0.82822	2.05812	1.20741
1085	18.923	15.689	39.004	0.82910	2.06123	1.20613	1243.5	18.954	15.688	38.991	0.82767	2.05707	1.20822
1093.5	18.366	15.631	38.393	0.85110	2.09046	1.17495	1253.5	18.879	15.675	38.931	0.83028	2.06209	1.20442
1105	18.975	15.682	39.128	0.82646	2.06212	1.20997	1265	18.359	15.612	38.353	0.85038	2.08901	1.17595
1123.5	18.812	15.674	38.911	0.83320	2.06840	1.20020	1283.5	18.506	15.657	38.510	0.84602	2.08093	1.18201
1135.5	18.893	15.679	38.972	0.82991	2.06283	1.20496	1293.5	18.998	15.694	39.069	0.82613	2.05652	1.21047
1145	18.827	15.663	38.908	0.83194	2.06662	1.20201							

Appendix 14: Pb Isotopes LC2

Appendix 15

LC2 – Biogenic Silica

Biogenic Silica							
Depth (cm)	**Wt, mg**	**%Si(opal)**	**%opal**	**Depth (cm)**	**Wt, mg**	**%Si(opal)**	**%opal**
1	40.26	34.98	83.95	522	40.71	0.28	0.67
43	43.12	0.49	1.17	563	42.73	18.23	43.75
123	42.48	0.63	1.52	643	38.92	0.36	0.87
183	41.53	23.67	55.66	702	45.91	17.98	43.14
223	43.05	22.70	54.49	702	41.87	13.49	32.37
223	41.17	21.26	51.03	702	42.04	23.24	55.77
223	42.08	18.41	44.19	Av. 702	39.40	23.49	56.39
Av. 223	42.10	20.79	49.90	764	42.15	8.47	20.34
283	41.50	1.84	4.41	793	39.62	5.22	12.52
403	42.02	0.35	0.84	913	45.20	0.17	0.41
494	40.65	12.92	31.01	1012	41.72	0.21	0.50
494	41.78	16.65	39.95	1143	52.37	0.33	0.79
494	42.35	13.38	32.12	1293	52.84	0.24	0.57
Av. 494	41.59	14.32	34.36				

Appendix 15: Biogenic Silica LC2

Appendix 16

LC2 – Microscope Analysis

Microscopic Analysis			
Depth (cm)	**Evidence of biogenic silica**	**Depth (cm)**	**Evidence of biogenic silica**
43	None	643	None
75	None	663	None
123	None	702	Yes - 20%
183	Yes - 40%	764	Yes - 20%
223	Yes - 10%	793	Yes - 15%
233	Yes - 5%	833	None
283	None	873	None
403	None	913	None
494	Yes - 20%	1012	None
513	None	1093	None
522	None	1143	None
563	Yes	1293	None

Appendix 16: Microscopic Analysis LC2

Appendix 17

LC2 – Bulk Density

Depth	**Dry weight**	**Volume**	**Density**	**Depth**	**Dry weight**	**Volume**	**Density**
(cm)	**(g)**	**(cm3)**	**(g/cm3)**	**(cm)**	**(g)**	**(cm3)**	**(g/cm3)**
5	4.47	4.47	0.12	235	2.26	2.26	0.06
15	3.99	3.99	0.11	245	2.60	2.60	0.07
25	2.79	2.79	0.08	255	2.92	2.92	0.08
35	2.54	2.54	0.07	265	2.31	2.31	0.06
45	2.67	2.67	0.07	275	2.09	2.09	0.06
55	2.12	2.12	0.06	285	2.41	2.41	0.07
65	2.52	2.52	0.07	295	2.38	2.38	0.07
75	2.21	2.21	0.06	305	2.49	2.49	0.07
85	2.17	2.17	0.06	315	2.52	2.52	0.07
95	2.11	2.11	0.06	325	2.10	2.10	0.06
105	1.63	1.63	0.05	335	2.12	2.12	0.06
115	1.07	1.07	0.03	345	1.99	1.99	0.06
125	1.27	1.27	0.04	355	1.71	1.71	0.05
135	1.30	1.30	0.04	365	1.74	1.74	0.05
145	1.37	1.37	0.04	375	1.71	1.71	0.05
155	1.33	1.33	0.04	385	1.77	1.77	0.05
165	1.40	1.40	0.04	395	1.93	1.93	0.05
175	2.32	2.32	0.06	405	1.75	1.75	0.05
185	4.08	4.08	0.11	415	1.95	1.95	0.05
195	2.98	2.98	0.08	425	1.52	1.52	0.04
205	2.21	2.21	0.06	435	1.44	1.44	0.04
215	2.42	2.42	0.07	445	1.29	1.29	0.04
225	2.63	2.63	0.07	455	1.56	1.56	0.04

Appendix 17: Bulk Density LC2

Depth (cm)	Dry weight (g)	Volume (cm3)	Density (g/cm3)	Depth (cm)	Dry weight (g)	Volume (cm3)	Density (g/cm3)
465	1.70	1.70	0.05	695	1.77	1.77	0.05
475	1.88	1.88	0.05	705	2.62	2.62	0.07
485	3.50	3.50	0.10	715	1.60	1.60	0.04
495	2.16	2.16	0.06	725	1.60	1.60	0.04
505	1.72	1.72	0.05	735	2.02	2.02	0.06
515	1.89	1.89	0.05	745	1.48	1.48	0.04
525	1.78	1.78	0.05	755	2.21	2.21	0.06
535	1.75	1.75	0.05	775	1.64	1.64	0.05
545	2.28	2.28	0.06	785	1.65	1.65	0.05
555	1.58	1.58	0.04	795	2.37	2.37	0.07
565	1.67	1.67	0.05	805	2.03	2.03	0.06
575	1.96	1.96	0.05	815	1.68	1.68	0.05
585	2.61	2.61	0.07	825	1.67	1.67	0.05
595	2.00	2.00	0.06	835	1.59	1.59	0.04
605	1.89	1.89	0.05	845	1.94	1.94	0.05
615	2.12	2.12	0.06	855	1.74	1.74	0.05
625	1.78	1.78	0.05	865	1.96	1.96	0.05
635	1.46	1.46	0.04	875	1.93	1.93	0.05
645	1.34	1.34	0.04	885	1.99	1.99	0.06
655	1.68	1.68	0.05	895	1.82	1.82	0.05
665	1.76	1.76	0.05	905	1.58	1.58	0.04
675	2.65	2.65	0.07	915	1.82	1.82	0.05
685	2.06	2.06	0.06	925	1.76	1.76	0.05

Appendix 17: Bulk Density LC2

Depth	**Dry weight**	**Volume**	**Density**	**Depth**	**Dry weight**	**Volume**	**Density**
(cm)	**(g)**	**(cm3)**	**(g/cm3)**	**(cm)**	**(g)**	**(cm3)**	**(g/cm3)**
935	1.79	1.79	0.05	1125	1.68	1.68	0.05
945	1.58	1.58	0.04	1135	1.70	1.70	0.05
955	1.84	1.84	0.05	1145	1.77	1.77	0.05
965	1.88	1.88	0.05	1155	1.42	1.42	0.04
975	2.12	2.12	0.06	1165	1.18	1.18	0.03
985	1.85	1.85	0.05	1175	1.35	1.35	0.04
995	1.70	1.70	0.05	1185	1.17	1.17	0.03
1005	1.66	1.66	0.05	1195	1.09	1.09	0.03
1015	1.69	1.69	0.05	1205	0.87	0.87	0.02
1025	1.86	1.86	0.05	1215	2.50	2.50	0.07
1035	2.17	2.17	0.06	1225	2.43	2.43	0.07
1045	1.84	1.84	0.05	1235	2.38	2.38	0.07
1055	1.84	1.84	0.05	1245	1.96	1.96	0.05
1065	1.54	1.54	0.04	1255	1.81	1.81	0.05
1075	1.62	1.62	0.04	1265	2.46	2.46	0.07
1085	1.69	1.69	0.05	1275	1.95	1.95	0.05
1095	1.52	1.52	0.04	1285	2.33	2.33	0.06
1105	1.65	1.65	0.05	1295	1.88	1.88	0.05
1115	1.92	1.92	0.05				

Appendix 17: Bulk Density LC2

Appendix 18

Kylander et al., 2007 Abstract

Rare Earth Element and Pb isotope variations in a 55,000 year old peat core from Lynch's Crater (NE QLD, Australia): Proxy development and application to paleoclimate in the Southern Hemisphere

M.E. Kylander[1,2], J. Muller[3], D.J. Weiss[1,2], R.A.J. Wüst[3], K. Gallagher[1], R. Garcia-Sanchez[2] and B. J. Coles1[2]

1. Department of Earth Science and Engineering, Imperial College London, UK, SW7 2AZ

2. Department of Mineralogy, The Natural History Museum London, UK, SW7 5BD

3. School of Earth Sciences, James Cook University, Townsville, 4811, Queensland, Australia

Corresponding author: malin.kylander@imperial.ac.uk

Paper published in:

Geochimica et Cosmichimica Acta

2007, Volume 71, Issue 4*: *942-960

Appendix 18: Kylander et al., 2007

ABSTRACT

Accurate prediction of future climates scenarios is contingent on our understanding of its mechanisms. This is done in part through the reconstruction of past climate changes using environmental archives. Here, develop REE as an indicator of dust source changes and by extension as a new inorganic geochemical proxy of climate change. Using a peat core from Lynch's Crater in NE Queensland, Australia we present the first long-term (55,000 years) record of (with the exception of four lake periods) atmospheric REE deposition in the Southern Hemisphere. This core covers both glacial and interglacial times and is under minimal anthropogenic influence. The immobility of REE was established using a combination of correlation analyses, Al and Ti normalised profiles and elemental patterns. This is important as REE can be mobile under acid and organic rich conditions like those found in a peat bog. Based on the various types of volcanic provinces in eastern Australia, Eu anomalies were applied in a novel way to source trace dusts deposited at the bog. The base of the core 40,745-54,850-BP was found to be under the influence of long distance (>1500 km) transport from SE Australia. From 8860-40,370 BP regional sources (100-1500 km) dominate the deposited signals while in the upper part of the core (1815-8435 BP) the dust signal is controlled by local sources (<100 km). These findings are confirmed by Pb isotope data. Changepoint modelling refined the identification of these changes in source, recognizing concurrent shifts in our source tracing tools (Eu/Eu*PAAS and $^{206}Pb/^{207}Pb$). The timing of these changepoints was compared with other palaeoenvironmental records (pollen, lake levels and dune building) from Australia and found to be similar. Our results clearly demonstrate the application of REE as a reliable tool for tracing atmospheric mineral dusts and as a new proxy of climate change.

Appendix 18: Kylander et al., 2007